PEER/ATC 72-1

Modeling and acceptance criteria for seismic design and analysis of tall buildings

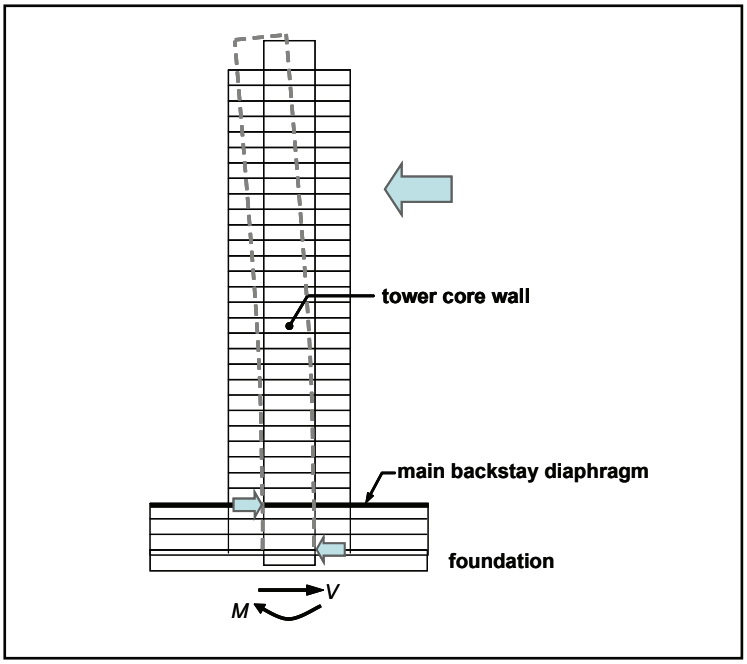

Applied Technology Council

Pacific Earthquake Engineering Research Center

Applied Technology Council

The Applied Technology Council (ATC) is a nonprofit, tax-exempt corporation established in 1973 through the efforts of the Structural Engineers Association of California. ATC's mission is to develop state-of-the-art, user-friendly engineering resources and applications for use in mitigating the effects of natural and other hazards on the built environment. ATC also identifies and encourages needed research, and develops consensus opinions on structural engineering issues in a non-proprietary format, thereby fulfilling a unique role in funded information transfer.

ATC is guided by a Board of Directors consisting of representatives appointed by the American Society of Civil Engineers, the National Council of Structural Engineers Associations, the Structural Engineers Association of California, the Western Council of Structural Engineers Associations, and at-large representatives concerned with the practice of structural engineering. Each director serves a three-year term.

Project management and administration are carried out by a full-time Executive Director and support staff. Project work is conducted by a diverse group of highly qualified consulting professionals, thus incorporating the expertise of individuals from academia, research, and professional practice who would otherwise not be available from any single organization. Funding for ATC projects is obtained from government agencies and from the private sector in the form of tax-deductible contributions.

2010-2011 ATC Board of Directors

Ramon Gilsanz, President
Marc Levitan, Vice President
Bret Lizundia, Secretary/Treasurer
H. John Price, Past President

Dan Allwardt
James A. Amundson
David A. Fanella
Manuel Morden
Charles Roeder
Spencer Rogers
Donald Scott
Joseph B. Shepard
Robert Smilowitz
Thomas L. Smith
Charles H. Thornton

Pacific Earthquake Engineering Research Center

The Pacific Earthquake Engineering Research (PEER) Center, with headquarters at UC Berkeley, is a consortium of western U.S. universities working in partnership with business, industry, and government to identify and reduce the risks from major earthquakes to life safety and to the economy.

PEER achieves its objectives of earthquake risk reduction through a coordinated program of research, education, and partnerships with users of research results. PEER's research program includes basic and applied components of geology, seismology, various branches of engineering, architecture, urban planning, and economics.

PEER is supported by funding from the United States Federal Government, State of California (various agencies), local governments, and the private sector.

PEER Reports can be ordered at
http://peer.berkeley.edu/publications/peer_reports.html

or by contacting:

Pacific Earthquake Engineering Research Center
1301 South 46th Street
Richmond, California 94804-4698
Tel: 510-665-3448
Fax: 510-665-3456
Email: peer_editor@berkeley.edu

PEER Director: Stephen Mahin
PEER Executive Director: Yousef Bozorgnia

Disclaimer and Notice

Cover Illustration: Courtesy of Joseph Maffei, Rutherford & Chekene, San Francisco, California

PEER/ATC-72-1

Modeling and Acceptance Criteria for Seismic Design and Analysis of Tall Buildings

Prepared by

APPLIED TECHNOLOGY COUNCIL
201 Redwood Shores Pkwy, Suite 240
Redwood City, California 94065
www.ATCouncil.org

in collaboration with
Building Seismic Safety Council (BSSC)
National Institute of Building Sciences (NIBS)
Federal Emergency Management Agency (FEMA)

Prepared for

PACIFIC EARTHQUAKE ENGINEERING RESEARCH CENTER (PEER)
Jack P. Moehle, Principal Investigator
Stephen Mahin, Director
Yousef Bozorgnia, Executive Director

TASK 7 PROJECT CORE GROUP
James O. Malley (Technical Director)
Gregory Deierlein
Helmut Krawinkler
Joseph R. Maffei
Mehran Pourzanjani
John Wallace
Jon A. Heintz

October 2010

Preface

In October 2006, the Applied Technology Council (ATC) began work on a contract assisting the Pacific Earthquake Engineering Research Center (PEER) in developing guidelines for the seismic design of tall buildings as part of the PEER Tall Buildings Initiative. The purpose of this work was to prepare recommendations for modeling the behavior of tall building structural systems and acceptance values for use in seismic design. Shortly thereafter, ATC secured additional funding on behalf of PEER from the Federal Emergency Management Agency (FEMA), through the Building Seismic Safety Council (BSSC) of the National Institute of Building Sciences, in support of this effort.

A *Workshop on Tall Building Seismic Design and Analysis Issues* was conducted in January 2007. The purpose of this workshop was to identify and prioritize seismic design and analytical challenges related to tall buildings by soliciting the opinions and collective recommendations of leading practitioners, regulators, and researchers actively involved in the design, permitting, and construction of tall buildings. The outcome of this workshop is recorded in a companion report, ATC-72 *Proceedings of Workshop on Tall Building Seismic Design and Analysis Issues*, which includes a prioritized list of the most important tall building modeling and acceptance criteria issues needing resolution, based on the opinions of those in attendance.

Using the workshop as a starting point, this report is the result of further work under the PEER Tall Buildings Initiative to develop modeling recommendations and acceptance criteria for design and analysis of tall buildings. It is intended to serve as a resource document for the *Guidelines for Seismic Design of Tall Buildings*, published as a companion report by PEER (2010).

ATC is indebted to the leadership of Jim Malley, Project Technical Director, and to the members of the PEER/ATC-72 Task 7 Project Core Group, consisting of Greg Deierlein, Helmut Krawinkler, Joe Maffei, Mehran Pourzanjani, and John Wallace, for their efforts in researching and assembling the information contained herein. A group of experts on tall building design and analysis was convened to obtain feedback on the

recommendations as they were being developed, and input from this group was instrumental in shaping the final product. The names and affiliations of all who contributed to this project are included in the list of Project Participants at the end of this report.

ATC also gratefully acknowledges Jack Moehle, Yousef Bozorgnia, and the PEER Tall Buildings Project Advisory Committee for their input and guidance in the completion of this report, Ayse Hortacsu and Peter N. Mork for ATC report production services, and Charles H. Thornton as ATC Board Contact.

Jon A. Heintz
ATC Director of Projects

Christopher Rojahn
ATC Executive Director

Table of Contents

Preface iii

List of Figures ix

List of Tables xvii

1. Introduction 1-1
   - 1.1 Background 1-1
   - 1.2 Pacific Earthquake Engineering Research Center Tall Buildings Initiative 1-2
   - 1.3 Workshop on Tall Building Seismic Design and Analysis Issues 1-3
   - 1.4 Issues in Tall Building Design 1-4
   - 1.5 Report Organization and Content 1-5

2. General Nonlinear Modeling 2-1
   - 2.1 Overview of Modeling Issues for Nonlinear Response History Analysis 2-1
     - 2.1.1 Types of Nonlinear Models 2-1
     - 2.1.2 Inelastic Component Attributes 2-3
     - 2.1.3 Energy Dissipation and Viscous damping 2-5
     - 2.1.4 Gravity Load effects in Nonlinear Analysis 2-5
     - 2.1.5 Acceptance Criteria 2-6
   - 2.2 Deterioration 2-8
     - 2.2.1 Modes of Deterioration 2-10
     - 2.2.2 Consequences of Deterioration on Structural Response 2-13
     - 2.2.3 Sources of Deterioration 2-14
     - 2.2.4 Modeling of Deterioration 2-15
     - 2.2.5 Analytical Modeling Options 2-25
     - 2.2.6 Sensitivity of Response to Deterioration 2-27
     - 2.2.7 Summary Observations for Modeling of Deterioration 2-29
   - 2.3 P-delta Effects 2-29
     - 2.3.1 Summary Observations for P-delta Effects 2-31
     - 2.3.2 Recommendations for Modeling P-delta Effects. 2-34
   - 2.4 Damping 2-35
     - 2.4.1 Physical sources of Damping 2-35
     - 2.4.2 Survey of Damping Assumptions in Design and Assessment 2-38
     - 2.4.3 Measurement of Damping in Buildings 2-39
     - 2.4.4 Modeling Techniques for Damping 2-47
     - 2.4.5 Recommendations for Nonlinear Analysis and Design 2-54
   - 2.5 Expected Properties and Uncertainty 2-56
     - 2.5.1 Statistical Characterization of Modeling Uncertainties 2-57

3. Modeling of Frame Components 3-1
3.1 Modeling Parameters for Frame Components 3-1
3.2 Nonlinear Modeling of Steel Beam and Column Components 3-2
3.2.1 Behavioral Considerations for Steel Beams 3-3
3.2.2 Quantification of Properties for Steel Beams 3-6
3.2.3 Recommendations for Modeling of Steel Beams 3-18
3.2.4 Behavioral Considerations for Steel Columns 3-19
3.2.5 Recommendations for Modeling of Steel Columns 3-21
3.2.6 Acceptance Criteria for Steel Beams and Columns 3-22
3.3 Nonlinear Modeling of Steel Panel Zones 3-23
3.3.1 Quantification of Properties for Steel Panel Zones 3-24
3.3.2 Acceptance Criteria for Steel Panel Zones 3-28
3.4 Nonlinear Modeling of Reinforced Concrete Beams, Columns, and Beam-Column Joints 3-28
3.4.1 Behavioral Considerations for Reinforced Concrete Frame Components 3-30
3.4.2 Quantification of Properties for Reinforced Concrete Beams and Columns 3-32
3.4.3 Quantification of Properties for Reinforced Concrete Beam-Column Joints 3-42
3.4.4 Recommendations for Modeling of Reinforced Concrete Frame Components 3-43
3.4.5 Acceptance Criteria for Reinforced Concrete Frame Components 3-44

4. Modeling of Shear Wall and Slab-Column Frame Systems 4-1
4.1 Modeling of Planar and Flanged Reinforced Concrete Shear Walls 4-1
4.1.1 Beam-Column Element Models 4-1
4.1.2 Fiber Beam-Column Models 4-2
4.1.3 Biaxial Fiber and Detailed Finite Element Models 4-3
4.1.4 Coupled Models (Shear-Flexure Interaction) 4-4
4.2 Quantification of Properties for Planar and Flanged Walls 4-5
4.2.1 Shear Behavior 4-5
4.2.2 Effective Flexural Stiffness 4-11
4.2.3 Material Models 4-16
4.2.4 Material Models in Commercially Available Software 4-17
4.2.5 Simulation of Tested Behavior 4-20
4.2.6 Model Sensitivity to Material and Model Parameters 4-26
4.2.7 Summary Recommendations for Modeling of Planar and Flanged Walls 4-29
4.3 Modeling of Coupling Beams 4-30
4.3.1 Effective Stiffness 4-30
4.3.2 Detailing Options and Force-Deformation Response 4-32
4.3.3 Implied Damage States 4-35
4.3.4 Simulation of Tested Behavior 4-37
4.3.5 Summary Recommendations for Modeling of Coupling Beams 4-39
4.4 Response and Behavior of Core Wall Systems 4-40

4.4.1 Core Wall Geometry, Configuration, and Modeling 4-40
4.4.2 Summary Findings for Core Wall Response and Behavior 4-48
4.5 Modeling of Slab-Column Frame Components and Connections 4-49
4.5.1 Quantification of Properties for Slab-Column Frames 4-49
4.5.2 Application to Core Wall Systems 4-53
4.5.3 Summary Recommendations for Modeling of Slab-Column Frames 4-57
4.6 Performance of Post-Tensioned Slab-Wall Connections 4-57

A. Modeling of Podium Diaphragms, Collectors, and Backstay Effects A-1
A.1 Podium and Backstay Effects A-1
A.1.1 Structural Elements of the Podium A-3
A.1.2 Seismic-Force-Resisting Elements of the Tower A-5
A.1.3 Consideration of Backstay Effects A-5
A.1.4 Impact of Structural System Type and Configuration on Backstay Effects A-5
A.2 Effects of Other Structural Configurations A-6
A.2.1 Buildings Without Backstay Effects A-6
A.2.2 Setback or Step-Back Effects A-6
A.2.3 Multiple Towers on a Common Base A-7
A.2.4 Buildings on Sloping Sites A-9
A.3 Nonlinear Seismic Response and Capacity Design A-9
A.3.1 Capacity Design A-9
A.3.2 Two-Stage Design Process A-11
A.4 Modeling of Structural Elements A-12
A.4.1 Bracketing of Stiffness Properties A-12
A.5 Collectors and Diaphragm Segments A-13
A.5.1 Role of Collectors A-13
A.5.2 Design for System Overstrength A-13
A.5.3 Collector Eccentricity and Diaphragm Segments A-14
A.6 Diaphragm Flexibility A-15
A.6.1 Relative Stiffness of Diaphragms and Vertical Elements A-17
A.6.2 Building Code Requirements A-17
A.7 Semi-Rigid Diaphragm Modeling A-18
A.7.1 Linear versus Nonlinear Analysis A-19
A.8 Design of Diaphragms and Collectors A-19
A.8.1 Diaphragm In-Plane Shear A-19
A.8.2 Strut-and-Tie Models A-19
A.8.3 Diaphragm In-Plane Flexure A-20
A.8.4 Distribution of Collector Forces A-20
A.8.5 Slab Reinforcement for Gravity and Seismic Forces A-21
A.9 Recommended Stiffness Properties for Modeling of Backstay Effects A-23
A.9.1 Lateral Stiffness for Passive Soil Resistance A-25

Glossary B-1
References C-1
Project Participants D-1

List of Figures

Figure 2-1 Comparison of nonlinear component model types 2-2

Figure 2-2 Illustration of modeling components for a reinforced concrete beam-column: (a) inelastic hinge model; (b) initial (monotonic) backbone curve; and (c) cyclic response model 2-4

Figure 2-3 Plots showing different rates of deterioration: (a) slow deterioration; and (b) rapid deterioration 2-9

Figure 2-4 Monotonic and cyclic experimental response of a steel beam 2-10

Figure 2-5 Hysteretic response of identical steel beam specimens under different loading histories 2-11

Figure 2-6 Hysteretic response of identical reinforced concrete column specimens under different loading histories 2-12

Figure 2-7 Incremental dynamic analysis (IDA) curves for a moment-resisting frame example using non-deteriorating and deteriorating component models 2-13

Figure 2-8 Parameters of the initial (monotonic) backbone curve of the Ibarra-Krawinkler model 2-18

Figure 2-9 Basic options for stable hysteresis characteristics: (a) bilinear; (b) peak oriented; and (c) pinching 2-19

Figure 2-10 Simulations obtained with a modified Bouc-Wen model 2-19

Figure 2-11 Ramberg-Osgood Model 2-20

Figure 2-12 Individual deterioration modes illustrated for a peak-oriented model 2-21

Figure 2-13 Ibarra-Krawinkler model calibration examples: (a) steel beam; and (b) reinforced concrete beam 2-22

Figure 2-14 Example of a simulation using the Sivalsevan-Reinhorn model showing: (a) experimental results; and (b) calibrated simulation 2-22

Figure 2-15 Song-Pincheira model: (a) backbone curve; (b) hysteresis rules for cycles of increasing deflection amplitude; (c) hysteresis rules for small amplitude or internal cycles....2-23

Figure 2-16 Monotonic and cyclic responses of identical specimens, and skeleton curve fit to cyclic response for: (a) steel beam (Tremblay et al., 1997); and (b) plywood shear wall panel....2-24

Figure 2-17 Illustration of four options for analytical component modeling....2-27

Figure 2-18 Effects of deterioration parameters on median collapse capacity of generic 8-story moment-resisting frame (MRF) and shear wall (SW) structures....2-28

Figure 2-19 Response history of a single degree of freedom system incorporating P-Delta effects....2-30

Figure 2-20 Pushover deflection profiles for an 18-story frame structure at different roof drifts with P-Delta excluded (thin line), and P-Delta included (thick line)....2-31

Figure 2-21 Effects of P-Delta on median collapse capacity (Sa_c/g) of: (a) 8-story moment-resisting frame; and (b) shear wall structure deforming in a flexural mode....2-32

Figure 2-22 Base shear versus roof displacement pushover curves for the SAC 20-story Los Angeles structure....2-32

Figure 2-23 Dynamic response of SAC 20-story Los Angeles structure using four different analytical models shown as: (a) response histories; and (b) incremental dynamic analyses....2-33

Figure 2-24 Damping and drift demand data from buildings excited by strong ground motions....2-41

Figure 2-25 Measured damping from buildings in Japan....2-43

Figure 2-26 Illustration of amplitude dependence of measured damping under wind loading....2-44

Figure 2-27 Variation in percent of critical damping for mass, stiffness, and Rayleigh proportional damping with $\zeta = 2\%$ at $T_1 = 5$ seconds....2-48

Figure 2-28 Suggested target limits on damping....2-56

Figure 3-1 Hysteretic response of a steel beam with composite slab....3-6

Figure 3-2 Plot showing comparison of deterioration model to experimental results 3-8

Figure 3-3 Cumulative distribution functions for pre-capping plastic rotation, θ_p, for: (a) full data sets; and (b) beam depths, $d \geq 21$ in 3-9

Figure 3-4 Cumulative distribution functions for post-capping rotation, θ_{pc}, for: (a) full data sets; and (b) beam depths, $d \geq 21$ in 3-10

Figure 3-5 Cumulative distribution functions for reference cumulative plastic rotation, Λ, for: (a) full data sets; and (b) beam depths, $d \geq 21$ in..... 3-10

Figure 3-6 Dependence of pre-capping plastic rotation, θ_p, on beam depth, d, for non-RBS connections, full data set.... 3-11

Figure 3-7 Dependence of pre-capping plastic rotation, θ_p, on shear span to depth ratio, L/d, for non-RBS connections, full data set..... 3-11

Figure 3-8 Dependence of modeling parameters on h/t_w, for beam depths $d \geq 21$ in., and RBS and non-RBS connections 3-13

Figure 3-9 Procedure for obtaining the modified backbone curve for modeling Option 3, and the ultimate rotation, θ_u, for modeling Option 4..... 3-19

Figure 3-10 Strong column factor, R_μ, required to avoid plastic hinging in columns for a 9-story moment-resisting frame structure 3-20

Figure 3-11 Representative results from tests on W14x176 column sections subjected to an axial load and cyclic bending moment: (a) moment versus story drift response for $P/P_y = 0.35$; and (b) peak moment versus story drift for $P/P_y = 0.75$ 3-21

Figure 3-12 Analytical predictions of flexural cyclic response of: (a) W27x146 columns for $P/P_y = 0.35$; and (b) W27x194 columns for $P/P_y = 0.55$ 3-22

Figure 3-13 Analytical model for panel zone..... 3-24

Figure 3-14 Cyclic shear behavior of weak panel zone..... 3-24

Figure 3-15 Trilinear shear force and shear distortion relationship for panel zone..... 3-27

Figure 3-16 Moment and shear forces at a connection due to lateral loads 3-27

Figure 3-17 Use of two springs to model trilinear behavior 3-27

Figure 3-18 Shear force-distortion response for a typical panel zone 3-27

Figure 3-19 Reinforced concrete flexural member: (a) idealized flexural element; (b) monotonic backbone curve and hysteretic response; and (c) monotonic and modified backbone curves. 3-29

Figure 3-20 Idealization of reinforced concrete beam-column joint 3-30

Figure 3-21 Definitions of secant elastic stiffness 3-33

Figure 3-22 Comparison of effective stiffness values of reinforced beam-columns 3-34

Figure 3-23 Modified force-deformation response curve 3-39

Figure 3-24 Comparison of plastic rotation parameters for modeling Option 3 versus ASCE/SEI 41-06 *Supplement No. 1* for: (a) pre-capping rotation capacity; and (b) post-capping rotation capacity 3-40

Figure 3-25 Comparison of ultimate plastic rotation versus ASCE/SEI 41-06 *Supplement No. 1* acceptance criteria at the Collapse Prevention performance level for: (a) Option 4; and (b) Option 3 3-42

Figure 3-26 Recommended rigid end zone offsets for reinforced concrete beam column joints based on relative column and beam strengths 3-43

Figure 4-1 Equivalent beam-column element representation of a reinforced concrete shear wall 4-2

Figure 4-2 Fiber element representation of a reinforced concrete shear wall. 4-2

Figure 4-3 Biaxial fiber model for bending in two-dimensions 4-4

Figure 4-4 Coupled model and results for a low-aspect ratio wall 4-5

Figure 4-5 Shear force-deformation curves based on: (a) FEMA 356; and (b) ASCE/SEI 41-06 Supplement No. 1 4-6

Figure 4-6 ASCE/SEI 41-06 variation in column shear strength versus ductility demand 4-9

Figure 4-7 Shear force-deformation results for lightly reinforced wall piers 4-11

Figure 4-8 Roof displacement response correlation studies for: (a) 10-story walls; and (b) 7-story walls 4-12

Figure 4-9 Upper-bound and lower-bound wall flexural stiffness versus: (a) axial load ratio; and (b) displacement ratio 4-13

Figure 4-10 Impact of wall flexural strength on effective stiffness 4-14

Figure 4-11 Comparison between predicted and tested effective stiffness values for: (a) rectangular walls; and (b) T-shaped walls 4-14

Figure 4-12 Comparison of modeled and tested moment versus curvature relations for: (a) slender wall; and (b) bridge column 4-15

Figure 4-13 Uniaxial material models commonly used in fiber models 4-16

Figure 4-14 Material models in commercially available software 4-18

Figure 4-15 Comparison of wall tests versus model results generated by commercially available software 4-19

Figure 4-16 Behavior of a rectangular wall section subjected to constant axial load and reverse cyclic loading 4-20

Figure 4-17 Comparison of model and test results for a rectangular wall section 4-21

Figure 4-18 Comparison of simulated results using two different concrete constitutive models 4-21

Figure 4-19 Comparison of measured versus modeled average strain in a rectangular wall section 4-22

Figure 4-20 Curvature profiles for a rectangular wall section at three levels of drift 4-22

Figure 4-21 Behavior of a flanged (T-shaped) wall section subjected to constant axial load and reverse cyclic loading 4-23

Figure 4-22 Comparison of model and test results for a T-shaped wall 4-24

Figure 4-23 Distribution of concrete strains in the flange of a T-shaped wall 4-24

Figure 4-24 Distribution of reinforcing steel strains in the flange of a T-shaped wall 4-25

Figure 4-25 Distribution of concrete strains in the flange of a T-shaped wall 4-25

Figure 4-26 Influence of reinforcing steel stress-strain relation on force-deformation response for: (a) elastic-perfectly-plastic; and (b) strain hardening behavior 4-27

Figure 4-27 Influence of mesh size on force-deformation response for: (a) 91 elements; and (b) six elements 4-27

Figure 4-28 Influence of mesh size on wall strain distribution 4-28

Figure 4-29 Coupling beam effective flexural stiffness ratios. 4-32

Figure 4-30 Coupling beam reinforcement detailing for: (a) prior ACI 318 provisions; and (b) current ACI 318 provisions 4-32

Figure 4-31 Coupling beam reinforcement detailing 4-33

Figure 4-32 Coupling beam load-deformation relations for specimens B1, B2, B3, and B4 4-34

Figure 4-33 Comparison of: (a) effective stiffness; and (b) backbone relations for coupling beam test results 4-34

Figure 4-34 Crack patterns in a coupling beam with an aspect ratio of l_n/h=3.33 at different drift levels 4-36

Figure 4-35 Schematic coupling beam models: (a) moment hinge; and (b) shear-displacement hinge 4-37

Figure 4-36 Rigid plastic rotational springs for moment-hinge model (half-scale test specimens) 4-37

Figure 4-37 Load-deformation relations for moment- and shear-hinge models 4-38

Figure 4-38 Configuration and plan section of tall core wall building system used in parametric studies 4-40

Figure 4-39 Variation in shear force over height in the: (a) north-south direction; and (b) east-west direction, for each case of relative stiffness 4-42

Figure 4-40 Variation in moment over height in the east-west direction, for each case of relative stiffness 4-43

Figure 4-41 Comparison of shear force distribution over height for fiber-hinge and fiber-all models 4-44

Figure 4-42 Comparison of moment distribution over height for fiber-hinge and fiber-all models 4-44

Figure 4-43 Comparison of shear force distribution over height for fiber-hinge and fiber-all models, for each case of relative stiffness 4-45

Figure 4-44 Comparison of moment distribution over height for fiber-hinge and fiber-all models, for each case of relative stiffness. 4-45

Figure 4-45 Distribution of maximum compression and tension strains over height for elements along the north wall of the core. 4-46

Figure 4-46 Distribution of maximum compression and tension strains over height for elements along the east wall of the core 4-47

Figure 4-47 Comparison of shear and moment distributions over height for the 100% Steel and Reduced Steel models 4-48

Figure 4-48 Normalized effective stiffness factors for interior slab-column frames based on Equations 4-10 through 4-12.... 4-51

Figure 4-49 Model of slab-column connection 4-51

Figure 4-50 Unbalanced moment transferred between the slab and column in a torsional connection element..... 4-52

Figure 4-51 ASCE/SEI 41-06 *Supplement No. 1* modeling parameter *a* for reinforced concrete and post-tensioned slab-column connections..... 4-53

Figure 4-52 Floor plan and simplified model of the combined slab-column frame and core wall system..... 4-54

Figure 4-53 Application of effective width model to core wall 4-54

Figure 4-54 Schematic of the slab model 4-55

Figure 4-55 Comparison of story drifts in the north-south and east-west directions for the core wall model and coupled core-slab model 4-56

Figure 4-56 Comparison of column axial stress in the north-south and east-west directions for the core wall model and coupled core-slab model 4-56

Figure 4-57 Slab-to-wall connection details for Specimen 1 (left) and Specimen 2 (right) 4-58

Figure 4-58 Overall test specimen geometry..... 4-58

Figure 4-59 Force-displacement relations for slab-wall connection Specimens 1 and 2 4-59

Figure 4-60 Observed cracking at 2.5% drift in Specimen 1 (left) and Specimen 2 (right) 4-60

Figure A-1 Example of a tall building structural system with a concrete core wall superstructure and below-grade perimeter retaining walls forming a podium A-2

Figure A-2 Construction of a concrete core and below-grade levels of a high-rise building A-3

Figure A-3 Construction of concrete walls for a high-rise apartment building. The structural system has two individual walls, at left, and a concrete core, at right A-4

Figure A-4 Example of a setback in a concrete core wall building in which an additional concrete wall extends above the lower podium, but not the full height of the building A-7

Figure A-5 Example of two towers on a common base A-8

Figure A-6 Desirable nonlinear mechanisms for: (a) cantilever wall; and (b) coupled wall A-10

Figure A-7 Example location of a collector (shown hatched). A-14

Figure A-8 Eccentric collector and reinforcement into, and alongside, a shear wall A-15

Figure A-9 Relative stiffness assumptions associated with diaphragm flexibility models A-16

List of Tables

Table 2-1 Selected Results of Measured Damping in Tall Buildings under Wind-Induced Vibration 2-45

Table 2-2 Measured Damping versus Level of Damage from Shaking Table Tests 2-46

Table 2-3 Comparison of Effective Damping with Inelastic Softening and Period Elongation 2-52

Table 3-1 Modeling Parameters for Various Beam Sizes (non-RBS connections) Based on Regression Equations with Assumed Beam Shear Span L=150 in., L_b/r_y= 50, and Expected Yield Strength, F_y=55 ksi 3-16

Table 3-2 Modeling Parameters for Various Beam Sizes (with RBS connections) Based on Regression Equations with Assumed Beam Shear Span L=150 in., L_b/r_y= 50, and Expected Yield Strength, F_y=55 ksi 3-16

Table 3-3 Empirical Plastic Rotation Values, θ_p and θ_{pc}, for a Representative Column Section 3-37

Table 4-1 New Zealand Standard 3101 Coupling Beam Coefficients 4-31

Table 4-2 Parametric Variation in Stiffness Parameters 4-41

Table A-1 Diaphragm Flexibility and Applicability of Modeling Assumptions A-15

Table A-2 Recommended Stiffness Assumptions for Structural Elements of a Podium and Foundation A-24

Table A-3 Recommended Stiffness Assumptions for Structural Elements of a Tower and Foundation A-24

Chapter 1
Introduction

1.1 Background

Seismic design provisions and construction practice in regions of high seismicity have been based primarily on an understanding of the anticipated behavior of low- to mid-rise construction. In extrapolating design and detailing provisions for use in high-rise construction, structural systems have been limited in height, or not permitted, where combinations of spectral response acceleration parameters, site class, and building occupancy result in Seismic Design Categories D or higher, as defined in ASCE/SEI 7-10 *Minimum Design Loads for Buildings and Other Structures* (ASCE, 2010). Recent trends in high-rise residential construction have resulted in a variety of unusual configurations, innovative structural systems, and high performance materials that challenge current design practice.

Questions have arisen regarding the applicability of prescriptive code provisions to tall building structural systems, and whether or not these provisions can adequately ensure acceptable performance of this class of buildings. Building departments, with active input from peer review committees and advisory groups, have been considering performance-based methods to assess the adequacy of these new designs. Use of alternative performance-based design procedures has led to challenges in the plan check and enforcement process, and use of currently available performance-based analytical methods has led to questions regarding the ability of these methods to reliably predict performance of tall building structural systems.

The seismic design of modern tall buildings, defined as buildings exceeding 160 feet in height, introduces a series of challenges that need to be met through consideration of scientific, engineering, and regulatory issues specific to the modeling, analysis, and acceptance criteria appropriate for these unique structural systems. This report represents a compilation of the latest available information on analytical simulation, system and component behavior, material properties, and recommendations specific to the seismic design of tall building structural systems.

1.2 Pacific Earthquake Engineering Research Center Tall Buildings Initiative

The Pacific Earthquake Engineering Research Center (PEER) has conducted a multi-year collaborative effort, called the Tall Buildings Initiative, to develop performance-based seismic design guidelines for tall buildings. Guidelines resulting from this initiative are intended to promote consistency in design approaches, facilitate design and review, and help ensure that tall building designs meet safety and performance objectives consistent with the intent of current building codes and the expectations of various stakeholder groups.

Major collaborators on the PEER Tall Buildings Initiative include (in alphabetical order):

- Applied Technology Council (ATC),
- California Geological Survey,
- California Governor's Office of Emergency Services
- California Seismic Safety Commission
- The Charles Pankow Foundation,
- Department of Building Inspection, City & County of San Francisco (SFDBI),
- Federal Emergency Management Agency (FEMA),
- Los Angeles Tall Buildings Structural Design Council (LATBSDC),
- Los Angeles Department of Building and Safety (LADBS),
- Building Seismic Safety Council (BSSC) of the National Institute of Building Sciences (NIBS),
- National Science Foundation (NSF),
- Southern California Earthquake Center (SCEC),
- Structural Engineers Association of California (SEAOC), and
- United States Geological Survey (USGS).

The PEER Tall Buildings Initiative includes consideration of performance objectives, ground motion selection and scaling, modeling, acceptance criteria, and soil-foundation-structure interaction issues specific to the design of tall buildings. Guideline development activities were organized around the following tasks:

Task 1 - Establish and Operate the Tall Buildings Project Advisory Committee (T-PAC)

Task 2 - Develop consensus on performance objectives

Task 3 - Assessment of ground motion selection and scaling procedures

Task 4 - Synthetically generated ground motions

Task 5 - Review and validation of synthetically generated ground motions

Task 6 - Guidelines on selection and modification of ground motions for design

Task 7 - Guidelines on modeling and acceptance values

Task 8 - Input ground motions for tall buildings with subterranean levels

Task 9 - Presentations at conferences, workshops, seminars

Task 10 - Development of a design framework and publication of design guidelines

The recommendations on modeling and acceptance criteria included herein represent the outcome of work on Task 7. This report represents one part of the overall process, and is intended to serve as a resource document for the *Seismic Design Guidelines for Tall Buildings*, published as a companion report by PEER (2010).

1.3 Workshop on Tall Building Seismic Design and Analysis Issues

PEER Task 7 was focused on the technical development area of modeling, simulation, and acceptance criteria. A *Workshop on Tall Building Seismic Design and Analysis Issues* was conducted in January 2007, as an integral part of this work. The purpose of this workshop was to identify design and modeling issues of critical importance to various tall building stakeholder groups involved in the design, permitting, and construction of tall buildings, and to establish priorities for issues that should be addressed by the PEER Task 7 work.

The outcome of this workshop is recorded in a companion report, ATC-72 *Proceedings of Workshop on Tall Building Seismic Design and Analysis Issues* (ATC, 2007). This report includes a prioritized list of the most important tall building modeling and acceptance criteria issues needing resolution, based on the opinions of practitioners, regulators, and researchers in attendance.

1.4 Issues in Tall Building Design

Scientific, engineering, and regulatory issues specific to tall building design have been identified as part of the PEER Tall Buildings Initiative. The

following issues form the basis of the major technical development areas addressed by the overall scope of the Tall Buildings Initiative:

- *Building concepts and materials.* Functional requirements for tall residential buildings have led to new building configurations and systems that do not meet the prescriptive definitions and requirements of current building codes. These configurations include more efficient framing systems with reduced redundancy, and high-strength materials or specialized products to help meet the unique challenges posed by these structural systems.
- *Performance objectives and hazard considerations.* High occupancy levels, associated safety considerations, and interest in continued occupancy following an earthquake, have led to a reconsideration of performance objectives and ground shaking hazards. As a minimum, tall buildings must be safe from collapse in rare (low-probability, long-return period) ground shaking demands and significant aftershocks. Serviceability for more frequent events is also considered.
- *Ground motion time histories.* Selection, scaling, and spectral modification of ground motion time histories all have a significant impact on the results of nonlinear response history analysis of tall buildings. Validated seismological methods can be used to generate ground motion time histories that incorporate near-fault rupture directivity effects and basin effects to appropriately represent the duration and long period energy content necessary for design of tall buildings.
- *Modeling, simulation, and acceptance criteria.* Seismic design provisions in current codes and standards are based on design requirements established for low- to mid-rise construction. Because the dynamic and mechanical aspects of response that control the behavior of tall buildings are different, current provisions do not adequately specify appropriate modeling, analysis, and acceptance criteria for very tall structural systems. Criteria that address reliability, safety, capital preservation, re-occupancy, and functionality are needed.
- *Input ground motions for tall buildings with subterranean levels.* Tall building systems are commonly configured with several levels below grade. Interaction between the soil, foundation, and structure can significantly affect the character and intensity of the motion that is input to the superstructure, and this interaction should be considered in defining the input ground motions for tall buildings with subterranean levels.

- *Instrumentation.* Instrumentation in tall buildings would serve multiple purposes, including rapid assessment for re-occupancy following an earthquake, confirmation that building performance has met design expectations, and basic research leading to improved design criteria and analytical methods. Guidance on tall building instrumentation, and appropriate use of this information, is needed.

1.5 Report Organization and Content

This report is a compendium of the latest available research, information, and recommendations on analytical modeling and acceptance criteria for the design and analysis of tall structural systems. It addresses one in a series of issues specific to seismic design of tall buildings, and is intended to serve as a resource document for the companion report, *Seismic Design Guidelines for Tall Buildings* (PEER, 2010).

Chapter 1 provides background information and context for the overall PEER Tall Buildings Initiative.

Chapter 2 provides general guidance on issues related to nonlinear modeling, including selection of component model types, modeling of deterioration, capture of P-Delta effects, consideration of damping, quantification of expected properties, and uncertainty.

Chapter 3 provides recommendations for characterizing nonlinear properties of frame components including steel and reinforced concrete beams, columns, and beam-column joints.

Chapter 4 provides recommendations for characterizing nonlinear properties of reinforced concrete shear walls and slab-column frame systems, simulation of observed experimental behavior, and calibration with experimental results.

Appendix A provides guidance on design and analysis of the podium substructure, and consideration of backstay effects in tall building systems.

A glossary of important terms, references cited, and a list of all project participants are provided at the end of this report.

Chapter 2
General Nonlinear Modeling

This chapter discusses general issues associated with nonlinear modeling of building response. It provides guidance on selection of component model types, modeling of deterioration, capture of P-Delta effects, consideration of damping, quantification of expected properties, and consideration of uncertainty.

2.1 Overview of Modeling Issues for Nonlinear Response History Analysis

Nonlinear response history analysis is the best tool currently available for predicting building response at varying levels of ground motion intensity. Various aspects of nonlinear analysis, such as acceptance criteria, element discretization, and assumptions on modeling of energy dissipation through viscous damping, must be tailored to the specific features of the analytical representation of the system, and the extent to which various behavioral effects will be captured in the nonlinear component models.

Nonlinear response history analysis aims to simulate all significant modes of deformation and deterioration in the structure from the onset of damage to collapse. However, given present analytical capabilities and the practical constraints of design, it is usually not feasible, and perhaps not warranted, to directly simulate all modes of nonlinear behavior in the analysis.

2.1.1 Types of Nonlinear Models

Inelastic structural component models can generally be distinguished by the degree of idealization in the model. A comparison of three idealized model types for simulating the nonlinear response of a reinforced concrete beam-column is shown in Figure 2-1. At one extreme are detailed continuum finite element models that explicitly model the nonlinear behavior of the materials and elements that comprise the component. A continuum model might include finite elements representing the concrete, longitudinal reinforcement, and shear reinforcement, in which associated constitutive models would represent: (1) concrete crushing, cracking, and dilation; (2) steel yielding, buckling, and fracture; and (3) bond transfer between steel and concrete. Continuum models generally do not enforce any predefined behavioral modes and, instead, seek to model the underlying physics of the materials

and elements. They do not require definitions of member stiffness, strength or deformation capacity, as these effects are inherently captured in the model through the material properties.

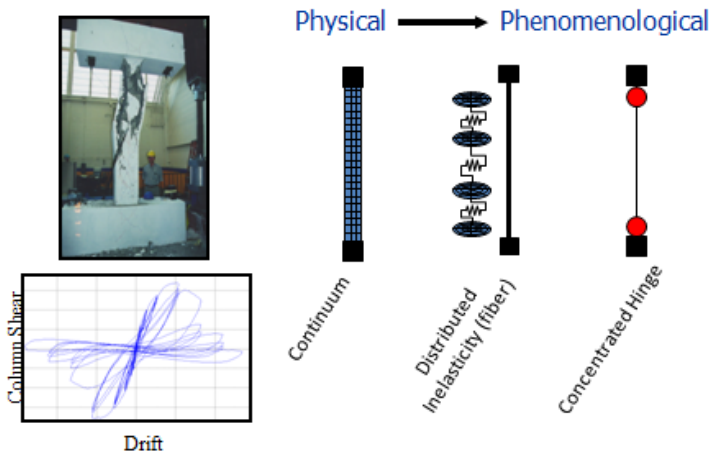

Figure 2-1 Comparison of nonlinear component model types.

At the other extreme are lumped plasticity (concentrated hinge) models, which are defined entirely by the phenomenological description of the overall force-deformation response of the component. For example, a concentrated hinge might represent axial force-moment interaction through a stress resultant (P-M) yield surface with inelastic deformation rules that are associated with observed behavior and hysteretic test data of beam-column components.

In between the two extremes are distributed inelasticity (fiber) models, which capture some aspects of behavior implicitly, such as integration of flexural stresses and strains through the cross section and along the member, and other effects explicitly, such as definition of effective stress-strain response of concrete as a function of confinement. These models typically enforce some behavior assumptions (e.g., plane sections remain plane) in combination with explicit modeling of uniaxial material response.

Continuum and distributed inelasticity models can more accurately capture behaviors such as initiation of concrete cracking and steel yielding, but they can be limited in their ability to capture strength degradation such as reinforcing bar buckling, bond slip, and shear failure. While, continuum models should not require calibration to component response, in practice, they do require some phenomenological calibration to account for behavior that is not captured by the formulation.

Concentrated hinge models, however, can capture strength degradation effects, but in a more empirical manner. Concentrated hinge models are also

more consistent with common limit state checks related to stress resultants (forces) and concentrated deformations (hinge or spring deformations) in current building codes and standards. Since current practice for analytical modeling tends to rely more on lumped plasticity (concentrated hinge) and distributed inelasticity (fiber) component models, recommendations in this report are focused on these model types.

2.1.2 Inelastic Component Attributes

With the objective of accurately simulating structural performance, nonlinear response history analysis models should be based on the expected properties of materials and components, rather than nominal or minimum specified properties that are otherwise used in design. These properties will generally include the stiffness, strength and deformation characteristics of the components. The term "expected" refers to properties that are defined based on median values from a large population of materials and components that are representative of what occurs in the structure. Use of expected structural properties is important for providing an accurate and unbiased measure of the expected response of the overall system. Equally important is the use of expected values throughout the model to accurately characterize the relative force and deformation demands between components of indeterminate structural systems. The goal is to avoid any systematic bias that could result from the use of nominal instead of expected properties for some components, and not others, in a structure.

Figure 2-2 illustrates the key features of an inelastic hinge model for reinforced concrete beam-column elements. The features of this element are generally applicable to other types of elements. This example is taken from a study of reinforced concrete columns by Haselton et al. (2008) making use of a degrading cyclic model developed by Ibarra and Krawinkler (2005). In this example, inelastic response is idealized by a backbone curve (Figure 2-2b) that relates moment to rotation in the concentrated hinges. The definition of the backbone curve and its associated parameters depend on the specific attributes of the nonlinear model used to simulate the hysteretic cyclic response (Figure 2-2c). The following important features of this model will be highlighted in later sections of this report:

- The backbone curve is generally expected to capture both hardening and post-peak softening response. The peak point of the curve is sometimes referred to as the "capping point," and the associated deformation capacity is the "capping deformation." The extent to which cyclic deterioration is modeled in the analysis will determine the extent to which the backbone curve is calibrated to initial or degraded component

response, and how the characteristic points on the curve correspond to component acceptance criteria for the onset of damage and significant deterioration.

- The cyclic model incorporates deterioration in strength and stiffness, which degrades the backbone curve as a function of the damage and energy dissipated in the component. Accordingly, the initial backbone curve (Figure 2-2b) is calibrated to component response that is representative of monotonic loading. When properly calibrated, cyclic deterioration enables the model to capture the deteriorated cyclic response of the component. However, not all models can capture this strength and stiffness deterioration. Where the cyclic deterioration is not accounted for in the model, the backbone curve should be modified by appropriate reductions in the peak strength and inelastic deformation quantities. This sort of reduction is implicitly incorporated into the idealized component response curves of ASCE/SEI 41-06, *Seismic Rehabilitation of Existing Buildings* (ASCE, 2007a) through calibration to a cyclic envelope (skeleton) curve from experimental data that naturally incorporates cyclic strength and stiffness degradation.

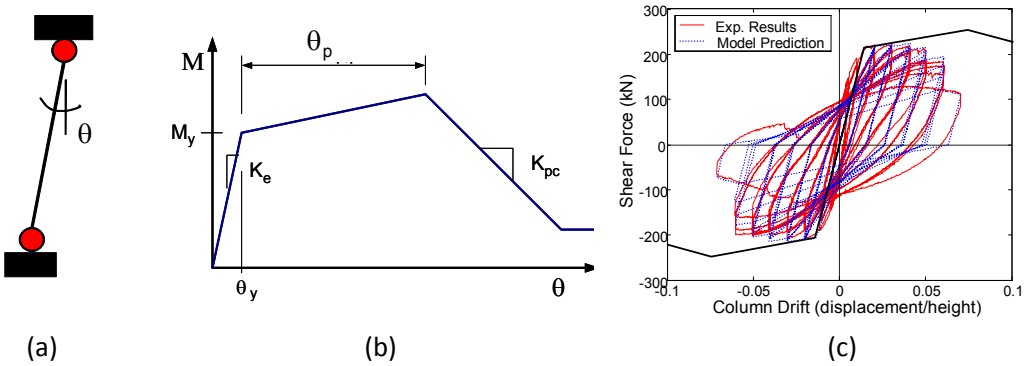

(a) (b) (c)

Figure 2-2 Illustration of modeling components for a reinforced concrete beam-column: (a) inelastic hinge model; (b) initial (monotonic) backbone curve; and (c) cyclic response model (Haselton et al. 2008).

- The backbone curve and cyclic deterioration properties should be calibrated to the median response of the component. In this way, basic modeling results will represent a median (or statistically neutral) assessment of response. Variability in component properties, or system response, can then be applied to establish appropriate margins against exceeding certain limit states, as evaluated through acceptance criteria (forces or deformations) on structural components, or the overall system.

2.1.3 Energy Dissipation and Viscous Damping

Traditionally, viscous damping has been used as a convenient way to idealize energy dissipation in elastic response history analyses. In nonlinear response history analyses, it is important to identify the sources of energy dissipation, and to determine how these effects are represented in the analytical model. For components that are modeled with nonlinear elements, most of the energy dissipation will be modeled explicitly through hysteretic response. However, energy dissipation that is modeled at low deformations may vary significantly with the type of model used. For example, continuum finite element models for reinforced concrete tend to capture damping effects due to concrete cracking that is not captured in concentrated hinge models (Figure 2-1).

In tall buildings, the relative contribution of damping from certain components can be substantially different from values typically assumed in low-rise buildings. For example, measured data show that levels of damping tends to be lower in tall buildings, suggesting that there may be proportionally less damping. Possible reasons for this include soil-foundation-structure interaction or special "isolation" detailing of nonstructural partitions and other components.

2.1.4 Gravity Load Effects in Nonlinear Analysis

Unlike linear analyses, nonlinear analyses are load path dependent, in which the results depend on the combined gravity and lateral load effects. For seismic performance assessment using nonlinear analysis, the gravity load applied in the analysis should be equal to the expected gravity load, which is different from factored gravity loads assumed in standard design checks.

In general, the expected gravity load is equal to the unfactored dead load and some fraction of the design live load. The dead load should include the structure self weight, architectural finishes (partitions, exterior wall, floor and ceiling finishes), and mechanical and electrical services and equipment. The live load should be reduced from the nominal design live load to reflect: (1) the low probability of the nominal live load occurring throughout the building; and (2) the low probability of the nominal live load and earthquake occurring simultaneously. Generally, the first of these two effects can be considered by applying a live load reduction multiplier of 0.4 and the second by applying a load factor of 0.5 (such as is applied to evaluation of other extreme events).

The net result is a load factor of 0.4 x 0.5 = 0.2, which should be applied to the nominal live load. For example, in a residential occupancy with a

nominal live load of 40 psf, an expected live load of 0.2 x 40 psf = 8 psf should be considered in the nonlinear analysis. Accordingly, a general load factor equation for gravity loads applied in nonlinear analysis is:

$$1.0D + 0.2L \tag{2-1}$$

where D is the nominal dead load, and L is the nominal live load. In the case of storage loads, only the 0.5 factor would apply, and the net load factor on storage live loads should be taken as 0.5. Expected gravity loads should also be used as the basis for establishing the seismic mass to be applied in the nonlinear analysis.

Vertical gravity loads acting on the entire structure, not just the seismic-force-resisting elements, should be included in the analysis in order to capture destabilizing P-Delta effects. Nonlinear analysis should include leaning columns with applied gravity loads that rely on the seismic-force-resisting system for lateral stability.

2.1.5 Acceptance Criteria

Performance assessment using nonlinear response history analysis requires a set of criteria defining acceptable performance. *Seismic Design Guidelines for Tall Buildings* (PEER, 2010) discusses two levels of assessment: (1) service level evaluation; and (2) Maximum Considered Earthquake (MCE) level evaluation, which generally involve comparisons of force and deformation demands imposed by the specified earthquake hazard to corresponding limit state capacities of the structural components and systems.

In this report, the emphasis is on defining capacities for two structural limit states: (1) the onset of structural damage requiring repair; and (2) the onset of significant degradation in structural components. The onset of structural damage requiring repair is envisioned as one of several possible metrics for assessing direct economic losses and disruption of building functionality. Initiation of structural damage also corresponds to the point at which elastic analysis may no longer be adequate for assessing performance.

The onset of significant degradation is related to structural integrity and collapse assessment. While component criteria alone are not sufficient for assessing collapse, collapse can be interpreted through limit states ranging from local onset of degradation in individual components, to global instability in the overall structural system, depending on the ability of the analytical model to simulate cyclic strength and stiffness degradation.

Given the inherent uncertainty in prediction of demands and estimation of capacities, it is envisioned that the use of recommended acceptance criteria for these two limit states will be established in a probabilistic framework. To the extent that data are available, criteria are defined in terms of expected (or median) values and dispersion of these values. Specific recommendations regarding parameters associated with these limit states are provided in Chapters 3 and 4.

2.1.5.1 Onset of Structural Damage

In general, it is presumed that the onset of structural damage will typically occur at forces and deformations beyond the yield point, with some permanent deformation associated with yielding of steel and cracking of concrete. For reinforced concrete components, the onset of damage is likely to involve slight spalling, slight yielding of longitudinal reinforcement, and cracking of concrete with residual crack widths of about 0.02 inch (Brown and Lowes, 2007). Repairs associated with this damage state include epoxy injection of cracks and patching of concrete. This degree of damage is generally consistent with the use of effective "elastic" component stiffness coefficients employed in elastic analyses, or the initial elastic region of nonlinear plastic hinge models employed in nonlinear analyses. For steel components, the onset of damage is likely to involve yielding and slight residual local buckling (peak distortion of 0.1 inch) in plastic hinge regions of beams, columns, and braces. For compact sections, local buckling of this magnitude occurs after yielding, and can be accepted without the need to initiate repair actions.

For the prediction of demands prior to the onset of structural damage, it is expected that the use of elastic analysis concepts (i.e., modal superposition based on three-dimensional elastic response spectrum analysis) should be adequate.

2.1.5.2 Onset of Significant Structural Degradation

The onset of significant strength and stiffness degradation in individual structural components is a prerequisite to deterioration in the overall system response, and eventual collapse. While significant component degradation is not always synonymous with collapse, it is an important indicator for when structural collapse should be a concern. The onset of significant component degradation is also an important indicator for gauging the accuracy of the analysis and the extent to which the model can accurately capture the strength and stiffness degradation that occurs at larger deformations.

Response evaluation associated with the onset of significant degradation is intended to provide for adequate safety against collapse. It does not provide a quantifiable margin of safety against collapse, but can demonstrate that collapse does not occur under selected ground motions (i.e., the structure maintains stability, and forces and deformations are within acceptable limits).

The capability to predict the probability of collapse given ground motion intensity exists (Zareian and Krawinkler, 2007), but the process of collapse prediction is complex. It is based on the presumption that the force and deformation characteristics of all important structural components can be modeled over the full range of deformations associated with inelastic behavior leading to collapse. At this time there is not sufficient knowledge to model such behavior, with full confidence, for all components that might be utilized in tall building structural systems.

Since modeling of component behavior beyond the onset of significant degradation is an immature science, it is prudent to set conservative limits on deformations associated with this limit state. These limits will typically be deformation values that are beyond the capping point (δ_c), but prior to the ultimate deformation capacity (δ_u) in the load-deformation response of the component.

While the relationship between local component response and global response varies depending on the structural system, the onset of significant degradation will typically occur at peak story drift ratios on the order of 0.01 to 0.02 for stiff systems (e.g., shear walls and braced frames), and 0.03 to 0.05 for flexible systems (e.g., moment frames).

2.2 Deterioration

Performance assessment can involve evaluating the performance of a system at different seismic hazard levels. Given the need to assess behavior over the full range of response from serviceability limit states to near-collapse limit states, it becomes necessary to develop hysteretic models that incorporate all important phenomena contributing to response as the structure approaches collapse. This section discusses modeling of deterioration at relatively large inelastic deformations.

Collapse implies that the structural system is no longer able to maintain its gravity load-carrying ability in the presence of seismic effects. Local collapse may occur, for instance, if a vertical load-carrying component fails in compression, or if shear transfer is lost between horizontal and vertical components (e.g., punching shear failure between a flat slab and a column). Global collapse occurs if a local failure propagates, or if an individual story

displaces to the point that the second order P-Delta effects exceed first order story shear resistance. Collapse assessment requires hysteretic models capable of representing all important modes of deterioration that are observed in experimental studies.

Modeling of deterioration is equivalent to modeling the consequences of damage on the hysteretic behavior of structural components. Damage occurs due to monotonic loading, and is accentuated by cyclic loading (cumulative damage). It affects all limit states, but becomes a predominant issue as a structure approaches collapse.

Deterioration can occur slowly or rapidly, as illustrated in Figure 2-3, obtained from tests of a steel beam welded to a column flange. In Figure 2-3a, relatively slow deterioration is caused by local instability, whereas in Figure 2-3b rapid deterioration is caused by crack propagation and fracture at the beam-column flange weld.

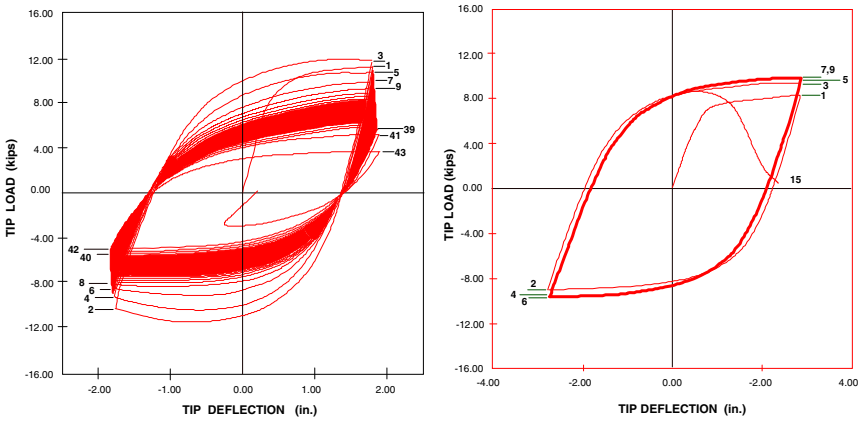

(a) (b)

Figure 2-3 Plots showing different rates of deterioration: (a) slow deterioration; and (b) rapid deterioration (ATC, 1992).

There is large uncertainty associated with prediction of the onset of rapid deterioration, and the consequences are usually a complete loss of strength. In general, rapid deterioration should be avoided in components that are subjected to inelastic deformation demands, unless such deterioration occurs at deformations that are clearly associated with Maximum Considered Earthquake (MCE) intensities, or larger.

In new construction, it is assumed that such failure modes are prevented through proper ductile detailing and separate demand versus capacity safety checks. As such, there should not be a need to explicitly model this type of behavior in the analysis, and modeling for tall buildings is focused on

behavior associated with relatively slow deterioration of the type illustrated in Figure 2-3a. Nevertheless, an analysis should include verification that demands occurring in the model do not exceed limits associated with rapid deterioration in the components.

2.2.1 Modes of Deterioration

The need for analytical models that incorporate deterioration is evident in Figure 2-4, which shows a monotonic load-displacement response and a superimposed quasi-static cyclic response of identical steel beams, based on data from Tremblay et al. (1997). The monotonic test result shows that strength is "capped" and is followed by a negative tangent stiffness. Thus, beyond a certain deformation there is strength deterioration evident under monotonic loading.

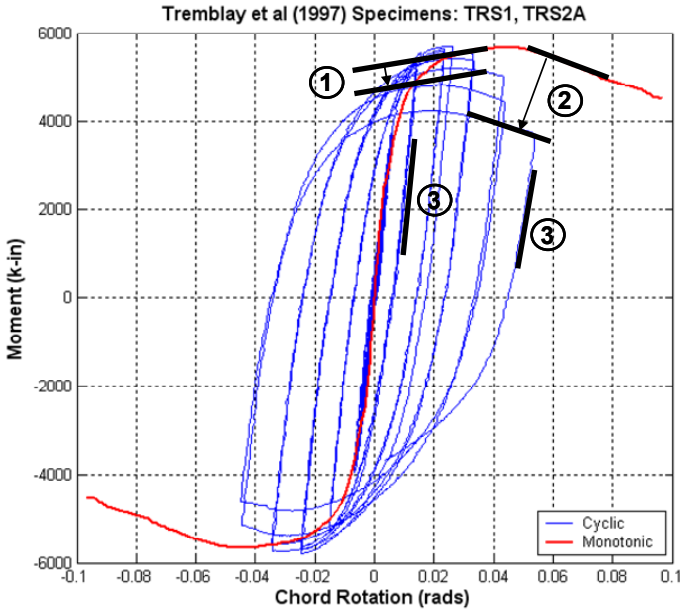

Figure 2-4 Monotonic and cyclic experimental response of a steel beam (data from Tremblay et al., 1997).

Cyclic loading causes additional modes of deterioration that may be classified as follows (Ibarra et al., 2005):

- *Basic strength deterioration.* Strength deteriorates with the number and amplitude of cycles, even if the displacement associated with the strength cap has not been reached (Mode 1 in Figure 2-4). This can be represented by a translation (and possibly rotation) of the pre-capping strength bound towards the origin (see also Figure 2-12a).
- *Post-capping strength deterioration.* Strength deteriorates further when a negative tangent stiffness is attained (Mode 2 in Figure 2-4). This can

be represented by a translation (and possibly rotation) of the post-capping strength bound towards the origin (see also Figure 2-12b).

- *Unloading stiffness deterioration.* Unloading stiffness deteriorates with the number and amplitude of cycles (Mode 3 in Figure 2-4). This can be represented by a rotation of the unloading slope (see also Figure 2-12c).
- *Accelerated reloading stiffness deterioration.* For a given deformation amplitude, the second cycle indicates a smaller peak strength than the first cycle; however, the resistance increases and the strength envelope is attained if the amplitude of the second cycle is increased (this mode is not evident in Figure 2-4, but is observed, for instance, in reinforced concrete beams subjected to a high shear force). This can be represented by movement of the point at which the strength envelope is reached away from the origin (see Figure 2-12d). If the strength envelope is attained upon increasing the deformation amplitude in subsequent cycles, then the deterioration is not strength deterioration, it is accelerated reloading stiffness deterioration.

The first three modes of cyclic deterioration are observed in the cyclic response of all structural components. The fourth mode (accelerated reloading stiffness deterioration) is not discernible in components with behavior that is controlled by flexure, and is represented by "fat" hysteresis loops (Figure 2-5).

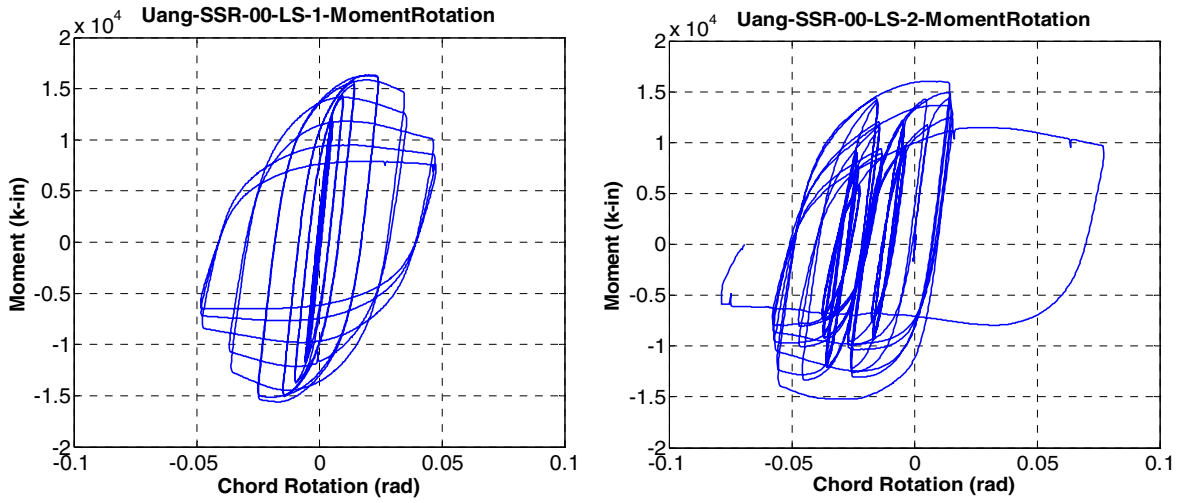

(a) (b)

Figure 2-5 Hysteretic response of identical steel beam specimens under different loading histories (Uang et al., 2000).

For the case illustrated in Figure 2-5a, it is also observed that the hysteresis loops stabilize at large inelastic cycles, which indicates that there is a residual

strength that will be maintained until a "final" failure occurs. In steel components, for example, this usually means ductile tearing at locations of severe local buckling.

The consequence of cyclic deterioration is a lack of stability in the load-deformation response of a structural component. Also, the point at which maximum strength is attained moves continuously as a function of the loading history. In most practical cases, this point moves towards the origin under cyclic loading (i.e., the maximum strength that is attained is smaller, and in some cases much smaller, than the maximum strength associated with monotonic loading). This is an important issue when assessing the deformation capacity of structural components, which is often predicted from concepts based on monotonic loading (see Section 2.2.4).

In Figure 2-6a, the stable drift capacity of the column appears to be at least 8%, but in Figure 2-6b cyclic deterioration appears to set in around 4% drift. The stable monotonic drift capacity is quite possibly larger than 8% because the load was reversed at 8% even though no decrease in strength was evident.

In Figure 2-6b, it was arbitrarily decided to increment the amplitude in each cycle by a small amount. This leads to apparent strength deterioration at drifts larger than 4%, but much of this deterioration is accelerated reloading stiffness deterioration rather than strength deterioration. Thus, more elaborate modeling is needed in order to identify important behavior aspects associated with deterioration of these components.

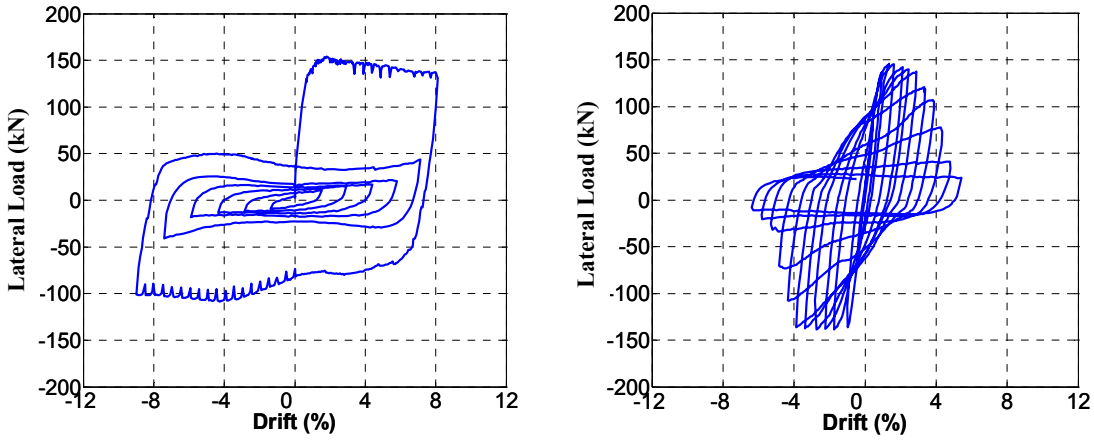

(a) (b)

Figure 2-6 Hysteretic response of identical reinforced concrete column specimens under different loading histories (Kawashima, 2007).

2.2.2 Consequences of Deterioration on Structural Response

The importance of deterioration on the dynamic response of structures depends on many variables, including the intensity and frequency characteristics of the ground motion, the type of structural system, the level of deformation, the importance of P-Delta effects, and the deterioration properties of important structural elements. The following is an illustration for a relatively ductile low-rise moment-resisting frame structure.

Figure 2-7 shows two incremental dynamic analysis (IDA) curves showing spectral acceleration at the first mode period of the structure versus computed maximum story drift, for one specific ground motion and one specific frame structure. One curve was obtained from analysis with non-deteriorating structural component models (i.e., the hysteretic response is assumed to be bilinear and no monotonic or cyclic deterioration modes are considered). Since P-Delta effects are not large enough to overcome the strain-hardening effects inherent in the component models, the IDA curve continues to rise to large drifts of more than 20%, until the analysis was stopped.

The second curve was obtained from analysis with deteriorating component models. At relatively small drifts, the responses are identical, but the curves diverge once cumulative damage sets in. The slope of the second IDA curve decreases rapidly between $S_a(T_1)$ of 2.5g and 2.8g, where it approaches zero. At this point, a small increase in intensity causes a large increase in story drift, which indicates dynamic instability in the analytical model. Presuming that the model is accurate, this implies sidesway collapse of a single story or a series of stories in the structural system. The ground motion intensity level associated with dynamic instability can be denoted as the collapse capacity of the specific structure, given the specific ground motion.

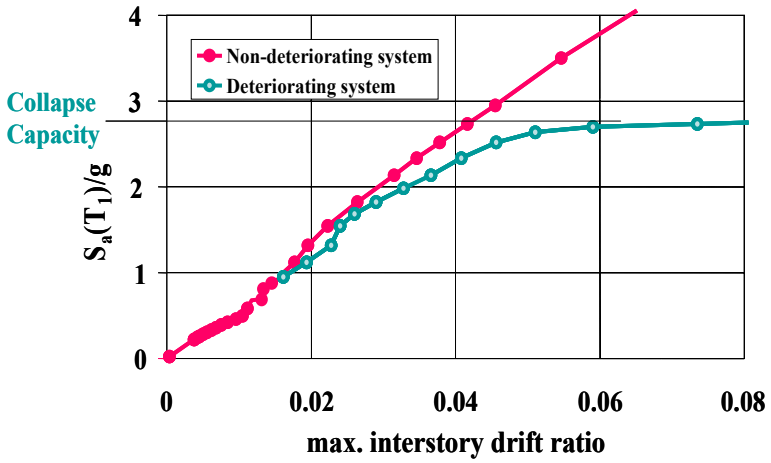

Figure 2-7 Incremental dynamic analysis (IDA) curves for a moment-resisting frame example using non-deteriorating and deteriorating component models.

Figure 2-7 demonstrates that incorporation of deterioration becomes critical when a structure approaches collapse. Performing this type of analysis using a series of representative ground motions provides collapse fragility curves, which, when combined with measures of modeling uncertainties, can be utilized to evaluate the probability of collapse (or collapse margin) for the structure (Ibarra et al., 2002; Ibarra and Krawinkler, 2005; Zareian, 2006; Haselton and Deierlein, 2007; Zareian and Krawinkler, 2007; FEMA, 2009b). These studies found that the deformation associated with the capping point and the post-capping tangent stiffness are the primary parameters on which collapse capacity depends, followed closely by the rate of cyclic deterioration.

2.2.3 Sources of Deterioration

Structural analysis software does not recognize deterioration unless it is built explicitly into the programming, and deterioration parameters for strength and stiffness of structural components need to be incorporated explicitly in component models. Usually, it is left up to the user to proactively build deterioration into the model, which implies recognition of phenomena that may contribute to deterioration. Contributors to deterioration in structural components are listed below.

In structural steel components, the following phenomena can cause deterioration in plastic hinge regions of beams and columns, and the post-buckling response of braces:

- Local buckling of flanges or web
- Lateral-torsional buckling
- Ductile tearing

The following additional phenomena can cause deterioration in the behavior of connections, which either needs to be incorporated in the component response, or requires separate connection modeling:

- Crack propagation and fracture
- Bolt slippage, yielding, and bearing
- Block shear
- Prying action
- Local plate bending
- Plate compression buckling

- Shear buckling of plates (e.g., in eccentrically braced frame links or joint panel zones)

In reinforced concrete components, the following phenomena can cause deterioration:

- Concrete tensile cracking
- Concrete crushing and spalling
- Rebar buckling and fracture
- Bond slip
- Prying (dowel) action
- Reduction in confinement due to yielding and fracture of confinement reinforcement
- Loss of anchorage of transverse reinforcement
- Reduction in aggregate interlock
- Diagonal tension and horizontal shear cracking
- Sliding at cracked interfaces and construction joints
- Insufficient crack closure

Modeling of deterioration is a complex issue. In most practical cases reliance must be placed on experimental evidence, and simplifications must be made. It is a matter of engineering judgment to decide when a source of deterioration is a sufficiently important contributor to response, and must be incorporated in the analytical model.

2.2.4 Modeling of Deterioration

Accurate modeling of deterioration involves incorporating all relevant material and geometric properties that contribute to strength and stiffness degradation of structural components under random loading histories. Due to uncertainties inherent in material properties, detailing, design decisions, construction techniques, and human error, even the use of micro-mechanical models may not achieve the goal of an accurate deterioration model. At the same time, accurate answers might not be needed considering the significant uncertainties inherent in ground motion hazard characterization. On the other hand, neglecting deterioration will make it impossible to assess performance near collapse, or at other low-probability and high-consequence limit states associated with extreme (e.g., MCE) level ground motion intensities.

The use of more refined models, such as finite element or fiber models, must be associated with physical concepts that give consideration to all important sources of deterioration, and incorporate cyclic deterioration phenomena. There are a number of questions that need to be addressed in the use of cross-section based models (e.g., fiber models and moment-curvature models), such as:

- How will bond slip be incorporated in reinforced concrete?
- How do fiber elements account for phenomena that cannot be described adequately by cross-sectional properties, such as shear, bar buckling, dowel action, and spalling in reinforced concrete, or connection behavior, local instabilities, and post-buckling behavior in steel?
- How is cyclic deterioration represented in the model?

The following discussion focuses on global component models, but is not intended to discourage the use of more refined models. Sometimes cross-section or "region" models, such as the wall element in the commercial analysis program, Perform 3D, *Nonlinear Analysis and Performance Assessment for 3D Structures* (Computers and Structures, Incorporated), are the only viable options, but in such cases it is recommended that the concepts outlined below be used to account for deterioration phenomena unless all important modes of deterioration are built into the model.

2.2.4.1 Basic Concepts of Modeling Hysteretic Behavior Including Deterioration

The following concepts are specifically described for rotational springs that represent plastic hinge regions. They can be applied equally well to translational springs that represent shear force-deformation modes, and can be adapted to other localized or component or element force-deformation modes built into a structural analysis program.

Modeling of cyclic response including deterioration can be based on the following three concepts:

- A backbone curve, which is a reference force-deformation relationship that defines the bounds within which the hysteretic response of the component is confined,
- A set of rules that define the basic characteristics of the hysteretic behavior between the bounds defined by the backbone curve, and
- A set of rules that define various modes of deterioration with respect to the backbone curve.

There are many models utilizing these concepts available in the literature. One such model is the Ibarra-Krawinkler model (Ibarra et al., 2005; Ibarra and Krawinkler, 2005; Zareian, 2006), which is used to illustrate these concepts. For many realistic cases of steel, reinforced concrete, and wood components, this deterioration model provides satisfactory matching of experimental results with analytical calibrations. It has been used in numerous collapse assessment examples, such as those documented in FEMA P-695, *Quantification of Building Seismic Performance Factors* (FEMA, 2009b). Like any other model, it has its limitations, and should not be applied unless it fits the phenomena that are represented in the analysis. The concepts summarized here are general, and the specific model is used only for illustration.

Backbone Curve

The backbone curve is a reference force-deformation relationship that defines the bounds within which the hysteretic response of the component is confined. If no cyclic deterioration has occurred, the backbone curve is close to the monotonic loading curve, and is referred to as the *initial backbone curve*. Once cyclic deterioration sets in, the branches of the backbone curve move toward the origin and are continuously updated (they can translate and/or rotate). The instantaneously updated backbone curve is referred to as a *cyclic backbone curve,* but it must be understood that a cyclic backbone curve is dependent on the loading history and changes continuously after each excursion that causes damage in the component.

The initial backbone curve is close to, but is not necessarily identical to, the monotonic loading curve. It usually contains compromises that are made in order to simplify response description. For instance, it might account for an average effect of cyclic hardening (which is likely small for reinforced concrete components, but can be significant for steel components). In concept, the differences between the initial backbone curve and the monotonic loading curve are small, and the terms initial and monotonic are interchangeable for practical purposes.

A typical initial (monotonic) backbone curve and necessary definitions are illustrated in Figure 2-8. The quantities F and δ are generic force and deformation quantities. For flexural plastic hinge regions $F = M$ (moment) and $\delta = \theta$ (rotation). Refinements, such as more accurate multi-linear descriptions, can be implemented as deemed necessary. It is important, however, to note that the initial backbone curve incorporates monotonic strength deterioration for deformations exceeding the *capping point* (point of maximum strength under monotonic loading).

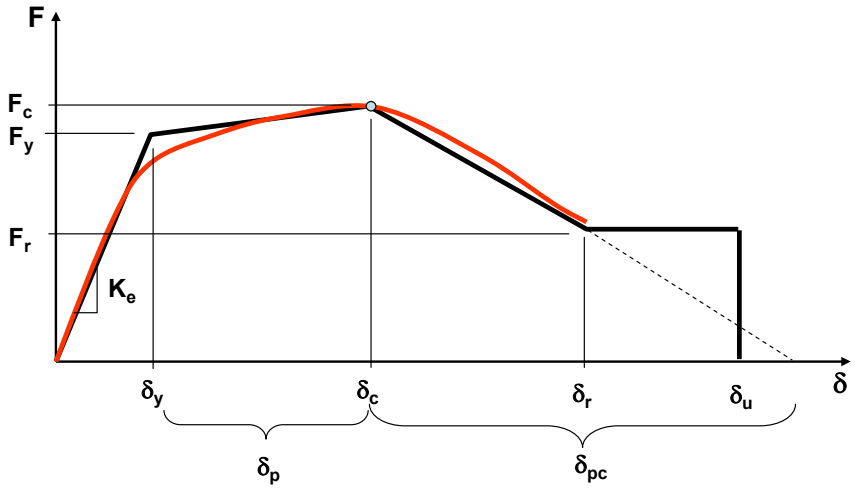

- Effective yield strength and deformation (F_y and δ_y)
- Effective elastic stiffness, $K_e = F_y/\delta_y$
- Strength cap and associated deformation for monotonic loading (F_c and δ_c)
- Pre-capping plastic deformation for monotonic loading, δ_p
- Effective post-yield tangent stiffness, $K_p = (F_c\text{-}F_y)/\delta_p$
- Post-capping deformation range, δ_{pc}
- Effective post-capping tangent stiffness, $K_{pc} = F_c/\delta_{pc}$
- Residual strength, $F_r = \kappa F_y$
- Ultimate deformation, δ_u

Figure 2-8 Parameters of the initial (monotonic) backbone curve of the Ibarra-Krawinkler model.

The properties of the initial (monotonic) backbone curve in the positive and negative directions can be different, as necessitated, for instance, by the presence of a slab on a steel beam or unequal reinforcement in a reinforced concrete beam. There might also be additional considerations that affect the construction of a backbone curve. If the initial stiffness is very different from the effective elastic stiffness, response can be affected, even close to collapse, and initial stiffness should become part of the modeling effort.

Residual strength (F_r in Figure 2-8) may or may not be present. Residual strength is present in most steel components, unless fracture occurs before the component strength stabilizes at a residual value. The ultimate deformation capacity usually is associated with a sudden, catastrophic failure mode. In steel components, this can be ductile tearing associated with severe local buckling, or fracture at weldments. It is possible that the ultimate deformation capacity, δ_u, is smaller than the deformation at which a residual strength is reached, δ_r.

As defined here, the initial backbone curve presumes that cyclic deterioration will be incorporated in the analytical component model. If this is not

feasible, (i.e., cyclic deterioration is ignored), then the initial backbone curve must be modified in order to account for the fact that cyclic loading usually leads to a decrease in the capping deformation (at which the tangent stiffness becomes negative) and the ultimate deformation (at which the component loses most or all of its strength).

Basic Hysteretic Modeling

Rules defining cyclic behavior without special consideration of cyclic deterioration should be adapted to the mode of deformation that dominates the behavior of the component. When appropriate, basic hysteresis rules can follow well established concepts such as those of linearized bilinear, peak-oriented, or pinching hysteretic behavior (Figure 2-9). This does not preclude the utilization of more refined hysteresis models such as multi-linear models or more general curvilinear models such as the Bouc-Wen model (Bouc, 1967; Baber and Wen, 1981), modified Bouc-Wen (Foliente, 1995), Ramberg-Osgood (Carr, 2003), or the hysteresis model in Perform 3D. Results from a modified Bouc-Wen model are shown in Figure 2-10, and the characteristics of a Ramberg-Osgood model are illustrated in Figure 2-11.

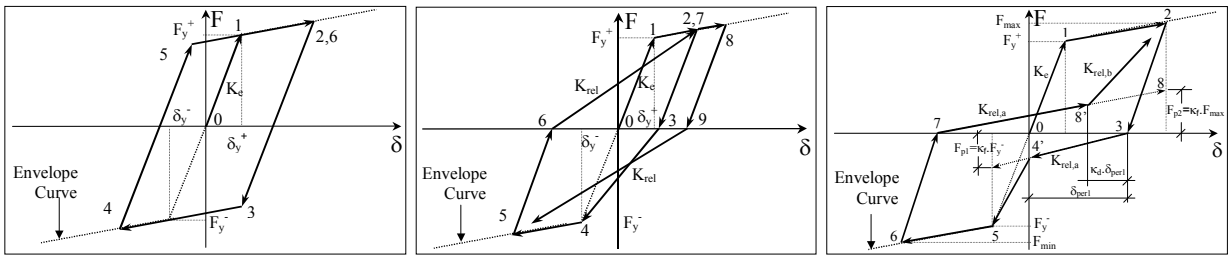

Figure 2-9 Basic options for stable hysteresis characteristics: (a) bilinear; (b) peak oriented; and (c) pinching (Medina and Krawinkler, 2003).

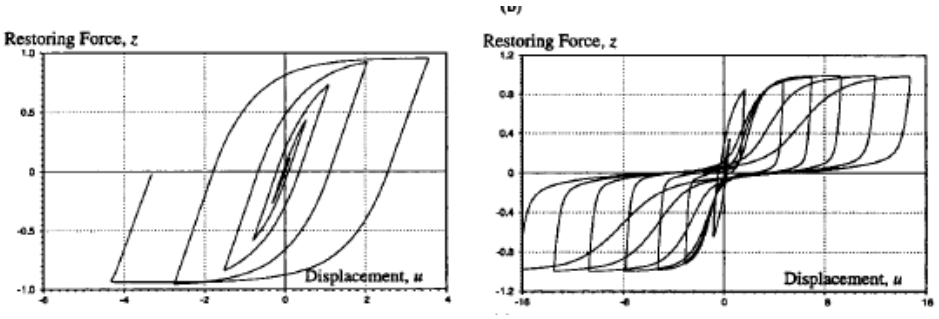

Figure 2-10 Simulations obtained with a modified Bouc-Wen model (Foliente, 1995).

Most seismic demand studies employ hysteresis models, which have hysteresis rules that either ignore stiffness deterioration (bilinear model) or

account for stiffness deterioration by modifying the path in which the reloading branch approaches the backbone curve (peak-oriented or pinching models). In 1970, Takeda developed a model with a trilinear backbone curve that degrades the unloading stiffness based on the maximum displacement of the system (Takeda et al., 1970). This model was developed specifically for reinforced concrete components, and the backbone curve is trilinear because it includes a segment for uncracked concrete.

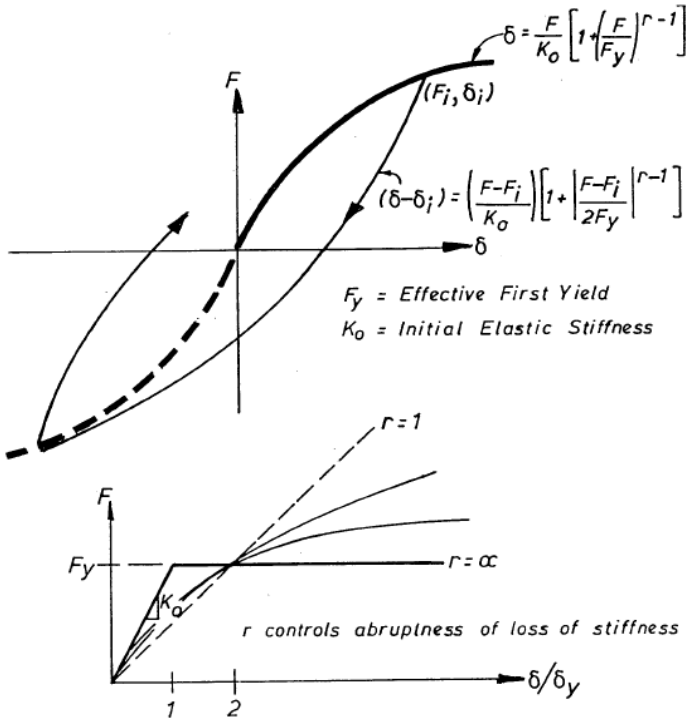

Figure 2-11 Ramberg-Osgood Model (Carr, 2003).

Rules Defining Cyclic Deterioration

In many models, cyclic deterioration is based on the hysteretic energy dissipated when the component is subjected to cyclic loading. In the Ibarra-Krawinkler model, it is postulated that every component possesses an inherent reference hysteretic energy dissipation capacity, regardless of the loading history applied to the component (Ibarra et al., 2005). Cyclic deterioration in excursion i is defined by the parameter β_i, which is given by Equation 2-2.

$$\beta_i = \left(\frac{E_i}{E_t - \sum_{j=1}^{i} E_j} \right)^c \tag{2-2}$$

where:

β_i = parameter defining the deterioration in excursion i

E_i = hysteretic energy dissipated in excursion i

E_t = reference hysteretic energy dissipation capacity, expressed as a multiple of $F_y\delta_p$, i.e., $E_t = \lambda F_y\delta_p$ (for bending it is convenient to use $E_t = \Lambda M_y$, with $\Lambda = \lambda\theta_p$ denoting the reference cumulative plastic rotation capacity)

ΣE_j = hysteretic energy dissipated in all previous excursions

c = exponent defining the rate of deterioration (at this time all calibrations are based on a value of c of 1.0)

Applications of this energy-based deterioration parameter to the four modes of deterioration listed in Section 2.2.1 are presented in Figure 2-12 for a peak-oriented model.

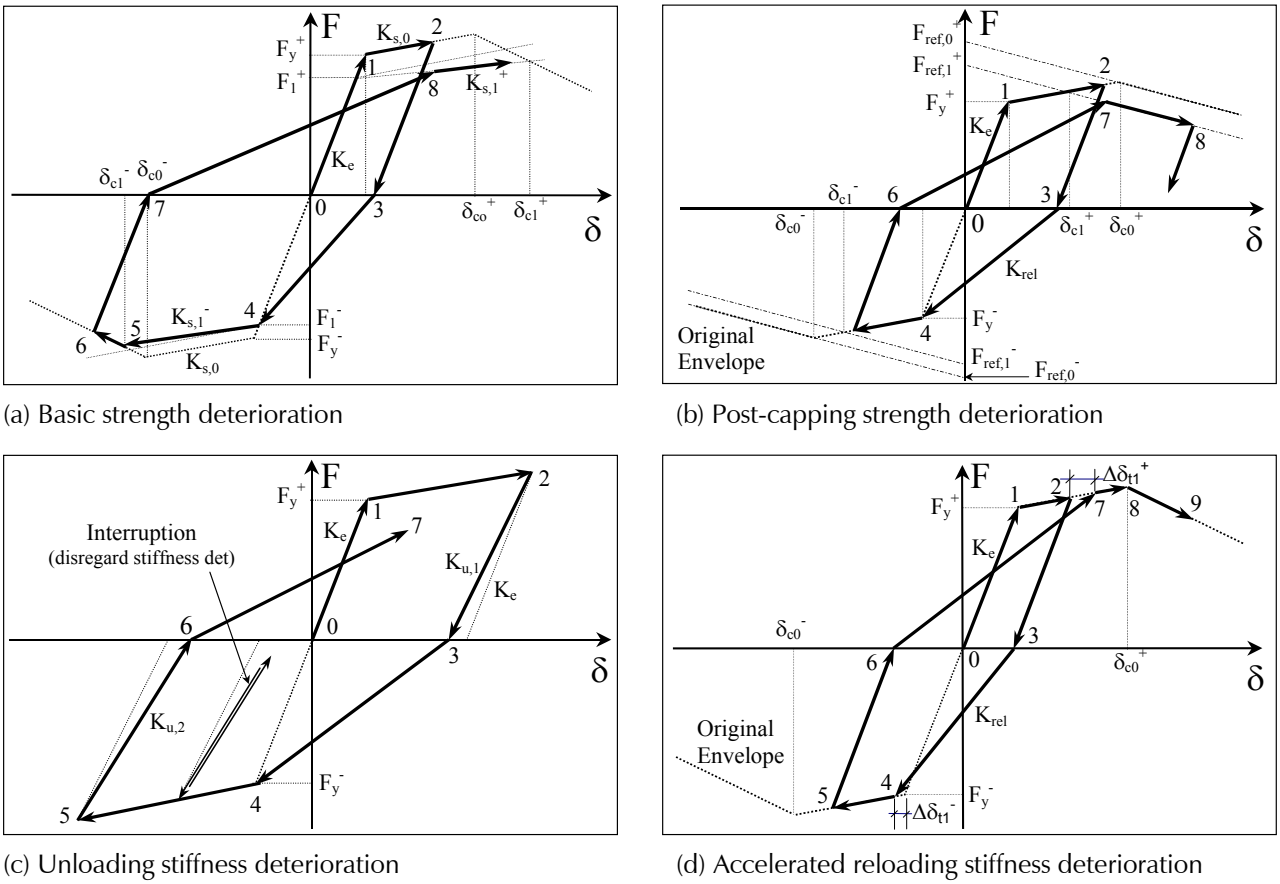

(a) Basic strength deterioration

(b) Post-capping strength deterioration

(c) Unloading stiffness deterioration

(d) Accelerated reloading stiffness deterioration

Figure 2-12 Individual deterioration modes illustrated for a peak-oriented model (Ibarra and Krawinkler, 2005).

The Ibarra-Krawinkler model was tested on about 700 cyclic load-deformation histories obtained from experiments on steel, reinforced

concrete, and wood components. Adequate simulations were obtained in most cases by tuning the model parameters to the experimental data. Examples of calibrations are presented in Figure 2-13. Clear patterns have been observed from these calibrations, which form part of the quantitative information presented in Chapter 3.

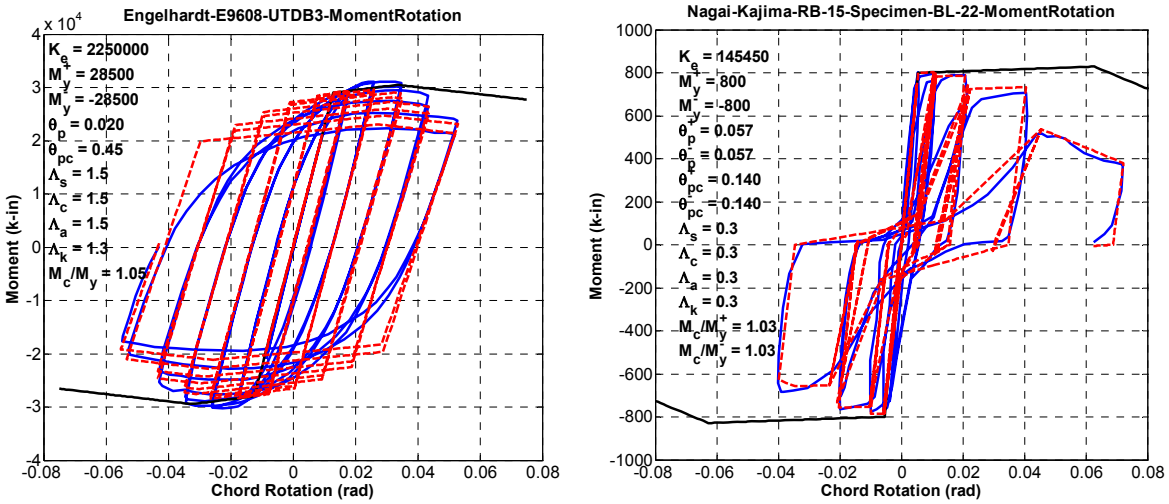

(a) (b)

Figure 2-13 Ibarra-Krawinkler model calibration examples: (a) steel beam; and (b) reinforced concrete beam.

The need to simulate structural response far into the inelastic range has led to the development of other versatile models, such as the smooth hysteretic degrading model developed by Sivaselvan and Reinhorn (2000), which includes rules for stiffness and strength deterioration as well as pinching. An example of a simulation using the Sivaselvan-Reinhorn model is shown in Figure 2-14.

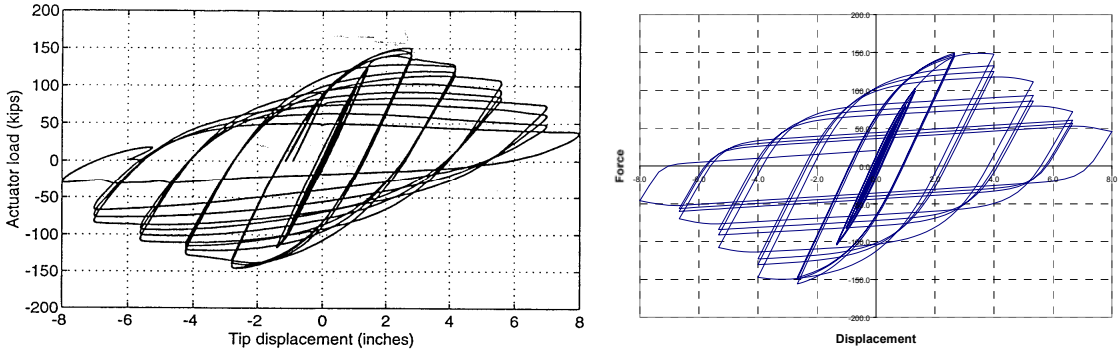

(a) (b)

Figure 2-14 Example of a simulation using the Sivalsevan-Reinhorn model showing: (a) experimental results; and (b) calibrated simulation (SAC, 1999b).

The model developed by Song and Pincheira (2000) is capable of representing cyclic strength and stiffness deterioration based on dissipated hysteretic energy. It is essentially a peak-oriented model that considers pinching. The backbone curve includes a post-capping negative tangent stiffness and a residual strength branch, but basic and post-capping strength deterioration is not incorporated (Figure 2-15).

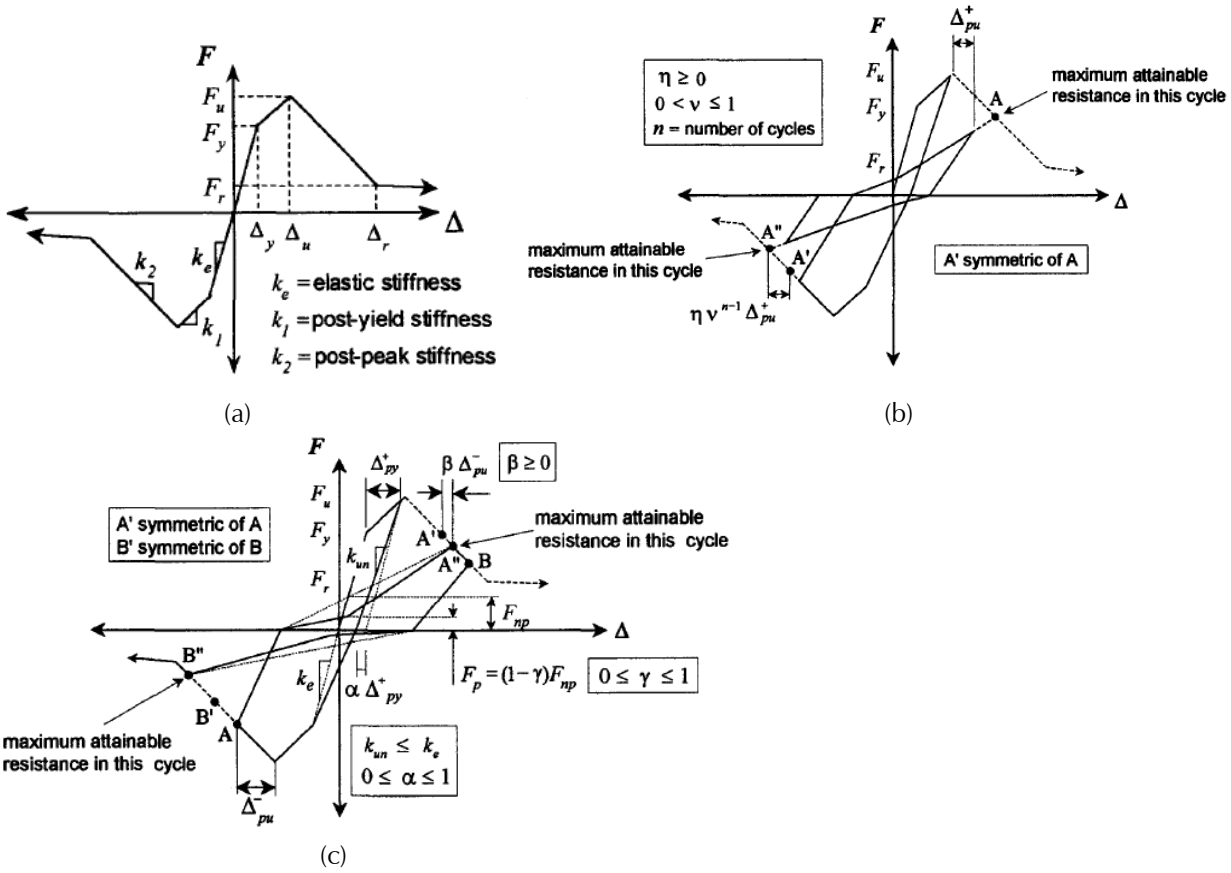

Figure 2-15 Song-Pincheira model: (a) backbone curve; (b) hysteresis rules for cycles of increasing deflection amplitude; (c) hysteresis rules for small amplitude or internal cycles (Song and Pincheira, 2000).

2.2.4.2 Backbone Curve versus Cyclic Envelope (Skeleton) Curve

The initial backbone curve can incorporate approximations in strength and stiffness to accommodate simplicity and account for phenomena that are not included in the deterioration model, such as average cyclic hardening. There is some judgment involved in its quantification, but the three basic approaches for obtaining initial backbone curve are: (1) refined analytical modeling (a formidable task because modeling needs to account for post-capping behavior); (2) a monotonic test; or (3) back-figuring from a cyclic test. The best approach is likely a combination of the three.

When information for the initial backbone curve is derived from cyclic test data, it is important to acknowledge the differences between an initial backbone curve obtained from monotonic tests and the cyclic envelope (skeleton) curve obtained from cyclic load tests. As defined here, the *cyclic envelope (skeleton) curve* is the curve formed by connecting the peak points in the first loading cycle under increasing deformations. Figure 2-16 shows results from two test series in which cyclic tests as well as a monotonic test were performed. The cyclic envelope (skeleton) curve is shown in bold.

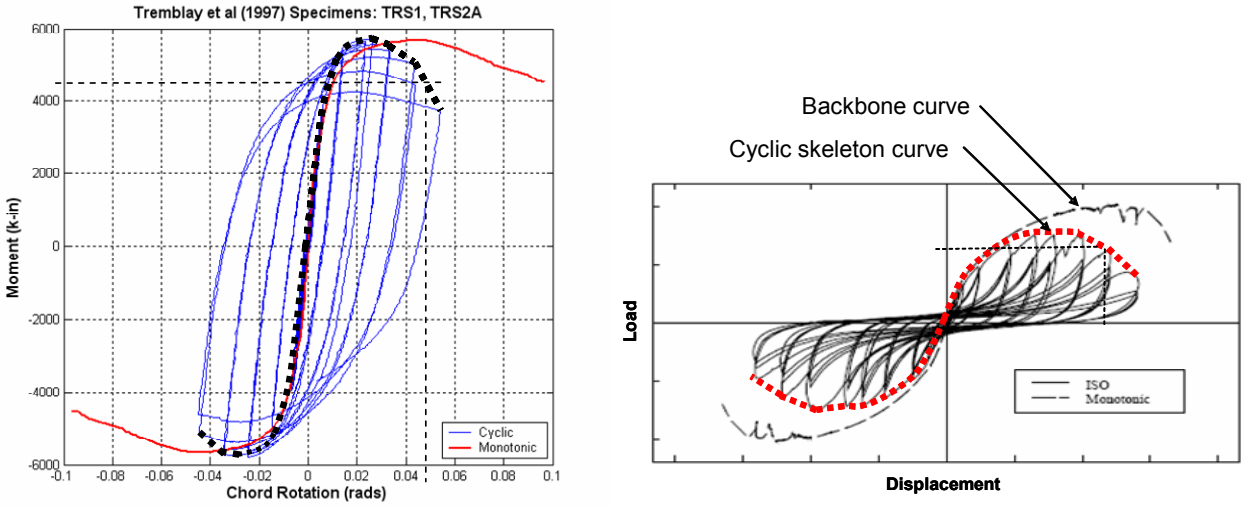

(a) (b)

Figure 2-16 Monotonic and cyclic responses of identical specimens, and skeleton curve fit to cyclic response for: (a) steel beam (Tremblay et al., 1997); and (b) plywood shear wall panel (Gatto and Uang, 2002).

The following general observations can be made:

- Except at small deformations, the cyclic envelope (skeleton) curve falls clearly below the monotonic loading curve.
- At relatively small deformations, the cyclic envelope curve exceeds the monotonic loading curve (Figure 2-16a) because the cyclic hardening effect exceeds the deterioration effect. This can be accounted for by assigning an effective yield strength to the initial backbone curve that is somewhat larger than the monotonic yield strength.
- The cyclic envelope curve is loading history dependent. The choice of amplitude in each cycle is up to the experimentalist, and affects the location of the peak in each cycle. If any one of the intermediate cycles had been executed with a larger amplitude, then the cyclic envelope curve would be different. Thus, an initial backbone curve is nearly unique, while a cyclic envelope curve is not.

- Dependence on loading history makes a cyclic envelope (skeleton) curve an ambiguous measure of cyclic performance, unless the executed loading history is close to what the component experiences in the response history analysis. In general, the cyclic skeleton curve does not vary by a large amount, provided it is obtained from a cyclic test that follows generally acceptable principles of symmetric cyclic loading histories.
- An initial backbone, when used as a stable (unchanging) boundary surface for cyclic loading, is also inappropriate because it ignores the effect of cyclic deterioration.

2.2.5 Analytical Modeling Options

To properly account for cyclic deterioration, four options for analytical modeling of component behavior are listed below. Figure 2-17 illustrates these four options for a typical experimental cyclic loading history and a peak-oriented hysteresis model.

- *Option 1 – explicit incorporation of cyclic deterioration in analytical model*. Cyclic deterioration is explicitly incorporated in the analytical model using the initial backbone curve as a reference boundary surface that moves "inward" (towards the origin) as a function of the loading history (see Figure 2-17a).
- *Option 2 – use of cyclic envelope (skeleton) curve as a modified initial backbone curve; no cyclic deterioration of the backbone curve included in analytical model*. If the cyclic envelope (skeleton) curve is known (e.g., from a cyclic test that follows a generally accepted loading protocol) then it is acceptable to use this curve as the modified backbone curve for analytical modeling, and to ignore additional cyclic deterioration (see Figure 2-17b). The bounds established by the cyclic envelope (skeleton) curve must not be exceeded in the analysis (i.e., the ultimate deformation, δ_u, should be limited to the maximum deformation recorded in the cyclic test). When using this approximation, the negative stiffness (deformation or strain softening) portion of the cyclic envelope curve must be included as part of the modified backbone curve in the analytical model.
- *Option 3 – use of factors for modification of an initial backbone curve; no cyclic deterioration included in analytical model*. If only the initial (monotonic) backbone curve is known, and cyclic deterioration is not incorporated in the analytical model (i.e., the initial backbone curve remains a non-moving boundary for cyclic loading), then the shape of the backbone curve must be modified to account for cyclic deterioration

effects in an approximate manner (see Figure 2-17c). Numerical values of the modification factors might depend on the material and configuration of the structural component. Based on an evaluation of database information for reinforced concrete and steel structural components (Haselton and Deierlein, 2007; Lignos and Krawinkler, 2007; Lignos, 2008) it is clear that such modification factors should be applied even though there is considerable variability in the values of these factors. Until more accurate component-specific data become available, the following values for the parameters of a modified backbone curve are recommended:

- Capping strength F_c': taken as 0.9 times the initial backbone curve value F_c, but not less than F_y
- Pre-capping plastic deformation δ_p': taken as 0.7 times the initial backbone curve value δ_p
- Post-capping deformation range δ_{pc}': taken as 0.5 times the initial backbone curve value δ_{pc}
- Residual strength F_r': taken as 0.7 times the initial backbone curve value F_r
- Ultimate deformation δ_u': taken as 1.5 times δ_c of the initial backbone curve

Note that Option 2 and Option 3 are similar in concept, except that in Option 2, the cyclic skeleton curve is based on test data, while in Option 3 it is based on factors applied to the initial backbone curve.

- *Option 4 – no strength deterioration in analytical model*. If the post-capping (negative tangent stiffness) portion of a modified backbone curve is not incorporated in the analytical model (i.e., a non-deteriorating model is employed), then the ultimate deformation of a component should be limited to the deformation associated with 80% of the capping strength on the descending branch of the modified backbone curve, as obtained using Option 2 or Option 3. No credit should be given for undefined strength characteristics beyond this deformation limit in the analysis (see Figure 2-17d).

Of the options presented, Option 1 is believed to be the most realistic, but also the most complex to implement. Options 2 and 3 are compromises in which the initial backbone curve is modified to account for cyclic deterioration implicitly. Also, post-capping behavior is considered explicitly while cyclic deterioration is considered implicitly. In Option 4, no deterioration is considered, but a strict deformation limit is established

beyond which no reliance can be placed in the modeling of component behavior. At this point, it is assumed that the resistance drops to zero. The choice of the most appropriate component modeling option, and of the basic hysteresis model used to represent the cyclic response of structural components, is a matter of engineering judgment, and should be included as part of the documentation for the analysis.

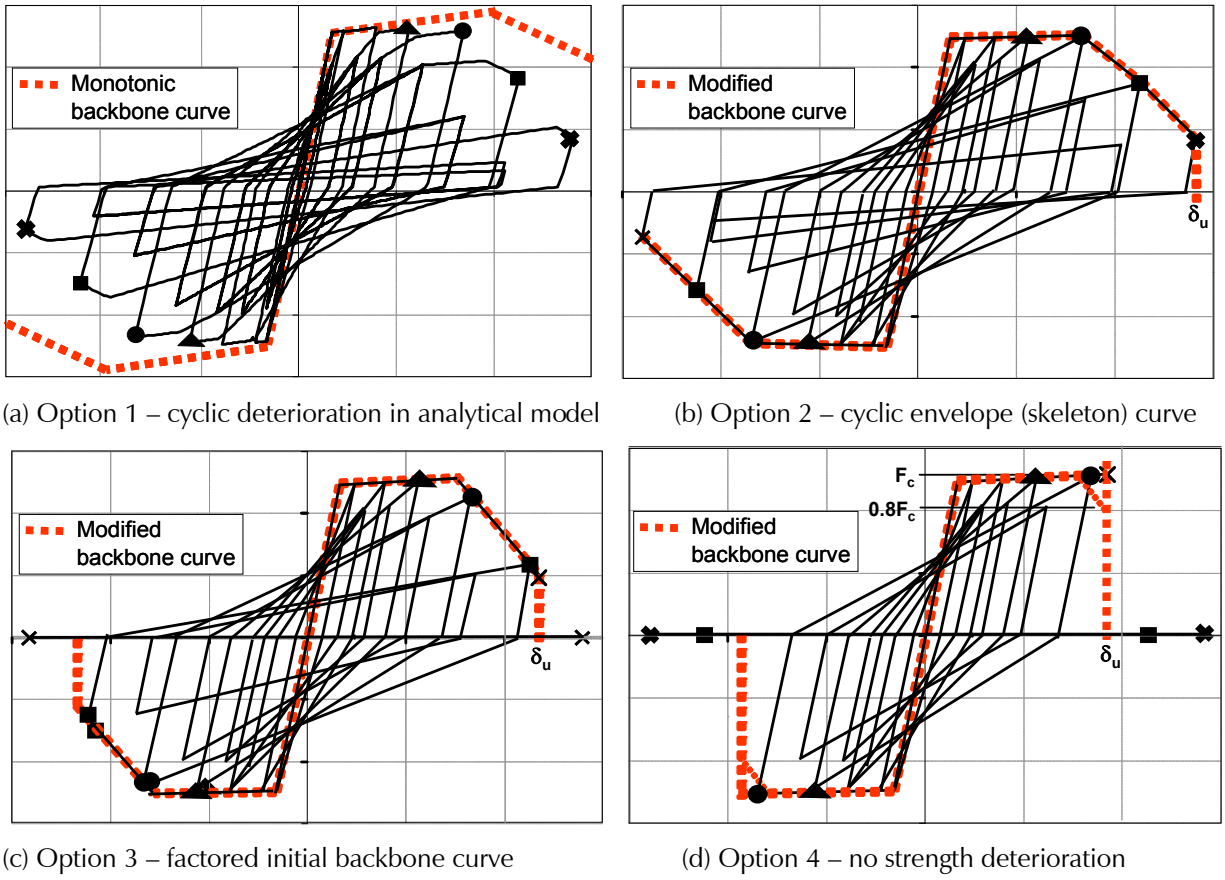

(a) Option 1 – cyclic deterioration in analytical model

(b) Option 2 – cyclic envelope (skeleton) curve

(c) Option 3 – factored initial backbone curve

(d) Option 4 – no strength deterioration

Figure 2-17 Illustration of four options for analytical component modeling.

In Figure 2-17, it can be seen that the greater the simplification in component modeling, the more the inelastic deformation capacity is reduced. This is most evident in Figure 2-17d, in which the attainment of the estimated δ_u severely limits the inelastic deformation capacity.

2.2.6 Response Sensitivity to Deterioration

Implementation of deterioration models in nonlinear response history analysis adds complexity and increases modeling effort. Additional effort is necessary and justified if the structural response is indeed sensitive to degradation of strength and stiffness, which is generally the case for

performance evaluation at MCE level ground motion intensities, and for assessing the collapse capacity of a structure.

The sensitivity of the median collapse capacity, η_c, to the strength parameter $\gamma = V_y/W$, pre-capping plastic rotation, θ_p, post-capping rotation, θ_{pc}, and the cyclic deterioration parameter, $\lambda = E_t/(M_y\ \theta_p)$ from Equation 2-2, is shown in Figure 2-18, for generic 8-story structures (Zareian, 2006).

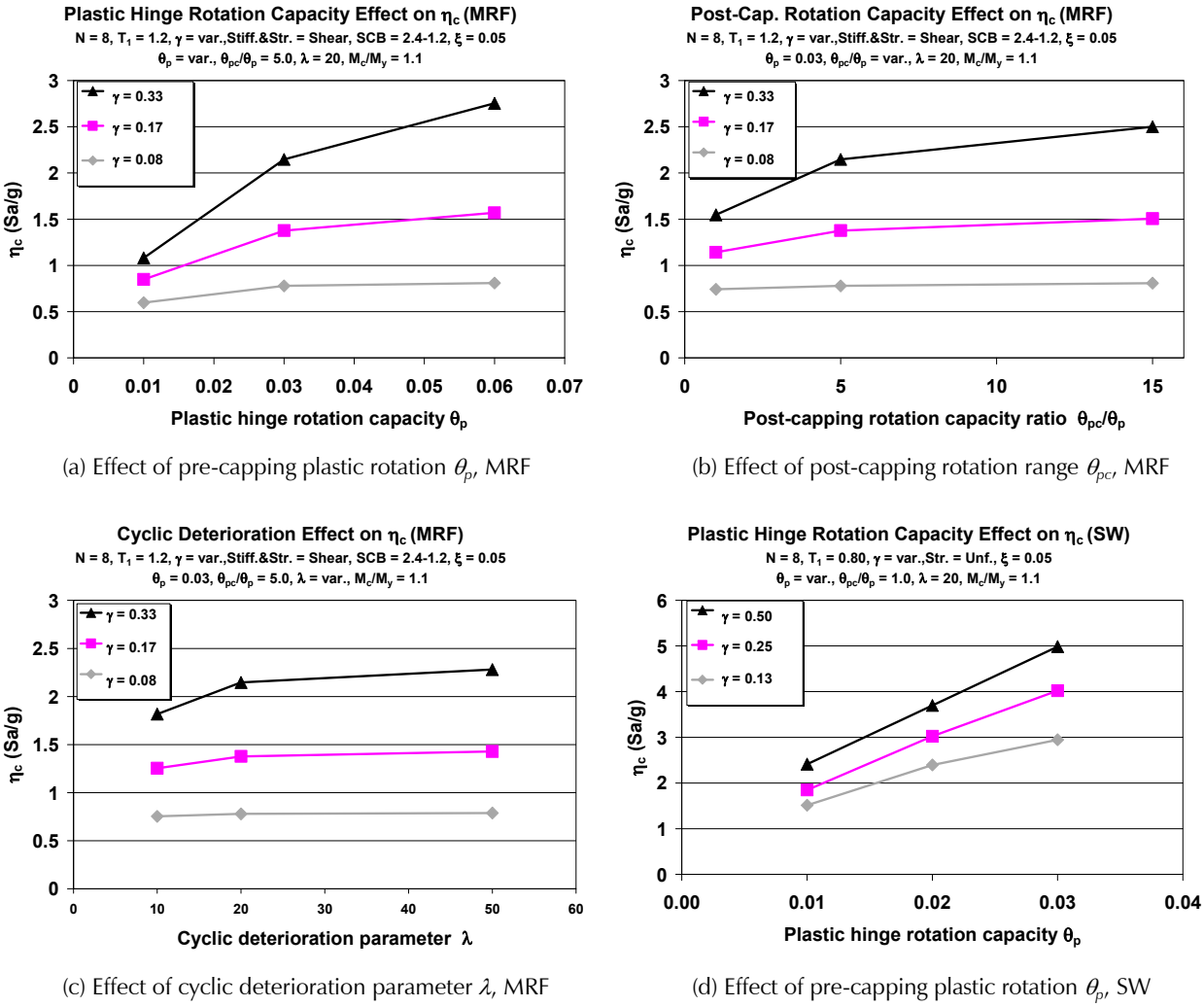

(a) Effect of pre-capping plastic rotation θ_p, MRF

(b) Effect of post-capping rotation range θ_{pc}, MRF

(c) Effect of cyclic deterioration parameter λ, MRF

(d) Effect of pre-capping plastic rotation θ_p, SW

Figure 2-18 Effects of deterioration parameters on median collapse capacity of generic 8-story moment-resisting frame (MRF) and shear wall (SW) structures (Zareian, 2006).

Figures 2-18a, 2-18b, and 2-18c are for generic 3-bay moment-resisting frames, and Figure 2-18d is for generic shear wall structures that develop a flexural hinge at the base. Except for the moment frame system with low base shear strength ($\gamma = 0.08$), the results show a clear dependence on the deterioration parameters. The exception in the case of low base shear

strength is caused be sensitivity to P-Delta effects, which renders the dependence on deterioration parameters secondary.

2.2.7 Summary Observations for Modeling of Deterioration

Deterioration implies loss in strength or stiffness in the response characteristics of a component. It occurs under monotonic loading and is accelerated under cyclic loading. The consequences of component deterioration are: (1) loads must redistribute to other components; (2) basic demand parameters such as story drift and roof drift increase; and (3) the failure mechanism of a structure can change. Modeling of deterioration is necessary if components will undergo deformations beyond which deterioration significantly affects response.

It is assumed that rapid deterioration, usually associated with a sudden loss of component resistance is prevented through good detailing and the application of capacity design concepts. For this reason, the need to model rapid deterioration is not anticipated, and recommendations are focused on modeling of relatively slow deterioration. If nonlinear response analysis discloses the existence of rapid modes of deterioration (e.g., brittle weld fracture, or shear failure in reinforced concrete beams or columns), then additional precautions should be taken to ensure that the structure response does not exceed the available force or deformation capacity.

The deterioration characteristics of a component can be described by a backbone curve, a basic hysteresis model, and additional deterioration rules that account for the effect of cyclic loading. The parameters defining deterioration in a component can be derived from advanced analytical models that account for all the behavior modes that might contribute significantly to deterioration. Physical data from experimental testing, when combined with first principles and mechanics models, provide information from which deterioration parameters can be derived empirically or analytically.

2.3 P-Delta Effects

P-Delta effects are caused by loads acting on the deformed configuration of the structure. *Structure P-Delta* is concerned with the global effects of gravity loads acting on the displaced location of the joints, while *member P-delta* is concerned with the local effects of loads acting on the deflected shape of a member between the joints. Local member P-delta effects are rarely important in seismic response analysis, so this section is focused on global structure P-Delta effects.

From a static perspective, structure P-Delta can be visualized as an additional lateral load that increases member forces and lateral deflections, reduces lateral load resistance in the structure, and causes a negative slope in the lateral load-displacement relationship at large displacements. From a dynamic perspective, structure P-Delta can lead to significant amplification in displacement response if the displacement demands in an earthquake are large enough to enter the range of negative tangent stiffness. This is illustrated in Figure 2-19, which shows the dynamic response of a single-degree-of-freedom system with bilinear hysteretic behavior, including P-Delta effects that lead to a negative post-yield tangent stiffness of 5% of the elastic stiffness. The presence of the negative post-yield stiffness leads to ratcheting of the displacement response in one direction, which causes the system to collapse.

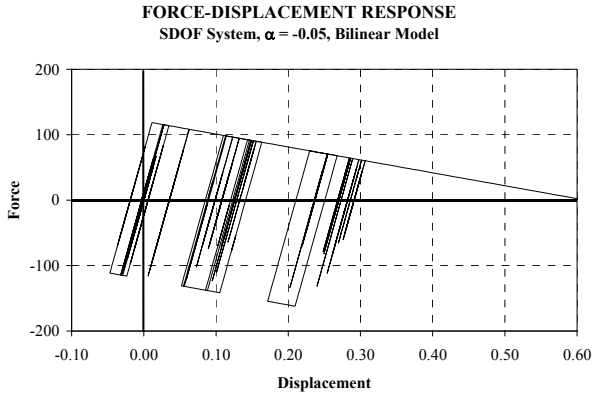

Figure 2-19 Response history of a single degree of freedom system incorporating P-Delta effects (FEMA, 2000b).

P-Delta effects are usually under control if the effective stiffness at maximum displacement is positive. If the effective stiffness becomes negative, the amplification of drift can become significant enough to cause lateral dynamic instability, and the potential for collapse exists. The presence of post-capping strength deterioration greatly accelerates this effect, but a negative effective stiffness can be attained even if no post-capping strength deterioration occurs.

The elastic story stability coefficient $\theta = P\Delta/(Vh)$, which is employed in ASCE/SEI 7-10, *Minimum Design Loads for Buildings and Other Structures* (ASCE, 2010) to estimate the importance of P-Delta effects, is not a reliable indicator of the importance of P-Delta in the range of large inelastic deformations. Inelastic behavior will lead to a redistribution of forces and story drifts, and both may be affected greatly by P-Delta effects.

This is illustrated in Figure 2-20, which shows pushover deflection profiles for elastic and inelastic behavior of an 18-story frame, with and without incorporation of P-Delta effects in the analytical model. In the elastic range, the deflection profiles with and without P-Delta effects are essentially equal, but in the inelastic range they deviate significantly. At a roof displacement equal to 1.75 times the yield displacement, the drift in the lower stories considering P-Delta effects is about four times as large as the drift predicted without consideration of P-Delta effects.

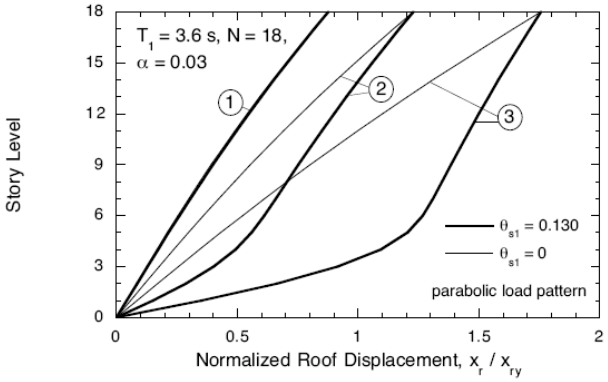

Figure 2-20 Pushover deflection profiles for an 18-story frame structure at different roof drifts with P-Delta excluded (thin line), and P-Delta included (thick line), from Adam et al. (2004).

2.3.1 Summary Observations for P-Delta Effects

Much information exists in the literature on the effects of P-Delta on the seismic response of single- and multiple-degree-of-freedom systems. Bernal (1998) presents predictive models for P-Delta effects in frame structures. Challa and Hall (1994), SAC (1999a), FEMA (2000b), and Adam et al. (2004) provide examples of the importance of P-Delta effects in multi-story steel frame structures. Summary of observations from recent literature are provided below.

1. Figure 2-21 illustrates the effect of P-Delta on the median collapse capacity (i.e., spectral acceleration, S_{ac}, at fundamental period causing collapse), for 8-story moment-resisting frames and shear wall structures of various yield strengths. There is a clear difference in the importance of P-Delta effects for frame structure versus shear wall structures. Deterioration that leads to negative post-capping component stiffness occurs in both structure types, but concentration of story drifts occurs mainly in frame structures. The effect of P-Delta on the collapse capacity is therefore larger in frame structures than in wall structures, provided the wall structure develops a flexural plastic hinge mechanism and not shear failure.

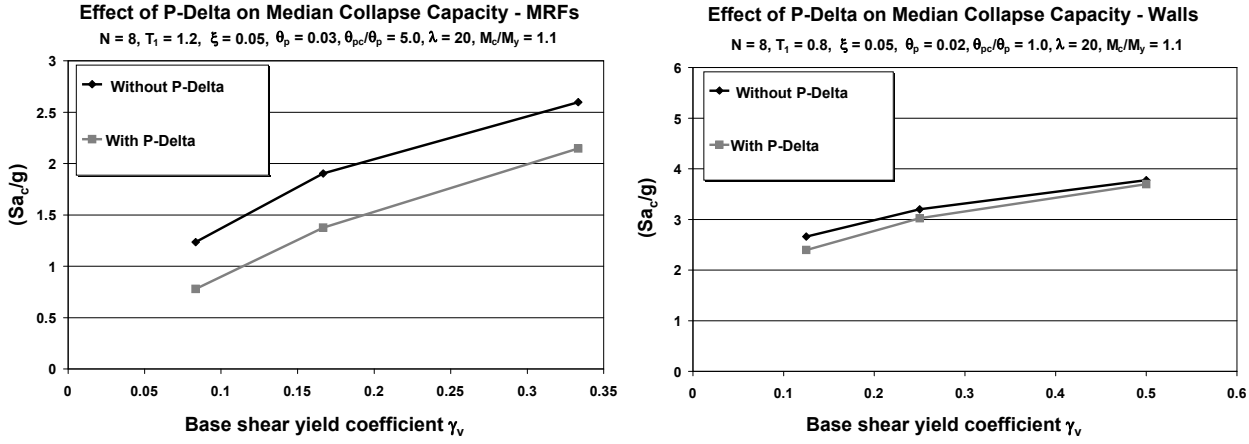

(a) (b)

Figure 2-21 Effects of P-Delta on median collapse capacity (Sa_c/g) of: (a) 8-story moment-resisting frame; and (b) shear wall structure deforming in a flexural mode (Zareian, 2006).

2. Equivalent single degree of freedom systems should not be used to predict the importance of P-Delta effects unless appropriate modifications are made to account for the fact that inelastic redistribution can radically change the effective post-yield stiffness of an equivalent single-degree-of-freedom system (Adam et al., 2004).

3. A static pushover analysis is useful for understanding the behavior of a structure and identifying P-Delta sensitivity. This type of analysis provides an estimate of the drift levels at which a negative post-yield stiffness is attained. This is illustrated in Figure 2-22, which shows global pushover curves of the SAC 20-story Los Angeles structure, both with and without consideration of P-Delta effects.

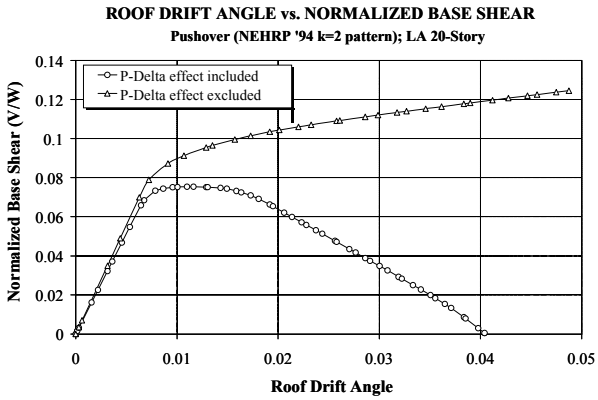

Figure 2-22 Base shear versus roof displacement pushover curves for the SAC 20-story Los Angeles structure (FEMA, 2000b).

4. The nonlinear dynamic response of structures can be very sensitive to modeling assumptions. This is illustrated in Figure 2-23, which shows

the response of the SAC 20-story Los Angeles structure to the Tabas record using four different analytical models (FEMA, 2000b). Model M1 is a bare centerline frame model in which the effects of the joint panel zones are ignored; Model M2 is a bare frame model in which the joint panel zone is modeled explicitly; and models M1A and M2A are models in which the contributions of the floor slab and gravity frame to strength and stiffness are considered. Large differences are evident in the response histories shown in Figure 2-23a, and in the incremental dynamic analysis results in Figure 2-23b. P-Delta is responsible for much of this difference, particularly when the structural model approaches lateral dynamic instability (i.e., the slope of the IDA curves approaches zero).

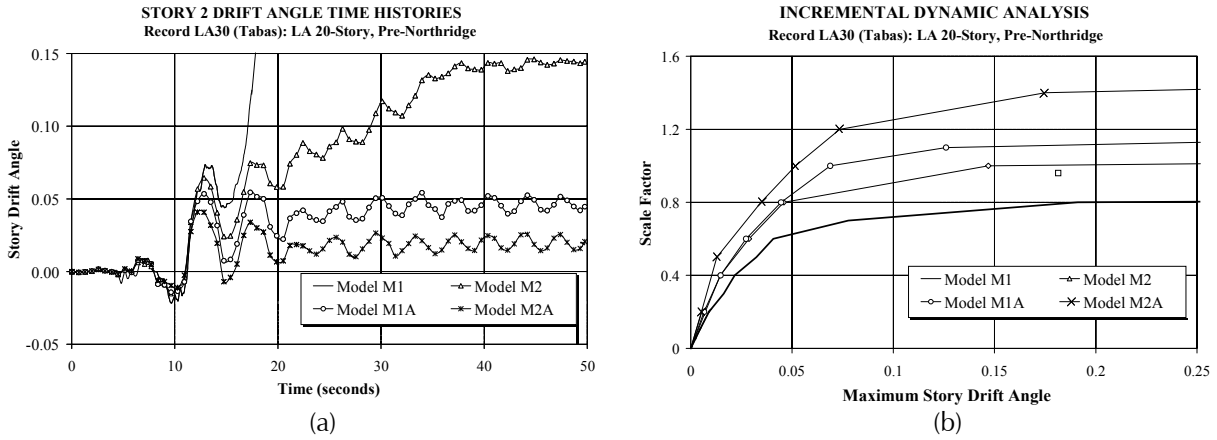

Figure 2-23 Dynamic response of SAC 20-story Los Angeles structure using four different analytical models shown as: (a) response histories; and (b) incremental dynamic analyses (FEMA, 2000b).

5. P-Delta effects become critical when the ground motion is sufficiently large to drive one or more stories of the structure into the range of negative tangent stiffness.

6. The potential for dynamic instability is relatively high in flexible moment frame structures in which one or more of the lower stories deforms in a shear mode, and tributary gravity loads are large enough that P-Delta will lead to a significant amplification of story drift demands.

7. Incorporation of elements that are not intended to resist seismic effects but contribute to lateral strength and stiffness can significantly improve seismic behavior. For instance, the interior gravity system in perimeter moment frame structures can provide adequate additional stiffness to delay the onset of negative stiffness once the primary system forms a mechanism.

8. The effects of P-Delta on seismic response increase when the structural components deteriorate and enter the post-capping range (negative tangent stiffness). The combination of P-Delta and post-capping deterioration will greatly increase the collapse potential of structures.

9. The duration of ground motions can have a large effect on story drift amplification because: (1) cyclic deterioration is a function of the number and amplitudes of inelastic excursions; and (2) ratcheting will bring the structure closer to collapse if the strong motion duration is long.

10. Because of the increasing importance of P-Delta effects on long-period structures, the collapse potential for tall frame systems increases with period, unless additional minimum strength criteria, such as R_{di} (FEMA, 2009a), are enforced.

2.3.2 Recommendations for Modeling P-Delta Effects

1. Nonlinear response history analysis should incorporate structure P-Delta effects. A small elastic story stability coefficient does not guarantee that the P-Delta effects are benign in the inelastic range.

2. If there are columns that carry gravity loads but are not part of the seismic-force-resisting system, then the P-Delta tributary to these columns must be represented in the analytical model.

3. The length and slope of the strain hardening region (i.e., θ_p and M_c/M_y) and of the post-capping region (i.e., θ_{pc}) of the structural components can greatly affect the lateral drift under severe ground motions because of ratcheting of the response in individual stories. For this reason estimates of these parameters should be reasonable and conservative (low). The implication is that Option 4 for analytical modeling of components should be used only if the post-capping portion of the non-deteriorating model is relatively small compared to the strain hardening portion.

4. Any deformation mode that leads to concentration of inelastic deformation in a single story (or to partial mechanisms involving several stories) should be incorporated in the analytical model. This pertains to possible plastic hinging in columns of moment frames, severe deterioration of bracing elements and/or connections in a braced frame, and shear failure in shear walls.

5. If the analytical model incorporates the strengthening and stiffening effects of components that are not part of the seismic-force-resisting system (e.g., gravity columns, simple connections, slab effects), then it should be shown that these components maintain their effective strength

and stiffness over the full range of deformation response experienced by the structure.

2.4 Damping

Damping is generally associated with reduction in dynamic (vibration) response due to energy dissipation in structural and nonstructural components of the building and foundation. While straightforward in concept, the quantification and representation of damping is complicated by the relationship between its mathematical representation and the underlying physical sources. For example, measured damping is a characteristic of recorded vibration motions, while underlying contributors to damping are many, and can be mathematically modeled in a variety of ways, including friction damping, hysteretic damping, or viscous damping. In the context of nonlinear structural analysis, it has been suggested that a more appropriate terminology for damping is "un-modeled energy dissipation," based on a common interpretation of "damping" as the portion of energy dissipation that is not captured in the hysteretic response of components that have been included in the model.

Largely for mathematical convenience, damping is often modeled as equivalent viscous damping, usually as a percentage of critical damping in one or more vibration modes. The damping matrix can be defined in a variety of ways, but for routine applications it is usually defined as either a linear combination of the mass and stiffness matrices (e.g., Rayleigh damping), or modal damping. Whereas Rayleigh and modal damping have clear relationships to elastic modes and computational benefits in the context of elastic modal analysis, these do not hold for nonlinear response history analysis. Thus, the main justification for selecting either of these definitions is practical convenience and familiarity in defining damping as a percentage of critical damping. For inelastic analyses under strong ground motions, traditional or classical damping models developed within the context of elastic analysis may be inappropriate, and need to be re-evaluated. This is particularly true for tall buildings subjected to earthquake effects, where data and observations from past earthquakes are limited, as is experience in utilizing nonlinear analysis for design.

2.4.1 Physical Sources of Damping

Proper modeling of damping effects requires an appreciation for the physical sources of damping, and how these may vary depending on the specific characteristics of a building. This is especially true for tall buildings, where

the structural systems, foundations, and non-structural components can be quite different from those in conventional low- to mid-rise construction.

Damping of earthquake-induced motions can generally be distinguished between contributions from structural components, nonstructural components, and the substructure and foundation. Where nonlinear analysis is used, damping contributions from structural components can be further distinguished between those components that are explicitly modeled in the analysis and those that are not. Further details of each damping source are described in the sections that follow.

2.4.1.1 Structural Components Explicitly Modeled in the Analysis

Structural components that are explicitly modeled in the analysis generally consist of components that are designed to resist earthquake effects. The nonlinear behavior of these elements is explicitly accounted for in the model and directly contributes to the calculated response. Such elements include the components of the structural wall and frame systems, such as: (a) reinforced concrete or steel plate shear walls and associated coupling beams; (b) reinforced concrete or steel moment frame beams, columns, and beam-column joints; (c) beams, columns, and braces of steel braced frames; and (d) combinations of these.

The extent to which all of the energy dissipation in these elements is captured through hysteretic response in the nonlinear analysis depends on the specific characteristics of the model. For example, concentrated plasticity (discrete hinge) models in beams and columns may not capture energy dissipated by gradual steel yielding or concrete cracking prior to the formation of a hinge. On the other hand, fiber-type analyses will do a better job of capturing energy dissipation at lower values of deformation, but may still not capture all the sources of energy dissipation (such as through reinforcing bar bond deterioration and bolt slip). Since it is common practice to mix elastic and nonlinear elements (e.g., modeling the lower hinging portion of shear walls with nonlinear fiber-type analysis and the upper portions elastically), energy dissipation associated with yielding and cracking in the portions of the structure that are modeled with elastic elements will not be captured.

Another factor that contributes to energy dissipation is the increase in material strengths (yield strength in steel and compression/cracking strengths in concrete) due to strain rate effects, which are usually ignored or discounted when establishing the structural component strengths in seismic applications.

2.4.1.2 Structural Components Not Explicitly Modeled in the Analysis

For practical reasons, there are many structural components that are not explicitly modeled in the analysis, but are expected to undergo inelastic deformations. Chief among these are components of the gravity system, including floor slabs, gravity beams, gravity columns, and their associated connections. Yielding and cracking of gravity components and connections caused by imposed lateral deformations is a source of energy dissipation in the system that should be implicitly accounted for in the analysis when not explicitly included in the model.

2.4.1.3 Nonstructural Components of the Superstructure

Nonstructural components that are likely to contribute to damping include interior partitions, exterior cladding, and various mechanical and electrical systems. The stiffening and damping effects provided by these components will depend to a large extent on the materials of construction and the manner in which they are attached to the structure.

Given that tall buildings can experience significant story drifts due to service wind load, interior partitions, curtain walls, and mechanical and electrical risers in tall buildings are usually detailed to minimize their interaction with the structure. Accordingly, these components will tend to contribute less damping in tall buildings than they provide in low-rise buildings. However, the contribution of each will tend to vary from building to building depending on the architectural layout (e.g., amount of interior walls per floor area) and the method of attachment to the structure.

Based on the assumption that nonstructural components contribute less than 5% to the total lateral strength of the system, and possess 10% viscous damping, Priestly and Grant (2005) reason that nonstructural components contribute less than 0.5% equivalent viscous damping in buildings.

2.4.1.4 Substructure, Foundation, and Site

While damping effects associated with soil-foundation-structure interaction are widely acknowledged, there is relatively little information available to quantify these effects. Nevertheless, when interpreting measurements of building response, or making estimates of damping, it is important to consider the potential contribution of damping associated with the foundation and its interaction with the surrounding soils.

For example, structures with below-grade levels embedded in soil are expected to exhibit higher damping than structures with shallow foundations supported on rock. Other effects, such as rocking response of shear wall

foundations, will also tend to damp out response as compared to structures that do not tend to rock. However, given that the vibration frequencies are small (periods are long) for tall buildings, radiation damping through the foundation is expected to be low.

As with other damping effects, the extent to which soil-foundation damping should be included in some equivalent viscous damping component will depend on whether it is explicitly modeled in the analysis. For example, if the soil-foundation interface is modeled with springs and dashpots, then the amount of soil-foundation damping attributed to viscous damping should be adjusted.

2.4.2 Survey of Damping Assumptions in Design and Assessment

Existing guidelines for damping effects in dynamic analysis of buildings can generally be distinguished between those intended for wind design and those intended for earthquake design, the primary difference being the amplitude of deformations that are expected. Damping assumptions to assess wind-induced vibrations are fairly well established, and can provide guidance for response of buildings in the elastic range at low displacement amplitudes (e.g., story drift ratios up to about 1/500 or 0.2%). Damping assumptions applicable in the inelastic range under larger displacement amplitudes are less established, and will depend on the extent to which inelastic material response is modeled explicitly in the analysis.

2.4.2.1 Wind Engineering

Wind design criteria for tall buildings generally consider two limit states: one associated with occupant comfort and a second associated with structural safety. The designs are often based on wind-tunnel studies, with two levels of equivalent viscous damping assumed for each limit state. Given that damping is amplitude dependent, smaller values are typically specified for serviceability (occupancy comfort) than for safety (structural member design).

Serviceability checks are usually defined in terms of limiting values of floor accelerations to ensure occupant comfort during frequent wind events. Damping values assumed for these checks range from about 0.5% to 1% of critical damping for steel-framed buildings, and 1% to 1.5% for reinforced concrete buildings. For strength limit state checks (usually defined at component design strengths corresponding to the onset of significant yielding) damping assumptions are increased somewhat, to values of 1.0% to 1.5% for steel-framed buildings, and 1.5% to 2% for reinforced concrete

buildings. The ISO standard, *Wind Actions on Structures* (ISO, 1997), specifies equivalent viscous damping values of 1% steel systems and 1.5% for reinforced concrete systems for analysis of strength checks for wind loads.

2.4.2.2 Earthquake Engineering

Only recently has nonlinear response history analysis been regularly applied in structural engineering design of buildings to resist earthquakes. As a result, many of the currently available guidelines on damping are intended for use with elastic dynamic analysis. For example, the Los Angeles Tall Buildings Structural Design Council (LATBSDC) seismic design requirements for tall buildings specify equivalent critical viscous damping values of 5% for steel framed buildings and 10% for reinforced concrete buildings for analysis at design-level ground motions, and 7.5% for steel and 12% for reinforced concrete buildings for analysis at MCE-level ground motions (Harder, 1989; Martin and Harder, 1989). Since these damping values are intended to account for inelastic (hysteretic) effects within the context of elastic response history analysis, they are inappropriate and should not be used with nonlinear dynamic analyses.

Examples of more recent recommendations intended for use with elastic analysis include 2% equivalent viscous damping used in the steel frame building studies conducted as part of the SAC Joint Venture (SAC, 1996) and an upper limit of 5% specified in the San Francisco Department of Building Inspection Administrative Bulletin, AB-83 (SFDBI, 2007). The seismic design working group of the Council on Tall Buildings and the Urban Habitat (CTBUH, 2008) reports that current practice in Japan is to use viscous damping values of 2% for steel structures and 3% for reinforced concrete structures. The report also notes that values of 2.5% to 5% for steel structures, and 5% for reinforced concrete structures, which are commonly used in nonlinear analytical studies of low- to mid-rise buildings, are probably too large for high-rise buildings. In assessing the dynamic response of a tall building in China, Li et al. (2002) report that the Chinese code of practice for seismic design specifies 3% critical damping.

2.4.3 Measurement of Damping in Buildings

With the advent of lower cost systems for building instrumentation and monitoring, data on measured response of buildings are becoming increasingly available. Much of the data are limited to small amplitude vibrations, typically excited by wind, mechanical shakers, or small earthquakes. There are some data available from buildings subjected to

strong ground motions (Goel and Chopra, 1997). These data, however, are similarly limited to small amplitude vibrations, with maximum story drift ratios of about 0.005 to 0.01.

Damping measured from vibration data cannot be related uniquely back to either the type of damping (e.g., viscous versus hysteretic) or the source of damping (e.g., structural components, nonstructural components, or foundations). Rigorous interpretation of measured damping requires detailed analyses to iteratively compare modeling assumptions to measured response. Since this is rarely done, most interpretation is based on judgment and reasonable assumptions as to the relative contributions of damping source and type.

Damping measurements can also vary depending on the specific techniques used to infer damping from time-history data. For example, methods based on Fourier analyses of power spectral density generally cannot distinguish whether there are changes in damping response over time, whereas methods based on time-domain decrement response can more readily detect changes that occur during a loading event. As reported by Kijewski-Correa and Pirnia (2007), differences in system identification algorithms can also result in significant variations in measured damping. Using a time domain decrement method, they calculated damping values for wind-induced motions of three tall buildings that ranged from 0.8%, 1.2%, and 1.0%. Using spectral analysis, they calculated values of 1.5%, 1.3% and 1.7%. Kijewksi-Correa and Pirnia argued that the time domain decrement method was a more accurate method for quantification of damping.

On the other hand, many studies of buildings in the United States subjected to strong ground motions have utilized spectral system identification techniques to calculate the damping (Celebi, 1998), which may tend to overestimate damping effects. Jeary (1986) provides further discussion on methods that are commonly used to quantify damping, and emphasizes the inherent limitations of certain methods, and the errors that can arise when methods are misapplied. These differences should be considered when attempting to calculate small damping values from low amplitude vibrations from random loading events.

2.4.3.1 Buildings Subjected to Earthquakes

Goel and Chopra (1997) compiled and analyzed recorded strong motion data for 85 buildings that were subjected to strong ground motions from eight earthquakes in California, from the 1971 San Fernando earthquake through the 1994 Northridge earthquake. With the primary purpose of examining

natural vibration periods of various buildings, this study included calculation of damping characteristics. Damping data from this study are summarized in Figures 2-24a through 2-24c.

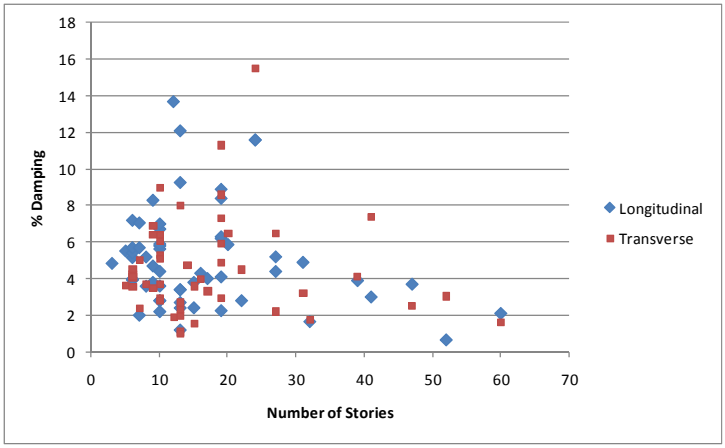

(a) damping versus number of stories

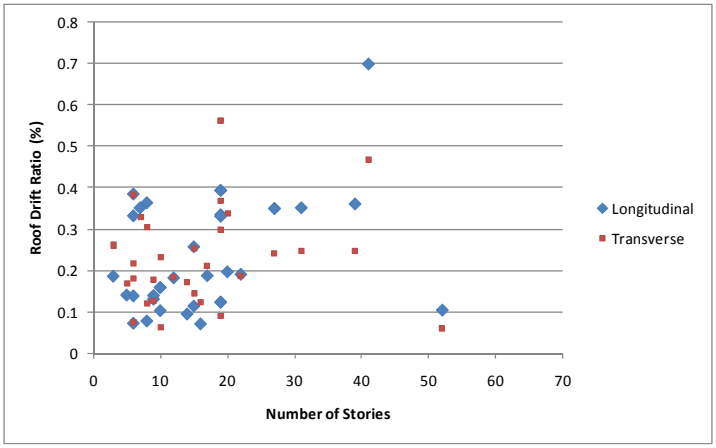

(b) roof drift demand versus number of stories

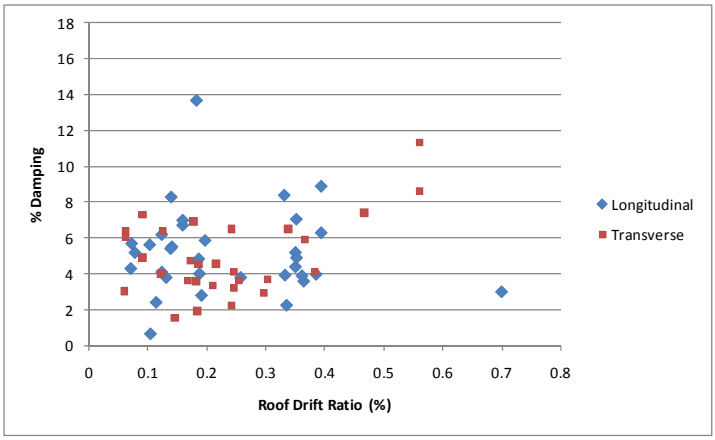

(c) damping versus roof drift demand

Figure 2-24 Damping and drift demand data from buildings excited by strong ground motions (based on Goel and Chopra, 1997).

The buildings ranged in height from 2 to 60 stories, and included 27 reinforced concrete moment frames, 42 steel moment frames, and 16 reinforced concrete shear wall structures. Data in Figure 2-24a show a clear trend between building height and the measured equivalent viscous damping for the first sway modes of vibration. Below 35 stories, the measured damping ranges from about 2% to 12% of critical, whereas above 35 stories the damping is generally in the range of 2% to 4% of critical. A possible reason for the large observed difference is that shorter buildings might have experienced larger displacements than the taller buildings in the earthquakes studied.

To examine this further, roof drift ratios are plotted versus the number of stories in Figure 2-24b, and the damping ratio is plotted versus roof drift ratio in Figure 2-24c. Both plots suggest that there are no discernable trends between drift demand and story height that play a major role in the variation of observed damping.

Data reported by Goel and Chopra reflect similar findings in other studies of measured strong motion response in the United States over the past thirty years, including Bradford et al. (2004), Celebi (1998), Celebi (2006), Hudson and Housner (1954), Li and Mau (1997), Maragakis et al. (1993), Rodgers and Celebi (2006), Skolnik et al. (2006), Stephen et al. (1985) and Trifunac (1970).

2.4.3.2 Buildings Subjected to Induced (Forced) Vibrations

Damping data are also available from vibration tests of real buildings, where vibration is typically induced by a mechanical shaker. Since forcing functions are known, and tests can be repeated multiple times, force vibration tests have the advantage that data reporting and analysis are more comprehensive. However, displacement amplitudes in forced vibration tests are typically much smaller, so allowances are needed when comparing damping data from forced-vibration studies to data recorded from strong earthquake shaking.

Figure 2-25 shows measured damping data reported by Satake et al. (2003) for buildings in Japan. Data are reported for 127 steel frame buildings up to 280 meters (70 stories) in height, and 68 buildings of reinforced concrete or mixed steel/concrete construction up to 170 meters (45 stories) in height. Most of the steel frame buildings are office or hotel occupancies, and most of the reinforced concrete and mixed steel/concrete buildings are residential occupancies. About half of the data are from forced-vibration testing, and half are from micro-tremor or wind-induced vibration testing. A few of the

measurements are also from earthquakes, but Satake et al. (2003) do not distinguish the results on the basis of vibration source. Typical displacement amplitudes in the measurements corresponded to roof drift ratios of about 2 x 10^{-5} (0.002%), which is about one-hundredth of the typical maximum wind drift index of 1/500 (0.2%), and even smaller in comparison to large earthquake-induced motions. A variety of techniques were also used to extract the damping (and other) vibration parameters in the different studies.

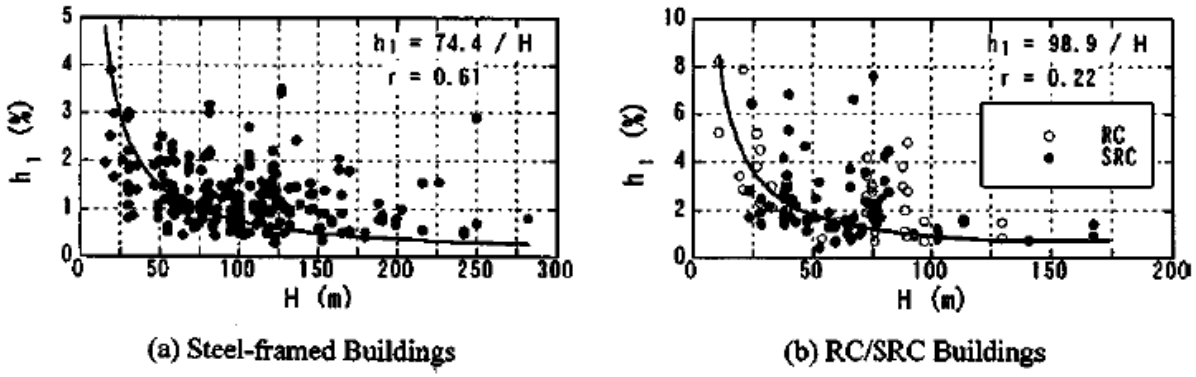

Figure 2-25 Measured damping from buildings in Japan (Satake et al., 2003).

The trend toward lower damping with increasing building height in Figure 2-25 is similar to the Goel and Chopra data in Figure 2-24, although in absolute terms, the damping values are lower. In Figure 2-25, the range of damping is from about 0.5% to 8% of critical damping, versus 1% to 15% of critical damping in Figure 2-24. The smaller values in Figure 2-25 are most likely due to the differences in the vibration displacement amplitudes between the two studies. Assuming a demarcation of 30 stories between low/mid-rise and high-rise buildings (roughly equivalent 120 meters), the maximum critical damping ratios plotted in Figure 2-25 range up to 4% (for steel) and 8% (for reinforced concrete) in low/mid-rise buildings, and up to 2% in high-rise buildings.

Also shown in Figure 2-25 is a simple regression formula that relates critical damping to the inverse of building height. Satake et al. (2003) attribute most of the change in damping with building height to the decreased significance of foundation and soil damping effects in taller buildings. They also examine other trends in the data and note that the damping ratios are slightly larger in apartment buildings than office buildings, which they suggest is related to the density of interior partitions.

2.4.3.3 Buildings Subjected to Wind

Measurements taken from buildings in strong wind storms are another source of data on damping effects. As buildings taller than 30 stories are a primary

focus of wind studies, there are more data available for tall buildings subjected to wind vibrations than to earthquake shaking, worldwide. Information from these studies, however, is still limited by the number of instrumented buildings and relatively small displacement amplitudes. Moreover, there are some differences in the loading effects between wind and earthquakes that can affect response. For example, wind introduces aero-elastic damping associated with fluid dynamics of airflow, which is not present under earthquake shaking. Also, nonlinearities in the soil-foundation-structure interface are expected to have a larger effect on earthquake-induced motions than wind-induced motions.

The amplitude dependence of damping for wind vibration in buildings has been well established by Jeary (1986) and others. Figure 2-26 shows a plot of damping measured by Fang et al. (1999) in a 30-story (120 meter) building that demonstrates the typical amplitude dependence considered in wind engineering. In this example, damping was calculated from wind vibration data collected over a two year period, which provided measurements at various amplitudes. As shown, damping increases from negligible amounts, to about 0.5% critical damping in the so-called "high amplitude plateau."

It should be noted, however, that even the largest recorded amplitudes in the high amplitude plateau are on the order of 0.02% roof drift. This is well below the amplitudes associated with serviceability or safety limit states for strong ground motions (i.e., drifts on the order of yield-level drifts of 0.5% to 1%). Unfortunately, there are no studies relating damping at the high amplitude plateau for wind loading to damping at larger drifts expected under earthquake shaking.

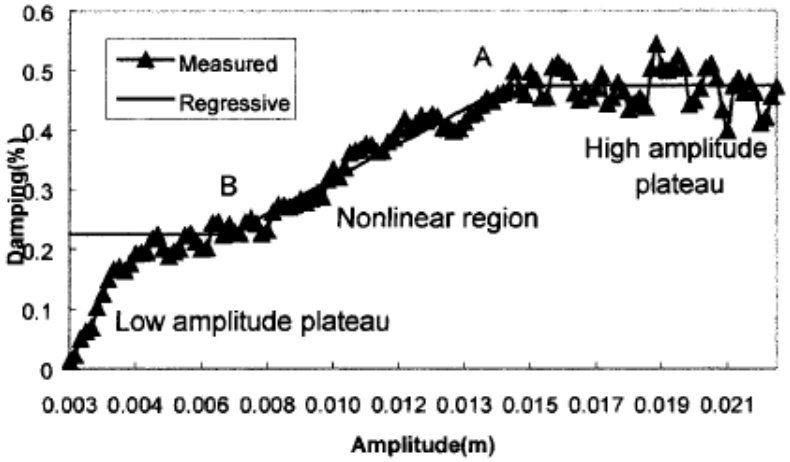

Figure 2-26 Illustration of amplitude dependence of measured damping under wind loading (Fang et al., 1999).

Damping data from several tall buildings subjected to wind vibration are summarized in Table 2-1. With critical damping percentages in the first mode ranging from 0.3% to 1.4%, these data further illustrate the relatively low damping values and relatively small displacement amplitudes that have been measured in tall buildings.

Table 2-1 Selected Results of Measured Damping in Tall Buildings under Wind-Induced Vibration

Building Description	*Damping (% critical)*	*Reference*
57-story steel frame office building	0.8%	Kijewski-Correa et al. (2007), case B1
73-story reinforced concrete shear wall with outrigger frames	0.8% to 1.2%	Kijewski-Correa et al. (2007), case S1
>50-story steel perimeter tube system	0.9%	Kijewski-Correa et al. (2007), case C1
>50-story reinforced concrete shear wall with frames	1.4%	Kijewski-Correa et al. (2007), case C2
>50-story steel frame tube system	1.0%	Kijewski-Correa et al. (2007), case C2
79-story reinforced concrete core with outriggers	0.4%	Li et al. (2002)
70-story composite braced frame	0.5%	Li et al. (2000)
78-story reinforced concrete shear wall	0.5%	Li et al. (2003)
63-story reinforced concrete shear wall	0.3%	Li et al. (2004)

2.4.3.4 Dynamic Shaking Table Tests

Dynamic shaking table tests are another source of data on structural damping. Usually damping is inferred from decrements in peak-to-peak response in free vibrations following table shaking or pull-release tests. The amplitude of displacement cycles is usually small (less than 0.1% drift ratio), however, in a controlled laboratory environment damping can be systematically interrogated after the structure has sustained large inelastic deformations and damage.

Measured damping data from various shaking table tests are summarized in Table 2-2. The table includes data for reduced scale (1/3 to 1/2 scale) tests of reinforced concrete frame (or frame-wall) systems and steel braced frame systems. Data are reported in terms of the percentage of critical damping in the first mode. In the initial or undamaged condition, damping in reinforced concrete frames ranges from 1% to 3% of critical. In structures that have

undergone modest levels of shaking (less than 1% drift) and sustained slight damage (i.e., hairline cracking, minor spalling), damping values increase to about 4%. Following significant damage, damping increases beyond 5% up to a maximum measured value of 11% of critical. In steel braced frames, damping in the undamaged state is about 0.7% to 1.3% of critical, or about half of that measured in the reinforced concrete structures.

Table 2-2 Measured Damping versus Level of Damage from Shaking Table Tests

Test Description	*Measured Damping (% critical) versus Level of Damage*		*Reference*
RC Frames (2) 1-story, 3-bay (1/2 scale)	Undamaged: Yielded: Significant:	1.4% to 1.9% 2.1% to 3.7% 3.9% to 5.4%	Elwood and Moehle (2003)
RC Wall-Frame 7-story (1/5 scale)	Undamaged: Slight: Significant:	1.9% to 2.2% 3.5% to 3.7% 6.9% to 7.5%	Aktan et al. (1983); Bertero et al. (1984)
RC Flat Plate-Frame 2-story, 3-bay (1/3 scale)	Undamaged: Slight: Moderate: Significant:	1.2% to 1.7% (negligible drift) 2.4% to 2.6% (0.002 to 0.011 drift) 5.0% (0.017 to 0.034 drift) 7.2% (0.053 drift)	Diebold and Moehle (1984)
RC Frame 2-story, 1-bay (1/3 scale)	Undamaged: Damaged:	1.9 to 2.2% 3.9 to 5.3%	Oliva (1980)
RC Frame 3- to 6-story, 2-bay (1/3 scale)	Undamaged: Moderate: Significant:	2.7% to 3.7% (0.001 to 0.003 drift) 4.9% to 6.4% (0.012 drift) 9.6% to 11.1% (0.015 to 0.02 drift)	Shahrooz and Moehle, (1987)
RC Frames (12) 1-story, 3-bay (1/3 scale)	Undamaged:	1.4% to 2.9% (2.1% avg., 0.31 COV)	Shin and Moehle (2007)
RC Frame 3-story, 3-bay, (1/3 scale)	Undamaged:	1.9%	Moehle et al. (2006)
Steel EBF 1 bay, 6-story (1/3 scale)	Undamaged:	0.7%	Whittaker et al. (1987)
Steel CBF 1 bay, 6-story (1/3 scale)	Undamaged:	0.7% to 1.3%	Whittaker et al. (1988)

Damping effects measured in shaking table tests can also be inferred from comparisons with nonlinear analyses of the tests. For example, nonlinear analyses with 2% viscous damping resulted in accurate comparisons to the shake table tests by Shin and Moehle (2007). For shaking table tests of a reinforced concrete bridge pier, Petrini et al. (2008) compared various viscous damping assumptions made using fiber-type and plastic hinge

models. For fiber-type models, the best agreement was obtained using zero damping. For plastic hinge models, the best agreement was obtained using 5% stiffness-proportional viscous damping, where the damping was based on the tangent stiffness matrix (i.e., the damping terms were reduced in proportion to the changes in the tangent stiffness during the analysis). Thus, when compared to models with constant damping, effective damping in the plastic hinge models was probably much less than 5%.

Recommendations from Gulkan and Sozen (1971) equate dissipated energy to equivalent viscous damping. While originally envisioned for elastic analyses, their recommendations help relate damping effects to displacement amplitudes. They recommended a threshold value for damping in an undamaged reinforced concrete structure at 2% of critical damping, and demonstrated how equivalent damping quickly increased to 5% at an imposed displacement ductility of 1.4, and 10% at an imposed ductility of 2.8. In the context of nonlinear analysis, these findings suggest a minimum value of 2% critical damping, where any increase in viscous damping beyond this value would depend on how well the nonlinear analysis captured hysteretic energy dissipation in the structural components.

2.4.4 Modeling Techniques for Damping

The quantification and definition of damping are integrally linked with how damping is modeled. For elastic analyses, damping is defined in terms of equivalent viscous damping through the velocity dependent term, [C], in the equation of motion, as follows:

$$[M]\{\ddot{x}\}+[C]\{\dot{x}\}+[K]\{x\}=-[M]\{\ddot{x}_g\}+[P] \tag{2-3}$$

This is done for mathematical convenience, since the velocity is out of phase with displacement and acceleration, and thus provides an easy way to incorporate a counteracting force to damp out motions in a linear analysis. To facilitate modal analyses, the damping matrix is often defined using either the classical Rayleigh damping assumption, where [*C*] is calculated as a linear combination of the mass [*M*] and stiffness [*K*] matrices, or modal damping, where [*C*] is a combination of specified damping amounts for specific vibration modes (usually elastic vibration modes). These damping formulations are explained below.

Rayleigh Damping. The damping matrix and resulting critical damping ratios are calculated as follows:

$$[C]=a_M[M]+a_K[K] \tag{2-4}$$

$$\zeta_n = \frac{a_M T_n}{4\pi} + \frac{a_K \pi}{T_n} \tag{2-5}$$

where a_M and a_K are proportionality constants for mass and stiffness, respectively, and ζ_n is the fraction of critical damping for the n^{th} vibration mode with the period T_n. Since there are two constants, a_M and a_K can be chosen to provide a specified fraction of critical damping, ζ, in two modes, in accordance with:

$$a_M = 4\pi\zeta \frac{1}{\left(T_i + T_j\right)} \text{ , and } \quad a_K = \frac{\zeta}{\pi} \frac{T_i T_j}{\left(T_i + T_j\right)} \tag{2-6}$$

Figure 2-27 shows a comparison of the percentage of critical damping as a function of vibration period for mass, stiffness, and Rayleigh proportional damping. The plot is drawn assuming critical damping of ζ=2% at a first mode period of 5 seconds (representative of tall buildings).

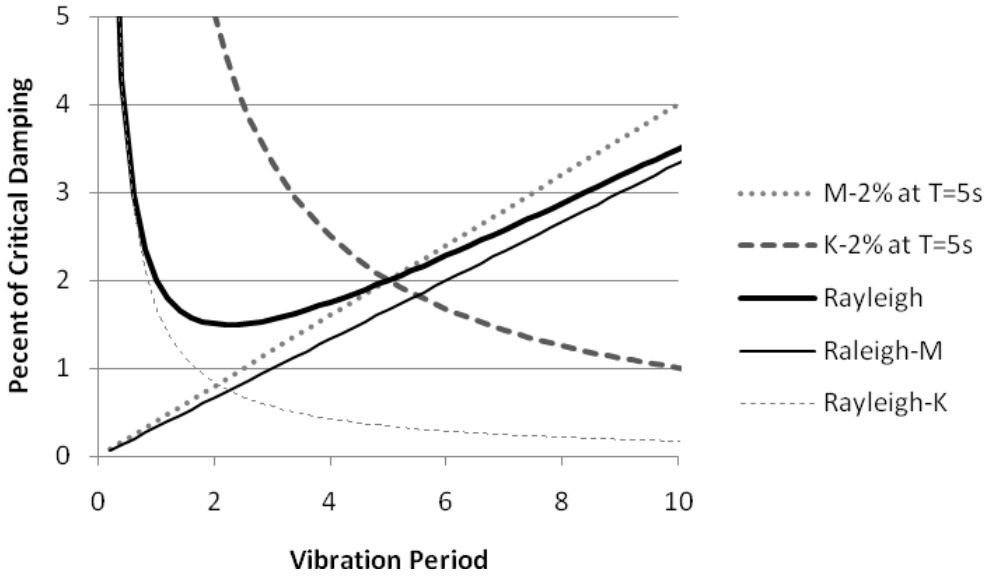

Figure 2-27 Variation in percent of critical damping for mass, stiffness, and Rayleigh proportional damping with ζ = 2% at T_1 = 5 seconds.

Coefficients for the mass-only and stiffness-only proportional cases are calculated using Equation 2-4 with ζ_n=0.02 and T_n = 5 seconds, and coefficients for the Rayleigh damping are calculated using Equation 2-6 with ζ=0.02, T_i = 5 seconds, and $T_j = 0.2T_i$ = 1 second. Note that the Rayleigh-M and Rayleigh-K lines show the contribution of each term to the

total Rayleigh damping, whereas the other mass and stiffness damping terms are for mass-only and stiffness-only damping.

Figure 2-27 illustrates the following well-known features of each type of damping: (1) effective damping for stiffness-only proportional damping is high at periods below the target fundamental period, and decreases at longer periods; (2) mass-proportional damping increases linearly with period; and (3) using Rayleigh damping, effective damping is constrained close to the target amount between the two specified periods, increases sharply below T_j, and increases close to linearly above T_i. Further analysis of the Rayleigh damping terms would reveal that damping at, and above, the fundamental period, T_i, is controlled by the mass-proportional damping term, and damping at, and below, the lower period is controlled by the stiffness-proportional term.

Modal Damping. Using a modal damping formulation, the damping matrix [C] is defined by the following equation:

$$[C] = \left[\Phi^T\right]^{-1}[c_i][\Phi]^{-1} \tag{2-7}$$

Where [Φ] is the matrix of eigenvectors (mode shapes) and [c_i] is a diagonal matrix of damping coefficients for each mode. Following Chopra (2007), Equation 2-7 can be implemented through the following equation:

$$[C] = [M]\left(\sum_{n=1}^{N}\frac{4\pi\zeta_n}{TM_n}\phi_n\phi_n^T\right)[M] \tag{2-8}$$

Where [M] is the diagonal mass matrix, ζ_n, T_n, and ϕ_n are the percent critical damping, period, and eigenvector (mode shape) for mode n, M_n ($=\phi_n^T[M]\phi_n$) is the generalized mass for mode n, and N is the number of modes included in the calculation. In elastic analyses, a key advantage of modal damping over Rayleigh or mass/stiffness-proportional damping is that the target damping amounts in each vibration mode can be independently specified. It is not clear whether or not this attribute of modal damping has the same benefits in nonlinear analyses, where the vibration modes are not uniquely defined.

2.4.4.1 Selection of Target Damping

In linear-elastic response history analyses, using either modal response history or direct integration, the magnitude of damping is chosen to represent, in an approximate sense, the amount of energy dissipation at the

expected deformation levels. At low deformation levels, prior to significant yielding or damage to structural components, damping values are typically in the range of 0.5% to 5% critical damping in the primary vibration modes. At higher deformation levels, damping values up to 20% of critical (or more) may be specified to approximate hysteretic effects that are not otherwise represented in the analysis.

In nonlinear response history analysis, there are several important factors to consider when specifying viscous damping:

- From a computational standpoint, there are few (if any) advantages of defining [*C*] using Rayleigh or modal damping since the dynamic equilibrium equations are integrated in their full form (i.e., without any modal decomposition). While the resulting direct integration of nonlinear equations presents a large computational effort, the generality of these methods opens up the possibility to define [*C*] in alternative forms, such as through the assembly of explicit elements to represent various damping effects in the building. For example, story shear dampers could be used to model the damping of interior partitions or exterior walls.
- The magnitude of the viscous damping should be chosen carefully, to avoid double-counting damping effects that are modeled explicitly through hysteretic damping.
- Depending on the type and configuration of elements in the model, there is a potential for significant force imbalances to occur as certain elements soften due to inelastic effects. In general, problems associated with force imbalances need to be dealt with through the analysis formulation and software implementation, but analysts should be aware of the potential problems, and when they can arise.

2.4.4.2 Damping in Nonlinear Analysis

Unlike linear analysis, where the elastic stiffness and percentage of critical modal damping remain constant, in nonlinear analysis the stiffness matrix softens due to inelastic effects, and the relative significance of damping can change dramatically during the analysis. For example, consider a case where the damping matrix, [*C*], is defined based on the initial elastic stiffness and the fundamental period of vibration. If the damping matrix is fixed during the analysis, then as the structure softens and the effective first-mode period elongates, the percentage of damping in the elongated fundamental mode will tend to increase. This increase can be reasoned from the equation of motion (Equation 2-3), where the relative significance of the damping matrix would

increase as the stiffness matrix softens. It is also apparent from the trends between effective damping and period shown for mass- and stiffness-proportional damping in Figure 2-27.

Aside from an apparent increase in effective damping as portions of the structure soften, the damping forces that occur across softening components can, in some cases, lead to large force imbalances across those components, as reported in Bernal (1994), Charney (2006), and Hall (2005). This can occur since the damping forces are not captured in the force recovery for the components, and do not generally reduce in proportion to the structural softening. Hall also points out that mass-proportional damping terms can lead to unrealistically large forces in structures with large rigid body motion. One can imagine that rigid body motion effects could be more significant in analyses of tall buildings, where drifts in the upper portions of the building are due, in part, to deformations that occur in lower levels of the building.

In general, solutions to these potential problems require modification to the nonlinear analysis formulation and implementation. Charney (2006) examines issues associated with the stiffness-proportional term of Rayleigh damping and proposes three alternatives to define [C]: (1) based on the initial elastic stiffness matrix and held constant during the analysis; (2) based on the tangent (softened) inelastic stiffness matrix and updated throughout the analysis using the initial proportionality constants, a_M and a_K; and (3) based on the tangent stiffness matrix and updated throughout the analysis, where the proportionality constants, a_M and a_K, are updated to maintain a specified critical damping percentage for the inelastic vibration modes.

Charney (2006) shows how the third option provides the most insurance against developing excessive damping forces, although there is not a clear physical basis for reducing the damping matrix to maintain a fixed critical damping percentage for pseudo-vibration modes based on the tangent stiffness. There are differing views on which of these options are most appropriate. A number of researchers, such as Charney (2006) and Petrini et al. (2008), have advocated the second option (i.e., fixing proportionality constants applied to the updated tangent stiffness matrix) as a practical way to avoid excessive damping in inelastic analysis, but others have countered that the first option (i.e., constant damping) is legitimate.

To illustrate the issues, Powell (2008) examined how the choice of damping formulation influences the effective damping in structures where the initial period has elongated. Table 2-3 summarizes illustrative data from this analysis, where effective damping coefficients are compared for a structure with an initial elastic period of T_1 = 1 second, a higher mode period T_{higher} =

0.15 seconds, critical damping of 4%, Rayleigh damping at T_1 and at T_2, and 4% modal damping at T_1 and T_{higher}. The columns, labeled "Initial Elastic" indicate the amount of effective damping in the first mode and in the assumed higher mode for initial elastic conditions. The columns labeled "Elongated T_1 = 1.5 sec" correspond to a scenario in which the first-mode period is assumed to have elongated from 1 second to 1.5 seconds, corresponding to an effective secant stiffness reduction to 0.44 of the initial stiffness.

Table 2-3 Comparison of Effective Damping with Inelastic Softening and Period Elongation

Case	Damping Formulation	Damping in First Mode (T_1 = 1 sec)		Damping in Higher Mode (T_{higher} = 0.15 sec)	
		Initial Elastic	Elongated T_1=1.5 sec	Initial Elastic	Elongated T_1=1.5 sec
1	$a_m M + a_k K_o$	4%	6%	5.8%	8.7%
2	$a_m M + a_k K_T$	4%	5.7%	5.8%	4.3%
3	$a_k K_o$	4%	6%	26.7%	40%
4	$a_k K_T$	4%	2.7%	26.7%	17.8%
5	$a_m M$	4%	6%	0.6%	0.9%
6	Modal	4%	6%	4%	6%

Based on this information, the following observations can be made:

1. In the higher mode, for both the initial elastic and yielded (elongated) conditions, Case 3 and Case 4 with stiffness-only proportional damping exhibit excessive damping, and Case 5 with mass-proportional damping exhibits very low damping.
2. For the inelastic (elongated) condition, all models, except for Case 4 with tangent stiffness-proportional damping, exhibit effective first-mode damping values about 1.5 times the initial effective damping of 4%.
3. For Rayleigh damping, the differences in effective damping between initial stiffness (Case 1) versus tangent stiffness (Case 2) are relatively insignificant at the fundamental mode due to the dominance of the mass-proportional term, but are significant at higher modes, where tangent stiffness damping is more conservative than constant initial stiffness damping.

Overall, these observations suggest that: (1) stiffness-proportional damping (Cases 3 and 4) should not be used for multi-degree of freedom structures, since this will tend to overdamp higher modes; (2) mass-proportional

damping (Case 5) will conservatively underdamp higher mode effects; and (3) modal damping provides the best control of damping for elastic higher modes and tends to provide reasonable effective damping values for inelastic (elongated) modes.

2.4.4.3 Spurious Damping Effects

Issues regarding spurious damping effects include:

- *Spurious damping associated with inelastic elements with large initial stiffness:* Stiffness-proportional damping (or the stiffness-proportional term of Rayleigh damping) can lead to excessively large damping effects and potential force imbalances in yielding elements that have artificially large initial stiffnesses. This situation can occur in plastic hinge regions that are idealized with springs that have very large initial stiffnesses (to simulate rigid behavior) relative to their inelastic stiffness. Similar problems can arise in gap-type elements or materials that have large stiffness changes between tension and compression loading. Gap-type elements include fiber models used to model reinforced concrete members (including walls), where the initial uncracked (gross) stiffness is much larger than the cracked (effective) stiffness. Short of not using such models, one strategy to avoid potential force imbalances is to exclude the stiffness terms associated with these components from the stiffness-proportional portion of the damping matrix (Charney, 2006). Other strategies include: (1) enforcing upper bounds on the stiffness-proportional damping terms (Hall, 2005); or (2) condensing out certain degrees of freedom (that would lead to spurious damping forces) when formulating the damping matrix (Bernal, 1994). In the commercial analysis program Perform 3D, spurious damping with fiber-type reinforced concrete elements is avoided by using only 15% of the total fiber area stiffness when calculating the stiffness-proportional part of the damping matrix (Powell, 2008).
- *Spurious damping associated with large mass-proportional damping forces:* Hall (2005) describes several situations where large rigid body motions can lead to excessive mass-proportional damping forces. He cites, for example, the case of a base-isolated structure, where large relative velocities between the superstructure and the ground can lead to large mass-proportional damping forces. While Hall does not specifically address tall buildings, one can draw similarities between the base isolated example to a tall building example, where large velocities can occur in the upper floors, giving rise to mass-proportional damping forces that are large and unrealistic. Of particular concern are the forces resisted by mass-proportional damping reacting against fictitious

supports that are not carried through the structure. Hall suggests solutions to minimize or eliminate mass-proportional damping, through greater reliance on stiffness-proportional damping or introducing discrete damping elements. The significance of these large mass-proportional damping forces, and whether or not they are realistic, will depend on the nature of the underlying energy dissipation mechanisms in the structure. The significance of the damping model assumption increases as the magnitude of the damping forces increases relative to other forces in the analysis.

2.4.4.4 Explicit Damping Elements

Considering potential problems that can be encountered using Rayleigh (mass- and stiffness-proportional) or modal damping with inelastic analysis, another strategy is to define explicit damping elements to represent the likely sources of damping. For example, damping provided by partition walls and the exterior facade could be modeled as shear damping elements, which act between adjacent floors up the building height. Damping provided by the foundation and surrounding soils could be modeled using springs and dashpots.

Such an approach would have the advantage of more accurately representing the physical sources of damping. In doing so, one would need to identify and model all significant sources of damping, considering the spatial distribution in the building. This would include the challenging task of quantifying the damping parameters for each such damping element, and accounting for forces developed in the elements. Since the target damping would likely still be based on overall damping response, one would need to relate the contributions of the individual damping elements to the overall response and calibrate the damper properties accordingly, and the question of whether or not the damping assigned to each explicit damping element should vary with displacement and/or velocity amplitudes would still need to be addressed.

2.4.5 Recommendations for Nonlinear Analysis and Design

For nonlinear analysis, damping (energy dissipation) effects are included through a combination of hysteretic and viscous damping. In general, damping effects caused by structural components of the seismic-force-resisting system are implicit to the analysis through the hysteretic response of the inelastic component models. Damping effects caused by other structural members (e.g., gravity framing), soil-foundation-structure interaction, and nonstructural components that are not otherwise modeled in the analysis can be incorporated through equivalent viscous damping. The amount of viscous

damping should be adjusted based on specific features of the building design, and may be represented by either modal damping, explicit viscous damping elements, or a combination of stiffness- and mass-proportional damping (e.g., Rayleigh damping). Among the various alternatives, it is generally recommended to model viscous damping using modal damping, Rayleigh damping, or a combination of the two. Care should be taken when specifying stiffness-proportional damping components of Rayleigh damping to avoid overdamping in higher modes, or force imbalances in gap-type elements and rigid-plastic materials and components.

Generally, the amount of damping is quantified in terms of a percentage of critical damping in one or more elastic vibration modes, although it is also recognized that distinct vibration modes and frequencies do not exist for nonlinear response as they do with elastic analysis. Existing guidelines suggest the use of viscous damping values ranging from 2% to 5% of critical for nonlinear response history analyses of typical buildings subjected to strong ground motions. Laboratory tests suggest that damping values of about 1% for steel frame structures and 2% to 3% for reinforced concrete structures be used to model energy dissipation that occurs in bare structural systems, under small deformations, that is not accounted for in typical hysteretic models. Measured data from earthquake induced motions of actual buildings suggest damping values in the range of 1% to 5% for quasi-elastic response of buildings over 30 stories tall. Measurements in actual buildings indicate that the damping in tall buildings is lower than damping in low- to mid-rise buildings.

The following values of equivalent viscous damping are suggested as appropriate for use in nonlinear response history analysis of typical buildings, in which most of the hysteretic energy dissipation is accounted for in the nonlinear component models of the structural members of the seismic-force-resisting system:

$$D = \alpha/30 \quad (\text{for } N < 30) \tag{2-9}$$

$$D = \alpha/N \quad (\text{for } N > 30) \tag{2-10}$$

where D is the maximum percent critical damping, N is the number of stories, and α is a coefficient with a recommended range of $\alpha = 60$ to 120. In general, structural steel systems would tend toward the lower range of damping ($\alpha = 60$), and reinforced concrete systems of would tend toward the upper range ($\alpha = 120$). Figure 2-28 shows damping ranges between 2% to 4% for 30-story buildings and 1% to 2% for 70-story buildings. Damping

values for specific buildings should reflect the structural material and system, the foundation conditions, and the nonstructural partition walls.

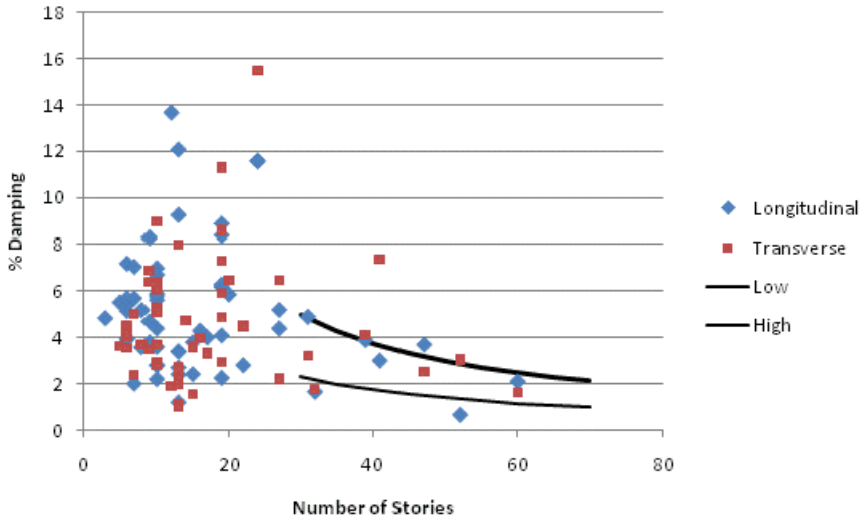

Figure 2-28 Suggested target limits on damping.

Given uncertainty in the appropriate values of assumed damping, and the alternative ways in which damping can be mathematically modeled, it is generally advisable to ascertain the sensitivity of the building response to the assumed value of damping. Sensitivity studies should be conducted at appropriate earthquake ground motion intensities that reflect the amplitude of motions expected for various limit states. Where inelastic response is significant, as might be expected under Maximum Considered Earthquake (MCE) level ground motions, spurious damping forces should be checked for, and the methods outlined above should be employed to mitigate their effects.

2.5 Expected Properties and Uncertainty

Component model parameters should be defined based on median properties, as opposed to nominal or minimum-specified properties that are otherwise used in design. Use of median structural properties is important for providing an accurate and unbiased measure of the expected response of the overall system. Nonlinear response assessment based on median values permits calculation of median (50^{th} percentile) values of response for one or more levels of ground motion intensity. The goal is to avoid any systematic bias that could result from the use of nominal instead of expected properties in a structure.

For practical reasons, and because data to characterize the properties of structural parameters are incomplete, median values are not available, and "expected values" (or mean values) are often used. For parameters that are

normally distributed, the median and mean values are equal. However, many properties of structural materials and components have skewed distributions that are often approximated by lognormal distributions. In lognormal distributions, median values tend to be somewhat lower than mean values.

While, in theory, it is most appropriate to base the structural analysis on median values, in practice, the mean and median are often close enough to result in similar response prediction. Many available sources for expected material properties are based on mean rather than median values, such as the R_y factors used to calculate effective steel yield strengths. Hence, it is common and generally accepted practice to base modeling parameters on the mean (expected) values when median values are not available.

2.5.1 Statistical Characterization of Modeling Uncertainties

Variability in component response quantities should be assessed, taking into account underlying sources of uncertainty. Variability in component response is important for estimating the overall system response variability, either based on judgment or sensitivity studies. Some variability can be determined from test data statistics; however, a significant portion of the variability is often associated with factors that may not be reflected in typical laboratory testing programs. For example, whereas comparisons to test data can help establish how well the predicted model parameters agree with the test data, these comparisons do not capture differences that can arise due to modeling (epistemic) uncertainty when the model is applied to component configurations and member properties that are different from those tested and used to develop the model. Additional uncertainties are introduced by material variability, dimensional tolerances, and construction quality, the full effects of which are rarely captured in laboratory tests.

Variability is generally described through the standard deviation of the data. For data that follow a normal distribution, the coefficient of variation (standard deviation divided by the average value) provides a more intuitive index of the variability. For data that follow a lognormal distribution, the standard deviation of the natural logarithm of the data is a common measure of dispersion. This measure is close to the coefficient of variation when the variability is lower than 0.3.

In general, lognormal distributions tend to be a reasonably good fit to many types of data, such as strength and deformation quantities, where the distribution is skewed towards larger values. This tendency, combined with mathematical advantages of modeling all parameters in a simulation with the

same type of distribution, make it common to assume lognormal distributions to describe the uncertainties in modeling parameters.

Generally speaking, variability is less for strength parameters than for stiffness and deformation parameters. For example, a study of test data for reinforced concrete beam columns by Haselton and Deierlein (2007) reported dispersions in member strengths to be on the order of 0.1, while dispersions in capping or post-capping deformation parameters were 0.5 to 0.6. These values considered variations in measured response from a large database (over 200 tests) of reinforced concrete beam-columns. The larger dispersion at large deformations was due, in part, to the sparse amount of data and greater reliance on empirical models to simulate response at large deformations.

Porter et al. (2007) recommend a default dispersion value ("β-value") of 0.4 in the absence of compelling evidence for smaller values. Based on these observations, the following values of modeling parameter dispersion are suggested when no other information is available:

- 0.2 for dispersion in strength,
- 0.3 for dispersion in stiffness and yield deformation, and
- 0.5 for dispersion in capping and post capping deformation.

Currently, there is no consensus on how variability in modeling parameters (modeling uncertainties) should be considered in nonlinear analysis. It has been suggested that, given the large uncertainties associated with extreme ground motions, modeling uncertainties should be ignored. At the other extreme, Monte Carlo methods can be used to explicitly simulate variability introduced by all significant uncertainties in modeling parameters.

A related question is the extent to which variability affects both the demand and capacity side of the equation. In elastic analyses, it is relatively straightforward to separate the demand and capacity effects. In nonlinear analyses, demand and capacity are coupled. Variability in plastic hinge properties will affect both the calculated demands and the rotation limits that are used to assess the response.

Liel et al. (2008) have used several approaches to demonstrate that dispersions in collapse fragility introduced by modeling uncertainties is on the order of 0.5, which is the same order of magnitude as dispersion caused by ground motion record-to-record variability (0.4). Assuming that these two sources of uncertainty are independent, the combined uncertainty is obtained by a square-root-sum-of-squares (SRSS) combination of the values,

which in this case is equal to 0.65. Liel et al. (2008) have also demonstrated challenges associated with rigorously accounting for modeling uncertainties, which include assumptions on the correlation of variability between the many components that comprise a building structure.

In FEMA P-695, modeling uncertainty is considered through adjustments in the collapse fragility curve. These adjustments are based on judgments related to the accuracy and robustness of the underlying test data, modeling parameters, and attributes of the analytical model. In the FEMA P-695 methodology, total system collapse uncertainty, β_{TOT}, varies between 0.43 for systems in which the input parameters and the model are well-defined, and 0.95 where the information is not so well-defined.

In the absence of a more comprehensive evaluation of the sources of variability in a response history analysis, the following values of composite uncertainty are suggested:

- 0.5 for systems that are well-defined, with elastic or near elastic response, and
- 0.65 for systems with highly nonlinear response.

These values can be used in conjunction with median predicted displacement response (or component force demands) to evaluate important limit states on a probabilistic basis (e.g., to determine the probability at which a calculated demand quantity will exceed a specified capacity limit).

Chapter 3
Modeling of Frame Components

This chapter describes recommendations for modeling of steel and reinforced concrete frame components, and the derivation of modeling parameters and acceptance criteria from available sources of experimental data.

3.1 Modeling Parameters for Frame Components

Modeling parameters for nonlinear analysis depend on the details and assumptions inherent in the component model formulations. Nonlinear models can be distinguished by their fundamental (physical) versus phenomenological (behavioral) characteristics. Parameters for physical models tend to be defined in terms of basic material properties, while parameters for phenomenological models are defined based on the overall component response.

Parameters of interest for nonlinear modeling of frame components are identified in the reference force-deformation relationship introduced in Figure 2-8. Key modeling parameters, which are either specified explicitly (in concentrated hinge models) or modeled implicitly (in finite element models), can be characterized as follows:

- *Stiffness Parameters:* Key stiffness parameters include the pre-yield (elastic) stiffness, post-yield (strain hardening/softening) stiffness, and the post-capping (degrading) stiffness. Stiffness prior to yielding is usually characterized by an effective or secant stiffness, which can vary depending on the type of model and limit state of interest. When evaluating serviceability limit states at low deformation levels, the pre-yield stiffness is the initial stiffness. Alternatively, when evaluating behavior at large deformations, it is more appropriate to calibrate the pre-yield stiffness to a secant slope evaluated at some fraction (40% to 100%) of the yield strength. Post-yield and post-capping stiffness parameters are characterized by a tangent slope.
- *Strength Parameters:* Key strength parameters include the yield strength, maximum strength, and residual strength at large deformations. In general, yield and maximum strength parameters are needed in all nonlinear analyses. The extent to which residual strength is important depends on how far the structure is responding beyond the deformation

at which degradation occurs. Basic strength parameters are usually defined on the basis of the initial (monotonic) force-deformation curve, unless hysteretic energy dissipation (cyclic deterioration) adjustments are made.

- *Deformation Parameters:* Key deformation parameters include the deformations associated with each key strength parameter (e.g., yield deformation, capping deformation, and ultimate deformation). Deformation parameters together with the strength parameters define the characteristic backbone curve.

Nonlinear modeling of frame components also requires consideration of cyclic deterioration, either explicitly or implicitly. The anchor points of the initial monotonic backbone curve, or the modified cyclic (skeleton) curve, will depend on how cyclic deterioration is handled in the model. Options for modeling cyclic deterioration are described in Section 2.2.5, and illustrated in Figure 2-17.

While fiber or finite element models can be used, recommendations for modeling of frame components are focused on global force-deformation response parameters for concentrated hinge models, including effective stiffness, strength, and plastic deformation. If fiber or finite element modeling formulations are used, the resulting behaviors should be consistent (i.e., calibrated) with the global response parameters provided herein.

3.2 Nonlinear Modeling of Steel Beam and Column Components

Modeling recommendations for steel beam and column components of frames are based on the assumption that beams and columns are modeled as lumped plasticity elements, consisting of elastic elements with concentrated plastic hinges at each end. Concentrated plastic hinges are represented by rotational springs with properties determined by principles of engineering mechanics supplemented with backbone parameters and deterioration rules based on data from experimental studies.

Use of lumped plasticity elements requires concentrated hinge locations to be decided up front. Concentrated hinges should be located in the model where they best represent the integrated effect of distributed inelasticity. In moment-resisting frames, the joint panel zone is generally modeled as a separate element, and concentrated hinges are placed outside the panel zone region. For conventional steel moment-resisting connections, with no flange reinforcement or flange reductions, the concentrated hinge can be placed at the column face. For reinforced connections (e.g., cover plates, haunches

and fins), and reduced beam section (RBS) connections, the concentrated hinge should be located away from the column face, as recommended in FEMA 350, *Recommended Seismic Design Criteria for New Steel Moment Frame Buildings* (FEMA, 2000a).

3.2.1 Behavioral Considerations for Steel Beams

Modeling of plastic hinge regions in beams could be based on standard material stress-strain curves, curvature analysis, and integration of curvatures to obtain rotations, if the base material controlled behavior, and no local failure or deterioration modes occurred. Unfortunately, this is rarely the case, and a curvature analysis without consideration of special behavior modes for steel beams can be misleading.

3.2.1.1 Connection Type

Modeling and acceptance criteria depend on the type of connection that is used to transfer forces (moments, shears, and axial forces) between beams and columns. Types of connections include unrestrained, partially-restrained, and fully-restrained beam-column connections.

In unrestrained (simple) connections it is usually assumed that moment transfer is negligible. Experiments have shown, however, that the rotational strength and stiffness of composite shear tab connections can be substantial (Liu and Astaneh-Asl, 2000 and 2004). Lateral strength and stiffness contributions from the gravity system can provide significant benefits for lateral stability at large displacements when P-Delta and component degradation effects are strongly influencing response. Incorporation of gravity system strength and stiffness in the analytical model is at the discretion of the user. FEMA 355D, *State of the Art Report on Connection Performance* (FEMA, 2000c) and Liu and Astaneh-Asl (2000 and 2004) provide data for the basis of assumed properties.

Partially restrained connections, in which there is significant rotational stiffness, can be an intended part of the seismic-force-resisting system. In such cases, the hysteretic behavior relating beam and column rotation must be modeled explicitly. If the connection is of sufficient strength to develop inelastic actions in the beam, separate modeling of beam-column joint flexibility and concentrated hinging in the beam is necessary. Partially restrained connections include:

- Extended end plate connections,
- Bolted flange plate connections,
- T-stub connections,

- Double flange angle connections, and
- Shear tab connections in a composite floor system.

Under specific conditions some of the connections listed above may also be considered fully restrained. Information on hysteretic modeling of moment-rotation relationships for partially restrained connections, including deterioration characteristics, is summarized in FEMA 355D.

Fully restrained connections are those in which the relative rotation between the beam and the column is small in comparison with joint rotations and panel zone distortions. In such connections, the rotation capacity can be limited by localized fractures from a variety of sources, including:

- Inadequate weld material quality or workmanship,
- Inadequate ductility of base material,
- Early cracking at web copes (weld access holes),
- Stress and strain concentrations in the beam flanges at weldments,
- Excessive shear deformations in joint panel zones,
- Bolt slippage in the web shear tab connection, and
- Net section fracture in the case of cover-plated bolted connections.

Occurrence of these failure modes should be avoided through proper design and detailing, since it is difficult to realistically incorporate these failure modes in currently available nonlinear component models. It is assumed that proper design criteria have been applied so that these localized failure modes need not be considered in the analytical modeling of tall buildings.

Localized failures in fully restrained connections have been extensively investigated, and criteria have been developed to prevent or at least delay such failure modes over the range of cumulative deformations expected in large earthquakes. Appropriate design criteria for preventing such failures are provided in FEMA 350, FEMA 355D, AISC 358 *Prequalified Connections for Special and Intermediate Steel Moment Frames for Seismic Applications* (AISC, 2005a), and AISC 341 *Seismic Provisions for Structural Steel Buildings* (AISC, 2005b).

3.2.1.2 Local and Lateral-Torsional Buckling

Local and lateral-torsional buckling control deterioration in the hysteretic behavior, and these deterioration modes become noticeable at relatively small plastic rotations, even if code requirements for compact sections and seismic lateral bracing are satisfied.

Local and lateral-torsional buckling have been studied for decades, but the consequence of these phenomena cannot be quantified analytically with confidence. Gioncu and Mazzolani (2002) point out the complexities of the phenomena, and advocate the use of a plastic collapse mechanism method based on yield line theory to capture and quantify local instabilities, but fall short on providing practical solutions that can be applied directly in global analytical modeling of structures.

The same is true for the many finite element models that have been developed and published in the literature. At this time this is not quite feasible, thus, the only practical solution is to develop empirical rules for adjusting of the backbone curve and cyclic deterioration parameters for local and lateral-torsional buckling. Data for this purpose are discussed in Lignos and Krawinkler (2009).

3.2.1.3 Residual Strength

Most steel elements with hysteretic behavior that deteriorates due to local instabilities approach stabilization of the hysteretic response at large inelastic deformations. This stabilization occurs at a residual strength level that is some fraction of the yield strength. It happens when stresses originally carried in the buckled portions of the cross section have redistributed to unbuckled portions of the cross section. While full stabilization rarely occurs, it is observed that the rate of deterioration becomes small enough to be neglected in analytical modeling.

3.2.1.4 Ductile Tearing

At very large plastic rotations, cracks can develop in the steel base material at the apex of the most severe local buckle, followed by rapid crack propagation, ductile tearing, and essentially complete loss of flexural strength. The deformation associated with this rapid strength loss is termed the ultimate plastic rotation.

3.2.1.5 Slab Effect

Steel beams are often part of a composite slab system. The presence of a composite slab will move the neutral axis, change the moment-rotation relationship, and affect the bending strength in both the positive and negative directions (Ricles et al., 2004). This effect is not captured in tests of bare steel connection subassemblies. In the positive moment direction (top flange in compression), the presence of a slab will delay local instabilities but will cause higher tensile strain demands in the bottom flange and welds. In the

negative moment direction (bottom flange in compression), the presence of a slab can accelerate the occurrence of lateral-torsional buckling.

If the slab is thick, or the beam depth is small, this increase in strength can be a dominant factor. In the example shown in Figure 3-1, the capping rotation is unsymmetric in the two loading directions (about 3% in positive bending versus 1.2% in negative bending).

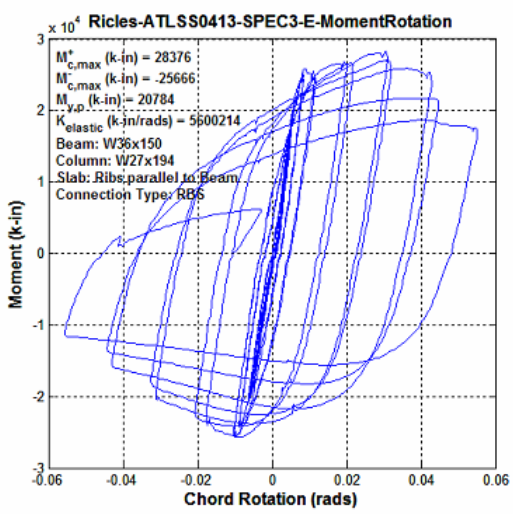

Figure 3-1 Hysteretic response of a steel beam with composite slab (data from Ricles et al., 2004).

Unfortunately, the majority of currently available experimental test data come from tests that do not include a composite slab. Because of the scarcity of data on slab effects, recommended modeling parameters are based on bare steel beam tests without the presence of a composite slab.

3.2.1.6 Axial restraint

In an actual system, the floor slab and adjacent columns will restrain axial contraction or expansion of the top and bottom flanges of a steel beam, reducing the effect of local instabilities on rotation capacities. In most experimental tests, however, the beam is free to contract or expand in the axial direction. Axial restraint that is provided by the slab and adjacent columns will have a positive effect on rotation capacity that is not captured in currently available experimental data. The extent to which this effect helps in increasing rotation capacity is unknown, but estimated to be significant. Additional testing is necessary to reliably quantify this effect for use in nonlinear analysis.

3.2.2 Quantification of Properties for Steel Beams

This section describes the basis for quantification of steel beam parameters including the pre-capping plastic rotation, θ_p, and post-capping rotation, θ_{pc}, for the initial moment-rotation backbone curve defined in Figure 2-8, as well as the reference cumulative plastic rotation parameter, Λ, defined as part of Equation 2-2 for calculating the hysteretic energy dissipation parameter (for cyclic deterioration). These parameters are needed to develop a moment-rotation model that explicitly incorporates cyclic deterioration, (modeling Option 1 presented in Section 2.2.5).

Lumped plasticity (concentrated hinge) and distributed inelasticity models for steel components are available in the literature (e.g., Ziemian et al., 1992a and 1992b; Liew et al., 1993a and 1993b; Kilic, 1996; Kunnath, 2000) and reinforced concrete components (e.g., Spacone et al., 1996; Taylor et al., 2003; Scott et al., 2004). Few of these models, however, consider all of the behaviors that can contribute to strength and stiffness deterioration, which are important when predicting structural response at Maximum Considered Earthquake (MCE) level intensities, or near-collapse.

Unless otherwise specifically identified, observations and recommendations are based on an evaluation of an extensive database of steel beams tests. The database contains results from over 300 experiments on beam-column subassemblies, currently available at http://www.nees.org.

3.2.2.1 Experimental Data

Experimental data from steel beam tests have been collected in several databases (PEER, 2007; Kawashima, 2007; Lignos and Krawinkler, 2007; Lignos and Krawinkler, 2009). These data were used to quantify properties for nonlinear modeling of steel beams.

The experimental results documented in Lignos and Krawinkler (2007 and 2009) are also utilized to some extent in FEMA 355D and ASCE/SEI 41-06, *Seismic Rehabilitation of Existing Buildings* (ASCE, 2007a). It should be noted, however, that a direct comparison with the recommendations contained in FEMA 355D and criteria presented in ASCE/SEI 41-06 cannot be made because of differences in how key parameters have been defined. For example, the parameter "θ_p" in FEMA 355D differs from the definition in Figure 2-8. In FEMA 355D, "θ_p" is essentially the plastic component of the ultimate deformation as defined in modeling Option 4 (Section 2.2.5) where no strength deterioration is included in the analytical model.

Data on backbone curve parameters (θ_p and θ_{pc}) and cyclic deterioration (reference cumulative plastic rotation, Λ) are obtained from calibrations in which the parameters of the deterioration model are matched to experimental moment-rotation relationships (Lignos and Krawinkler, 2009).

A typical match between experimental results and analytical modeling is shown in Figure 3-2. Data presented here are for inelastic deformations in the beams only, even though in many tests additional inelastic deformations occurred in the joint panel zones and in the columns. Tests in which brittle fracture occurred at the beam-column connection have not been included in the data.

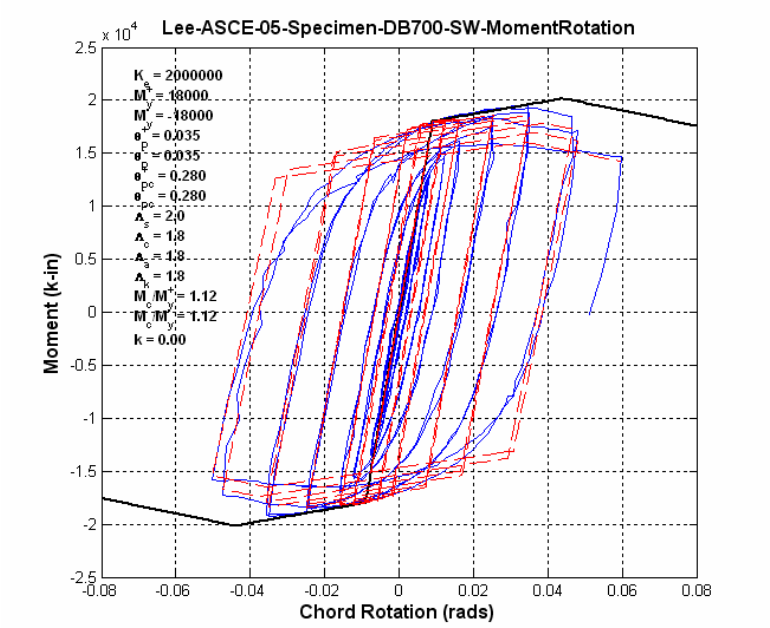

Figure 3-2 Plot showing comparison of deterioration model to experimental results.

The following four data sets were used to obtain statistical information on trends between modeling parameters and selected geometric properties:

- All tests on beams with non-RBS connections, for beam depths, d, ranging from 4 inches to 36 inches, except tests with early fracture problems
- All tests on beams with RBS connections, for beam depths, d, ranging from 18 inches to 36 inches
- Applicable tests on beams with non-RBS connections, for beam depths, $d \geq 21$ inches
- Tests on beams with RBS connections, for beam depths, $d \geq 21$ inches

Except for reduced beam section (RBS) connections, no other distinction is made by connection type. The number of tests is too small and the trends are not sufficiently clear to justify additional distinctions based on other connection types. Because the data contain many tests on small section sizes, data sets for beam depths greater than 21 inches were created to observe trends in section sizes that are likely to be part of seismic-force-resisting systems in tall buildings. Tests on beams with composite slabs were not considered in any data set.

3.2.2.2 Statistical Information from Available Data Sets

Cumulative distribution functions (CDFs) for pre-capping plastic rotation, θ_p, post-capping rotation, θ_{pc}, and reference cumulative plastic rotation, Λ, obtained from the four data sets are shown in Figures 3-3, 3-4, and 3-5, respectively.

All specimens in each data set are represented, spanning a wide range of geometric and material properties. The curves shown represent log-normal distributions fitted to the data points. The plots reveal statistical characteristics, but do not display dependencies on individual properties.

Each plot shows CDFs for RBS and non-RBS ("other than RBS") connections. Results for the four data sets are comparable, but, in general, median values of parameters for beams with non-RBS connections are smaller (and the dispersion is larger) than for beams with RBS connections.

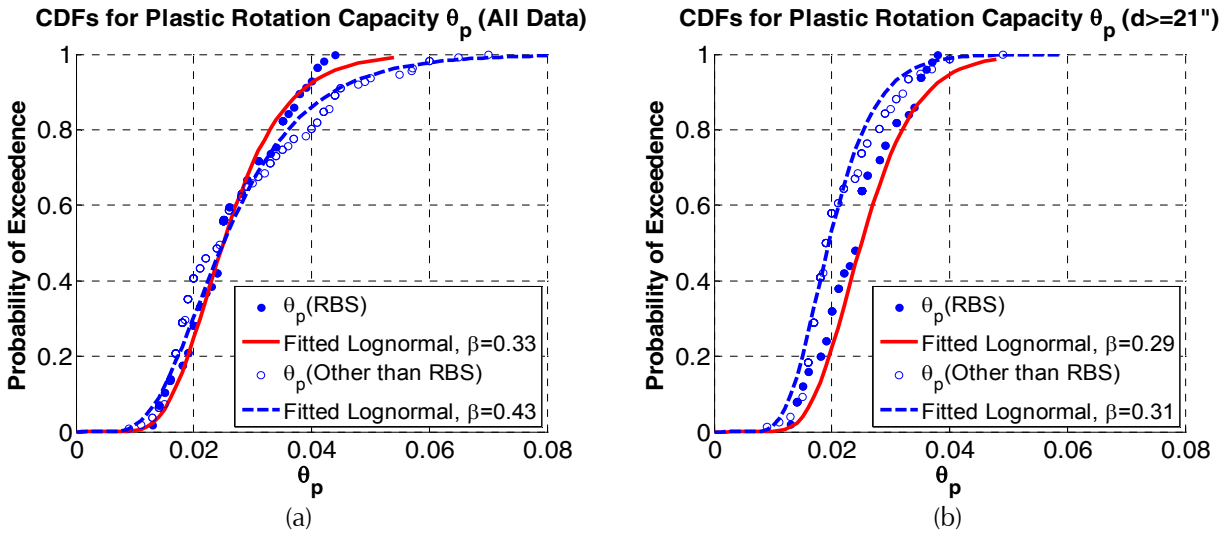

Figure 3-3 Cumulative distribution functions for pre-capping plastic rotation, θ_p, for: (a) full data sets; and (b) beam depths, $d \geq 21$ in.

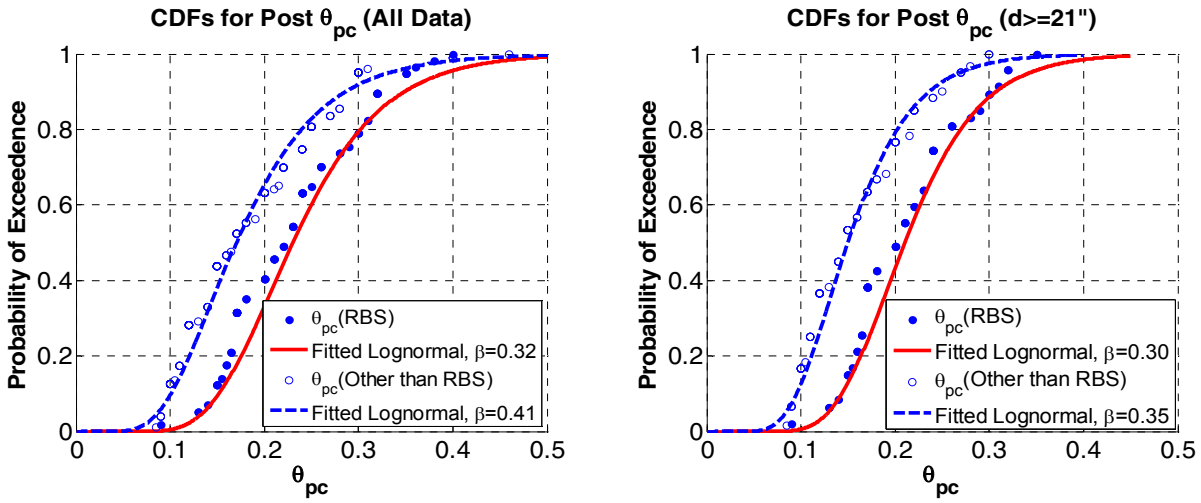

(a) (b)

Figure 3-4 Cumulative distribution functions for post-capping rotation, θ_{pc}, for: (a) full data sets; and (b) beam depths, $d \geq 21$ in.

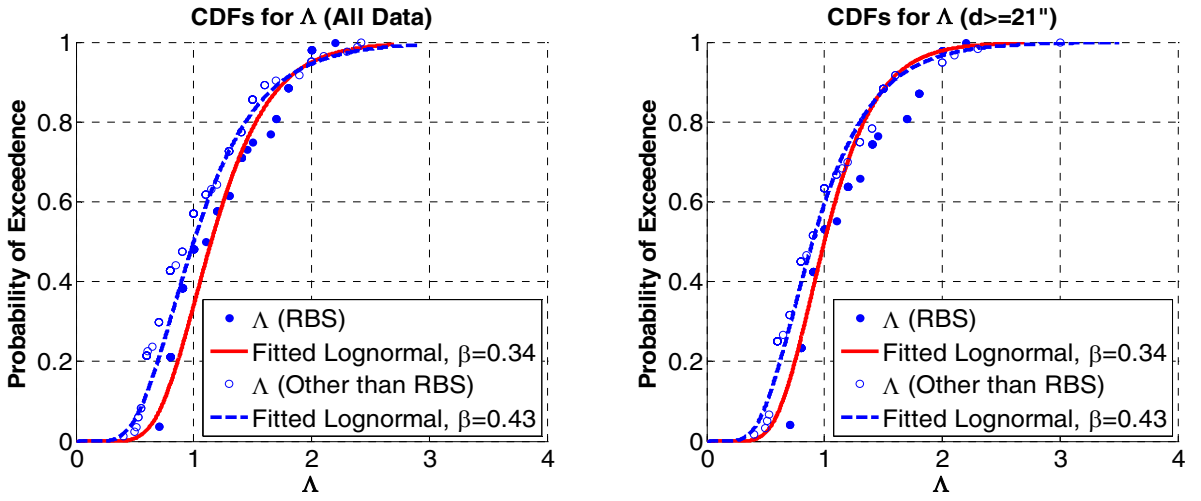

(a) (b)

Figure 3-5 Cumulative distribution functions for reference cumulative plastic rotation, Λ, for: (a) full data sets; and (b) beam depths, $d \geq 21$ in.

3.2.2.3 Observed Trends

Dependence on beam depth, d. An increase in beam depth, d, is usually associated with a decrease in plastic rotation capacity. This is evident in Figure 3-6, which shows a linear regression of data for pre-capping plastic rotation, θ_p, for all non-RBS data, with beam depths ranging from 4 inches to 36 inches. The dependence is driven, in part, by the incorporation of small sections in the database, and is smaller for the larger beam sizes of relevance to tall building systems ($d \geq 21$ inches). Others have noted the strong

dependence of the plastic rotation capacity on beam depth (FEMA 350 and FEMA 355D). Reasons for this dependence are presented in Roeder (2002a and 2002b).

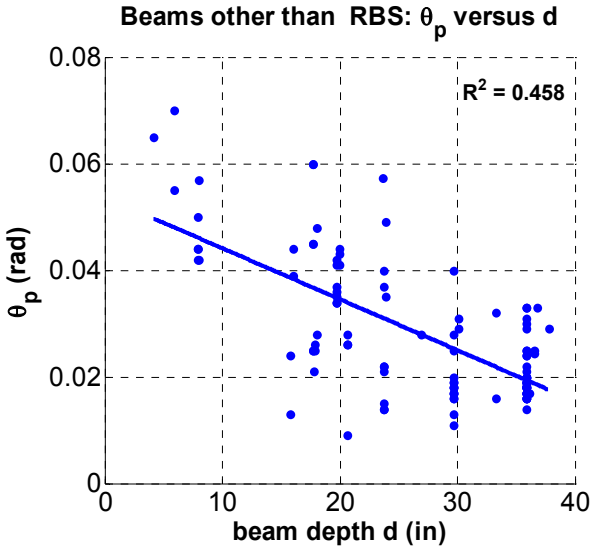

Figure 3-6 Dependence of pre-capping plastic rotation, θ_p, on beam depth, d, for non-RBS connections, full data set.

Dependence on shear span to depth ratio, L/d. The plastic rotation capacity for a given beam section is linearly proportional to the ratio between the beam shear span, L (distance from plastic hinge location to point of inflection) and depth, d. This proportionality is shown in Figure 3-7 for all non-RBS data (beam depths ranging from 4 inches to 36 inches), but this strong dependence on L/d does not hold true for beam depths larger than 21 inches.

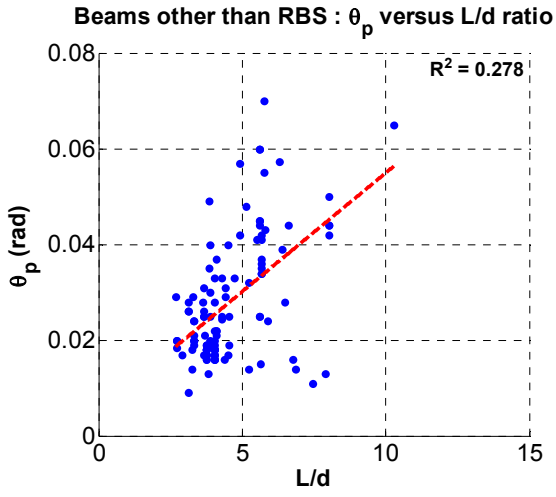

Figure 3-7 Dependence of pre-capping plastic rotation, θ_p, on shear span to depth ratio, L/d, for non-RBS connections, full data set.

For beams between 21 inches and 36 inches deep, the pre-capping plastic rotation capacity is only weakly dependent on L/d. The reason for this is that most deep beams are susceptible to a predominance of web buckling and lateral-torsional buckling, which increase with an increase in the L/d ratio. This phenomenon offsets the curvature integration effect of a larger plastic hinge length. The following observations are made for beams with depths larger than 21 inches:

- The pre-capping plastic rotation capacity and other modeling parameters are mildly sensitive to the shear span to depth ratio for beams that are susceptible to web buckling and lateral-torsional buckling. It does not hold true for beams in which both flanges are braced laterally at close intervals.
- A description of beam plastic deformation capacity in terms of the ductility ratio θ_p/θ_y is often misleading because θ_y increases linearly with L (for a given beam section), but θ_p does not.

Dependence on L_b/r_y. The ratio of L_b, defined as the distance from the column face to the nearest lateral brace, and r_y, the radius of gyration about the y-axis of the beam, is associated with protection against premature lateral-torsional buckling. Seismic codes require that this ratio be less than $2500/F_y$. Data indicate that the pre-capping plastic rotation is somewhat, but not greatly affected by L_b/r_y, provided the ratio is close to or smaller than the code-specified limit. Counterintuitively, providing lateral bracing close to the RBS portion of a beam does not lead to a significant improvement in θ_p. A similar observation was made by Yu et al. (2000).

Dependence on $b_f/2t_f$. Using beams with a small width/thickness ratio of the beam flange, $b_f/2t_f$, has only a small effect on the pre-capping plastic rotation capacity. This observation does not negate the benefit of using beams with small values of $b_f/2t_f$, it merely points out that none of the geometric parameters can be evaluated comprehensively in isolation. For most of the deeper beams in the database, a small $b_f/2t_f$ ratio implies a narrow-flange beam with small r_y and large d/t_w, both of which have a detrimental effect on θ_p. Moreover, the data show a clear benefit of a smaller $b_f/2t_f$ ratio for the parameters θ_{pc} and Λ.

Dependence on h/t_w. The depth to thickness ratio of the beam web, h/t_w, is important for all three modeling parameters. Figure 3-8 shows that all three modeling parameters decrease with increasing h/t_w ratios, for both RBS and non-RBS connections.

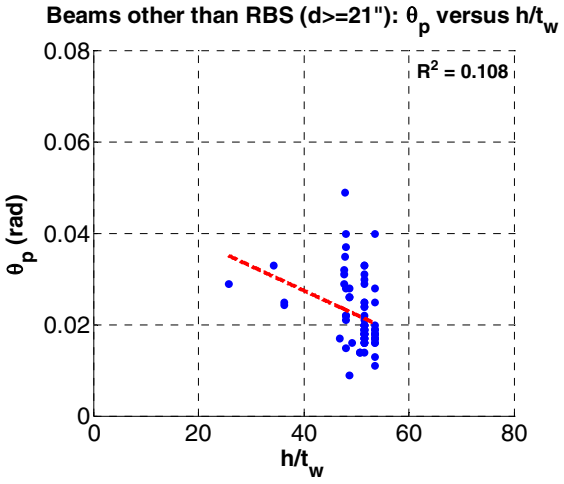

(a) Pre-capping plastic rotation, θ_p; non-RBS

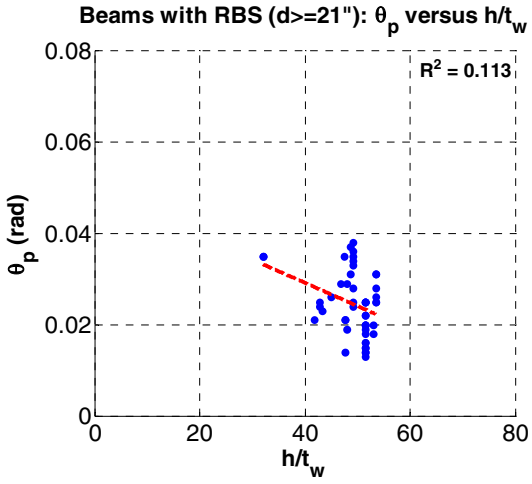

(b) Pre-capping plastic rotation, θ_p; RBS

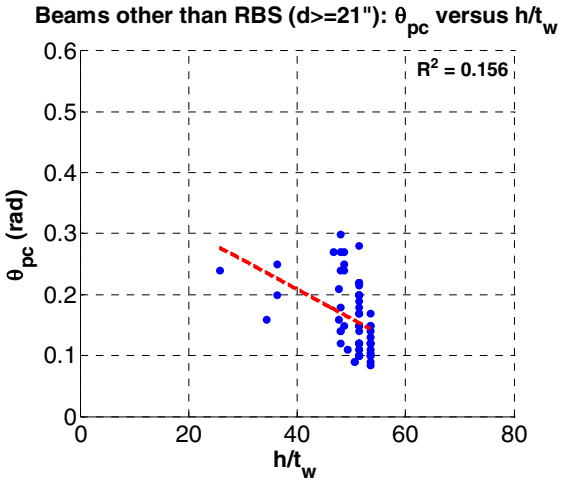

(c) Post-capping rotation, θ_{pc}; non-RBS

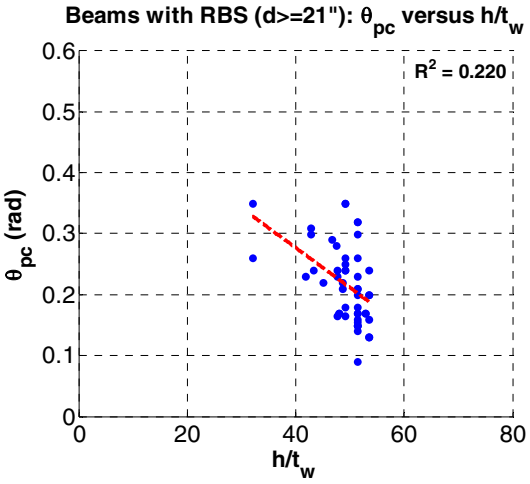

(d) Post-capping rotation, θ_{pc}; RBS

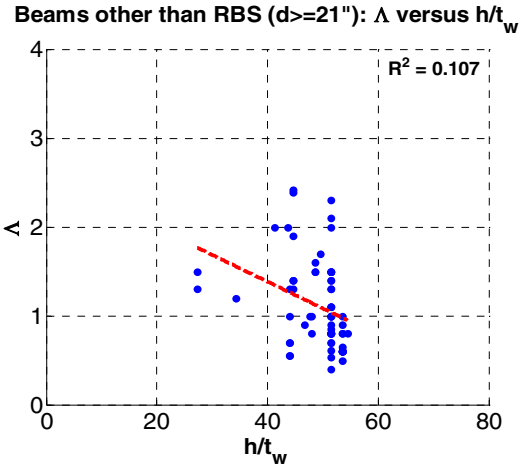

(e) Cumulative plastic rotation, Λ; non-RBS

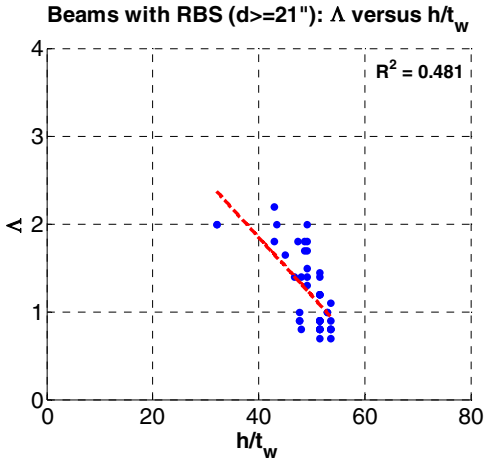

(f) Cumulative plastic rotation, Λ; RBS

Figure 3-8 Dependence of modeling parameters on h/t_w, for beam depths $d \geq 21$ in., and RBS and non-RBS connections.

3.2.2.4 Regression Equations for Modeling Parameters

It is understood that the trends alone do not provide sufficient information to fully quantify modeling parameters. Empirical equations based on multi-variate regression analysis that account for combinations of geometric and material parameters in the quantification of modeling parameters are suggested.

Data were exploited to derive regression equations for the modeling parameters θ_p, θ_{pc}, and Λ. The equations have been derived from the full RBS and non-RBS data sets, using the full range of beam depths available in each set (4 in. $\leq d \leq$ 36 in. for non-RBS connections, and 18 in. $\leq d \leq$ 36 in. for RBS connections). The following equations are suggested to estimate modeling parameters as a function of geometric and material parameters that were found to be statistically significant.

Pre-capping plastic rotation, θ_p, for beams with non-RBS connections:

$$\theta_p = 0.087 \cdot \left(\frac{h}{t_w}\right)^{-0.365} \cdot \left(\frac{b_f}{2 \cdot t_f}\right)^{-0.14} \cdot \left(\frac{L}{d}\right)^{0.34} \cdot \left(\frac{d}{c^1_{unit} \cdot 21"}\right)^{-0.721} \cdot \left(\frac{c^2_{unit} \cdot F_y}{50}\right)^{-0.23} \quad (3\text{-}1)$$

Pre-capping plastic rotation, θ_p, for beams with RBS connections:

$$\theta_p = 0.19 \cdot \left(\frac{h}{t_w}\right)^{-0.314} \cdot \left(\frac{b_f}{2 \cdot t_f}\right)^{-0.10} \cdot \left(\frac{L_b}{r_y}\right)^{-0.1185} \cdot \left(\frac{L}{d}\right)^{0.113} \cdot \left(\frac{d}{c^1_{unit} \cdot 21"}\right)^{-0.76} \cdot \left(\frac{c^2_{unit} \cdot F_y}{50}\right)^{-0.07} \quad (3\text{-}2)$$

Post-capping rotation, θ_{pc}, for beams with non-RBS connections:

$$\theta_{pc} = 5.70 \cdot \left(\frac{h}{t_w}\right)^{-0.565} \cdot \left(\frac{b_f}{2 \cdot t_f}\right)^{-0.80} \cdot \left(\frac{d}{c^1_{unit} \cdot 21"}\right)^{-0.28} \cdot \left(\frac{c^2_{unit} \cdot F_y}{50}\right)^{-0.43} \quad (3\text{-}3)$$

Post-capping rotation, θ_{pc}, for beams with RBS connections:

$$\theta_{pc} = 9.62 \cdot \left(\frac{h}{t_w}\right)^{-0.513} \cdot \left(\frac{b_f}{2 \cdot t_f}\right)^{-0.863} \cdot \left(\frac{L_b}{r_y}\right)^{-0.108} \cdot \left(\frac{c^2_{unit} \cdot F_y}{50}\right)^{-0.36} \quad (3\text{-}4)$$

Reference cumulative plastic rotation, Λ, for beams with non-RBS connections:

$$\Lambda = \frac{\mathrm{E}_t}{M_y} = 500 \left(\frac{h}{t_w}\right)^{-1.34} \cdot \left(\frac{b_f}{2 \cdot t_f}\right)^{-0.595} \cdot \left(\frac{c^2_{unit} \cdot F_y}{50}\right)^{-0.36} \quad (3\text{-}5)$$

Reference cumulative plastic rotation, Λ, for beams with RBS connections:

$$\Lambda = \frac{E_t}{M_y} = 592 \cdot \left(\frac{h}{t_w}\right)^{-1.138} \cdot \left(\frac{b_f}{2 \cdot t_f}\right)^{-0.632} \cdot \left(\frac{L_b}{r_y}\right)^{-0.205} \cdot \left(\frac{c^2_{unit} \cdot F_y}{50}\right)^{-0.391} \quad (3\text{-}6)$$

where the parameters used in these equations are defined as:

h/t_w = ratio of fillet-to-fillet depth to web thickness. Range of experimental data: $20 \le h/t_w \le 55$ for non-RBS; $21 \le h/t_w \le 55$ for RBS.

L_b/r_y = ratio of unbraced length, L_b, to radius of gyration about the weak axis of the cross section. Range of experimental data: $20 \le L_b/r_y \le 80$ for non-RBS; $20 \le L_b/r_y \le 65$ for RBS.

$b_f/2t_f$ = ratio of flange width to thickness. Range of experimental data: $4 \le b_f/2t_f \le 8$ for non-RBS; $4.5 \le b_f/2t_f \le 7.5$ for RBS.

L/d = ratio of shear span to depth. Range of experimental data: $2.5 \le L/d \le 7$ for non-RBS; $2.3 \le L/d \le 6.3$ for RBS.

d = depth of beam. Range of experimental data: $4 \le d \le 36$ for non-RBS; $18 \le d \le 36$ for RBS.

F_y = yield strength of the flange in ksi. Range of experimental data: $35 \le F_y \le 65$ for non-RBS; $38 \le F_y \le 63$ for RBS.

c^1_{unit} = (and c^2_{unit}) coefficients for units conversion. If d is in meters and F_y is in MPa, $c^1_{unit} = 0.0254$ and $c^2_{unit} = 0.145$. Both coefficients are 1.0 if inches and ksi are used.

The coefficients and exponents are different for beams with RBS connections and those with non-RBS connections, but the equations lead to relatively similar predicted values, as shown in Table 3-1 and Table 3-2. The range of experimental data covered by each parameter is listed along with the definitions. Missing from the data set are results for heavy W14 sections and heavy, deep beam sections. Values resulting from these equations, however, were compared with data from a series of experiments on heavy W14 sections (Uang and Newell, 2007), and shown to provide conservative (low) values of predicted modeling parameters. Until more tests on heavy sections become available, the above equations represent the best available information.

Table 3-1 Modeling Parameters for Various Beam Sizes (non-RBS connections) Based on Regression Equations with Assumed Beam Shear Span L=150 in., L_b/r_y= 50, and Expected Yield Strength, F_y=55 ksi

Section Size	θ_p *(rad)*	θ_{pc} *(rad)*	Λ	h/t_w	$b_f/2t_f$	L_b/r_y	L/d	*d (cm)*
W21x62	0.031	0.14	0.90	46.90	6.70	50.00	7.14	53
W21x147	0.038	0.22	2.23	26.10	5.43	50.00	6.79	56
W24x84	0.028	0.15	1.00	45.90	5.86	50.00	6.22	61
W24x207	0.034	0.28	2.81	24.80	4.14	50.00	5.84	65
W27x94	0.024	0.13	0.83	49.50	6.70	50.00	5.58	68
W27x217	0.029	0.22	2.14	28.70	4.70	50.00	5.28	72
W30x108	0.021	0.12	0.82	49.60	6.91	50.00	5.03	76
W30x235	0.024	0.19	1.76	32.20	5.03	50.00	4.79	80
W33x130	0.019	0.11	0.79	51.70	6.73	50.00	4.53	84
W33x241	0.021	0.16	1.42	35.90	5.68	50.00	4.39	87
W36x150	0.017	0.12	0.81	51.90	6.38	50.00	4.18	91
W36x210	0.020	0.18	1.45	39.10	4.49	50.00	4.09	93

Table 3-2 Modeling Parameters for Various Beam Sizes (with RBS connections) Based on Regression Equations with Assumed Beam Shear Span L=150 in., L_b/r_y= 50, and Expected Yield Strength, F_y=55 ksi

Section Size	θ_p *(rad)*	θ_{pc} *(rad)*	Λ	h/t_w	$b_f/2t_f$	L_b/r_y	L/d	*d (cm)*
W21x62	0.028	0.16	0.97	46.90	6.70	50.00	7.14	53
W21x147	0.033	0.27	2.15	26.10	5.43	50.00	6.79	56
W24x84	0.026	0.19	1.08	45.90	5.86	50.00	6.22	61
W24x207	0.030*	0.34*	2.71*	24.80	4.14	50.00	5.84	65
W27x94	0.022	0.16	0.91	49.50	6.70	50.00	5.58	68
W27x217	0.026*	0.29*	2.12*	28.70	4.70	50.00	5.28	72
W30x108	0.020	0.16	0.89	49.60	6.91	50.00	5.03	76
W30x235	0.023	0.25	1.78	32.20	5.03	50.00	4.79	80
W33x130	0.018	0.16	0.86	51.70	6.73	50.00	4.53	84
W33x241	0.020	0.22	1.46	35.90	5.68	50.00	4.39	87
W36x150	0.017	0.16	0.89	51.90	6.38	50.00	4.18	91
W36x210	0.019*	0.25*	1.53*	39.10	4.49	50.00	4.09	93

*Values slightly outside the range of experimental data

3.2.2.5 Flexural Strength of Steel Beams

Flexural strength parameters for steel beams, including the yield strength, maximum strength, and residual strength, can be quantified as follows:

Effective yield strength, M_y. The effective yield strength, which forms the first point on the initial backbone curve, is obtained by providing a "best fit" bilinear diagram to the monotonic loading curve, with an allowance made for cyclic hardening that occurs before visible strength deterioration sets in. Lignos and Krawinkler (2009) report a mean value for M_y of $1.06M_p$ for beams with RBS connections and 1.17 M_p for beams with non-RBS connections, with $M_p = Z F_y$, where F_y is the measured flange yield stress. A value of $M_y = 1.1M_p$ is recommended, with M_p based on the expected yield stress.

Capping strength, M_c. Lignos and Krawinkler (2009) report a mean value of the ratio of capping strength to effective yield strength, M_c/M_y, of 1.09 for beams with RBS connections and 1.11 for beams with non-RBS connections. A value of 1.1 for this ratio is recommended in both cases.

Residual strength, M_r. Most steel elements whose hysteretic behavior deteriorates due to local instabilities approach stabilization of the hysteretic response at large inelastic deformations (usually before ductile tearing occurs). While full stabilization may not occur, it is observed that the rate of deterioration becomes small enough to be neglected in analytical modeling. Data in Lignos and Krawinkler (2009) suggest that a reasonable estimate of residual strength would be 0.4 times the effective yield strength, M_y. Additional experimental testing at large deformation cycles is needed to assess residual strength with more reliability.

3.2.2.6 Comparisons with ASCE/SEI 41-06

While they appear different, there are no evident conflicts between the data presented here and the modeling parameters for fully restrained moment connections presented in ASCE/SEI 41-06.

- In ASCE/SEI 41-06, modeling parameters *a* and *b* are defined for a model in which cyclic deterioration has already been taken into account. Parameters *a* and *b* are intended to be used in a pushover analysis, and do not provide information on how the post-capping negative tangent stiffness range of component response should be modeled.
- The values of pre-capping rotation, θ_p, presented in Figure 3-3 appear to be smaller than values for beams in flexure presented in Table 5-6 of ASCE/SEI 41-06. The values in ASCE/SEI 41-06 are presented in terms of multiples of θ_y, which is a questionable practice because θ_y is sensitive to the beam shear span to depth (L/d) ratio. Moreover, the definition of plastic rotation angle employed in ASCE/SEI 41-06 is different from the definition of pre-capping rotation used here.

- In ASCE/SEI 41-06 it is assumed, for simplicity, that the post-capping negative tangent slope is very steep due to cyclic deterioration. Data show that this is not the case for steel beams, and use of an ASCE/SEI 41-06 backbone model might significantly underestimate the actual deformation capacity.
- The values for plastic rotation angle for fully restrained moment connections in Table 5-6 of ASCE/SEI 41-06 appear to be equivalent and of similar magnitude to the plastic component, θ_{pu}, of the ultimate rotation, θ_u, associated with modeling Option 4 (Section 2.2.5).

3.2.3 Recommendations for Modeling of Steel Beams

Summary recommendations for lumped plasticity (concentrated hinge) modeling of steel beams are as follows:

1. Whenever feasible, quantification of modeling parameters should be based on results from full-scale experimental tests of the configuration for which the model is being developed. Guidelines for developing an experimental program for establishing modeling parameters are summarized in FEMA P-695, *Quantification of Building Seismic Performance Factors* (FEMA, 2009b).
2. The use of curvature-based models is not recommended, unless the effects of local and lateral-torsional buckling are built into these models, or conservative (lower-bound) estimates of the ultimate deformation capacity are established.
3. The preferred modeling option is the use of the initial monotonic backbone curve in conjunction with explicit consideration of cyclic deterioration, modeling Option 1 (Section 2.2.5).
4. When Option 1 is not feasible, modeling Options 2 or 3 should be used. Options 2 and 3 account for the negative slope of the post-capping tangent stiffness.
5. Caution must be exercised in using modeling Option 4 for steel beams. The post-capping range of response can be large, which means the tangent stiffness might be negative for a large portion of the inelastic response. Since component behavior is modeled without negative tangent stiffness in modeling Option 4, this can lead to serious underestimation of P-Delta effects.
6. Reasonable estimates of the modeling parameters θ_p, θ_{pc}, and Λ for steel beams can be obtained from the regression equations presented in Section 3.2.2.4.

7. Recommended values for the flexural strength parameters M_y, M_c, and M_r for steel beams are presented in Section 3.2.2.5. The effective post-yield tangent stiffness (strain hardening) is defined as $K_p = (M_c - M_y)/\theta_p$.

8. Quantitative values of the backbone curve parameters θ_p and θ_{pc}, and the cyclic deterioration parameter Λ, cannot be obtained directly from Table 5-6 of ASCE/SEI 41-06. The definitions of the quantities listed in that table are different from the modeling parameters as defined herein.

9. The plastic rotation angle for fully restrained moment connections listed in Table 5-6 of ASCE/SEI 41-06 can be used to estimate the ultimate plastic rotation for modeling Option 4 (Section 2.2.5), but cannot be related directly to the pre-capping plastic rotation, θ_p.

10. The process of obtaining a modified backbone curve using the factors for modeling Option 3 (Section 2.2.5) applied to the parameters of the initial monotonic backbone curve, and the ultimate rotation, θ_u (and its plastic component, θ_{pu}), for modeling Option 4 (taken as 80% of the values obtained using Option 3) is illustrated in Figure 3-9.

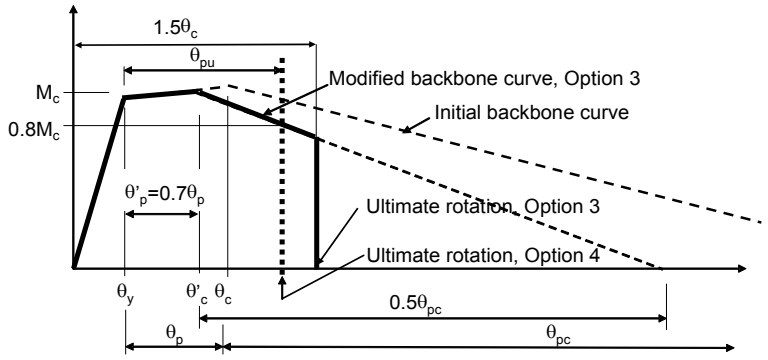

Figure 3-9 Procedure for obtaining the modified backbone curve for modeling Option 3, and the ultimate rotation, θ_u, for modeling Option 4.

3.2.4 Behavioral Considerations for Steel Columns

Column behavior is different from beam behavior, due to differences in support conditions, moment gradient, and axial load effects. Although seismic design provisions include a strong column-weak beam requirement, it is a misconception to believe that inelastic behavior in columns is prevented. Analytical studies, such as Gupta and Krawinkler (2000) and Medina and Krawinkler (2003), have shown that actual column flexural demands can be much larger than anticipated in design. The reason for this is that column moment diagrams during inelastic response can deviate significantly from the double-curvature shape assumed in elastic analyses.

As an example, values of the strong column factor, $R_\mu = [S_a(T_1)/g]/(V_y/W)$, which would be required to avoid plastic hinging in the columns of a 9-story moment-resisting frame, are shown in Figure 3-10. A required strong column factor of about 2.0 is indicated in the median, while a factor on the order of 1.0 will almost guarantee plastic hinging in columns in an MCE level event.

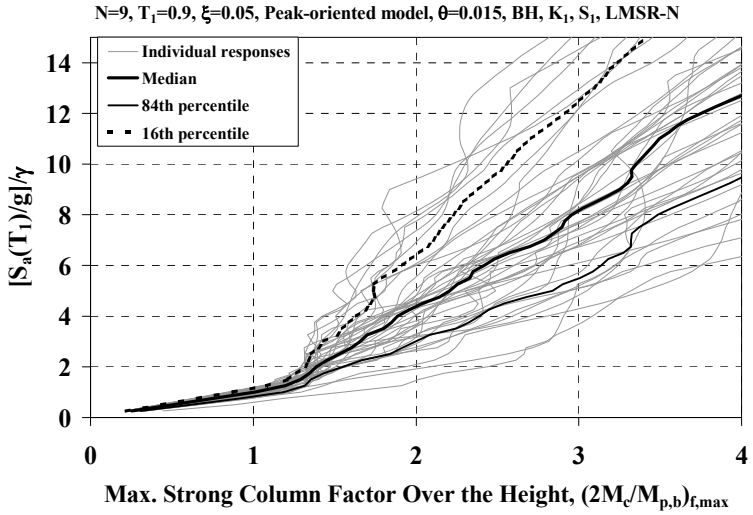

Figure 3-10 Strong column factor, R_μ, required to avoid plastic hinging in columns for a 9-story moment-resisting frame structure (Medina and Krawinkler, 2003).

Plastic hinging in moment frame columns is not an unlikely event, and should be simulated in an analytical model. The extent of inelastic deformation in the columns is sensitive to the strength distribution over the height of the building, redistribution of forces and deformations, and changes in the deflected shape, particularly when P-Delta effects become important.

Columns are susceptible to local and lateral-torsional buckling, as documented for beams. The susceptibility to lateral-torsional buckling, however, might be higher because: (1) the column boundary conditions at the top of a story are often ambiguous and depend on local detailing; (2) the column might be in single curvature bending between adjacent floors during inelastic response; and (3) axial loads are present. This is likely less of an issue for heavy W14 columns, but is more important for deep column sections, particularly those with large r_x/r_y and h/t_w ratios (FEMA 355D).

Bending strength in the presence of axial loads can be computed with confidence from either fiber models or yield surface models, but inelastic rotation parameters of the backbone curve (or backbone surface in the case of biaxial bending) are a matter of much judgment.

It is judged that the pre-capping plastic rotation, θ_p, of shallow, heavy, and wide column sections is large for the full range of axial force expected in a column, because of small values of d, L_b/r_y, $b_f/2t_f$, and h/t_w. This judgment is supported by column tests performed at University of California San Diego (Newell and Uang, 2008). Figure 3-11 shows representative results of this test series on heavy W14 sections.

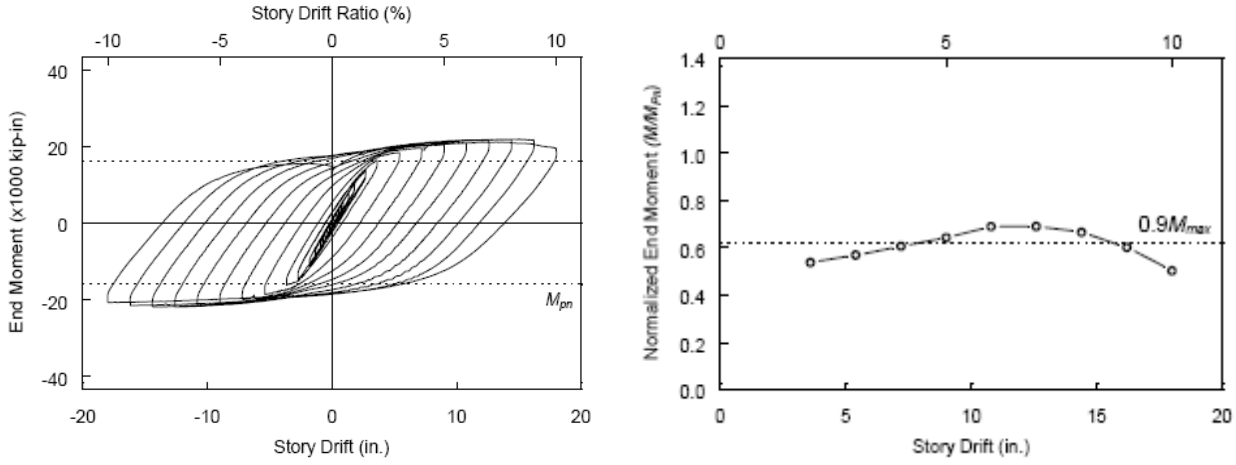

(a) (b)

Figure 3-11 Representative results from tests on W14x176 column sections subjected to an axial load and cyclic bending moment: (a) moment versus story drift response for $P/P_y = 0.35$; and (b) peak moment versus story drift for $P/P_y = 0.75$ (Newell and Uang, 2006).

Finite element analysis of three W27 column models, however, revealed a potential vulnerability of deep columns to combined high axial load and drift demand (Newell and Uang, 2006). Significant deterioration from flange and web local buckling was accelerated by the presence of a high axial load. Typical results of this analytical study are shown in Figure 3-12.

3.2.5 Recommendations for Modeling of Steel Columns

Only a small number of tests are available for steel elements subjected to combined axial load and inelastic deformations caused by cyclic bending moments. None of the available data incorporate the variation in moment gradient observed in nonlinear analytical studies, and no tests have been performed on deep column sections. Analytical modeling, therefore, must be based on a combination of incomplete column test data, principles of mechanics, and extrapolation from beam test results.

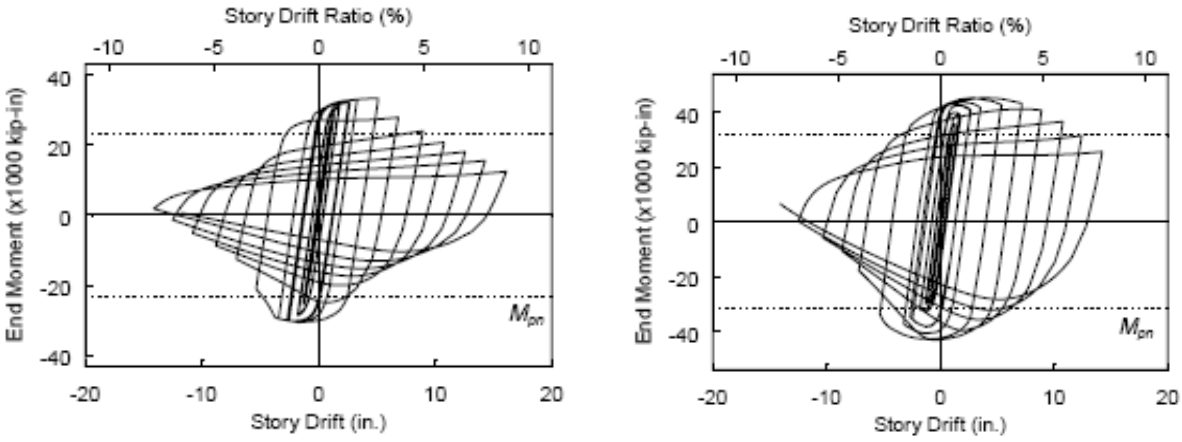

(a) (b)

Figure 3-12 Analytical predictions of flexural cyclic response of: (a) W27x146 columns for $P/P_y = 0.35$; and (b) W27x194 columns for $P/P_y = 0.55$ (Newell and Uang, 2006).

No specific recommendations for pre-capping plastic rotation, θ_p, post-capping rotation, θ_{pc}, and reference cumulative plastic rotation, Λ, for steel columns can be made at this time. Values provided for steel beams could serve as an upper bound for these parameters, but axial load effects in the form of accelerated lateral-torsional buckling and web buckling, and decreased residual strength, should be considered. In the case of low axial loads ($P/P_y < 0.2$), parameters for steel beams might be appropriate, provided that the column is well braced at the top and bottom of every story.

The values listed for "Columns-flexure" in Table 5-6 of ASCE/SEI 41-06 are believed to be unconservative, and should be re-evaluated. Also, they should be expressed in terms of plastic rotation angle, θ_p, rather than multiples of yield rotation, θ_y, since the moment gradient is expected to change significantly during inelastic response.

3.2.6 Acceptance Criteria for Steel Beams and Columns

Local acceptance criteria for steel beam and column components are provided for service level and Maximum Considered Earthquake (MCE) level evaluations. Additional local component acceptance criteria, and global acceptance criteria for the overall structural system, are provided in *Seismic Design Guidelines for Tall Buildings* (PEER, 2010).

3.2.6.1 Service Level

At the service level, structural response is usually predicted using elastic response spectrum analysis. For steel beams and columns, resulting force demands can be compared to strength capacities based on AISC 341 *Seismic*

Provisions for Structural Steel Buildings (AISC, 2005b), using expected material properties and resistance factors of $\phi = 1.0$. For ductile actions on steel beams, demand to capacity ratios can exceed 1.0, but should not exceed 1.5. For columns, demand to capacity ratios should not exceed 1.0.

3.2.6.2 Maximum Considered Earthquake Level

At the MCE level, structural response is usually predicted using nonlinear response history analysis. Failure modes leading to rapid deterioration should be prevented through appropriate capacity design and detailing requirements. For failure modes associated with relatively slow deterioration (as defined in Figure 2-3) the maximum deformation demand in each component should be less than the ultimate deformation capacity.

In the case of beams, deformation implies rotation. If the ultimate rotation capacity is exceeded, then the bending strength of the component should be taken as zero, and the component should be checked to verify that exceedance of the ultimate rotation capacity does not lead to failure that causes loss of gravity-load-carrying ability (e.g., loss of shear resistance in a beam).

3.3 Nonlinear Modeling of Steel Panel Zones

Shear deformation in steel panel zones contributes significantly to elastic and inelastic story drifts in steel frame structures. The shear strength of a panel zone controls the distribution of inelastic deformations between beams and columns, and therefore controls the collapse mode of steel frame structures.

Mathematical models for the behavior of the panel zone in terms of shear force-shear distortion relationships have been proposed by many researchers, including Krawinkler (1978), Tsai and Popov (1988), Kim and Engelhardt (1995), and Jin and El-Tawil (2005), based on either experimental observations or finite element modeling. The models differ in their representation of inelastic behavior, but agree well in their representation of the elastic shear stiffness, K_e, and the yield strength in shear, V_y.

In frame analysis programs that utilize line elements, panel zone behavior can be modeled by creating a panel zone with rigid boundaries as illustrated in Figure 3-13. The model requires the use of 8 rigid elements per panel zone that are connected with hinges at the four corners. These 8 rigid elements create an assembly that deforms into a parallelogram. The strength and stiffness properties of the panel zone can be modeled by adding one (or two) rotational springs to one of the four panel zone corners, or by adding

one (or two) translational springs crossing the panel zone diagonally and connected at two opposite corners.

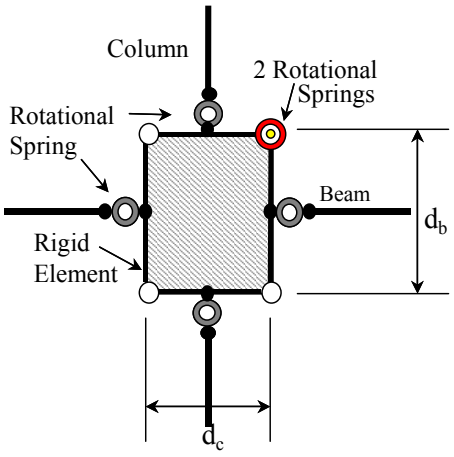

Figure 3-13 Analytical model for panel zone (Gupta and Krawinkler, 1999).

3.3.1 Quantification of Properties for Steel Panel Zones

Under lateral deformation, steel panel zones are subjected to large shear forces. If the panel zone is relatively thin, shear yielding will propagate from the center towards the boundaries, followed by inelastic bending of the adjacent column flanges. This behavior is characterized by stable inelastic cycles of the type shown in Figure 3-14.

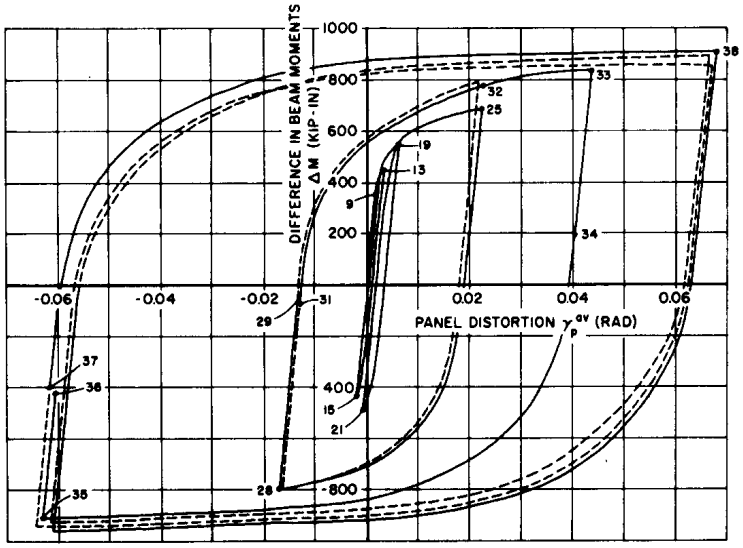

Figure 3-14 Cyclic shear behavior of weak panel zone (Krawinkler, 1978).

Experimental evidence indicates that deterioration in the shear force and shear distortion response of a panel zone is limited, unless shear buckling or fracture of a welded doubler plate occurs. Since code detailing criteria

adequately control shear buckling, this type of behavior is not likely. It should be acceptable to neglect deterioration in the modeling of steel panel zones, unless there is clear indication that deterioration will occur within the range of deformations expected at the MCE level. In the following discussion, deterioration in the steel panel zone is not considered.

If the panel zone is relatively strong, and only limited inelastic behavior is expected, then a simple bilinear hysteretic model should be sufficient. If the panel zone is expected to contribute significantly to the inelastic story drift, then a trilinear model is recommended to account for an increase in strength that occurs after initial yielding, which cannot be adequately captured in a bilinear model.

Use of a bilinear model with a realistic initial yield strength produces an unrealistic concentration of inelastic deformations in the panel zone, underestimating inelastic rotation demands in the adjacent beams and columns. Use of a bilinear model with an unrealistically large yield strength to capture strength gain penalizes beam and column rotation demands more than necessary.

The model proposed in Krawinkler (1978), and presented in FEMA 355C, *State of the Art Report on System Performance of Steel Moment Frames Subject to Earthquake Ground Shaking* (FEMA, 2000b) is summarized here. The trilinear shear force and shear distortion relationship for this model is shown in Figure 3-15. The control values for this model are:

$$V_y = \frac{F_y}{\sqrt{3}} A_{eff} = \frac{F_y}{\sqrt{3}} (0.95 d_c t_p) \approx 0.55 F_y d_c t_p \tag{3-7}$$

where V_y is the panel zone shear yield strength, F_y is the yield strength of the material, A_{eff} is the effective shear area, d_c is the depth of the column, and t_p is the thickness of the web including any doubler plates. The corresponding yield distortion, γ_y, is given as:

$$\gamma_y = \frac{Fy}{\sqrt{3} \times G} \tag{3-8}$$

The elastic stiffness, K_e, of the panel zone can then be written as:

$$K_e = \frac{V_y}{\gamma_y} = 0.95 d_c t_p G \tag{3-9}$$

where G is the shear modulus of the column material.

Additional shear resistance, which is mobilized primarily after yielding of the panel zone, is attributed to the resistance of the column flanges at the panel zone corners, which must bend in order to accommodate the shear distortion mode of the panel zone. The full plastic shear resistance of the joint, V_p, can be estimated as:

$$V_p = V_y\left(1+\frac{3K_p}{K_e}\right) \approx 0.55F_y d_c t_p\left(1+\frac{3b_c t_{cf}^{\,2}}{d_b d_c t_p}\right) \tag{3-10}$$

where K_p is the post-yield stiffness, b_c is the width of the column flange, and t_{cf} is the thickness of the column flange. This strength is assumed to be attained at a value of $4\gamma_y$. Beyond $4\gamma_y$, an appropriate value of strain-hardening can be assumed to fully define the trilinear shear force and shear distortion relationship of the panel zones.

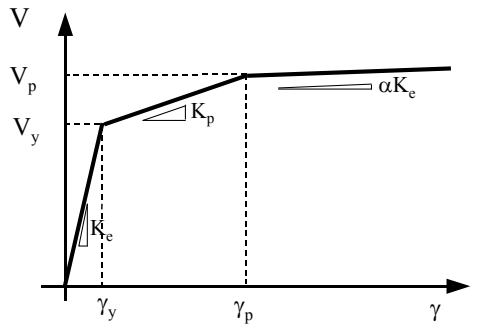

Figure 3-15 Trilinear shear force and shear distortion relationship for panel zone (Gupta and Krawinkler, 1999).

The shear force demand on the panel zone, V, can be estimated using the following equation:

$$V = \left(\frac{\Delta M}{d_b} - V_{col}\right) \tag{3-11}$$

where $\Delta M = M_{bl} + M_{br}$, which is the net beam moment transferred to the column, and V_{col} represents the average of the shears in the column above and below the connection, as shown in Figure 3-16.

If rotational springs are used in one corner, the total spring stiffness is given as $d_b(V/\gamma)$. The use of two bilinear springs to model panel zone trilinear behavior is illustrated in Figure 3-17. A representative example of the panel zone dynamic response obtained with this model is shown in Figure 3-18.

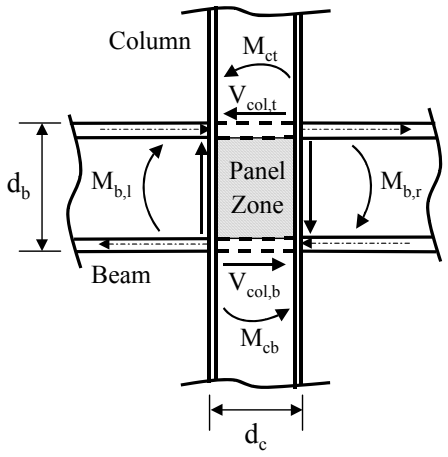

Figure 3-16 Moment and shear forces at a connection due to lateral loads.

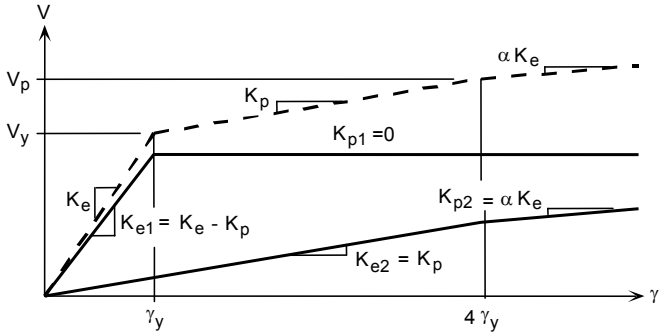

Figure 3-17 Use of two springs to model trilinear behavior (Gupta and Krawinkler, 1999).

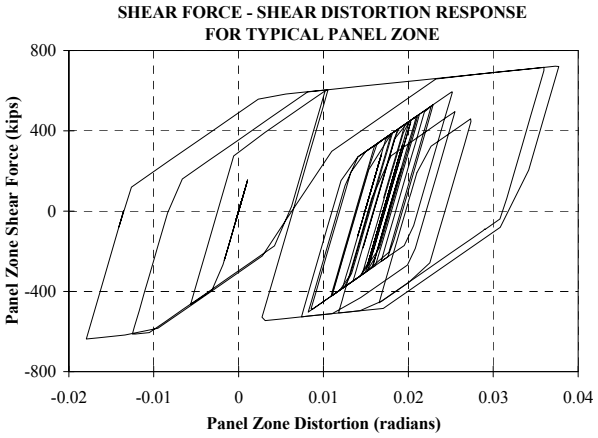

Figure 3-18 Shear force-distortion response for a typical panel zone (Gupta and Krawinkler, 1999).

The model illustrated here has been calibrated for cases in which the column flange thickness is less than 10% of the column depth. Recent research, such as Jin and El-Tawil (2005), has shown that this model overestimates the

ultimate shear strength for heavy W14 sections with very thick flanges. The choice of an appropriate model is left to the analyst. It is important to use as accurate a model as possible because the distribution of inelastic deformations to beams, columns, and the panel zone is sensitive to relative strength of these elements.

3.3.2 Acceptance Criteria for Steel Panel Zones

Local acceptance criteria for steel panel zones are provided for service level and MCE level evaluations. Additional local and global acceptance criteria are provided in *Seismic Design Guidelines for Tall Buildings* (PEER, 2010).

3.3.2.1 Service Level

At the service level, the shear force demand in the panel zone should be less than 1.5 times the yield strength, V_y, if elastic analysis is used. This value is judgmental, and is based on the following two assumptions: (1) no remedial action needs to be taken; and (2) the effect of panel zone yielding on the deformation capacity of the beam-column connection is accounted for in acceptance criteria at the MCE response level.

3.3.2.2 Maximum Considered Earthquake Level

For frames in which panel zone shear distortion does not contribute to the incident of fractures at the beam-column connection, a shear distortion angle of 0.08 radians, presently accepted for link elements in eccentrically braced frames in AISC 341 (AISC, 2005b), should be used.

If panel zone shear distortion causes kinking at the panel zone corners that contributes to fractures at the beam-column connection, then the shear distortion angle should be limited to 0.02 radians, unless a larger (or smaller) value is justified based on experimental evidence.

3.4 Nonlinear Modeling of Reinforced Concrete Beams, Columns, and Beam-Column Joints

Seismic response of reinforced concrete moment frames is modeled through nonlinear element representations of beams, columns, and beam-column joints. Nonlinear element formulations that are available for reinforced concrete frame components range from three-dimensional continuum finite element models to lumped plasticity concentrated hinge models.

As in the case of steel frame components, modeling recommendations for reinforced concrete frame components are based on the assumption that beams and columns are modeled as lumped plasticity elements, consisting of elastic elements with concentrated plastic hinges at each end. Concentrated

plastic hinges are represented by rotational springs with backbone and cyclic deterioration properties that have been calibrated to results from experimental studies. This does not preclude the use of fiber or finite element formulations, however, results from these component models should be calibrated with test data and other evidence to verify consistent and accurate measures of performance.

Figure 3-19 shows an example of a concentrated hinge model for a reinforced concrete flexural member, which could represent a beam or column. The element is idealized as a quasi-elastic member with inelastic hinges at one or both ends. The term quasi-elastic refers to the fact that the elastic properties of the element are adjusted to account for concrete cracking, bond slip, and other factors that occur prior to yield. The inelastic response is modeled through the nonlinear springs, where the spring properties are calibrated to match the backbone and cyclic response of the overall chord rotation of the member.

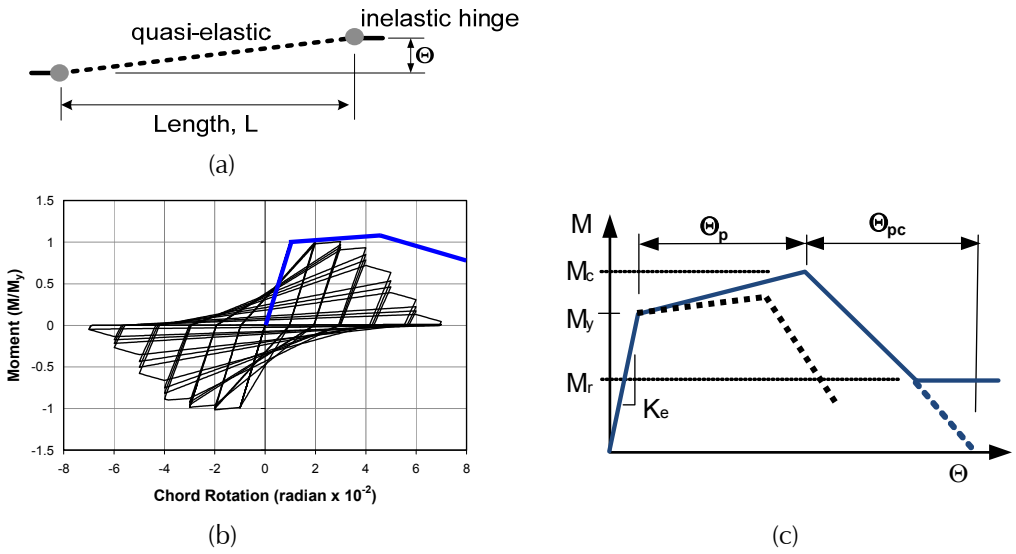

Figure 3-19 Reinforced concrete flexural member: (a) idealized flexural element; (b) monotonic backbone curve and hysteretic response; and (c) monotonic and modified backbone curves.

Figure 3-19 also illustrates component modeling options described in Section 2.2.5, as applied to a reinforced concrete flexural member. Figure 3-19b shows Option 1, in which the properties are based on the initial monotonic backbone curve, and the deteriorating hysteretic response is explicitly included in the analytical model to capture cyclic deterioration. Figure 3-19c shows a modified backbone curve, which is used in Options 2 and 3, in lieu of explicit inclusion of cyclic deterioration. In Option 2, the modified backbone parameters are based on cyclic test results, and in Option 3, the

modified backbone parameters are based on empirical factors applied to the initial monotonic backbone curve.

Since a considerable portion of the inelastic response of reinforced concrete beams and columns occurs in bond-slip and yield penetration into the beam-column joints, inelastic modeling of the beams, columns, and joints are inter-related. Figure 3-20 illustrates one way to idealize a reinforced concrete beam-column joint region. It includes five inelastic springs, coupled through kinematic constraints to represent the finite joint size.

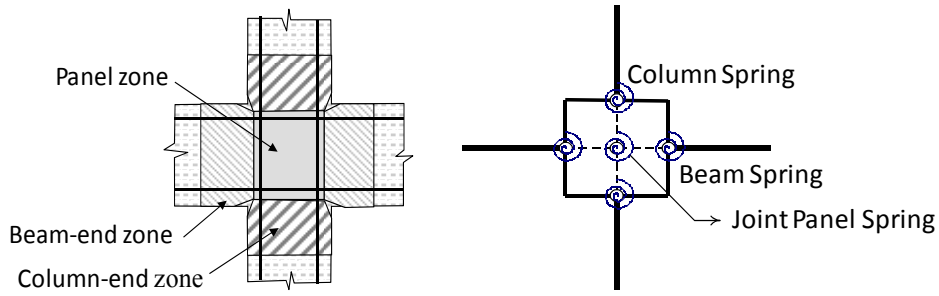

Figure 3-20 Idealization of reinforced concrete beam-column joint.

In this idealization, each of the four springs connecting the joint to the adjacent beam or column is common to the joint and the connected element. As such, these springs are calibrated to model both the inelastic deformations in the member plastic hinge and the bond-slip/yield penetration into the joint, and are the same as the springs at each end of the flexural member in Figure 3-19. The spring at the center of the joint is calibrated to model joint panel deformations due to the large shear force transfer through the joint. Clear distinction and accounting of deformations associated with the flexural response of the member, anchorage into the joint, and joint panel shear are important when calibrating flexural hinges for reinforced concrete frame components.

3.4.1 Behavioral Considerations for Reinforced Concrete Frame Components

In general, the modeling and acceptance criteria for reinforced concrete beams, columns, and beam-column joints should consider all significant modes of deformation and deterioration in reinforced concrete components, including:

- Flexural hinging of beams, including the effects of concrete cracking and crushing, longitudinal bar yielding, buckling and fracture, longitudinal bar bond slip and anchorage into the beam-column joint, and transverse reinforcing bar yielding and failure. Influence of the floor slab,

including slab reinforcement and post-tensioning (where present) should also be considered.

- Flexural hinging of columns under the combined effects of bending and axial loads, including the effects of concrete cracking and crushing, longitudinal bar yielding, buckling and fracture, longitudinal bar bond slip and anchorage into the beam-column joint or column foundation, and transverse reinforcing bar yielding and failure.
- Effect of shear forces and deformations on the response of beams and columns.
- Deformations in the beam-column joint, including bond-slip and anchorage of the longitudinal beam and column bars, joint shear forces, and joint shear deformations.
- Deformation compatibility in structural elements other than beams, columns, and joints of the moment-resisting frames. This would typically include gravity columns and their connections to the concrete floor slab. In dual or combined systems, interaction with other elements (e.g., walls, wall-to-slab connections, etc.) should also be considered.

Since the design of new tall buildings is expected to conform to current code and reference standard seismic design and detailing requirements, such as ACI 318 *Building Code Requirements for Structural Concrete* (ACI, 2008), recommended modeling and acceptance criteria are based on the following behavioral assumptions:

- *Member shear design*: It is assumed that shear capacity design provisions are in effect, which will prevent premature shear failures in beams and columns. Thus, while shear strength demand to capacity ratios should be checked, the inelastic hinge calibration is for components that are dominated by flexural effects, considering the interaction of axial load and moment.
- *Joint panel design:* It is assumed that the joint panel will be designed to resist shear and bar anchorage forces associated with flexural hinging of the connected members, which will preclude joint shear failure, limit bond slip, and prevent bar pullout. The joint shear strength demand to capacity ratios should be checked, but large inelastic panel deformations should not be permitted.
- *Longitudinal reinforcing bars:* It is assumed that the longitudinal reinforcing bar splices in beams and columns will be designed and detailed to prevent splice failure that would otherwise limit flexural hinging in the members and cause sudden strength degradation.

- *Transverse tie reinforcement:* It is assumed that transverse reinforcement will conform to ductile detailing requirements to control degradation of the confined concrete core and longitudinal reinforcing bars, and to maintain sufficient axial strength of columns to prevent axial load failure.

3.4.2 Quantification of Properties for Reinforced Concrete Beams and Columns

The following sections describe the basis for quantification of modeling parameters for reinforced concrete beams and columns, including elastic stiffness, pre-capping plastic rotation, post-capping plastic rotation, reference hysteretic energy dissipation capacity (cyclic deterioration), and flexural strength, based on the concentrated hinge models shown in Figure 3-19 and Figure 3-20. These parameters are needed to develop a backbone curve and moment-rotation model that explicitly incorporates cyclic deterioration, (modeling Option 1 presented in Section 2.2.5).

In general, parameters should be calculated based on expected values of material properties. For concrete, the expected compressive strength should be taken as $f'_{c,\exp} = 1.25\, f'_c$, where f'_c is the nominal specified minimum strength. The modulus should be calculated as $E_{c,\exp} = 57,000\sqrt{f'_{c,\exp}}$ where $f'_{c,\exp}$ and $E_{c,exp}$ are in given in psi. The expected reinforcing bar steel yield strength should be equal to $F_{y,exp} = 1.2F_y$, where F_y is nominal specified minimum strength.

3.4.2.1 Experimental Data

Recommended modeling parameters and acceptance criteria are based on recent studies by Haselton et al. (2008), Elwood and Eberhard (2006), and Elwood et al. (2007). While not exhaustive, these studies reflect much of the recent work in other published studies and guidelines. The investigation by Haselton et al. (2008) is based on data from 255 column tests that have been assembled in the PEER Structural Performance Database (PEER, 2007; Berry et al., 2004). The work by Elwood et al. (2007) evaluated some of the same data, and the results have been incorporated in ASCE/SEI 41-06 *Supplement No. 1* (ASCE, 2007b) for reinforced concrete structures.

3.4.2.2 Stiffness of Reinforced Concrete Beams and Columns

The initial stiffness coefficients of reinforced concrete beams and columns are typically defined in terms of a secant stiffness, which is calibrated to a specified load or deformation level. As shown in Figure 3-21, two common definitions are the secant stiffness to the yield point, K_y, or a larger stiffness,

K_{stf}, calibrated to a force at some fraction of the yield point. The yield stiffness, K_y, should be used in analyses where the component deformations are likely to exceed the yield rotation, as is common in MCE level assessments. The larger stiffness, K_{stf}, should be used in analyses where the component deformations are likely to be below the yield rotation, as is expected in service level assessments. For this purpose, values of K_{stf} corresponding to 0.4 times the yield point are suggested.

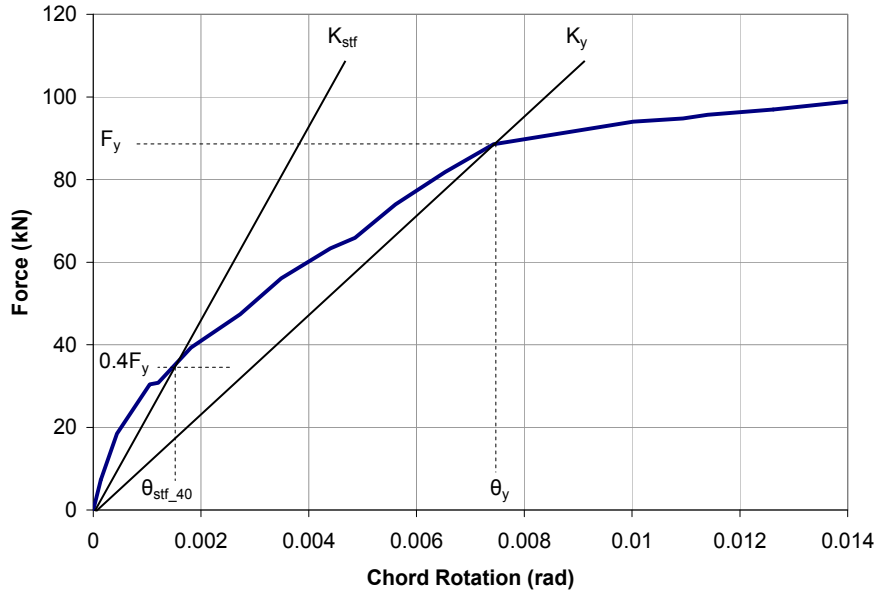

Figure 3-21 Definitions of secant elastic stiffness (Haselton et al., 2008).

Haselton et al. (2008) proposed the following equations for median estimates of K_y and K_{stf}, based on calibration to tests of reinforced concrete columns:

$$K_y: \quad \frac{EI_y}{EI_g} = -0.07 + 0.59\left[\frac{P}{A_g f_c'}\right] + 0.07\left[\frac{L_s}{H}\right] \quad \text{where} \quad 0.2 \le \frac{EI_y}{EI_g} \le 0.6 \tag{3-12}$$

$$K_{stf}: \quad \frac{EI_{stf}}{EI_g} = -0.02 + 0.98\left[\frac{P}{A_g f_c'}\right] + 0.09\left[\frac{L_s}{H}\right] \quad \text{where} \quad 0.35 \le \frac{EI_{stf}}{EI_g} \le 0.8 \tag{3-13}$$

In these equations, EI_g is the flexural stiffness of the gross section, P is the member axial (compression) load, A_g is the gross column area, f_c' is the concrete compressive stress, L_s is the shear span from the point of maximum moment to the inflection point (typically one-half of the member length), and H is the member depth. For median value estimates, material properties used to calculate the stiffness parameters should be based on expected values. Variations in stiffness tend to follow a lognormal distribution with a variation of $\sigma_{ln} = 0.28$ for K_y and $\sigma_{ln} = 0.33$ for K_{stf}. Note that these stiffness values

take into account the deformations associated with bond-slip into the member end anchorages, and have been calibrated assuming that shear deformations are incorporated using an effective shear stiffness of $0.4E_cA_g$.

Assuming a column height to depth ratio of $2L_s/H = 6$ subjected to reverse curvature, the yield stiffness in Equation 3-12 ranges from $0.20EI_g$ to $0.60EI_g$ for axial load ratios from zero to $0.6P/A_g f_c'$. The corresponding yield point ratios in Equation 3-13 are about 60% to 70% larger, with stiffness ratios ranging from $0.35EI_g$ to $0.80EI_g$. These values are lower than the common stiffness assumptions of $0.5EI_g$ for beams and $1.0EI_g$ for columns, due to bond slip at member ends and the deformation levels associated with the secant definitions.

Elwood et al. (2007) recommended effective stiffness values that have been adopted in ASCE/SEI 41-06 *Supplement No. 1*. These values range from $0.3EI_g$ to $0.7EI_g$, which are also lower than values that are commonly assumed. Figure 3-22 shows a comparison of the values contained in ASCE/SEI 41-06 *Supplement No. 1* (designated ASCE 41S in the figure) to the values obtained using Equation 3-12 and Equation 3-13.

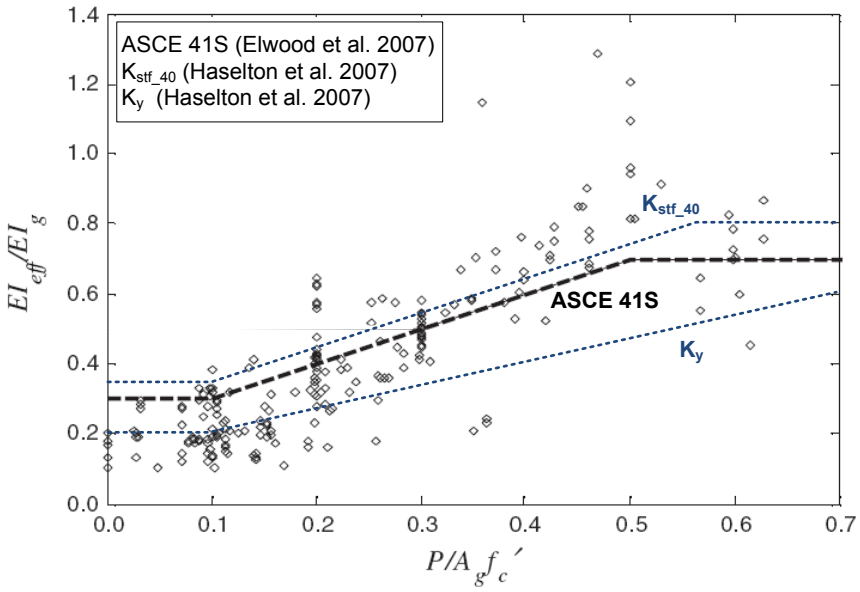

Figure 3-22 Comparison of effective stiffness values of reinforced beam-columns from Haselton et al. (2008) and Elwood et al. (2007).

Overall, the values given by the equations (K_y and K_{stf_40}) tend to bracket the values in ASCE/SEI 41-06 *Supplement No. 1*. While based on similar data and criteria, differences are likely due to variations in how the underlying data were processed to recover EI_{eff}, and differences in the intended statistical adjustments. While the values given by Equations 3-12 and 3-13 are

statistically rigorous (reporting median values and dispersions), the data in Figure 3-22 illustrate the large variability and the corresponding uncertainty in calculating deformations in the pre-yield range of response.

There are relatively few data available on reinforced concrete beams that are integral with the floor slab or that have post-tensioned reinforcing. In the absence of other data or information, the values for column stiffness at zero axial load can be used for beams without post-tensioning, where the EI_g is adjusted to account for the presence of a slab and reverse curvature bending. In reverse curvature bending, EI_g may be taken as the average of the gross stiffness for positive bending (based on an effective slab width equal to one-eighth the beam span on each side of the beam) and the gross stiffness of the beam section alone for negative bending. For beams with post-tensioned slabs, stiffness should be increased based on the axial load ratio induced by the post-tensioning over the effective slab width.

3.4.2.3 Pre-Capping Plastic Rotation of Reinforced Concrete Beams and Columns

Haselton et al. (2008) proposed the following empirical equation for calculating the pre-capping plastic rotation, θ_p, in the initial monotonic backbone curve, based on calibration to tests of reinforced concrete columns:

$$\theta_p = 0.12\left(1+0.55a_{sl}\right)\left(0.16\right)^{\upsilon}\left(0.02+40\rho_{sh}\right)^{0.43}\left(0.54\right)^{0.01c_{units}f_c'}\left(0.66\right)^{0.1s_n}\left(2.27\right)^{10.0\rho} \qquad (3\text{-}14)$$

where a_{sl} = 1 (unless bond slip of longitudinal bars is prevented), $\upsilon = P / f_c' A_g$ is the axial load ratio, $\rho_{sh}=A_{sh}/sb$ is the area ratio of transverse reinforcement in the hinge region (where A_{sh} is the bar area, s is the bar spacing, and b is the section width), c_{units} is a unit conversion factor on f_c' and F_y (equal to 1.0 for SI units in MPa, and 6.9 for Imperial units in ksi), $s_n=(s/d_b)(F_y/100)^{0.5}$ is a rebar buckling coefficient (where s is the tie spacing, d_b is the longitudinal bar diameter, and $F_y/100$ is the reinforcing bar strength ratio in SI units, or $F_y/14.5$ in Imperial units), and $\rho = A_s/bh$ is the ratio of longitudinal steel (where A_s is the steel area and b and h are the section dimensions).

The equation was calibrated to match the median response from column tests, with a reported dispersion (standard deviation of the logarithm of the data) of σ_{ln} = 0.54. To the extent that the reinforcement in beams is similar to the columns on which these data are based, Equation 3-14 can be applied to beams.

However, for beams with non-symmetric reinforcement, or for beams with significantly smaller shear and confinement reinforced in the beam, the equation does not apply. Based on an approach proposed by Fardis and

Biskinis (2003), Haselton et al. (2008) developed the following factor to adjust the pre-capping rotation of Equation 3-14 to account for members with non-symmetric reinforcement:

$$\theta_{p(non-symmetric)} = \left(\frac{\max\left(0.01, \frac{\rho' f_y}{f_c'}\right)}{\max\left(0.01, \frac{\rho \quad f_y}{f_c'}\right)} \right) \theta_{p(symmetric)} \qquad (3\text{-}15)$$

where ρ is the ratio of the tension steel reinforcement, defined as A_s/bd, ρ' is the ratio of the compression reinforcement, defined as A_s'/bd, and f_y and f_c' are the steel and concrete strengths, respectively.

3.4.2.4 Post-Capping Plastic Rotation of Reinforced Concrete Beams and Columns

Despite its importance in predicting the collapse response of reinforced concrete frames, research to define the post-capping rotation, θ_{pc}, has been limited. Key parameters affecting the post-capping response are the axial load ratio, v, and transverse steel ratio, ρ_{sh}. Based on the same set of reinforced concrete column test data, Haselton et al. (2008) proposed the following equation for post-capping rotation:

$$\theta_{pc} = (0.76)(0.031)^{v} (0.02 + 40\rho_{sh})^{1.02} \leq 0.10 \qquad (3\text{-}16)$$

This equation was calibrated to the median response from column tests, with a reported dispersion of $\sigma_{ln} = 0.72$. The larger dispersion for post-capping rotation reflects both the larger inherent uncertainty in degrading behavior, and a relative lack of available data. The upper bound of $\theta_{pc} < 0.10$ is a conservative assumption based on limited availability of data for elements with shallow post-capping slopes. Since this ultimate rotation is fairly large, and data to quantify the response at large deformations are lacking, the residual strength of the hinge, M_r, should be conservatively neglected, and taken as zero (or near zero).

Equation 3-16 is based on data from square and rectangular columns with symmetric reinforcement. Presumably, the equation can be similarly adjusted for cross sections with non-symmetric reinforcement, and applied to beams, using the modifier in Equation 3-15.

Empirical predictions of plastic rotation capacity for different values of axial load ratio, v, and confinement, ρ_{sh}, are summarized in Table 3-3. Values are reported for a representative column section with f_c' = 41 MPa (6 ksi), α_{sl} = 1

(bond slip included), s_n = 12.7 (longitudinal bar buckling), and ρ = 0.02 (longitudinal reinforcement ratio).

Table 3-3 Empirical Plastic Rotation Values, θ_p and θ_{pc}, for a Representative Column Section (Haselton et al., 2008)

$\nu = P / A_g f'_c$	ρ_{sh}	θ_p	θ_{pc}
0.1	0.002	0.031	0.052
	0.006	0.047	0.100
	0.020	0.077	0.100
0.6	0.002	0.012	0.009
	0.006	0.019	0.024
	0.020	0.031	0.077

For columns with low axial load ($0.1 f'_c A_g$), the pre-capping rotation ranges from θ_p = 0.031 radians for a column with minimal confinement, up to θ_p = 0.077 radians for a column with heavy confinement. For columns with higher axial loads ($0.6 f'_c A_g$) above the balance point, the pre-capping rotation is reduced to less than half of the corresponding values at lower axial loads, ranging from θ_p = 0.012 to 0.031 radians. In both cases, bond slip (incorporated through the α_{sl} parameter) accounts for about one-third of the total pre-capping rotation.

Similar to the trends for pre-capping rotation, post-capping rotation drops off dramatically for axial loads above the balance point and low confinement ratios. Values for post-capping rotation range from θ_{pc} = 0.10 for a column with low axial load and high confinement, down to θ_{pc} = 0.009 for a column with high axial load and low confinement.

3.4.2.5 Cyclic Deterioration

The parameter governing cyclic deterioration is the reference hysteretic energy dissipation capacity, E_t, which is defined as ΛM_y or $\lambda \theta_p M_y$ as part of Equation 2-1. Following the calibration done for other backbone parameters using test data for reinforced concrete columns, Haselton et al. (2010) proposed the following equation for the mean energy dissipation capacity parameter λ:

$$\lambda = (30)(0.03)^{\nu} \tag{3-17}$$

where ν is the axial load ratio. This equation was calibrated to the median response from column tests, with a reported dispersion of σ_{ln} =0.60. For a typical column with seismic detailing, typical values of the parameter λ are

on the order of 10 to 20, varying from a low of 2 for columns with high axial load, to a high of 30 for columns with no axial load.

3.4.2.6 Flexural Strength of Reinforced Concrete Beams and Columns

Flexural strength parameters for reinforced concrete beams and columns, including the yield strength, maximum strength, and residual strength, can be quantified as follows:

Effective yield strength, M_y. The flexural (yield) strength of reinforced concrete beams and columns, M_y, should be calculated based on conventional reinforced concrete flexure theory, i.e., assuming plane sections remain plane, negligible concrete tension strength, and an appropriate stress-strain model (or equivalent compression block factors) for concrete in compression. Calculations should be performed using expected material properties. For members with axial load below the balance point, M_y corresponds to the initiation of yielding in the tension steel. For members with axial loads above the balance point, M_y is equal to the moment associated with significant inelasticity in the concrete. Panagiotakos and Fardis (2001) have published equations to calculate flexural strength, $M_{y,\text{Fardis}}$, which compare well to the column data in the PEER database. Haselton et al. (2008) reported ratios $M_y/M_{y,\text{Fardis}}$ with a median value of 0.97 and a dispersion of σ_{ln}= 0.36, indicating reasonably good agreement.

Capping strength, M_c. While the capping strength, M_c, can, in theory, be determined through analysis, its calculation is complicated by assumptions regarding steel strain-hardening, concrete stress-strain behavior, and other factors. For the initial backbone curve, M_c, should incorporate the effects of cyclic hardening of steel. Regression analysis by Haselton et al. (2008) showed that the capping strength can be estimated from M_y by assuming a constant ratio of M_c/M_y = 1.13. The additional variability introduced by this ratio is σ_{ln}=0.10, which, when combined with the variability in M_y, results in a total variability on M_c that is equal to σ_{ln}=0.37.

Residual strength, M_r. Since values of ultimate plastic rotation, θ_{pc}, are fairly large, and data to quantify the response at large deformations are lacking, the residual strength, M_r, should be conservatively neglected, and taken as zero (or near zero).

3.4.2.7 Comparisons with ASCE/SEI 41-06

Figure 3-23 shows a modified version of the ASCE/SEI 41-06 idealized force-deformation response curve, defined as a function of the component yield strength, deformation parameters *a* and *b*, and the residual strength

parameter *c*. Since recent experimental data suggest that the sudden drop in strength from point C to D is unrealistic, and the steep negative slope is problematic for implementation in nonlinear analysis, many, including ASCE (2007b), have recommended the use of a modified slope to represent the post-peak degrading response (dashed line from points C to E).

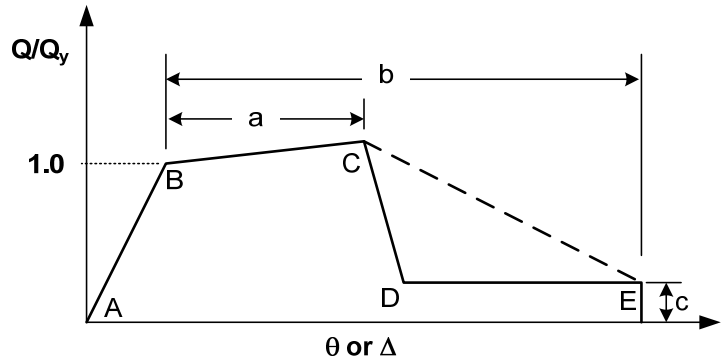

Figure 3-23 Modified force-deformation response curve (based on ASCE/SEI 41-06).

Component modeling Options 3 and 4 (Section 2.2.5) indirectly account for cyclic deterioration effects when degrading hysteretic behavior is not explicitly included in the analytical model. Option 3 uses factors to modify an initial monotonic backbone curve, and Option 4 uses conservative plastic deformation limits to control the level of component degradation in the model. These modeling options are analogous to the criteria contained in ASCE/SEI 41-06.

In modeling Option 3, the modified pre-capping plastic rotation, θ'_p, is set equal to $0.7\theta_p$, and the modified post-capping plastic rotation, θ'_{pc}, is set equal to $0.5\theta_{pc}$, where θ_p and θ_{pc} can be calculated using the empirical Equations 3-14, 3-15, and 3-16. In concept, these values are comparable to the rotation parameters (*a* and *b*) specified in ASCE/SEI 41-06 *Supplement No. 1* for reinforced concrete frame components.

Figure 3-24 shows comparisons between values based modeling Option 3 and rotation parameters *a* and *b* specified in ASCE/SEI 41-06 *Supplement No. 1*. Such a comparison is not exact, since the parameters have a somewhat different basis. Whereas the modified backbone curve values were based on a statistical regression of median response quantities, parameters *a* and *b* were based on a combination of test data and judgment, which tended to be biased on the conservative side. The dashed curves represent modeling Option 3, and the solid lines represent rotation parameters *a* and *b*. Values are plotted for different shear reinforcement ratios and different levels of shear demand.

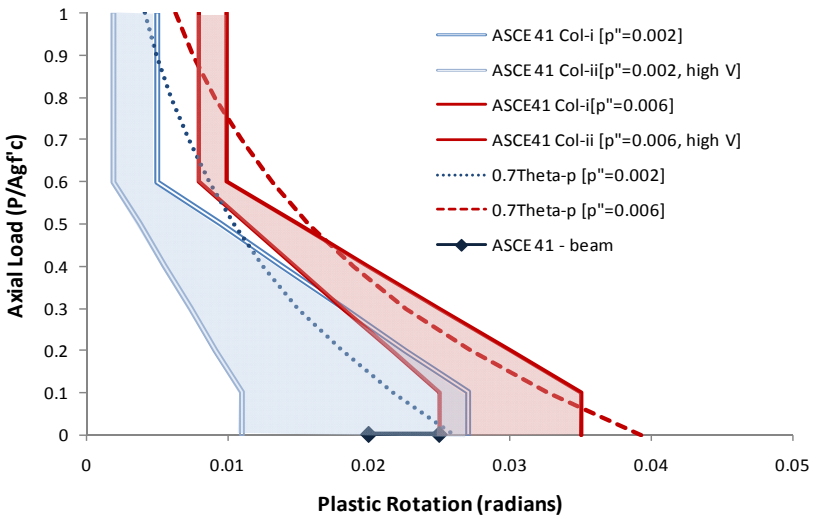

(a)

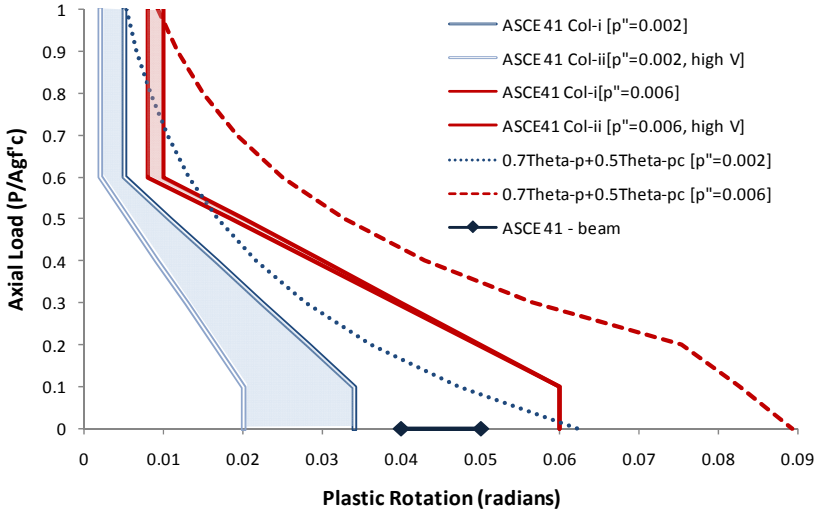

(b)

Figure 3-24 Comparison of plastic rotation parameters for modeling Option 3 versus ASCE/SEI 41-06 *Supplement No. 1* for: (a) pre-capping rotation capacity; and (b) post-capping rotation capacity.

Figure 3-24a compares values for modified pre-capping plastic rotation ($0.7\theta_p$) and rotation parameter a. For cases dominated by flexure, the values agree fairly well. Some difference is expected since the ASCE/SEI 41-06 *Supplement No. 1* values for flexure-controlled cases were reportedly about 30% less than mean values measured from tests. For cases dominated by shear, observed discrepancies are larger. This is also expected, since ASCE/SEI 41-06 *Supplement No. 1* values for high shear cases were reportedly about 55% less than mean values measured from tests. Since column data used by Haselton et al. (2008) included both flexure and flexure-

shear cases, large differences for high shear cases suggest that further work is needed to reconcile the effects of shear on flexural hinging.

Figure 3-24b compares values for modified post-capping plastic rotation ($0.7\theta_p + 0.5\theta_{pc}$) and rotation parameter *b*. Observed discrepancies are considerably larger for post-capping rotation values than for pre-capping rotation values. This is due to limited availability of data for quantifying performance of columns at very large deformations, and the increasing role that judgment plays in interpreting the data. Such differences highlight the additional uncertainty that is present when analyzing structural response out to large deformations beyond the capping point where significant degradation occurs.

Modified backbone curve parameters can also be used to determine ultimate rotation limits, which are analogous to ASCE/SEI 41-06 acceptance criteria at the Collapse Prevention performance level. The criteria are similar, though not always equivalent to the plastic rotation parameters *a* and *b* in Figure 3-23. In the case of primary components, Collapse Prevention criteria are set to avoid degradation, which is comparable to modeling Option 4. In the case of secondary components, Collapse Prevention criteria allow degradation, which is comparable to modeling Option 3.

In Option 4, the ultimate rotation is taken at the point of 20% strength loss on the descending branch of the modified backbone curve. Using the approach illustrated for steel beams in Figure 3-9, the resulting ultimate rotation limit would be $0.7\theta_p + 0.1\theta_{pc}$. In Option 3, a rotation limit of $1.5\theta_c$, or alternatively, a corresponding plastic rotation limit of $1.5\theta_p$, is used.

Figure 3-25 compares values of ultimate plastic rotation based on modeling Options 3 and 4 versus ASCE/SEI 41-06 *Supplement No. 1* acceptance criteria at the Collapse Prevention performance level. In the figure, dashed curves represent values for modeling Options 3 and 4, and solid lines represent ASCE/SEI 41-06 Collapse Prevention limits.

Plots show reasonably good agreement between the values for Option 4 and ASCE/SEI 41-06 Collapse Prevention limits for primary components, but values for Option 3 appear unconservative relative to ASCE/SEI 41-06 Collapse Prevention limits for secondary components. As noted previously, in cases with high shear demands, the discrepancies are larger, due, in part, to a conservative penalty that ASCE/SEI 41-06 places on components with high shear force demands.

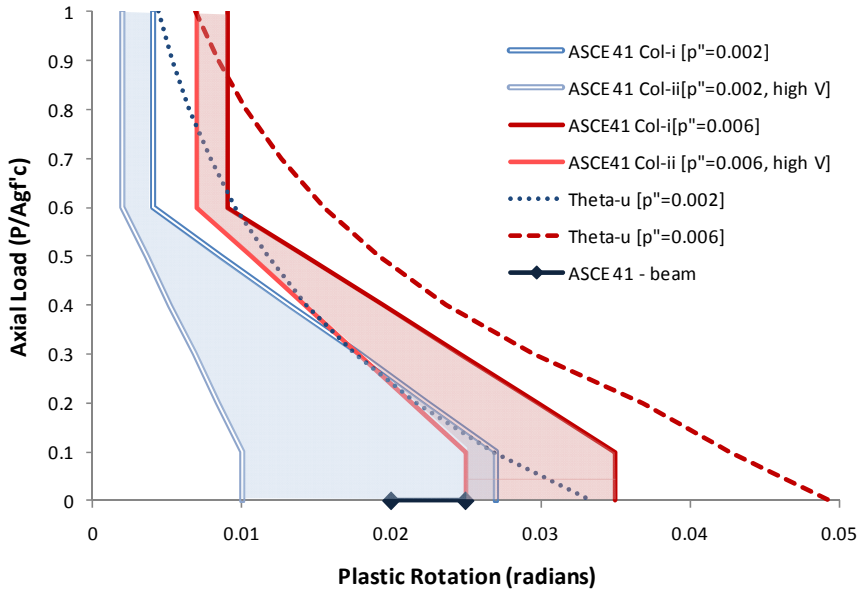

(a)

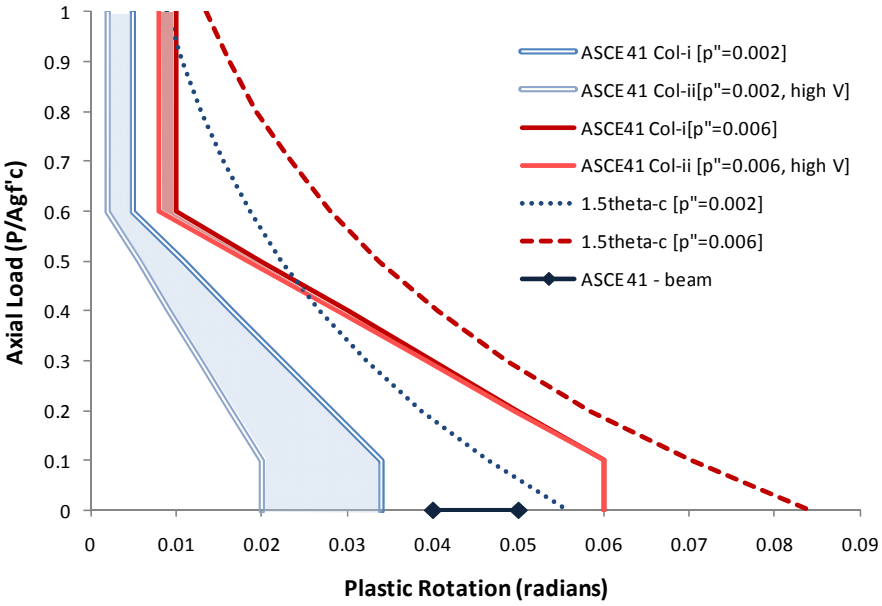

(b)

Figure 3-25 Comparison of ultimate plastic rotation versus ASCE/SEI 41-06 *Supplement No. 1* acceptance criteria at the Collapse Prevention performance level for: (a) Option 4; and (b) Option 3.

3.4.3 Quantification of Properties for Reinforced Concrete Beam-Column Joints

Code-conforming reinforced concrete frame systems used in new tall buildings are expected to have joints that can develop the flexural strength of the beams framing into the joint. Since joint shear failure is not expected to

occur, and deformations associated with bond slip and yielding penetration of beam and column reinforcing bars in the joint region are incorporated in the frame element models, modeling of joints is primarily concerned with capturing the effects of the finite joint size and the initial joint shear deformations. For model verification, however, resulting joint shear demands should be checked against the joint shear capacity, which can be calculated using recommendations in ASCE/SEI 41-06 based on the expected concrete strength and the appropriate joint configuration factors to account for confinement.

The finite joint size and shear panel deformations can generally be included explicitly, through a joint panel model as shown in Figure 3-20, or more approximately by defining effective rigid end offsets for elements framing into the joint. When modeled explicitly, the joint stiffness can be calculated using modified compression field theory (Mitra and Lowes, 2007) or by calibrating the effective initial stiffness to test data.

Alternatively, as proposed by Elwood et al. (2007), and incorporated into ASCE/SEI 41-06 *Supplement No.1*, it is reasonably accurate to model the joint using effective rigid end offsets as shown in Figure 3-26. The assumed rigid end offset is based on the relative strength of the columns and beams that are framing into the joint. For code-conforming special moment frames, in which the ratio of column to beam moment strength is required to be at least 1.2, the joints can be modeled as shown in Figure 3-26a, where the column elements have rigid end offsets equal to the depth of the beam, and the beam elements have no rigid offsets.

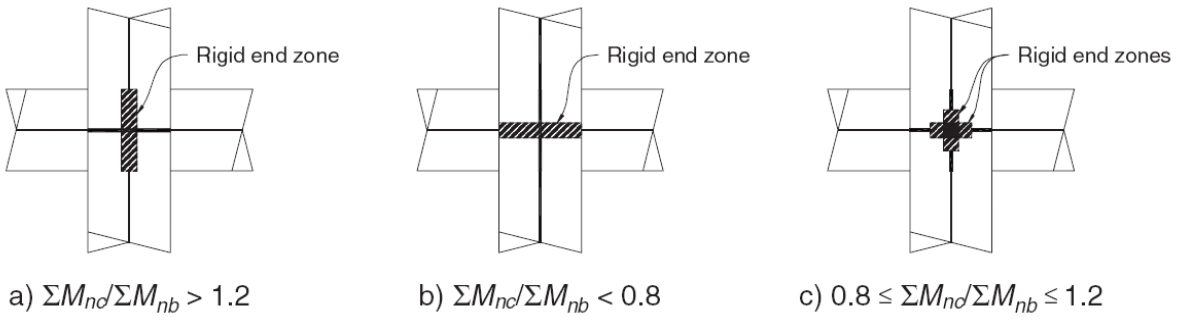

Figure 3-26 Recommended rigid end zone offsets for reinforced concrete beam column joints based on relative column and beam strengths (Elwood et al., 2007).

3.4.4 Recommendations for Modeling of Reinforced Concrete Frame Components

Summary recommendations for lumped plasticity (concentrated hinge) modeling of reinforced concrete frame components are as follows:

1. It is generally recommended to model reinforced concrete frame components using quasi-elastic elements. For nonlinear response history analyses at MCE level ground motions that are expected to cause extensive yielding, elements can be modeled using the effective yield stiffness given by Equation 3-12. At service-level ground motions, the stiffer secant stiffness, given by Equation 3-13, may be used.
2. Reasonable estimates of plastic rotation parameters for reinforced concrete frame components can be calculated using the empirical equations provided in Section 3.4.2.3 through 3.4.2.5, taking into account necessary adjustments for components with non-symmetric reinforcement, high shear demands, or other factors not explicitly considered in the models.
3. Recommended values for flexural strength parameters M_y, M_c, and M_r for reinforced concrete frame components are provided in Section 3.4.2.6.
4. For code-conforming frame systems, in which joints are proportioned to develop the flexural strength of members framing in, joint panels can be modeled with effective rigid offsets, as shown in Figure 3-26.
5. Modeling Option 1 is the preferred option. When Option 1 is not feasible, modeling Options 2, 3, or 4 can be used. Options 2 and 3 account for the negative slope of the post-capping tangent stiffness.
6. The approach illustrated for steel beams in Figure 3-9, is applicable for determining Option 3 and Option 4 modified backbone parameters for reinforced concrete frame components.
7. Caution must be exercised with ultimate rotation limits for reinforced concrete frame components determined using modeling Option 3, as these values have been shown to be unconservative relative to ASCE/SEI 41-06 Collapse Prevention limits for secondary components.

3.4.5 Acceptance Criteria for Reinforced Concrete Frame Components

Modeling parameters are calibrated to represent median response of a structure to input ground motions. As such, they are intended to be used in conjunction with strategies that account for inherent variability, and result in an appropriate level of reliability, for achieving the intended performance result. Values of dispersion characterizing the uncertainty in stiffness and plastic rotation parameters for reinforced concrete components are fairly large (typically on the order of σ_{ln} = 0.3 to 0.5) and should be considered in both the analysis (calculated demands) and the acceptance criteria (estimated capacities) for each performance limit state.

Local acceptance criteria for reinforced concrete frame components are provided for service level and MCE level evaluations. Additional local component acceptance criteria, and global acceptance criteria for the overall structural system, are provided in *Seismic Design Guidelines for Tall Buildings* (PEER, 2010).

3.4.5.1 Service Level

At the service level, force and deformation demands in reinforced concrete frame components should be limited to those corresponding to the onset of structural damage that would necessitate repair. A reasonable (although conservative) criterion for the onset of structural damage is the expected yield strength. At this level, components will have experienced limited cracking, with some potential for localized concrete spalling.

For comparison purposes, ASCE/SEI 41-06 specifies acceptance criteria for the Immediate Occupancy performance level corresponding to plastic hinge rotations of 0.2% to 0.5% in beams and columns, which is slightly beyond yield. In beam-column joints, plastic rotation is not permitted.

3.4.5.2 Maximum Considered Earthquake Level

At the MCE level, deformations in reinforced concrete frame components should be limited to levels that avoid significant strength and stiffness degradation. In terms of component backbone curves, this could be interpreted as somewhere in the range between the capping rotation, θ_c, and ultimate rotation, θ_u. Based on the modeling option selected, the following criteria are recommended:

Option 4: In Option 4, hinge rotation is limited to the rotation at 20% strength loss on the descending branch of the modified backbone curve. This criterion is appropriate for shear demands up to $V = 3\sqrt{f_c'}bd$, however, it is recommended that consideration be given to reducing this limit for reinforced concrete frame components when shear demands are high. For flexure-shear hinges with high shear demand, it is recommended that Option 4 acceptance criteria be reduced to one-half of the calculated values at a shear demand of $V > 6\sqrt{f_c'}bd$, with linear interpolation for values of shear demand between $3\sqrt{f_c'}bd < V < 6\sqrt{f_c'}bd$.

Option 3: In Option 3, the default criterion is to limit the plastic hinge rotation to $1.5\theta_p$. However, it was shown that for reinforced concrete frame components, the $1.5\theta_p$ limit for Option 3 is unconservative relative to Collapse Prevention criteria for secondary components. As such, it is suggested that the default criterion of $1.5\theta_p$ be reduced to$1.5\theta_p' = 1.5(0.7\theta_p) = 1.05\theta_p$ (which

applies the 1.5 factor to the *modified* plastic capping rotation). Additionally, for flexure-shear hinges with high shear demand, it is recommended to further reduce the criteria to one-half of the calculated values at $V > 6\sqrt{f_c'}bd$, with linear interpolation between $3\sqrt{f_c'}bd < V < 6\sqrt{f_c'}bd$.

Options 1 and 2: For Options 1 and 2, component deformation demands can extend to the ultimate rotation, θ_u (i.e., no other specific limiting criteria are proposed), provided that the analytical model captures all significant modes of deterioration.

Chapter 4

Modeling of Shear Wall and Slab-Column Frame Systems

This chapter describes recommendations for modeling of reinforced concrete shear wall and slab-column frame systems, and the derivation of modeling parameters based on available sources of experimental data. It presents recommended modeling approaches for shear wall and slab-column frame components, discusses response sensitivity, and assesses how available models compare to experimental behavior.

4.1 Modeling of Planar and Flanged Reinforced Concrete Shear Walls

The primary objective for modeling of planar and flanged reinforced concrete core walls involves capturing the load versus deformation responses related to flexure, shear, and bond in a reasonable manner. Modeling approaches typically used in the analysis and design of tall core wall buildings are discussed in the following sections.

4.1.1 Beam-Column Element Models

Equivalent beam-column element (lumped plasticity) models, such as those shown in Figure 4-1, have been used to model reinforced concrete walls. Shortcomings of these models include: (1) inability to account for migration of the neutral axis along the wall cross-section during loading and unloading; (2) interaction with the connecting components such as slabs and girders both in the plane of, and perpendicular to, the wall; (3) and influence of variation in axial load on the wall strength and stiffness. It is also more difficult to model non-planar walls, such as T- or L-shaped cross-sections, using beam-column element models. On the positive side, beam-column element models with rigid plastic hinges at the member ends are relatively easy to use, and are computationally efficient. Stiffness parameters and plastic hinge rotation limits are easily assigned.

Necessary modeling parameters for equivalent beam-column elements include effective stiffness values for flexure, $E_c I_{eff}$, and shear, $G_c A$, yield strengths, M_y and V_y, post-yield stiffness (typically taken as a fraction of the effective stiffness), deformation capacities, and residual strength. Modeling

parameters are typically defined using well-established procedures given in standards such as ACI 318-08, *Building Code Requirement for Structural Concrete* (ACI, 2008), ASCE/SEI 41-06, *Seismic Rehabilitation of Existing Buildings* (ASCE, 2007a), or values derived from test results. Flexural strength can be modeled assuming an average axial load (i.e., independent of changes in axial load) or using *P-M* interaction diagrams.

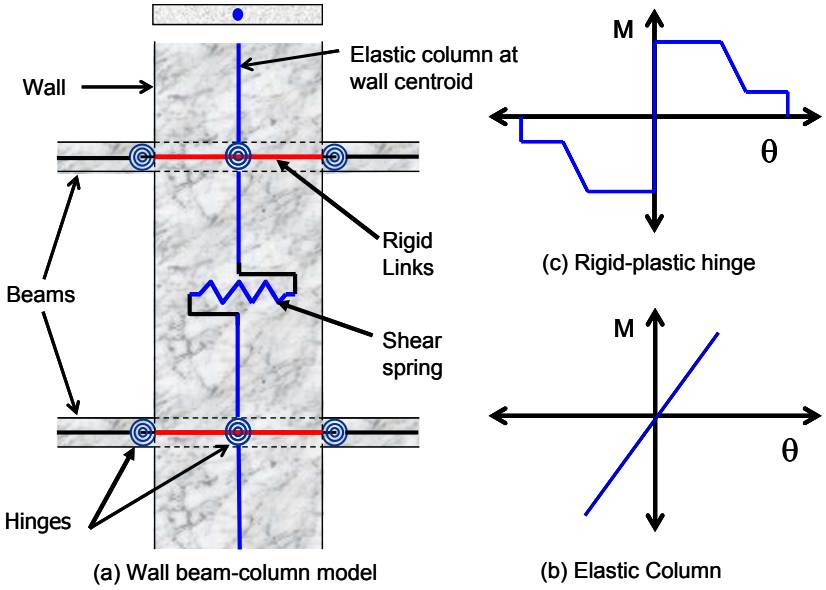

Figure 4-1 Equivalent beam-column element representation of a reinforced concrete shear wall.

4.1.2 Fiber Beam-Column Models

Fiber (distributed inelasticity) beam-column models, involve subdividing the wall section into concrete and steel fibers, as shown in Figure 4-2. Use of fiber models has become more common in practice as they have been implemented in commercially available analytical software. They address many of the shortcomings noted for equivalent beam-column models.

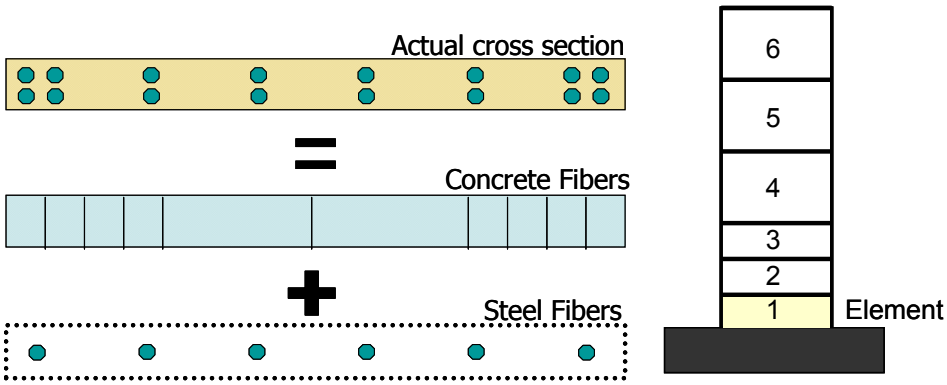

(a) Fiber model of cross-section (b) Elevation of wall

Figure 4-2 Fiber element representation of a reinforced concrete shear wall.

In a fiber model, the cross-section geometry is prescribed, and concrete and steel fibers are individually defined. In Figure 4-2a the concrete is sub-divided into ten fibers, and the reinforcement is grouped into six fibers. In Figure 4-2b, the elements are stacked to enable modeling of a planar wall. It is important to use a sufficient number of fibers along the cross-section to define the strain gradient at equilibrium for a given loading condition, and a sufficient number of elements over the height of the wall to capture the overall wall behavior. Use of too many fibers and elements, however, can substantially increase computer run time. Preliminary analytical studies for a given wall section can be used to determine the sensitivity of the selected fiber mesh on the predicted behavior, and to optimize the results.

Monitored response quantities in a fiber model include material strain limits, such as maximum concrete compressive strain and maximum reinforcement tensile strain. Selection of rotation or strain limits is based on available material standards, test results, or engineering judgment. ASCE/SEI 41-06, for example, specifies maximum usable strain limits for concrete and reinforcing steel. Limiting values for compressive strain in unconfined concrete are 0.002 (in pure compression) or 0.005 (other conditions), and maximum strains in reinforcing steel are 0.02 in compression and 0.05 in tension. A significant shortcoming associated with fiber models is the potential impact that assumed material relations and element sizes have on maximum computed strain values.

Use of a fiber model, with defined uniaxial material relations, implies several important differences relative to the use of an equivalent beam-column model. In an equivalent beam-column model, the elastic flexural stiffness is specified (e.g., $E_c I_{eff} = 0.5 E_c I_g$), whereas in a fiber model, the flexural stiffness is derived from the specified material relations, and varies depending on the magnitude of axial load. Also, in a beam-column model, the flexural strength is defined using simplified concrete theory (i.e., prescribed strains in the extreme steel or concrete fibers, linear concrete compressive behavior at yield moment, or Whitney Stress Block at nominal moment), whereas in a fiber model, the section strength depends on the prescribed material relations.

4.1.3 Biaxial Fiber and Detailed Finite Element Models

More sophisticated modeling options are available in commercially available software. For example, a uniaxial fiber model can be extended to two-dimensions, as shown in Figure 4-3. In a biaxial model, yielding is possible in both planes (horizontal and vertical), which can lead to complex yielding behavior. This is especially true in regions where a refined mesh is used;

therefore, careful examination of the analysis results is necessary to verify that predicted responses are consistent with expectations. Biaxial models might be convenient for structural systems with complex geometry, such as core walls, or elements subjected to bidirectional forces, such as floor diaphragms.

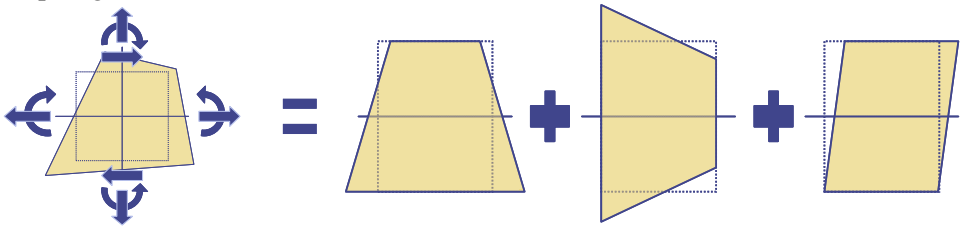

Figure 4-3 Biaxial fiber model for bending in two-dimensions.

Modeling of core wall systems using detailed finite element models with concrete elements (e.g., brick elements) and discrete modeling of reinforcement is possible with currently available commercial software. Although such models are available, they should be used with caution, as it is often difficult to determine if the resulting load versus deformation behavior of the components is within reasonable bounds. Given this difficulty, use of detailed nonlinear finite element models is not emphasized.

4.1.4 Coupled Models (Shear-Flexure Interaction)

Shear behavior in commonly available equivalent beam-column and fiber models is uncoupled from flexural behavior. In an uncoupled model, flexural yielding occurs in combination with elastic shear behavior, or shear yielding occurs with elastic flexural response, depending on geometry, materials, or loading conditions.

Available software programs generally do not account for coupled shear-flexure interaction behavior. Research, however, has shown that such interaction exists. Generally shear-flexure interaction results in increased flexibility and somewhat reduced strength (Oesterle et al., 1984; Elwood et al., 2007). Conceptually, as nonlinear flexural ductility increases, flexural and bond crack widths grow, and shear resistance degrades.

Modeling approaches are available that account for shear-flexure interaction (Petrangeli et al., 1999; Massone, 2006). Results for low-aspect ratio walls are presented in Figure 4-4, which compares uncoupled flexural response with coupled shear-flexure response determined by analysis and by test. In the figure, it can be seen that coupled shear-flexure behavior tends to significantly reduce lateral stiffness once shear cracking occurs, but only modestly reduces the shear strength.

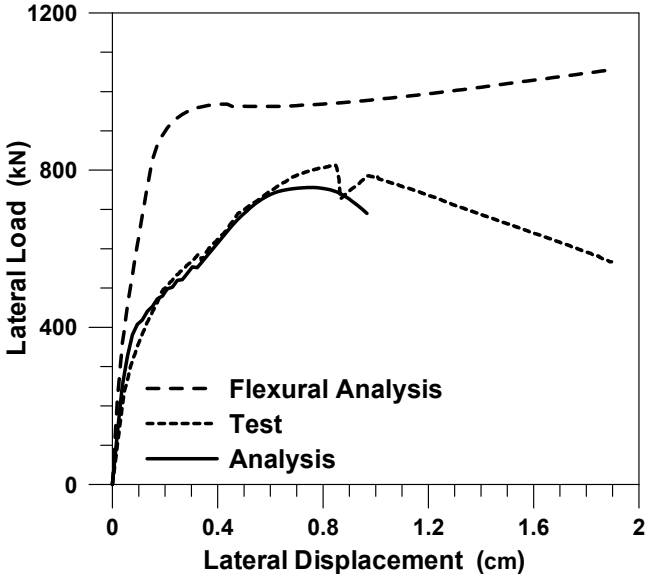

Figure 4-4 Coupled model and results for a low-aspect ratio wall (Massone, 2006).

Existing shear-flexure interaction models typically do not consider cyclic loading, and are not available in commercial software. Without commercially available software capable of incorporating coupled models, the potential impact of coupled behavior on strength and stiffness of low-aspect ratio walls should be considered with appropriate bounds on the lateral stiffness used to model these elements.

4.2 Quantification of Properties for Planar and Flanged Walls

In the following sections, available data from laboratory testing of planar (rectangular) and flanged (T-shaped) walls are used to quantify properties related to shear and flexural behavior, and assess the ability of current modeling approaches to capture important response quantities, such as overall lateral load versus displacement response, concrete and reinforcement strain demands in critical (yielding) regions, and plastic rotations over assumed plastic hinge lengths.

4.2.1 Shear Behavior

Shear force versus deformation response is often represented using a uniaxial shear spring with a prescribed shear-deformation behavior. Shear yield is often assumed to occur at the nominal shear strength.

4.2.1.1 Shear Force-Deformation Behavior

There are few studies focusing on the force versus deformation response of walls governed by shear behavior. Deformations corresponding to the onset of yield and shear strength degradation are based on limited test data, such as Hidalgo et al. (2002), Hirosawa (1975), and Massone (2006). Figure 4-5a shows the shear force-deformation relation (backbone curve) provided in FEMA 356, *Prestandard and Commentary for the Seismic Rehabilitation of Buildings* (FEMA, 2000d). Figure 4-5b shows an improved relation that is provided in ASCE/SEI 41-06 *Supplement No. 1* (ASCE, 2007b), which allows the backbone curve to be modified to include a pre-cracked stiffness and strength, followed by post-cracked stiffness up to the nominal (yield) strength.

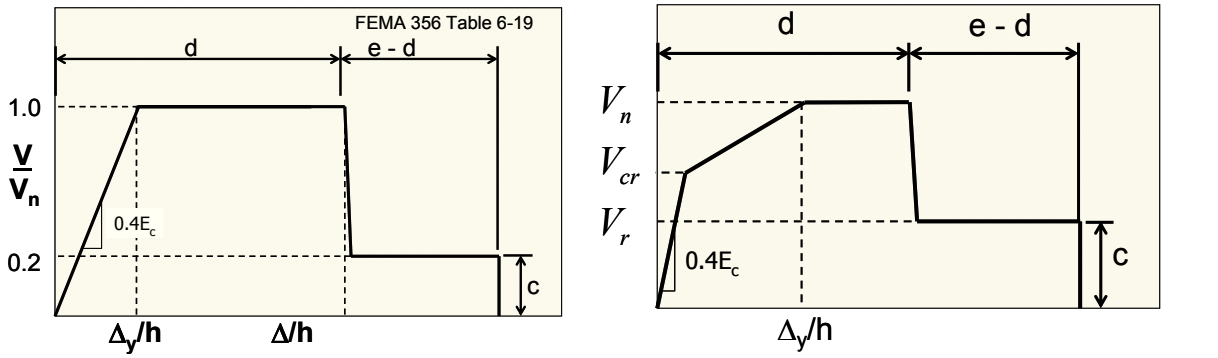

(a) Shear backbone curve (from FEMA 356) (b) Shear backbone curve (from Supplement No.1)

Figure 4-5 Shear force-deformation curves based on: (a) FEMA 356; and (b) ASCE/SEI 41-06 Supplement No. 1.

4.2.1.2 Shear Strength

The nominal shear strength of walls is typically defined using Equation 4-1, taken from ACI 318-08:

$$V_n = A_{cv}\left(\alpha_c \lambda \sqrt{f_c'} + \rho_t f_y\right) \tag{4-1}$$

where $\alpha_c = 3.0$ for a height-to-length ratio, $h_w/l_w \leq 1.5$, $\alpha_c = 2.0$ for $h_w/l_w \geq 2.0$, and varies linearly for $1.5 \leq h_w/l_w \leq 2.0$. In this equation, λ is 0.75 for lightweight concrete and 1.0 for normal weight concrete, A_{cv} represents the cross-sectional web area of a wall, f_c' is the compressive strength of concrete, ρ_t is transverse reinforcement ratio, and f_y, is the yield strength of transverse reinforcement. The variation of α_c for h_w/l_w values between 1.5 and 2.0 accounts for the observed strength increase for low-aspect ratio walls. An upper limit on nominal shear strength is set at $V_n = A_{cv}\left(10\sqrt{f_c'}\right)$ for a single wall, which is the same limit used for beams (ASCE-ACI, 1973), and

$V_n = A_{cv}\left(8\sqrt{f_c'}\right)$ for walls sharing lateral load. Test data were reviewed by Cardenas et al. (1973 and 1980) to show that the limit of $V_n = A_{cv}\left(10\sqrt{f_c'}\right)$ was satisfactory for design.

Limiting the wall shear stress to $V_n = A_{cv}\left(6\sqrt{f_c'}\right)$ has been suggested (Wang et al., 1975; Aktan et al., 1985) to ensure ductile response for reverse cyclic loading, and to avoid sliding shear failures, unless diagonal shear reinforcement is present (Paulay, 1980). Subsequent test results reported by Paulay et al. (1982) for walls controlled by flexural yielding indicated that ductile response, with displacement ductility ratios exceeding four, could be achieved for walls with a maximum shear stress of approximately $V_n = A_{cv}\left(8\sqrt{f_c'}\right)$, provided failure modes associated with diagonal tension, diagonal compression, and sliding shear were prevented. Test results also indicated that flanged walls, because of the reduced flexural compression depth, were more susceptible to shear strength degradation associated with sliding shear.

In contrast to shear strength of columns, the ACI 318-08 equation for shear strength of walls does not consider the effect of axial load. Orakcal et al. (2009) reported that wall shear strength is sensitive to axial load, with V_{test}/V_n values of approximately 1.5 for walls tested with an axial load of $P_u / A_g f_c' = 0.05$, and 1.75 for walls with an axial load of $P_u / A_g f_c' = 0.10$. Relatively few wall tests with reported shear failures have been conducted that include axial load, so insufficient information exists to systematically assess the impact of axial load on shear strength.

In the alternative backbone relation of Figure 4-5b, the shear strength at cracking is taken as:

$$V_{cr} = 4\sqrt{f_c'}\left(1+\frac{P_u}{4\sqrt{f_c'}A_{web}}\right)^{1/2} \le 0.6V_n \qquad (4\text{-}2)$$

where P_u is the factored axial load, and A_{web} is the cross-sectional area of the web, and other parameters are as defined in Equation 4-1.

Oesterle et al. (1984) used a truss analogy to determine the shear stress associated with web crushing of barbell and I-shaped wall cross-sections as:

$$v_{n,wc} = 0.14 f_c' + \frac{N_u}{2l_w h} \;\le\; 0.18 f_c' \qquad (4\text{-}3)$$

where N_u is the factored axial load normal to the cross-section. Tests conducted by by Wang et al. (1975), Barda et al. (1977), and Valenas et al. (1979), show that Equation 4-3 tends to slightly underestimate the measured

shear stress. ACI 318-08 limits the value of $\sqrt{f_c'}$ to 100 psi, indicating that the upper limit on shear stress for walls is $10\sqrt{f_c'}$ = 1,000 psi. Available test data suggest that this limit is conservative for concrete compressive strengths of approximately 6 ksi and higher.

Test data for walls with concrete strength exceeding 10 ksi are summarized by Kabeyasawa and Hiraishi (1998) and Farvashany et al. (2008). Kabeyasawa and Hiraishi (1998) reported on tests with concrete strengths ranging between 10 ksi and 15 ksi, and shear-span-to-depth ratios, M_u/V_uI_w, between 0.6 and 2.0. Wallace (1998) evaluated these data with respect to ACI 318-95 requirements (which are essentially equivalent to ACI 318-08). The median ratio of V_{test}/V_n was 1.38, with a standard deviation of 0.34, indicating that ACI 318 requirements provided a lower-bound estimate of tested wall shear strengths. For ratios of $\rho_t f_y / f_c' > 0.10$, ACI 318 tended to overestimate tested shear strengths, indicating that the contribution of web reinforcement to shear strength was overestimated. This is consistent with results reported by Wood (1990) for concrete compressive strengths ranging from 2.0 ksi to 6.0 ksi.

Farvashany et al. (2008) reported on tests of I-shaped walls with concrete strengths ranging between approximately 12 ksi and 15 ksi, and a shear-span-to-depth ratio, M_u/V_uI_w, of 1.36. For these tests, ratios of V_{test}/V_n varied from 2.6 to 3.8, but these walls were only subjected to monotonic loading.

4.2.1.3 Shear Strength versus Ductility Demand

Models that reduce shear strength with increasing ductility demand have been provided in references for design of columns, such as Sezen and Moehle (2004), Zhu et al. (2007), and ASCE/SEI 41-06. An analogous shear strength capacity relation for walls is:

$$V_n = k_\delta A_{cv}\left(\alpha_c \lambda \sqrt{f_c'} + \rho_t f_y\right) \tag{4-4}$$

where k_δ represents a reduction factor that reduces shear strength with increasing ductility, and all other parameters are as defined in Equation 4-1. Various relations have been proposed for k_δ. The relation used for columns in ASCE/SEI 41-06 is depicted in Figure 4-6, for three types of failure modes: shear, flexure-shear, and flexure.

In the case of walls, relatively sparse data exist for judging whether shear strength should be degraded with increasing ductility demand. Results from two small scale tests reported by Corley et al. (1981) show that deformation capacity is impacted by the level of shear stress, i.e., wall shear strength degrades with increasing ductility demand. Oesterle et al. (1984) suggest

that the reduction in drift capacity is related to increased contribution of inelastic shear deformations leading to web crushing failures.

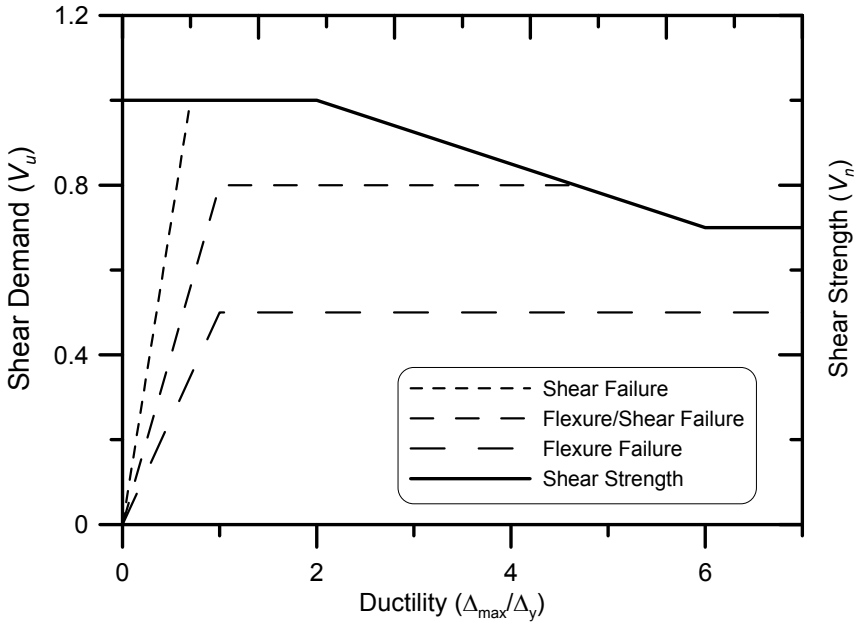

Figure 4-6 ASCE/SEI 41-06 variation in column shear strength versus ductility demand.

A specific recommendation for shear walls is not given here, as this issue requires further study. However, for performance-based design of core wall systems in tall buildings, it would appear prudent to consider some reduction in shear strength with increasing ductility demand.

4.2.1.4 Effective Shear Stiffness

The uncracked shear stiffness is typically taken as:

$$G_c A = \frac{E_c}{2(1+\nu)} A_{cv} = 0.4 E_c A_{cv} \tag{4-5}$$

where ν is Poisson's ratio, and A_{cv} is the cross-sectional area of the web. Based on the assumption that Poisson's ratio for uncracked concrete is approximately 0.2, the effective shear stiffness defined in ASCE/SEI 41-06 is $G_c A = 0.4 E_c A_w$.

From Mohr's circle, the shear strain at yield is twice the principal strain (approximately 0.002 for Grade 60 reinforcement); therefore, the effective shear stiffness at yield is approximately $G_c/20$ for walls with a shear strength of $5\sqrt{f_c'}A_{cv}$. For typical walls in new construction, the effective shear stiffness at yield doubles to approximately $G_c/10$ at a shear strength of about $10\sqrt{f_c'}A_{cv}$.

The post-cracked shear stiffness is substantially less than that given in Equation 4-5, although the presence of axial load increases shear stiffness (Wallace, 2007). Unfortunately, test data necessary for assessing wall shear stiffness at shear cracking and shear yielding are limited because of difficulties in instrumenting and measuring very small displacements in stiff walls, and assessing the relative contributions of flexural, shear, and slip deformations (Sozen and Moehle, 1993).

Sozen and Moehle (1993) studied load versus deformation behavior of low-rise walls and reported that a relatively simple model could be used to reasonably capture the measured load versus deformation response prior to strength degradation. The proposed model consists of three components to account for flexure, shear, and slip. For flexure, the force versus deformation behavior is defined for two points, cracking and yielding, along with an assumed post-yield stiffness equal to 3% to 15% of the yield stiffness. The moment capacities at cracking and yielding, and the associated deformations, are calculated using straightforward methods, such as those based on the results of a moment-curvature analysis.

For shear, two points, cracking and ultimate, are used to define the load versus deformation behavior. The cracking point is defined by:

$$v_c = 4\sqrt{f_c'}\sqrt{1+\frac{f_o}{4\sqrt{f_c'}}} \qquad \gamma_c = k\frac{v_c}{G_c} \tag{4-6}$$

where v_c is the cracking shear stress in psi, f_c' is the compressive concrete capacity in psi, f_0 is the average axial stress in psi, γ_c is the shear strain at shear cracking, G_c is the elastic shear modulus assumed as a fraction of Young's modulus, $0.4E_c$, Young's modulus, E_c, is assumed as $57{,}000\sqrt{f_c'}$ in psi, and k relates average shear stresses and strains (A_w/1.2 for rectangular wall cross-sections, A_w/1.1 for walls with flanges). The ultimate point is defined by:

$$v_{cu} = v_c + \rho_w f_y \qquad \gamma_{cu} = k\frac{v_{cu}}{n\rho_w G_c} \tag{4-7}$$

where v_{cu} is the ultimate shear stress in psi, γ_{cu} is the shear strain at shear capacity, ρ_w is the wall web reinforcement ratio (lesser of the two directions), n is the modular ratio, E_s/E_c, and f_y is the reinforcement yield stress. To convert from stress to force, the stresses at each point are multiplied by the area of the web.

For slip deformations, the rotation at an interface is calculated (e.g., at the cracking moment and the yield moment) and the additional deformation

associated with slip is added to the deformation associated with flexure (bending without slip). Various slip models appear in literature (e.g., Saatcioglu et al., 1992; Cho and Pincheira, 2006), but a detailed description of slip models is beyond the scope of this report.

The effective shear stiffness of low-rise walls was also examined by Elwood et al. (2007), focusing on lightly-reinforced wall segments. Figure 4-7 shows that the use of $0.4E_c$ is reasonable for modeling uncracked shear stiffness of lightly reinforced wall piers, provided that the flexural deformations are modeled independently (e.g., with a fiber model).

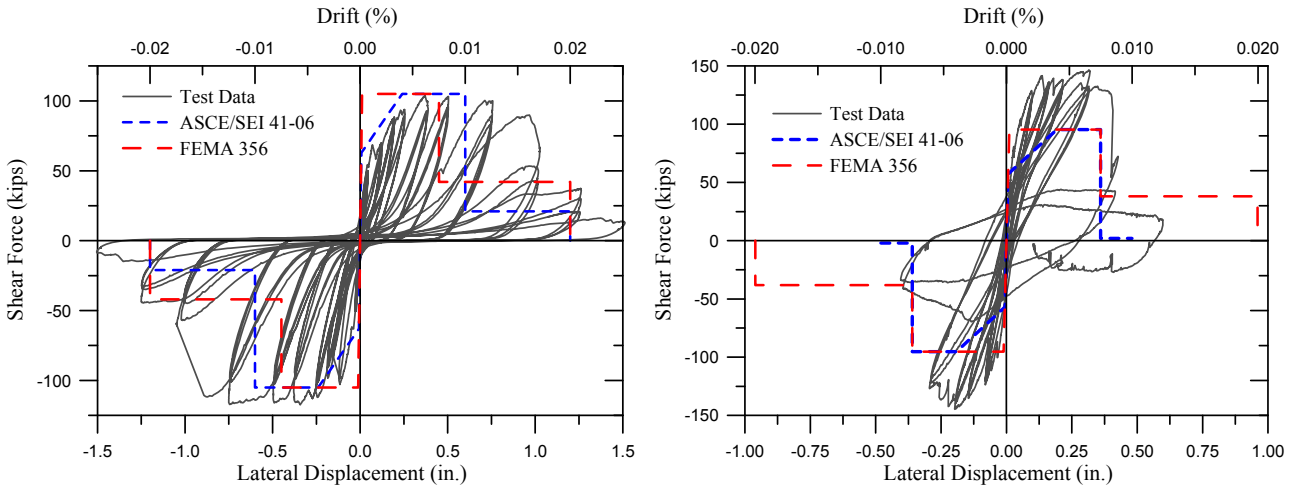

(a) Spandrel Test: $P=0.0A_g f'_c$ (b) Spandrel Test: $P=0.05A_g f'_c$

Figure 4-7 Shear force-deformation results for lightly reinforced wall piers (Elwood et al., 2007).

Given the influence of axial load and web reinforcement on shear strength, and the effects of cracking, selection of a single effective shear stiffness is problematic for analysis of shear wall systems. The impact of potential uncertainty in the effective shear stiffness of the wall should be considered to obtain bounds on important response quantities.

4.2.2 Effective Flexural Stiffness

In equivalent beam-column models, effective flexural stiffness is taken as a fraction of the gross inertia of the concrete cross-section. The reduction in stiffness is intended to account for the influence of concrete cracking, axial load, reinforcing bond slip, and anchorage extension. In ASCE/SEI 41-06, the specified effective flexural stiffness $E_c I_{eff}$ is $0.8E_c I_g$ for uncracked walls and $0.5E_c I_g$ for cracked walls.

Values in ASCE/SEI 41-06 are consistent with results obtained from analytical studies of ten-story walls subjected to low-to-moderate levels of earthquake shaking (Wallace et al., 1990), which indicate that values of $E_c I_{eff}$

between $0.4E_cI_g$ and $0.5E_cI_g$ resulted in good agreement between measured and modeled responses (Figure 4-8a).

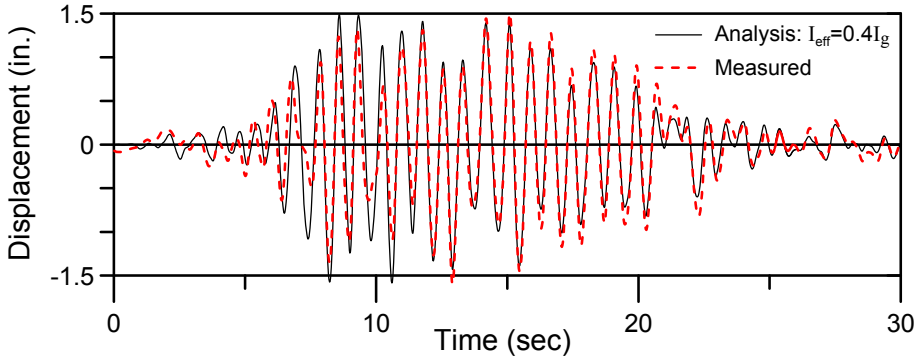

(a) 10-story walls (Yan and Wallace,1993)

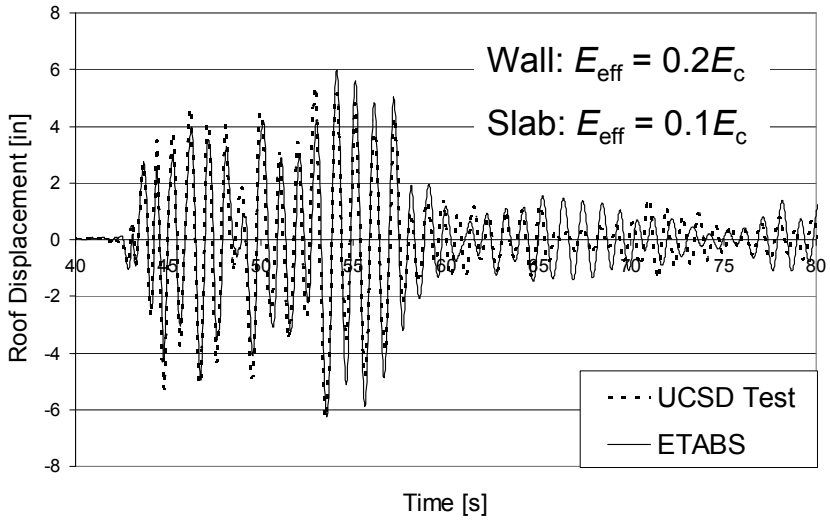

(b) 7-story walls (Panagiotou and Restrepo, 2007)

Figure 4-8 Roof displacement response correlation studies for: (a) 10-story walls; and (b) 7-story walls.

A value of $0.4E_cI_g$ was used with axial loads on the order of $P \approx 0.10A_g f_c'$, and a value of $0.5E_cI_g$ was used as a reasonable approximation for walls with modest axial load. However, displacement response history comparisons at the top of a 7-story wall tested by Panagiotou and Restrepo (2007) indicate that $0.2E_cI_g$ produced good agreement between tested and modeled results (Figure 4-8b). These disparate results indicate that appropriate effective stiffness values may vary depending on the specific characteristics of the wall.

The Canadian Code was recently modified to include recommendations for upper- and lower-bound flexural stiffness for linear analysis of walls using the following equations (Adebar et al., 2007):

$$I_e = \left(0.6 + \frac{P}{f_c' A_g}\right) I_g \le I_g \qquad \text{Upper-bound} \qquad (4\text{-}8a)$$

$$I_e = \left(0.2 + 2.5\frac{P}{f_c' A_g}\right) I_g \le 0.7\, I_g \qquad \text{Lower-bound} \qquad (4\text{-}8b)$$

Variations in the upper- and lower-bound values of effective moment of inertia predicted by Equations 4-8a and 4-8b are shown in Figure 4-9. In Figure 4-9a, the lower-bound effective stiffness is between $0.4E_cI_g$ and $0.5E_cI_g$ for axial load levels of $P \approx 0.10 A_g f_c'$, and is near $0.3E_cI_g$ for axial load levels of $P \approx 0.05 A_g f_c'$. These values are generally consistent with the results presented in Figures 4-8a and 4-8b.

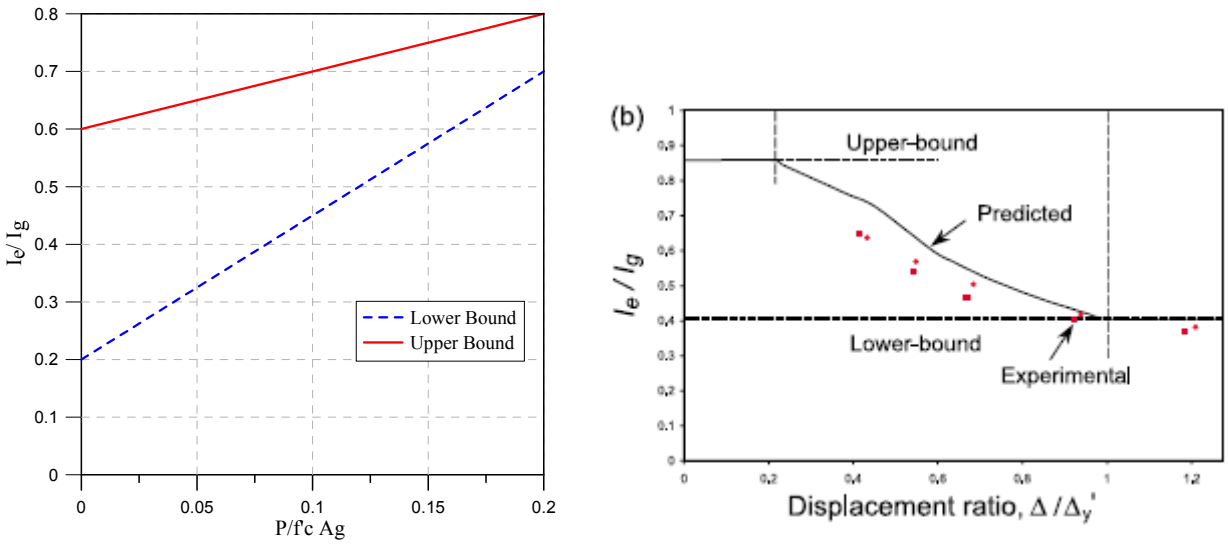

(a) Effective stiffness versus axial load ratio

(b) Effective stiffness versus displacement ratio

Figure 4-9 Upper-bound and lower-bound wall flexural stiffness versus: (a) axial load ratio; and (b) displacement ratio (Adebar et al., 2007).

Figure 4-9b shows that upper-bound values would be appropriate for uncracked walls with maximum (roof) displacement less than about 0.2 times the yield displacement, and lower-bound values would be appropriate when the maximum displacement is equal to, or exceeds, the yield displacement. This relationship can be useful in assigning effective flexural stiffness for service level analyses through an iterative approach, where a stiffness value is assumed, and then verified based on the analysis results. A lower-bound stiffness will most likely be appropriate in maximum considered earthquake-level (MCE) analyses.

Use of less longitudinal reinforcement would be expected to reduce the effective flexural stiffness prior to yield. Since yield curvature is primarily a

function of wall length, i.e., $\phi_y \approx (0.0025 \text{ to } 0.003)/l_w$, then a reduction in the nominal (yield) moment by a factor of two will produce a nearly equal reduction in the effective stiffness, as shown in Figure 4-10.

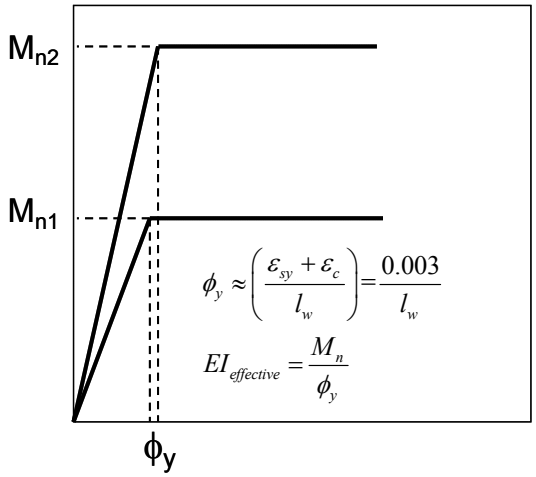

Figure 4-10 Impact of wall flexural strength on effective stiffness.

The test presented in Figure 4-8b was conducted for a relatively low axial load $\left(P \approx 0.05 A_g f_c'\right)$, and a primary objective of that study was to demonstrate that satisfactory lateral-load behavior could be achieved using approximately one-half the longitudinal reinforcement typically required in current codes. The lower value of effective stiffness observed in that test might, therefore, be an artifact of the test parameters.

Figure 4-11 shows a comparison between predicted and tested effective stiffness values for rectangular and T-shaped walls that were subjected to constant axial stress and reverse cyclic loading (Thomsen and Wallace, 2004).

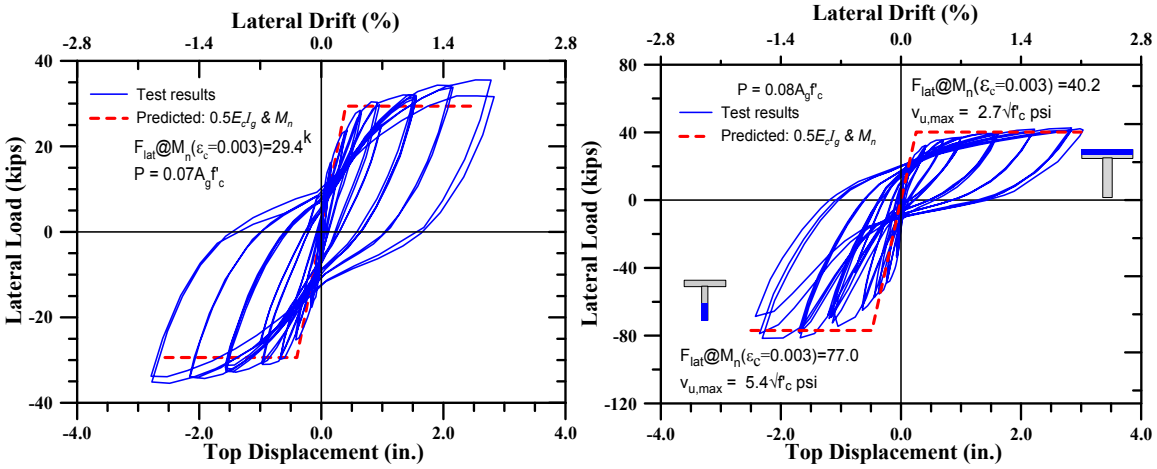

Figure 4-11 Comparison between predicted and tested effective stiffness values for: (a) rectangular walls; and (b) T-shaped walls.

Results indicate that $E_c I_{eff} = 0.5 E_c I_g$ reasonably estimates the effective stiffness, although the T-shaped wall is stiffer with the flange in tension and softer with the flange in compression.

Selection of an appropriate effective flexural stiffness is influenced by a number of parameters. Based on these limited studies, no single fraction of $E_c I_g$ is likely to work for all wall geometries, reinforcement ratios, and levels of axial load. Use of an effective linear stiffness of $0.4 E_c I_g$ to $0.5 E_c I_g$ appears appropriate for walls with axial stress levels near $P \approx 0.10 A_g f_c'$. For walls that do not have sufficient boundary reinforcement (flexural strength) to satisfy current code requirements, use of a lower value might be appropriate.

For lower levels of axial load, use of Equation 4-8b for the lower-bound effective stiffness is recommended to account for variation in axial load. Results from Adebar et al. (2007) suggest that higher axial stress levels, which would be expected to reduce cracking, are likely to yield higher effective stiffness values. At this time, however, there are insufficient test data available to assess the appropriateness of using higher effective linear stiffness values for higher levels of axial load.

Given the uncertainty in effective linear stiffness based on wall characteristics and axial load, use of a moment-curvature analysis (with appropriate uniaxial material relations for concrete and reinforcement) is likely the best approach for assessing flexural stiffness. Figure 4-12 shows a comparison of moment versus curvature relations obtained from section analysis and from tests on a slender wall (Taylor et al., 1998) and bridge column (Janoyan et al., 2006).

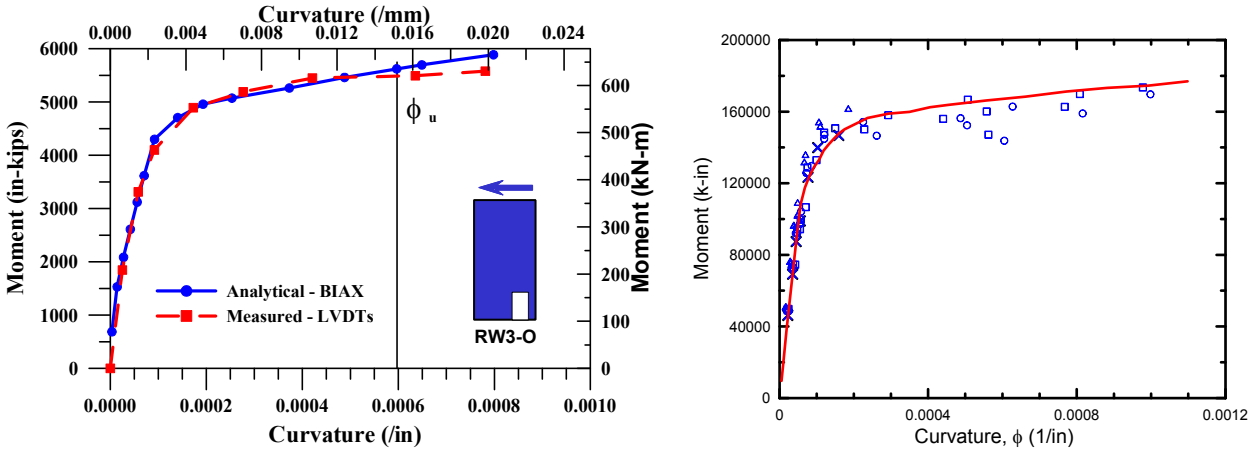

(a) Slender wall

(b) Bridge column

Figure 4-12 Comparison of modeled and tested moment versus curvature relations for: (a) slender wall; and (b) bridge column.

Results indicate that a moment versus curvature analysis does a reasonably good job at capturing the flexural stiffness for the range of axial loads in the two tests ($0.03A_g f_c'$ and $0.10A_g f_c'$). A moment-curvature analysis, however, does not consider the reduction in effective flexural stiffness due to slip deformations (Elwood et al., 2007; Sozen and Moehle, 1993), which should be considered. For the test results presented in Figure 4-12, slip deformations were negligible.

4.2.3 Material Models

In fiber element models, effective stiffness values are not used since load versus deformation response of a fiber model depends on the uniaxial material stress-strain relations specified for the concrete and steel fibers, level of axial load, and current condition of the element (considering hysteretic response in nonlinear response history analysis). Example stress-strain relations used to capture the uniaxial cyclic behavior of concrete and steel reinforcement are shown in Figure 4-13.

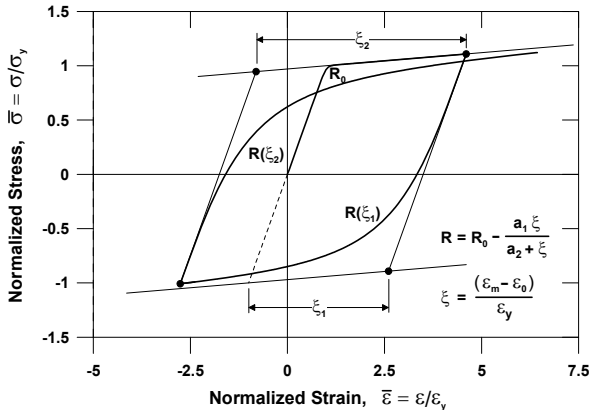

(a) Reinforcing steel (Menegotto and Pinto, 1973)

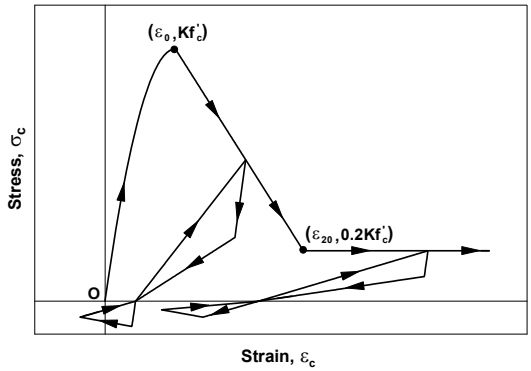

(b) Concrete (Yassin, 1994)

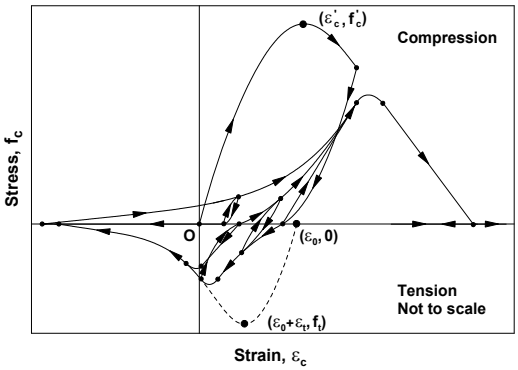

(c) Concrete (Orakcal and Wallace, 2004)

Figure 4-13 Uniaxial material models commonly used in fiber models.

Given that a fiber model can be used for both service level and MCE level analyses, the assumed uniaxial material models for concrete and reinforcing steel must reasonably represent the behavior of the materials used in construction over the full range of permissible response.

Cyclic behavior of steel reinforcement is typically modeled using the relationship proposed by Menegotto and Pinto (1973), as extended by Filippou et al. (1983). The model, shown in Figure 4-13a, incorporates cyclic degradation using a curvature parameter that accurately simulates the observed experimental behavior of cyclic reinforcement.

Common concrete material models include Yassin (1994) and Orakcal and Wallace (2004). The envelope of the concrete model in Figure 4-13b is based on the model from Scott et al. (1982), which considers both unconfined and confined concrete behavior, with the unloading and reloading rules described by Yassin (1994). Additional models are available, including envelope models proposed by Mander et al. (1988), Chang and Mander (1994), and Saatcioglu and Razvi (1992), and Razvi and Saatcioglu (1999).

Given substantial advances in modeling uniaxial concrete behavior, the model in Figure 4-13c represents a substantial improvement over the model in Figure 4-13b, with fairly complex unloading and reloading behavior, updated cyclic tensile behavior, and rules that better capture gradual crack closure. A comprehensive review of wall modeling, as influenced by the selection of material model parameters is provided by Orakcal et al. (2004) and Orakcal and Wallace (2006). Although improved comparisons between model and test results generally result when more sophisticated models are used, the results obtained using relatively simple models are generally acceptable.

4.2.4 Material Models in Commercially Available Software

Commercially available software typically employs simplified material relations, as shown in Figure 4-14. Typical models for reinforcing steel are bilinear, either with strain hardening and stiffness degradation on reverse loading (Figure 4-14a) or without (Figure 4-14b). The typical concrete model is derived from a trilinear relation (linear loading, plateau, linear degradation) and relatively simple unloading-reloading relations (Figure 4-14c).

Comparisons between wall tests and results generated using simplified material models in Perform 3D, *Nonlinear Analysis and Performance Assessment for 3D Structures* (Computers and Structures, Incorporated) are

shown in Figure 4-15. Results are compared for both rectangular (planar) and flanged (T-shaped) wall configurations.

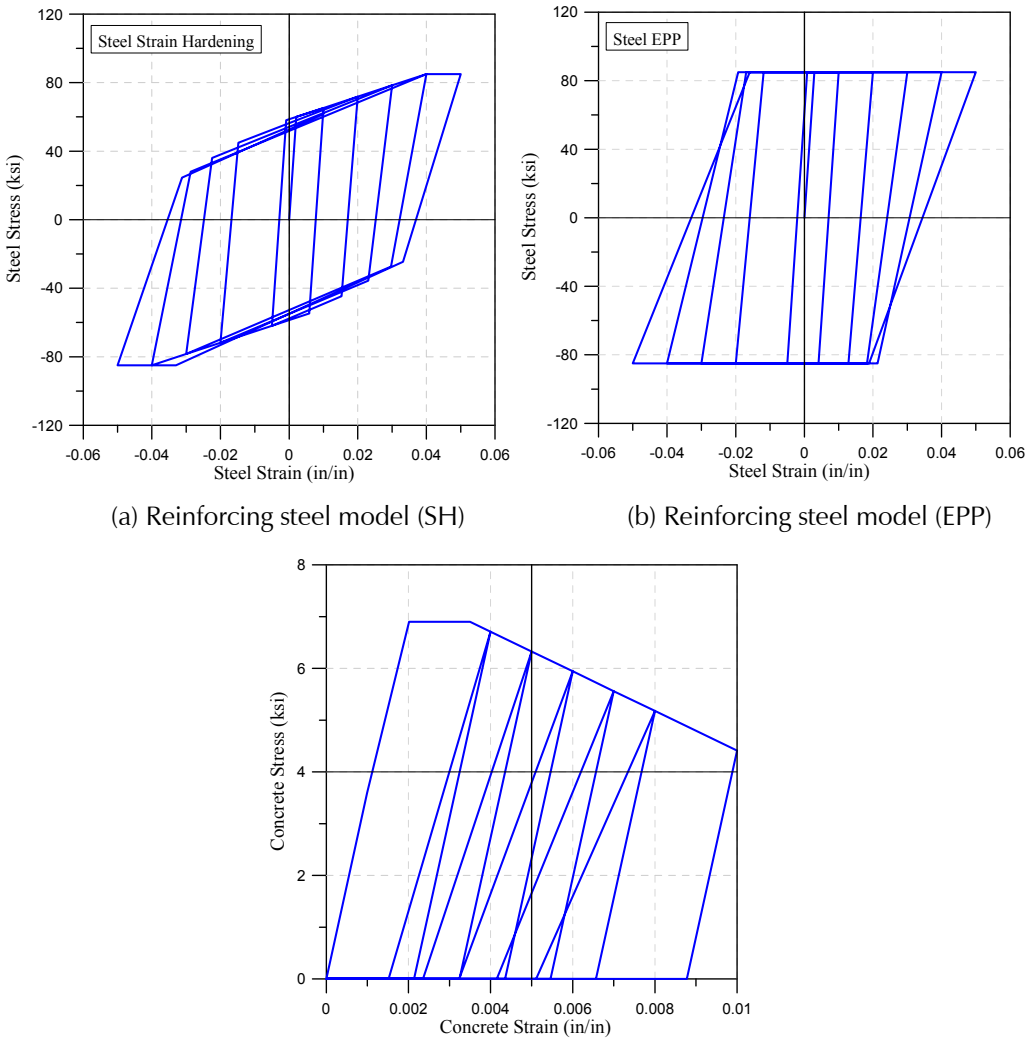

(a) Reinforcing steel model (SH)

(b) Reinforcing steel model (EPP)

(c) Concrete model

Figure 4-14 Material models in commercially available software.

An elevation of the fiber model is shown in Figure 4-15a, and the resulting strain gradient for the rectangular wall is shown in Figure 4-15b. Results show good agreement between the simple model (Perform 3D), complex model (MVLE), and test results at smaller drift ratios (e.g., on the order of 0.5%). At larger drift ratios, where differences in the unloading and reloading rules have more impact, somewhat more variation is observed between the results for different material models and the test results. The most significant discrepancies occur in the predicted concrete compressive strains, but the results obtained using both sets of material models are reasonably accurate.

Load-deformation response for a rectangular wall section and a T-shaped wall section are shown in Figure 4-15c and Figure 4-15d, respectively. Results for the rectangular wall section are predicted equally well in both the positive and negative loading directions, while the accuracy of the model for the T-shaped wall section varies depending on the direction of loading. Responses for the T-shaped wall are well-correlated in the positive direction, but more significant variation is observed in the negative direction. This variation is likely the result of several factors, including a large variation in tensile and compressive strains at the wall boundaries induced by the flanged shape of the cross-section.

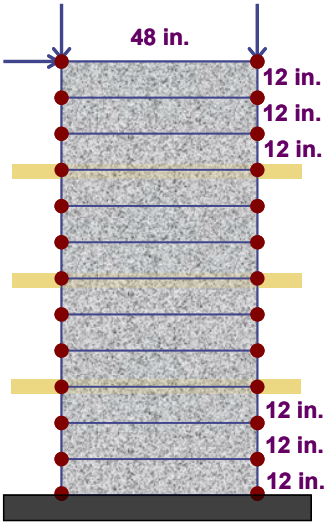

(a) Model elevation

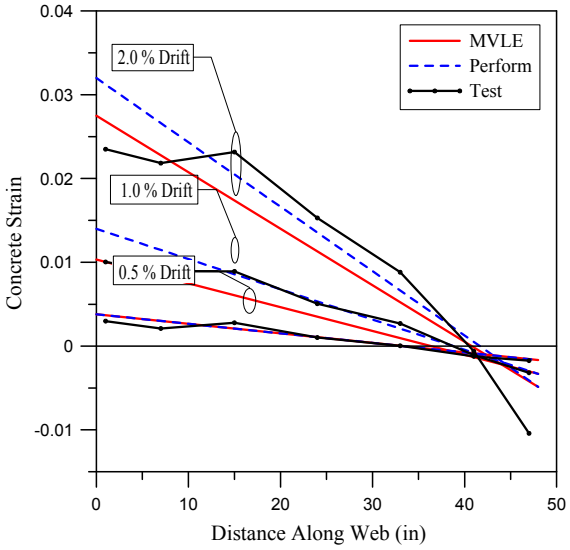

(b) Strain gradients on rectangular wall section

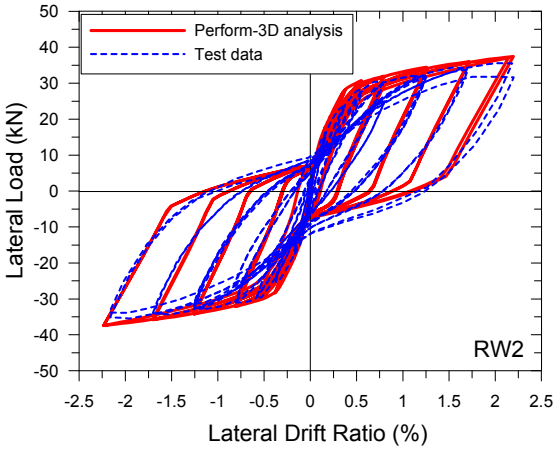

(c) Rectangular wall results

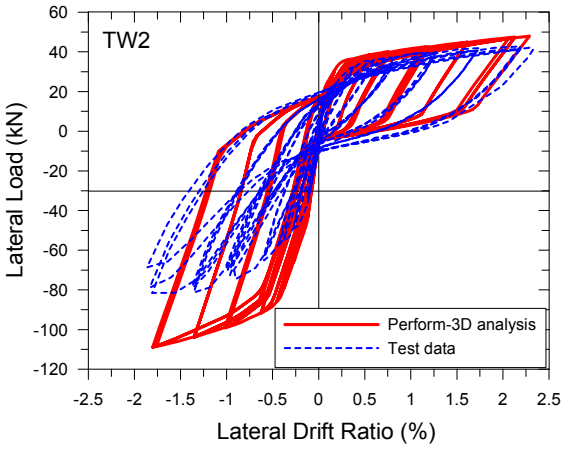

(d) Flanged (T-shaped) wall results

Figure 4-15 Comparison of wall tests versus model results generated by commercially available software.

Overall, the results generated using the simplified material relations in commercially available software are not as robust as those generated using research-oriented programs such as OpenSees, *Open System for Earthquake Engineering Simulation* (OpenSees, 2007); however, they are reasonable given the wall geometries, material behaviors, and loading histories evaluated in the test specimens. Results for overall load-displacement relations and strain distributions at the base of the walls indicate that the use of simplified material relations does not significantly impair the ability of the fiber model to simulate test results.

4.2.5 Simulation of Tested Behavior

Fiber models were used to investigate the ability to simulate observed behavior in laboratory tests of rectangular and flanged walls.

4.2.5.1 Rectangular (Planar) Walls

Typical behavior of rectangular wall sections can be observed in results from scaled tests of a cantilever planar wall subjected to a constant axial load of about $P \approx 0.10 A_g f_c'$ and reverse cyclic loading, shown in Figure 4-16. In this test, yield occurred at approximately 0.5% drift. At 1.5% and 2.0% drift, minor to moderate vertical splitting and concrete spalling occurred at the wall boundary. At 2.5% drift, rebar buckling occurred, accompanied by substantial concrete spalling. After rebar buckling, tensile fracture typically occured within the next few cycles due to low-cycle fatigue.

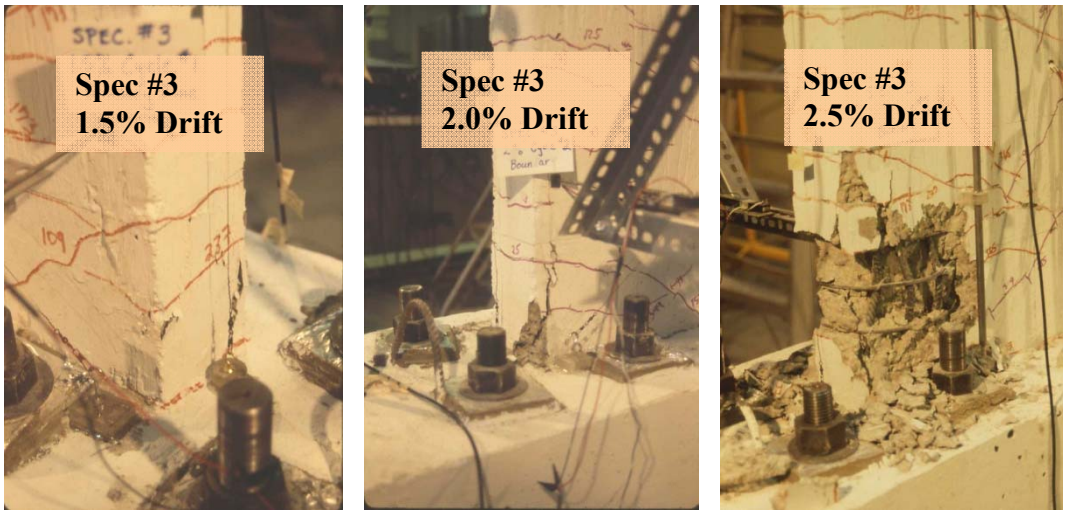

Figure 4-16 Behavior of a rectangular wall section subjected to constant axial load and reverse cyclic loading.

Results from a fiber model using fairly sophisticated material models for the concrete and reinforcing steel are presented in Figure 4-17. The model is capable of simulating the top flexural displacement measured in the tests, but

does not capture the strength degradation that was observed in the positive loading direction at the end of the test. Typically, strength degradation due to rebar buckling and fracture must be assessed independently. In general, rebar buckling and fracture are avoided by assigning appropriate strain limits in the model.

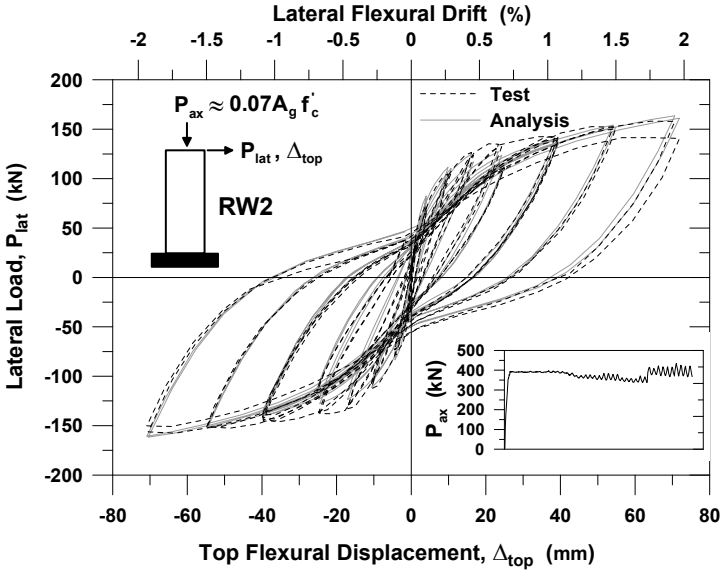

Figure 4-17 Comparison of model and test results for a rectangular wall section (Orakcal and Wallace, 2006).

The lateral load versus top displacement response using two different concrete material models (see Figure 4-13), are compared in Figure 4-18.

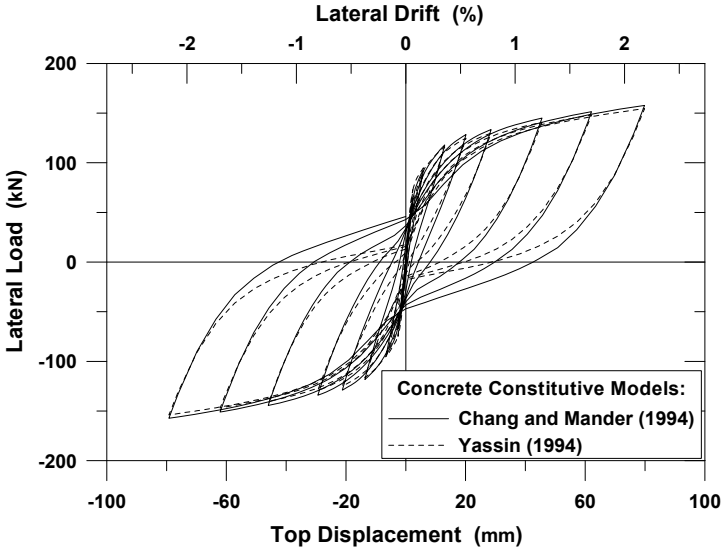

Figure 4-18 Comparison of simulated results using two different concrete constitutive models (Orakcal and Wallace, 2006).

Use of the more sophisticated concrete model shown in Figure 4-13c improved correlation between test and model results at low to moderate levels of drift. Use of the Yassin (1994) model exaggerated pinching behavior, however this discrepancy is relatively minor and either material model appeared to adequately capture the load versus displacement response of the test shown in Figure 4-17.

Figure 4-19 shows a comparison of the average strain measured at the base of the wall with results obtained from an analytical model. Figure 4-20 shows curvature profiles (strain distribution over the cross-section) for three levels of drift.

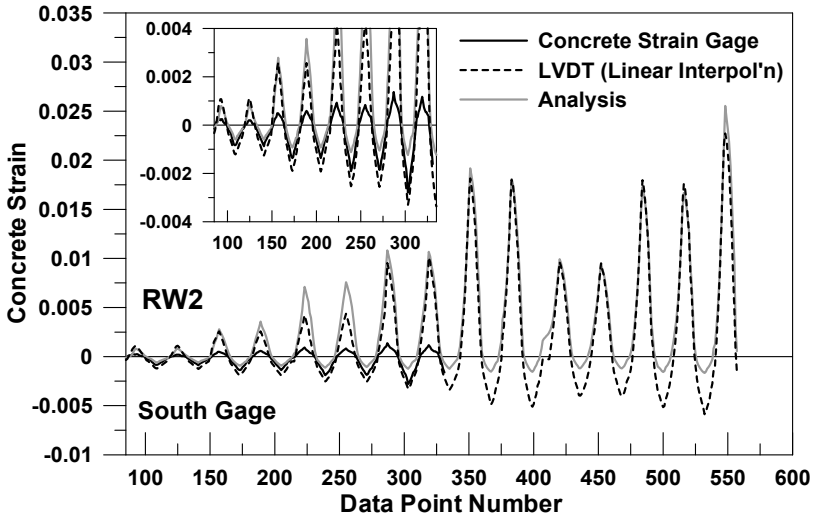

Figure 4-19 Comparison of measured versus modeled average strain in a rectangular wall section.

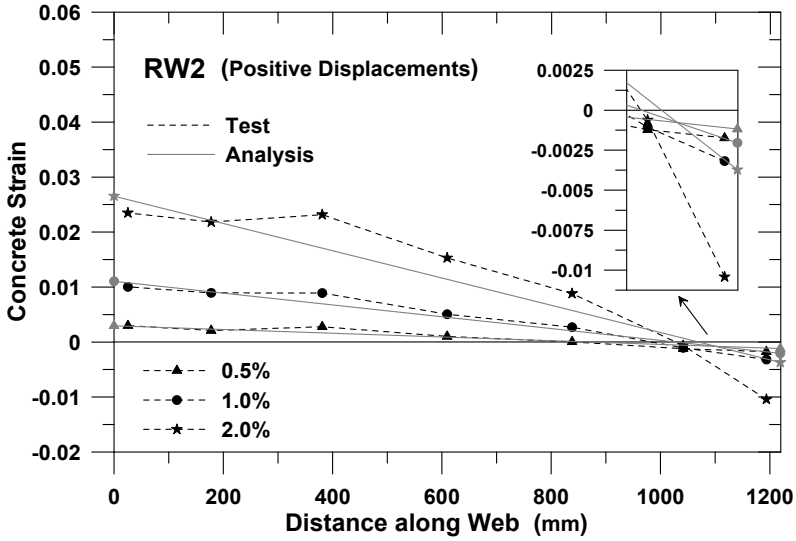

Figure 4-20 Curvature profiles for a rectangular wall section at three levels of drift.

Test data were processed to separate deformations due to flexure and shear using the procedure recommended by Massone and Wallace (2004), so the results shown include only the nonlinear flexural deformations obtained from the test. In both plots it can be observed that tensile strains were well represented, however, peak compressive strains were substantially underestimated in the model. In general, modeled compressive strains were about one-half of those measured during the tests.

4.2.5.2 Flanged (T-shaped) Walls

Typical behavior of flanged (T-shaped) wall sections can be observed in results from scaled tests shown in Figure 4-21. Yield drift ratios for a T-shaped wall were different in the positive and negative loading directions, but were generally within the same range as those for rectangular walls (approximately 0.5% drift).

At 1.5% and 2.0% drift, substantial concrete spalling was observed at the wall boundary opposite the flange. This is due to the larger moment capacity in the negative loading direction (flange in tension), due to the contribution of the longitudinal reinforcement in the flange. In contrast, concrete compressive strains were relatively low, and no spalling was observed in the positive loading direction (flange in compression), even for drift ratios approaching 3.0%.

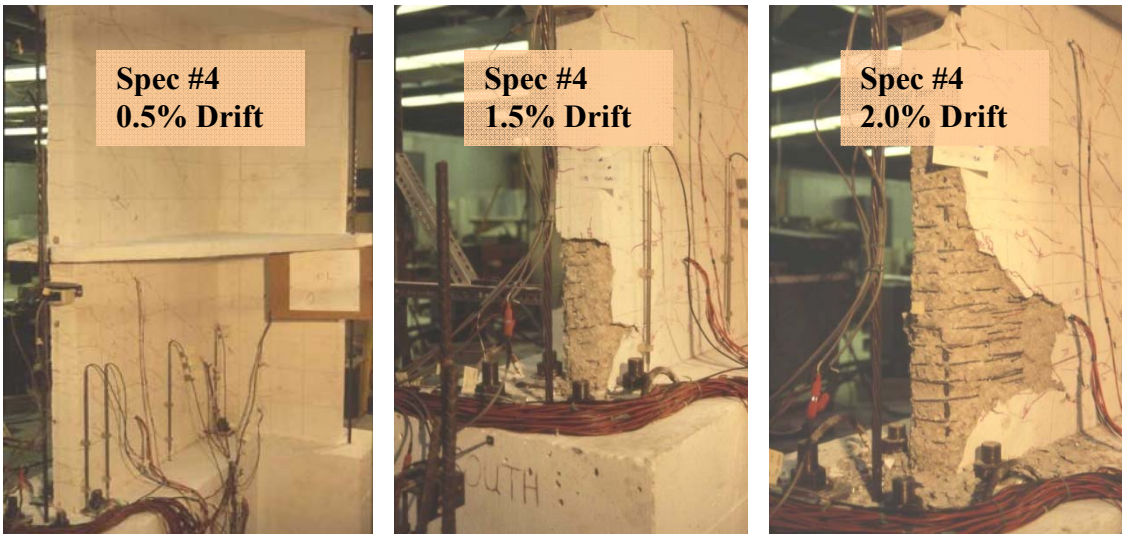

Figure 4-21 Behavior of a flanged (T-shaped) wall section subjected to constant axial load and reverse cyclic loading.

Results from a fiber model of the T-shaped wall section are presented in Figure 4-22. The model was capable of reasonably simulating the top flexural displacement measured in the tests, but somewhat overpredicted the strength of the wall when the flange was in tension. The likely reason for

this is that the model assumes the same strain gradient (plane sections remain plane) for the web and the flange, and is unable to capture the nonlinear tensile strain variation that occurs in the flange.

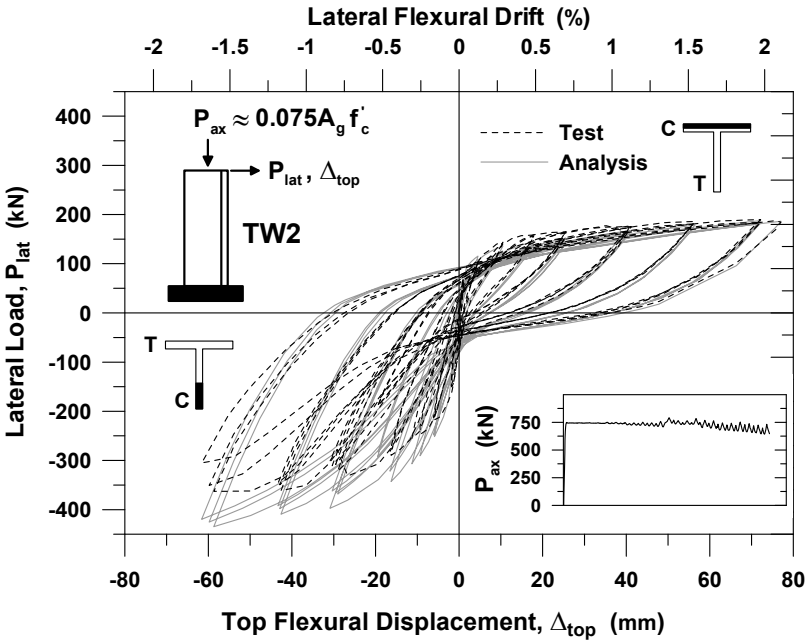

Figure 4-22 Comparison of model and test results for a T-shaped wall (Orakcal and Wallace, 2006).

Figure 4-23 shows the distribution of concrete strains in the flange for tension loading (negative displacements) and compression loading (positive displacements). With the flange in compression, the strain distribution was essentially uniform, indicating that the effective flange width in compression did not vary significantly with drift ratio.

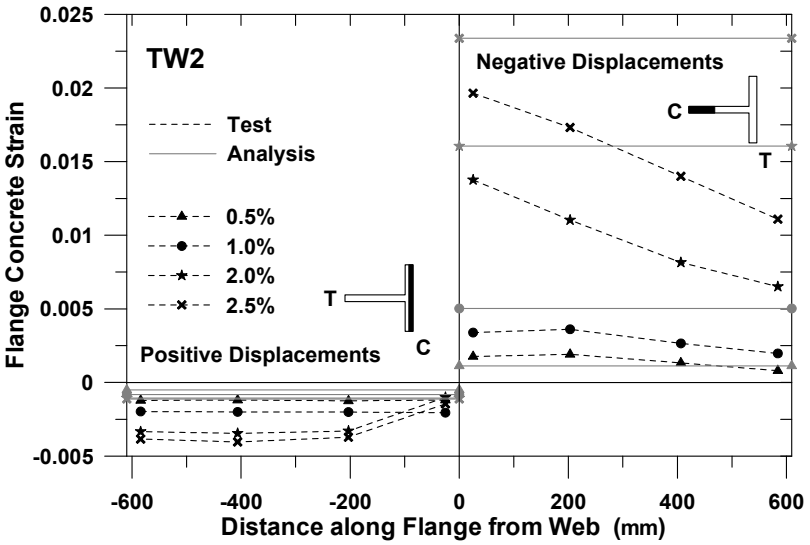

Figure 4-23 Distribution of concrete strains in the flange of a T-shaped wall.

Reinforcing steel strains in tension (negative displacements) varied significantly along the width of the flange, as shown in Figure 4-24. In very tall buildings, however, where the flange length is small in comparison with the wall height, the variation in tensile strain would be less pronounced than shown in the figure, and could be neglected.

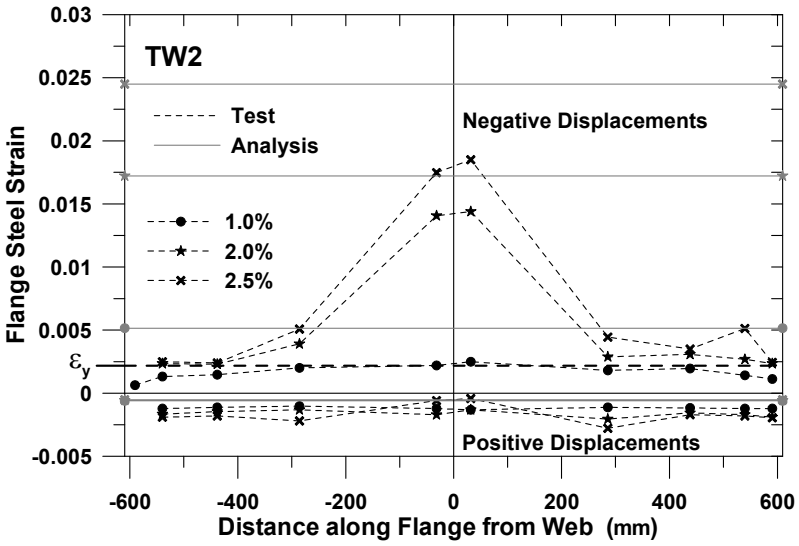

Figure 4-24 Distribution of reinforcing steel strains in the flange of a T-shaped wall.

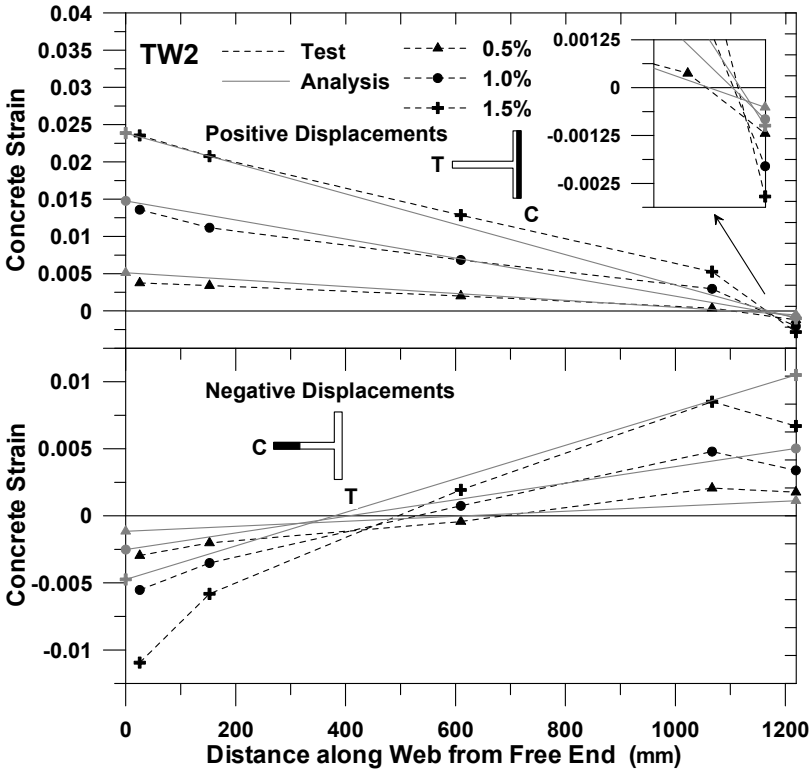

Figure 4-25 Distribution of concrete strains in the flange of a T-shaped wall.

A comparison of the concrete strain distribution in the web is shown in Figure 4-25. For positive displacements, the model and test results compared reasonably well. For negative displacements, web tensile strains were predicted with reasonable accuracy, except at the web-flange intersection, where measured tensile strains were observed to drop off. As in the case of rectangular wall sections, average concrete compressive strains were underestimated by a factor of about two. A possible reason for this discrepancy is shear-flexure interaction.

4.2.6 Model Sensitivity to Material and Model Parameters

It is well known that results obtained using finite element analyses can be sensitive to the mesh (or element size) used to define the structure or structural component. It is somewhat natural to assume that the use of more elements, especially within a yielding region, is advantageous. However, predicted material strains in reinforced concrete walls can vary substantially with differences in element height or length, depending on the material and model parameters used.

In the sections that follow, model and test results for lateral load versus top displacement response and element (local) strains are compared for a rectangular wall section. Additional information regarding the sensitivity of results to variations in wall model and material parameters are available in Orakcal et al. (2004) and Orakcal and Wallace (2006).

4.2.6.1 Influence of Reinforcing Steel Stress-Strain Relation

The influence of variation in the reinforcing steel stress-strain relation, given a constant mesh, is shown in Figure 4-26. Results for two material relations are presented, one for elastic-perfectly-plastic behavior (EPP), and the other assuming a 3% strain hardening slope (St Hard). Results indicate that including a modest strain hardening slope produces considerably better correlation with test results, given the same mesh and the same unloading and reloading material parameters. The most significant improvements were observed near the yield moment, where the EPP model overestimated the yield moment, and near zero load and displacement, where the EPP model produced abrupt changes in stiffness and significant differences from test results.

4.2.6.2 Influence of Mesh Size

The influence of mesh size on response, given both elastic-perfectly-plastic and strain hardening material behaviors is shown in Figure 4-27. Force-deformation response from models using 91 elements and six elements are presented. A model with six elements was selected because the element

height was equal to one-half of the wall length, which is a common value used to estimate the plastic hinge length at the base of a wall. Force versus displacement response was relatively insensitive to the number of elements. In this case, use of only six elements still produced good agreement between test and model results.

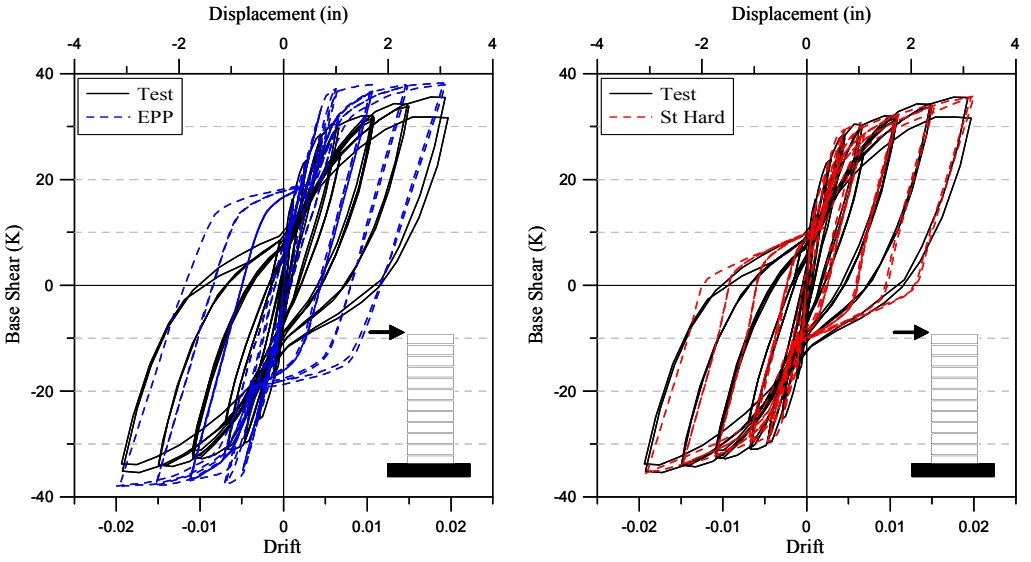

Figure 4-26 Influence of reinforcing steel stress-strain relation on force-deformation response for: (a) elastic-perfectly-plastic; and (b) strain hardening behavior.

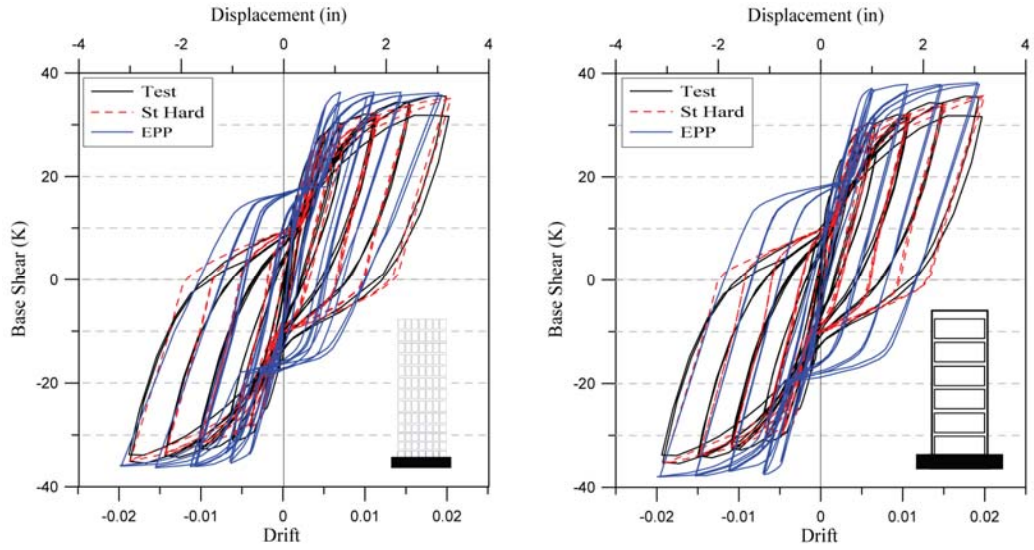

Figure 4-27 Influence of mesh size on force-deformation response for: (a) 91 elements; and (b) six elements.

The strain distribution over wall length (i.e., strain gradient or curvature) at the base is plotted in Figure 4-28 for models with 91 elements, 12 elements, and six elements. Although overall response was relatively insensitive to mesh size, local responses can vary significantly. When elastic-perfectly-plastic behavior is assumed, nonlinear deformations can concentrate in a single element and produce misleading results.

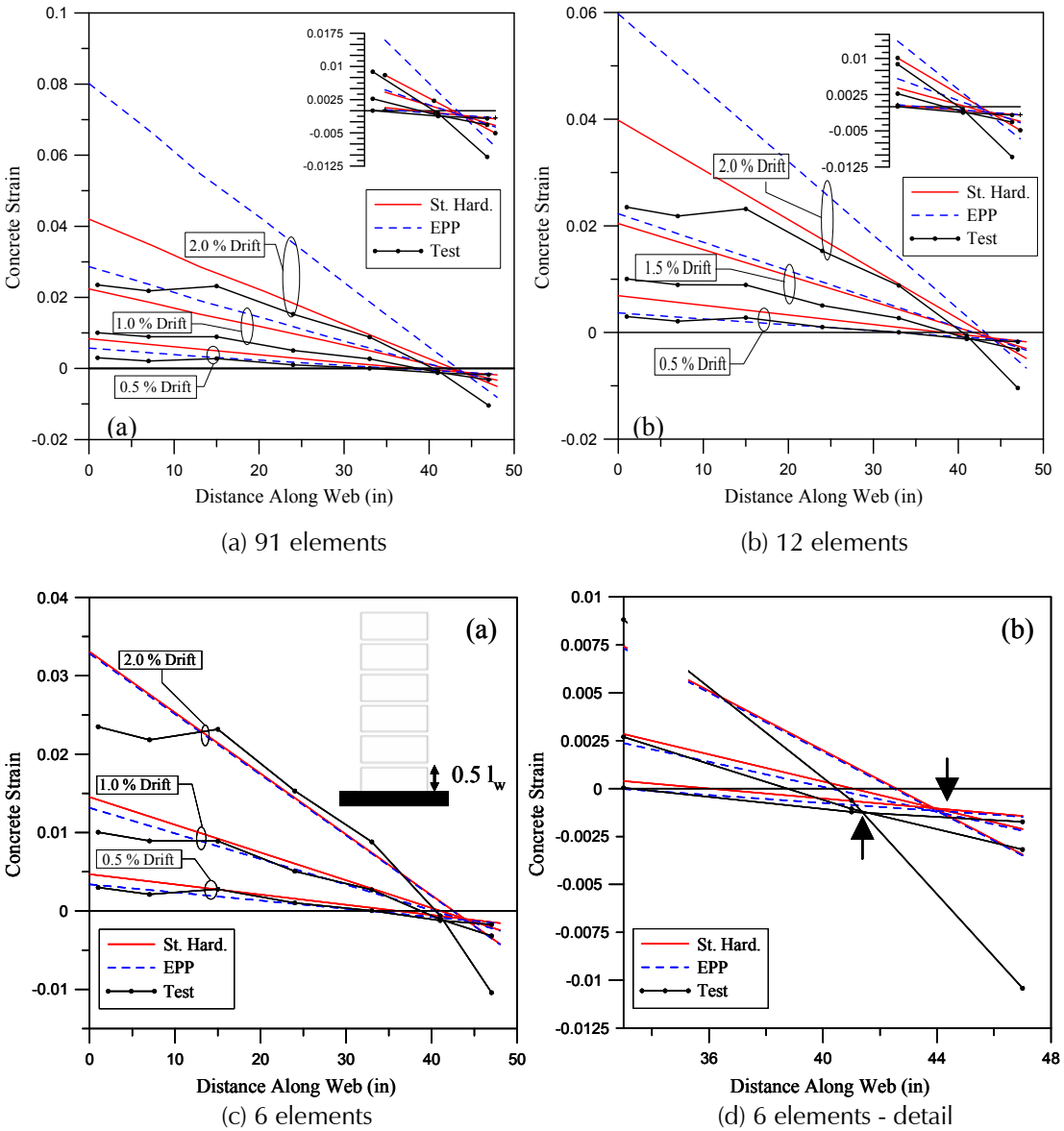

(a) 91 elements (b) 12 elements

(c) 6 elements (d) 6 elements - detail

Figure 4-28 Influence of mesh size on wall strain distribution.

Use of more elements (e.g., 91 elements or 12 elements), coupled with elastic-perfectly-plastic reinforcing steel behavior, resulted in higher modeled strains, especially at higher drift ratios. Use of a strain hardening material relation (St. Hard) improved correlation with test results, and

effectively eliminated this problem. Use of an element height equal to the plastic hinge length (e.g., six elements with a height of $0.5l_w$), produced good correlation with test results for both material models.

4.2.7 Summary Recommendations for Modeling of Planar and Flanged Walls

Summary recommendations for equivalent beam-column (lumped plasticity) and fiber (distributed inelasticity) modeling of planar and flanged reinforced concrete shear walls are as follows:

1. In equivalent beam-column models, the effective stiffness and strength properties are specified, whereas in a fiber model, stiffness and strength are derived from the specified material relations.

2. In general, use of section analysis (moment-curvature analysis) is recommended to verify the effective flexural stiffness values. In service-level analyses, where significant cracking is not expected, use of upper-bound effective stiffness values might be appropriate. In MCE level analyses, lower-bound effective stiffness values should be used and verified. The potential impact of slip deformations on flexural stiffness should be assessed. Slip deformations are typically more important for low-rise walls than for slender walls (e.g., wall aspect ratios exceeding three).

3. For effective flexural stiffness up to the yield point, values between $0.4E_cI_g$ and $0.5E_cI_g$ are appropriate for axial force levels of about $P \approx 0.10A_g f_c'$. For lower levels of axial load, use of Equation 4-8 for effective flexural stiffness is recommended to account for variation in axial load. Results from Adebar et al. (2007) suggest that higher axial stress levels could result in higher effective stiffness values, but there are insufficient test data available to make a firm recommendation at this time.

4. Effective shear stiffness at yield is approximately $G_c/20$ at a shear strength of $5\sqrt{f_c'}A_{cv}$, and $G_c/10$ at a shear strength of $10\sqrt{f_c'}A_{cv}$. Use of higher values for short walls with modest axial force levels, such as $P \geq 0.05A_g f_c'$, might be appropriate, but limited test data are available.

5. Alternatively, the model proposed by Sozen and Moehle (1993) can be used derive a shear force-deformation (backbone) relation.

6. Due to the sensitivity of shear stiffness with respect to cracking and axial load, uncertainty in the effective shear stiffness should be considered in

assessing the potential variation in important design and response parameters.

7. In fiber models, selection of material and modeling parameters can have a significant impact on model results. Use of a modest post-yield strain hardening slope (e.g., 3% to 5%) for reinforcing steel improves the correlation between tested and modeled results, independent of the mesh size used.

8. Use of an element size approximately equal to the estimated plastic hinge length improves correlation between tested and modeled strain distributions.

9. More sophisticated material models for concrete in tension produce modestly better correlation with test results, but relatively simple material models were found to produce results that were nearly as accurate.

10. Uniaxial material models provided in commercially available software, though relatively simple, produce results that are nearly as accurate as results obtained from fairly sophisticated research-based material models.

4.3 Modeling of Coupling Beams

A substantial volume of information related to reinforced concrete coupling beams is available in the literature. Prior tests have investigated placement of longitudinal and transverse reinforcement, clear span-to-depth ratios, l_n/h, near 1.0, and moderate-strength concrete (Paulay, 1971; Paulay and Binney, 1974; Barney et al., 1980; Tassios et al. 1996; Galano and Vignoli, 2000; Kwan and Zhao, 2002). None of these prior tests, however, included slabs.

A consistent finding from coupling beam studies is that the use of diagonal reinforcement improves the cyclic performance of beams with clear span-to-depth ratios ratios less than about four. For ratios greater than four, use of diagonal reinforcement is not practical given the shallow angle of the bars. Information on coupling beam effective stiffness, detailing, force-deformation behavior, and modeling is discussed in the sections that follow.

4.3.1 Effective Stiffness

ACI 318-08 provides specific provisions for determination of shear strength of diagonally reinforced coupling beams. For clear span-to-depth ratios typically used in tall core wall buildings (e.g., $2 \leq l_n/h \leq 4$), coupling beam

flexural strength also must be calculated to determine the minimum load (beam shear) that produces yielding (i.e., flexural or shear yielding).

ACI 318-08 provides guidance on effective flexural stiffness, recommending the use of $E_cI_{eff} = 0.35E_cI_g$. ASCE/SEI 41-06 recommends $E_cI_{eff} = 0.5E_cI_g$, and changes incorporated into ASCE/SEI 41-06 *Supplement No. 1*, recommend the use of $E_cI_{eff} = 0.3E_cI_g$. These effective flexural stiffness values are intended to provide an estimate of the secant stiffness to the yield point.

New Zealand Standard NZS 3101, *Concrete Structures Standard* (NZS, 1995), includes specific recommendations for effective flexural stiffness of diagonally-reinforced and conventionally-reinforced coupling beams. NZS 3101 defines the effective moment of inertia as:

$$I_e = \frac{A}{B + C\left(\frac{h}{l_n}\right)} I_g \tag{4-9}$$

where h is the total depth of the coupling beam, l_n is the clear span, and I_g is the gross concrete cross-section moment of inertia. Coefficients A, B, and C are provided in Table 4-1, based on the type of longitudinal reinforcement (diagonal or conventional) and on the anticipated ductility demand.

Table 4-1 New Zealand Standard 3101 Coupling Beam Coefficients

	Diagonally Reinforced			*Conventionally Reinforced*		
Ductility	*A*	*B*	*C*	*A*	*B*	*C*
1.25	1.00	1.7	1.3	1.00	1.0	5.0
3.0	0.70	1.7	2.7	0.70	1.0	8.0
4.5	0.55	1.7	2.7	0.55	1.0	8.0
6.0	0.40	1.7	2.7	0.40	1.0	8.0

NZS 3101 values for effective moment of inertia are intended for use with linear analysis, and are secant approximations at the given level of ductility. Values of the ratio I_e/I_g for a range of ductility demands (μ) and clear span-to-depth ratios are shown in Figure 4-29. For low ductility demands implying modest yielding (μ=1.25), NZS 3101 values are close to the ASCE/SEI 41-06 value of $0.5I_g$. For ductility demands of μ=3.0 and μ=4.5, NZS 3101 values are similar to the ACI 318-08 value ($0.35I_g$) and the ASCE/SEI 41-06 Supplement No. 1 value ($0.3I_g$) at clear span-to-depth ratios larger than 2.0.

Where a linear analysis is used for service level assessments, use of $E_cI_{eff} = 0.3E_cI_g$ appears appropriate. If a linear analysis is used for a design level

assessment, use of Equation 4-9 to estimate the reduction in secant stiffness is appropriate. For nonlinear response history analysis, an effective (secant) stiffness of $0.3E_cI_g$ to the yield point can be used, but results obtained from recent tests, summarized in the following sections, suggest that a lower value, on the order of $0.15E_cI_g$ to $0.2E_cI_g$, should be used.

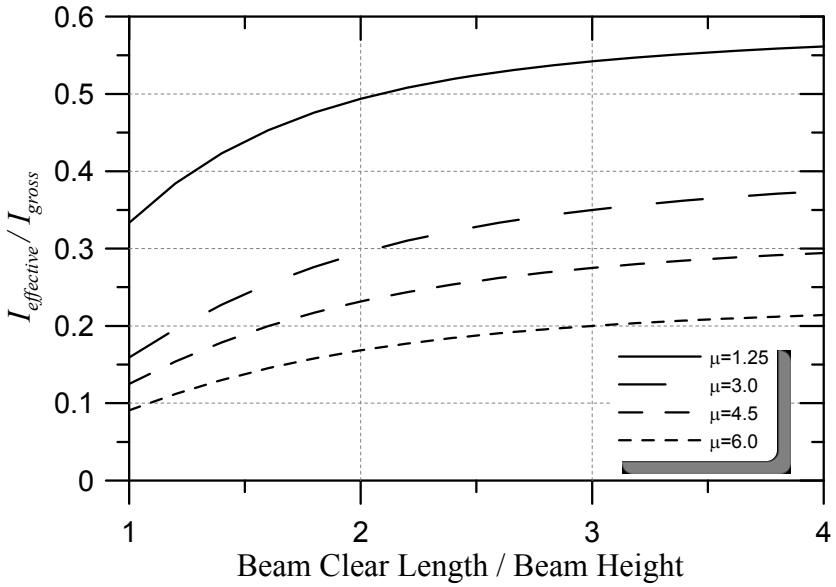

Figure 4-29 Coupling beam effective flexural stiffness ratios (based on NZS 3101).

4.3.2 Detailing Options and Force-Deformation Response

Prior code provisions for diagonally reinforced coupling beams (e.g., ACI 318-05) resulted in designs with substantial rebar congestion, especially at the beam-wall interface and the point at which the diagonals intersect. New detailing provisions were introduced in ACI 318-08 to address this issue (Figure 4-30).

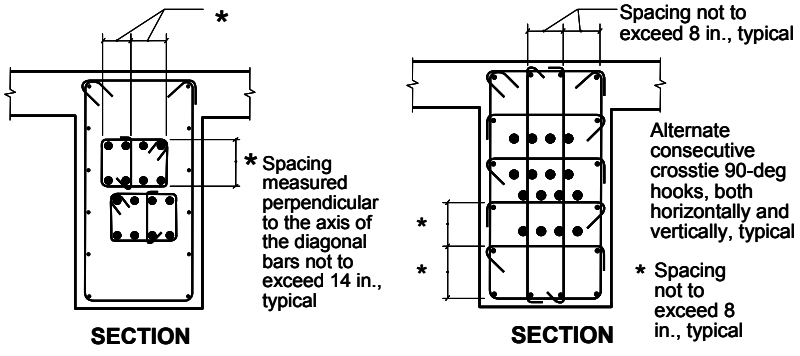

(a) ACI 318-05 (b) ACI 318-08

Figure 4-30 Coupling beam reinforcement detailing for: (a) prior ACI 318 provisions; and (b) current ACI 318 provisions.

The new provisions allow two options: (1) detailing similar to prior editions of ACI 318 with transverse reinforcement around the diagonal bars and modest transverse reinforcement around the entire beam section (Figure 4-30a); and (2) detailing with a larger quantity of transverse reinforcement provided around the entire beam section (Figure 4-30b).

Test results are available for coupling beams using the new ACI 318-08 detailing (Wallace, 2007; Naish et al., 2009). Test specimens were one-half scale, and test geometries and reinforcement detailing were selected to be representative of common span-to-depth ratios for residential construction (l_n/h=36”/15”=2.4) and office construction (l_n/h=60”/18”=3.33). Detailing for two groups of specimens are shown in Figure 4-31. Maximum expected shear stresses are approximately $v_{u,\max} = 6\sqrt{f_c'}$ psi and $v_{u,\max} = 10\sqrt{f_c'}$ psi for span-to-depth ratios of 3.33 and 2.4, respectively.

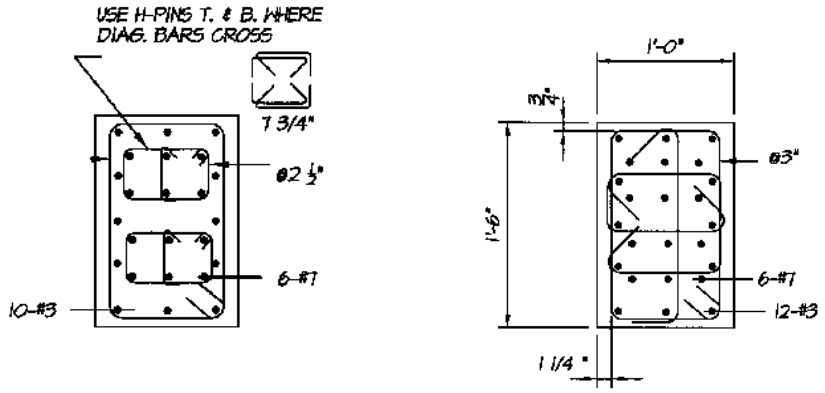

(a) ACI 318-08 Option 1 (diagonal) (b) ACI 318-08 Option 2 (full)

Figure 4-31 Coupling beam reinforcement detailing (Wallace, 2007).

Test results are presented in Figure 4-32 and Figure 4-33. Rotation levels of approximately 8% were achieved in all tests prior to any significant strength degradation. At each aspect ratio, specimens utilizing the two reinforcing options produced nearly identical force-deformation response (Figure 4-32), indicating that the transverse reinforcement detailing in Figure 4-31b is as effective as the detailing in Fig 4-31a.

The effective secant stiffness as a fraction of concrete gross section stiffness for each test specimen is shown in Figure 4-33a. For initial loading, an effective stiffness of approximately $0.25I_g$ to $0.40I_g$ was observed. This relatively low initial stiffness may have been influenced by initial cracking that existed in the test specimens. Figure 4-33a also presents test results for a coupling beam with a reinforced concrete slab, and a coupling beam with a post-tensioned slab (with nominal bonded reinforcement). Secant stiffness values for the tests with slabs were only moderately higher than those for the

rectangular beam, due to the development of cracks across the slab at the slab-wall interface.

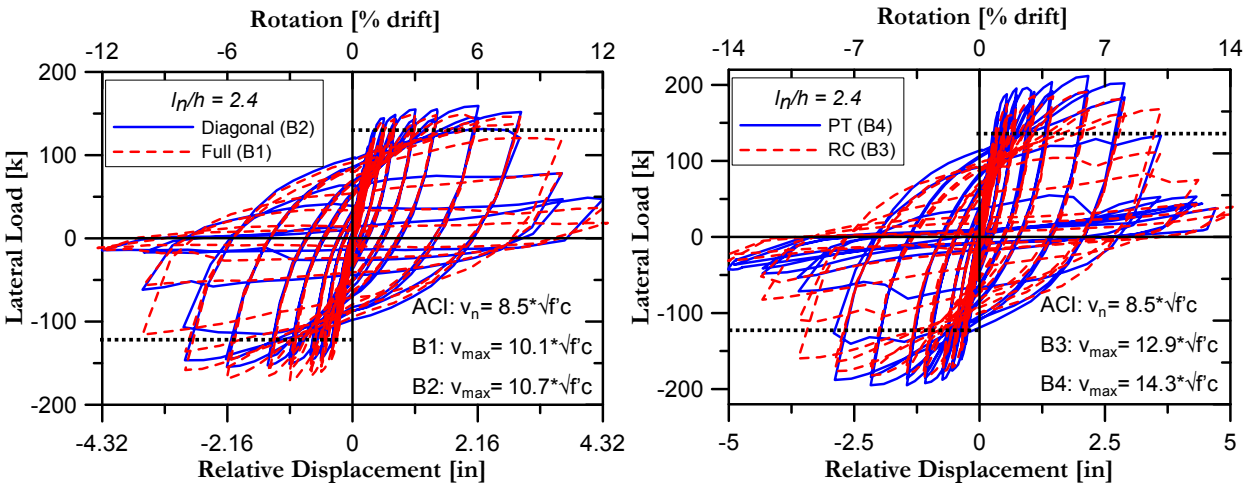

Figure 4-32 Coupling beam load-deformation relations for specimens B1, B2, B3, and B4.

Backbone relations derived from tests on beams with $l_n/h = 2.4$, both with and without slabs, are given in Figure 4-33b. The presence of a slab increased peak shear strength by 20% to 25%, but did not impact the beam deformation capacity.

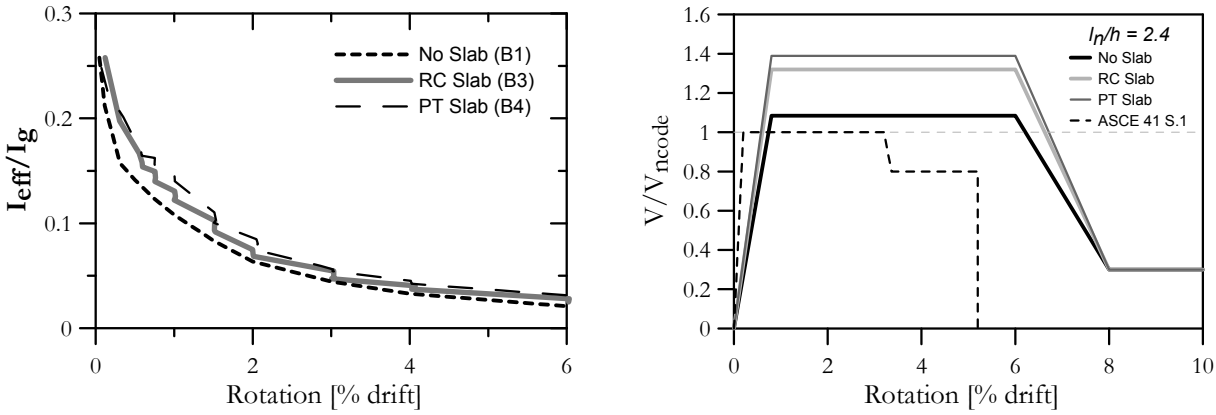

(a) Effective stiffness (b) Backbone relations for $l_n/h = 2.4$

Figure 4-33 Comparison of: (a) effective stiffness; and (b) backbone relations for coupling beam test results.

The backbone relation in ASCE/SEI 41-06 *Supplement No. 1* is also plotted in Figure 4-33b. The effective stiffness ($0.3E_cI_g$) is too stiff, and the relation underestimates the shear strength and deformation capacity relative to tests. In the tests, the effective stiffness to yield is on the order of $0.15E_cI_g$, which is considerably lower than specified in reference codes and standards. The lower stiffness value appears to be due to the added flexibility at the beam-wall interface due to slip/extension of the reinforcement. Comparison of

model and test results indicates that use of lower effective stiffness values results in good agreement between model and test results.

Prior test results reported by Paulay and Binney (1974) were reviewed to compare effective stiffness measurements. Coupling beams were 6 inches wide, 31 inches deep, and 40 inches long (l_n/h = 1.3). Assuming all deformations were associated with flexural deformations, effective stiffness values were $E_c I_{eff} \approx 0.08 E_c I_g$, or about half the values for the l_n/h = 2.4 and l_n/h = 3.33 tests discussed above. The difference is likely due to shorter beam span-to-depth ratios, which result in significant shear deformations. Yield rotations for the Paulay and Binney (1974) tests are close to the shear backbone yield relation illustrated in Figure 4-5. If the flexural stiffness is taken as $E_c I_{eff} \approx 0.15 E_c I_g$ based on the longer beam tests, then the deformations at yield resulting from flexure and shear are equal. This result is consistent with results reported by Massone (2006) for wall pier tests with l_n/h = 1.1 (i.e., equal flexural and shear deformations at yield). Therefore, for $E_c I_{eff} \approx 0.15 E_c I_g$, the effective shear stiffness should be taken as $G_{eff} \approx G_c / 4 = 0.4 E_c / 4 = 0.1 E_c$.

Tests on beams without diagonal reinforcement, with l_n/h ratios greater than 3, were conducted by Xiao et al. (1999) and Naish et al. (2009). In this discussion, "frame beams" refers to beams with standard (horizontal) longitudinal reinforcement. These tests, as well as others, reveal that "frame beams" display much more pronounced pinching behavior than diagonally-reinforced beams. This is especially true where no skin reinforcement is used. For beams tested with skin reinforcement, total rotations (drift ratios) at significant shear strength degradation exceeded 4%. The effective flexural stiffness for "frame beams" with $l_n/h \geq 3.0$ is also approximately $E_c I_{eff} \approx 0.15 E_c I_g$.

In summary, yield deformations for coupling beams with $l_n/h \geq 2.0$ are dominated by flexure, and use of $E_c I_{eff} \approx 0.15 E_c I_g$ and $G_c = 0.4 E_c$ are appropriate. For beams with $l_n/h \leq 1.4$, deformations due to flexure and shear are about equal, nonlinear behavior is dominated by shear deformations, and use of $E_c I_{eff} \approx 0.15 E_c I_g$ and $G_c = 0.1 E_c$ are appropriate. Linear interpolation of effective stiffness values for clear span-to-depth ratios $1.4 \leq l_n/h \leq 2.0$ is a reasonable approach.

4.3.3 Implicit Damage States

For linear analyses associated with either service-level or design-level events, reduced coupling beam stiffness values are often used to reduce link beam shear stresses to code-acceptable levels (e.g., $v_{n,\max} = 10\sqrt{f_c'}$ psi).

There is some concern that excessive crack widths and concrete spalling may be required to achieve stiffness values assumed in the analysis.

Test results indicate that the use of reduced stiffness values for coupling beams (e.g., $E_c I_{eff} \approx 0.25 E_c I_g$) is unlikely to produce excessive cracking or concrete spalling, either at service level or Maximum Considered Earthquake (MCE) level analyses. Tests summarized in Naish et al. (2009) indicate hairline to 1/64" diagonal crack widths, and 1/8" to 3/16" flexural crack widths at lateral drift levels of 3% to 4% (peak displacement). Residual crack widths at 4% drift were approximately 1/64" for diagonal cracking, and 1/32" for flexural cracking.

Photos of a test specimen with an aspect ratio of l_n/h = 3.33 are provided in Figure 4-34. Similar crack widths were observed for specimens with smaller aspect ratios of l_n/h = 2.4, even though shear stress levels of $10\sqrt{f_c'}psi$ to $14\sqrt{f_c'}psi$ were achieved. Substantial pullout of the diagonal bars was observed for these tests (without strength loss), even for cases where a reinforced concrete or post-tensioned slab was included.

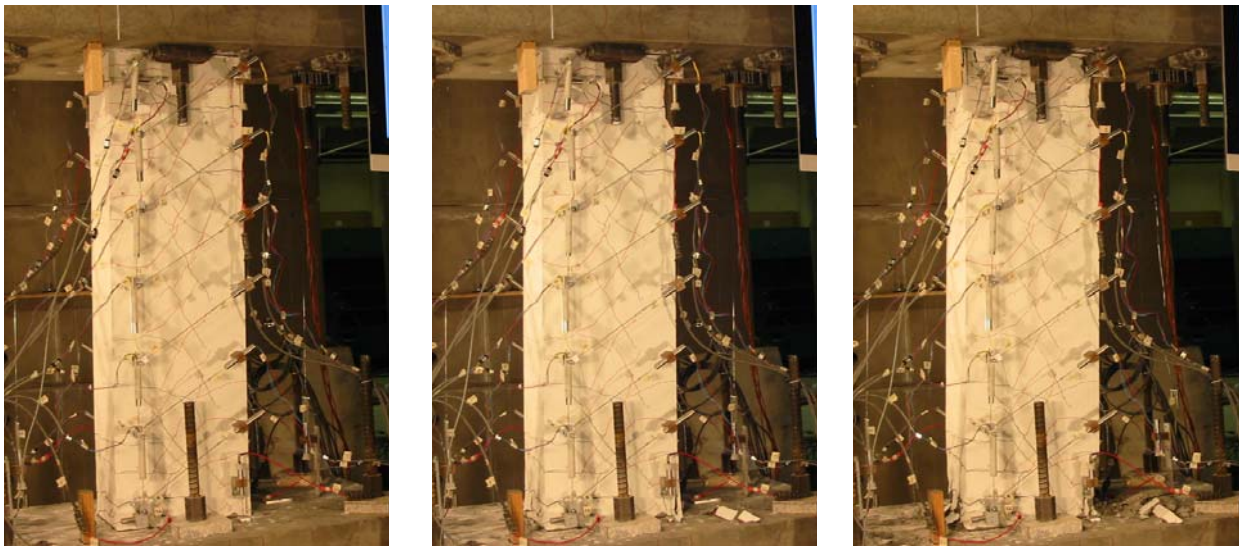

(a) 3% drift (b) 4% drift (c) 6% drift

Figure 4-34 Crack patterns in a coupling beam with an aspect ratio of l_n/h=3.33 at different drift levels.

Although a greater degree of damage has been observed in prior test programs (e.g., Paulay and Binney, 1974; Tassios et al., 1996), it is noted that prior tests were conducted on beams with lower aspect ratios, and transverse reinforcement in prior test specimens did not satisfy ACI 318-08 detailing requirements.

4.3.4 *Simulation of Tested Behavior*

Modeling studies were conducted to assess the ability of element and material modeling options available in commercially available software to simulate observed behavior in laboratory tests. Although fiber models could be used, concentrated (lumped plasticity) moment-hinge and shear-hinge models were used because they are relatively easy to implement and, as will be shown, are capable of reproducing test results with reasonable accuracy. Schematics of the models are shown in Figure 4-35.

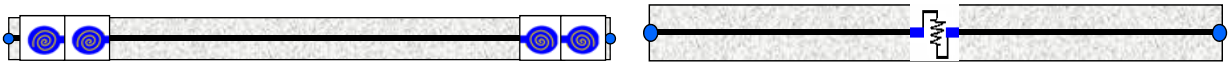

(a) moment hinge (rotational springs) (b) shear-displacement hinge.

Figure 4-35 Schematic coupling beam models: (a) moment hinge; and (b) shear-displacement hinge.

The moment-hinge model uses rigid plastic rotational springs at each end of the beam, with the properties shown in Figure 4-36. An effective bending stiffness of $0.5E_cI_g$ was used for both beam aspect ratios.

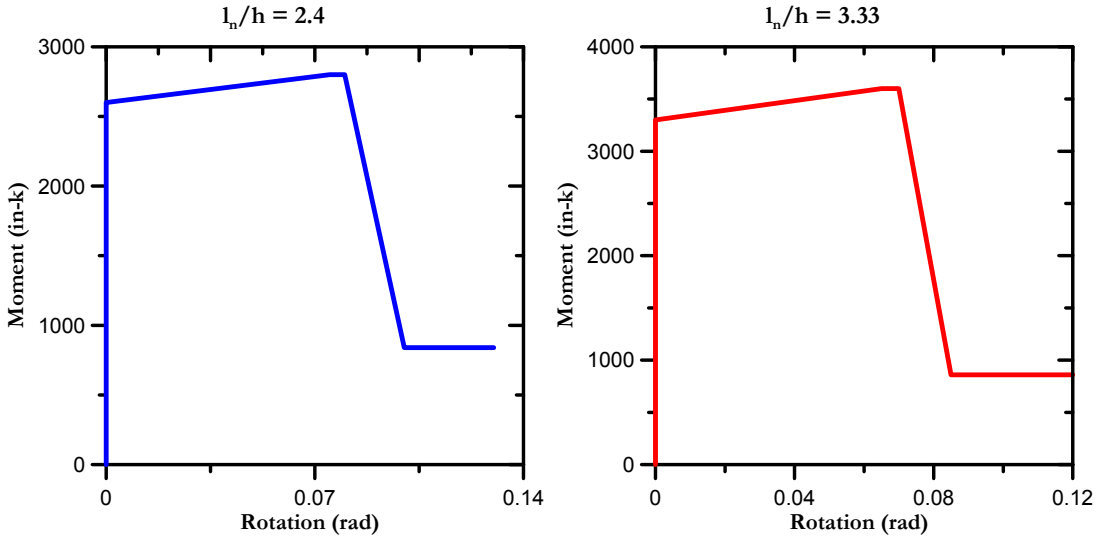

Figure 4-36 Rigid plastic rotational springs for moment-hinge model (half-scale test specimens).

The shear-hinge model was based on a slip/extension spring modeled using the approach proposed by Alsiwat and Saatcioglu (1992). The following specimen-specific spring stiffness values were used to model the added rotational flexibility at yield due to slip/extension: K_θ = 407,000 in-kips for l_n/h = 2.4, and K_θ = 825,000 in-kips for l_n/h = 3.33.

Use of $E_cI_{eff} = 0.5E_cI_g$ along with the slip/extension spring model was found to result in an effective flexural stiffness very close to $0.15E_cI_g$. An

alternative, and arguably more direct, approach would be to account for the added flexibility due to slip/extension indirectly by further reducing the effective flexural stiffness of the elastic portion of the beam. A similar approach was used in ASCE/SEI 41-06 *Supplement No. 1* for columns (Elwood et al., 2007). This approach was adopted for the shear-displacement hinge model, and an effective flexural stiffness of $E_c I_{eff} = 0.15 E_c I_g$ was used along with rigid plastic rotational springs.

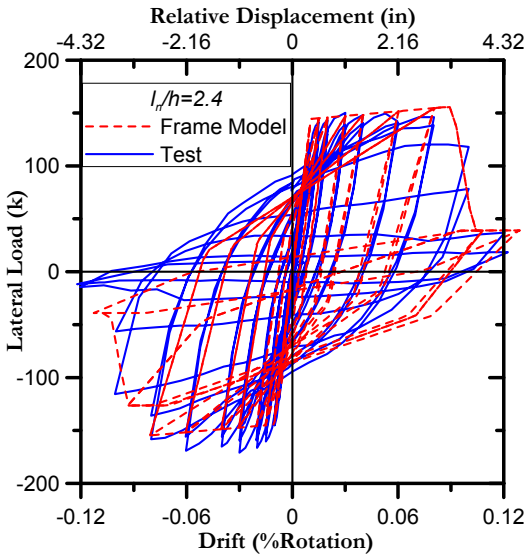

(a) Moment-hinge model (l_n/h = 2.4)

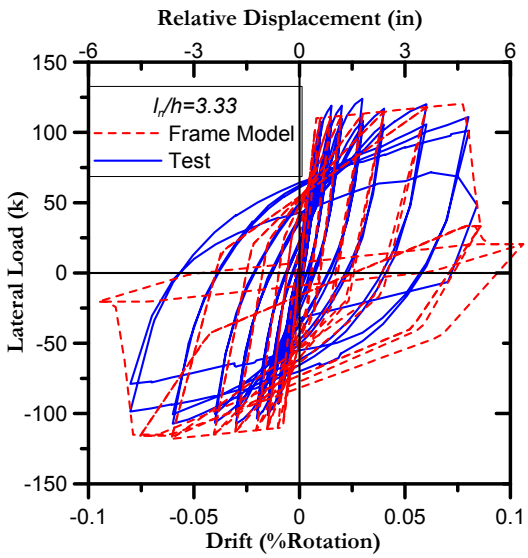

(b) Moment-hinge model (l_n/h = 3.33)

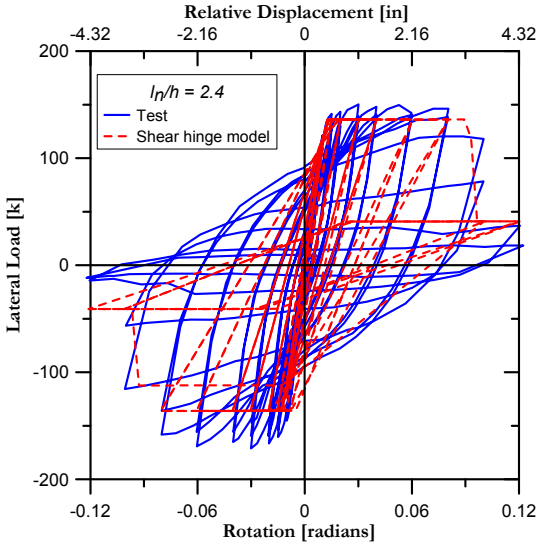

(c) Shear-hinge model (l_n/h = 2.4)

Figure 4-37 Load-deformation relations for moment- and shear-hinge models.

Model and test results presented in Figure 4-37 indicate that both moment-hinge and shear-hinge models reasonably capture the measured load versus deformation responses. Accounting for the added flexibility due to slip and

extension, either directly or indirectly, is necessary to improve the comparison between model and test results prior to yield.

The moment-hinge model does a slightly better job than the shear-displacement hinge model at representing the shape of the load-displacement loops at large displacements because the moment-hinge option includes more variables to control the shape of the hysteretic behavior. It is noted that the plastic rotation associated with significant loss of lateral load for both beam aspect ratios was arbitrarily assigned a value of approximately 0.08 based on the test results. This value substantially exceeds the values for modeling parameters $a = 0.03$ and $b = 0.05$ recommended in ASCE/SEI 41-06.

In the case of "frame beams" with no diagonal reinforcement, the force versus deformation response from laboratory tests indicates that greater "pinching" occurs. Modeling parameters should be selected that account for this behavior, which is typically accomplished by manipulating parameters associated with unloading stiffness and/or energy dissipation.

4.3.5 Summary Recommendations for Modeling of Coupling Beams

Summary recommendations for modeling of coupling beams are as follows:

1. New provisions for diagonally reinforced coupling beams are included in ACI 318-08 that allow two detailing options: one with transverse reinforcement around the groups of diagonal bars, and another with transverse reinforcement around the entire beam cross-section. Test results indicate that the force-displacement response for both detailing options is nearly the same.
2. Effective stiffness values derived from coupling beam tests are considerably lower than specified in reference codes and standards.
3. Yield deformations for coupling beams with $l_n/h \geq 2.0$ are dominated by flexure, and use of $E_c I_{eff} \approx 0.15 E_c I_g$ and $G_c = 0.4 E_c$ are appropriate. For beams with $l_n/h \leq 1.4$, deformations due to flexure and shear are about equal, nonlinear behavior is dominated by shear deformations, and use of $E_c I_{eff} \approx 0.15 E_c I_g$ and $G_c = 0.1 E_c$ are appropriate. Linear interpolation of effective stiffness values for clear span-to-depth ratios $1.4 \leq l_n/h \leq 2.0$ is a reasonable approach.
4. Both moment-hinge and shear-displacement hinge models are capable of capturing the load-deformation responses measured in tests using recommended effective stiffness values. The overall load–displacement response was better captured with moment-hinge models, because more parameters are available for adjusting the hysteretic behavior. In

conventionally-reinforced coupling beams, substantially more pinching is observed and modeling parameters should be calibrated to capture this behavior.

5. Plastic rotation limits observed in tests substantially exceed values recommended in ASCE/SEI 41-06. For diagonally reinforced beams with $l_n/h \geq 2.0$, observed peak (total) rotations prior to significant shear strength degradation were on the order of 0.06. For conventionally reinforced beams, peak rotations prior to significant shear strength degradation were on the order of 0.04.

4.4 Response and Behavior of a Core Wall System

The sensitivity of core wall system response quantities, such as diaphragm transfer forces and the distribution of moments, shear forces, and lateral displacements over the height of the building, are affected by modeling parameters. A parametric study of a tall core wall building was undertaken to demonstrate the potential impact of modeling parameters on response quantities of interest.

4.4.1 Core Wall Geometry, Configuration, and Modeling

A tall building system consisting of a core wall tower and a multi-level podium with perimeter walls was used to conduct parametric studies. The overall system configuration and plan section of the core wall is illustrated in Figure 4-38.

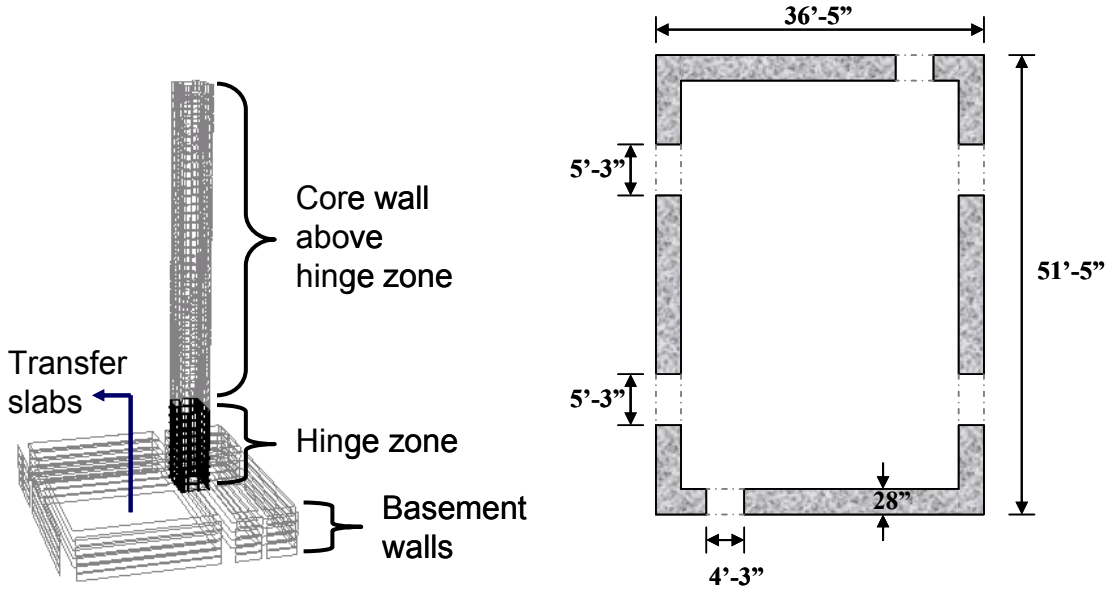

(a) System configuration (b) Core wall plan section

Figure 4-38 Configuration and plan section of tall core wall building system used in parametric studies.

The core wall consists of three regions: (1) an assumed hinge zone at the base of the core wall above the podium levels; (2) the portion of the wall above the hinge zone; and (3) the portion of the wall below the hinge zone (in the basement). Fiber elements with specified material models were used to capture axial-moment (P-M) interaction behavior, and bilinear springs were used to model shear response.

Modeling parameters that significantly influence system response include the effective stiffness of the wall, the relative stiffness values for the various elements that compose the structural system, and the variation in shear and flexural strength over the height of the wall. The stiffness values shown in Table 4-2 were used to parametrically assess the effects of stiffness on response. Longitudinal reinforcement over the height of the wall was varied to assess the effect of strength on response.

Table 4-2 Parametric Variation in Stiffness Parameters

Model Section	*Case 1: Stiff Diaphragm*	*Case 2: Soft Diaphragm*	*Case 3: Soft Hinge*	*Case 4: Stiff Hinge*	*No Factors: Uncracked*
Core Shear Wall, Hinge Zone	$0.5G_c$	$0.5G_c$	$0.25G_c$	$1.0G_c$	G_c
Core Shear Wall, Elsewhere	$0.75G_c$	$0.75G_c$	$0.75G_c$	$0.75G_c$	G_c
Diaphragm	$0.5G_c$	$0.1G_c$	$0.5G_c$	$0.1G_c$	G_c
Basement Wall	$0.75G_c$	$0.75G_c$	$0.75G_c$	$0.75G_c$	G_c

The following five cases of relative stiffness were considered. Case 5, with no factors applied to the uncracked shear stiffness (i.e., $G_c = 0.4E_c$), was used to assess the impact of cracking.

- Case 1: Stiff diaphragm, with modest stiffness reductions in all elements
- Case 2: Soft diaphragm
- Case 3: Soft hinge
- Case 4: Stiff hinge, with soft diaphragm
- Case 5: Uncracked, with no stiffness reductions

Nonlinear dynamic analyses were conducted for simultaneous application of the North-South, East-West, and vertical records for the Beverly Hills-14145 Mulholland (USC- 90013) station in the 1994 Northridge earthquake. Additional results, and a more detailed discussion of modeling parameters, are provided in Salas (2008).

Results for shear and moment over building height are summarized in Figure 4-39 and Figure 4-40. In Figure 4-39, shear forces within the hinge region and above are relatively insensitive to variations in shear stiffness parameters for the different relative stiffness cases. The greatest variation in core wall shear force occurs between Cases 3 (soft hinge) and 4 (stiff hinge, soft diaphragm), indicating that there is modest uncertainty in the magnitude of the force that is transferred through the podium level diaphragms. The influence of higher mode response on shear is apparent, as would be expected.

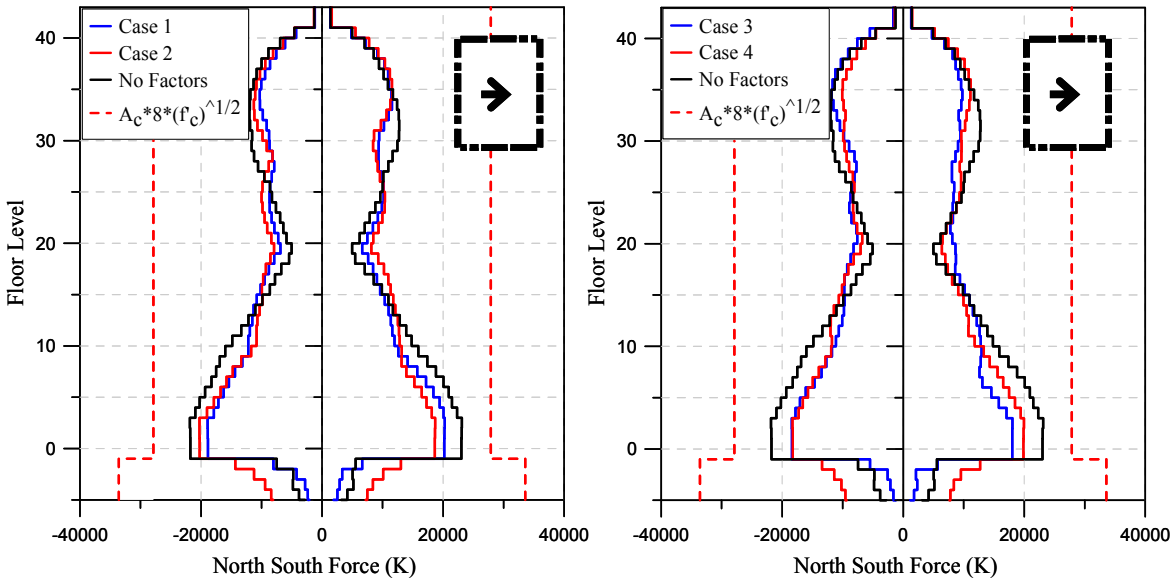

(a) North-south response

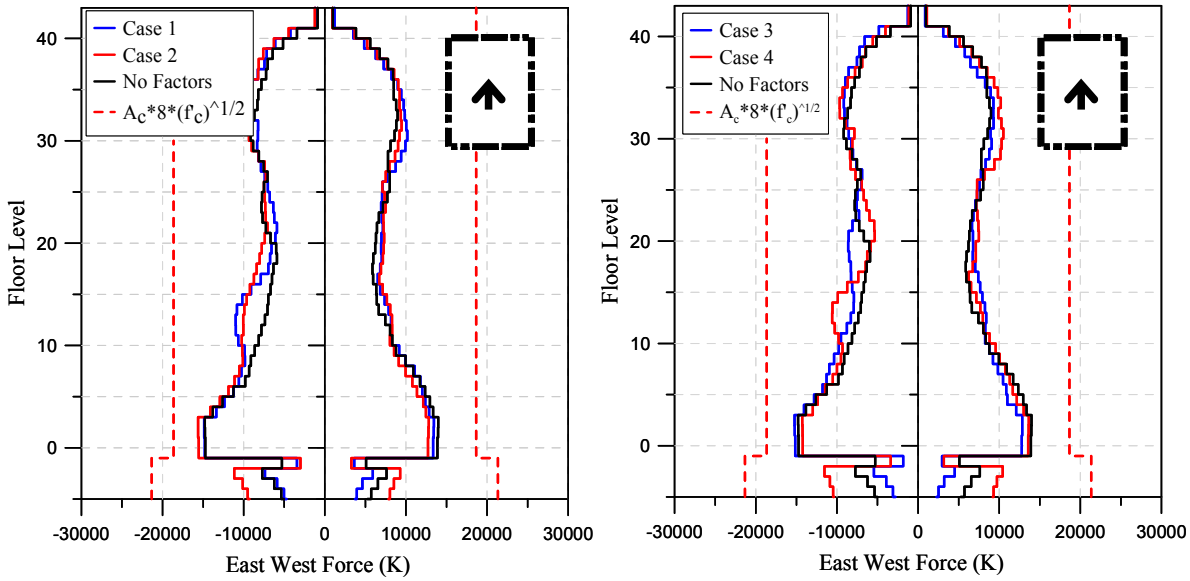

(b) East-west response

Figure 4-39 Variation in shear force over height in the: (a) north-south direction; and (b) east-west direction, for each case of relative stiffness.

Variation in moment over building height in Figure 4-40 shows that moment is insensitive to shear stiffness variation, with the exception of Case 5 (uncracked) in which no stiffness reduction factors were used. The figure also illustrates that the moment magnitude above the hinge zone exceeds the moment capacity in the hinge zone. This is a result of higher mode effects on the peak strains at various points along the core wall, and is an artifact of the model, which incorporated linear material modeling above the hinge zone to reduce computer run time. When the hinge region yields, higher-mode responses can produce very large moments in elastic elements in the upper levels. The moment magnitudes are such that it is not possible to provide sufficient flexural strength in the upper levels to avoid the potential for yielding.

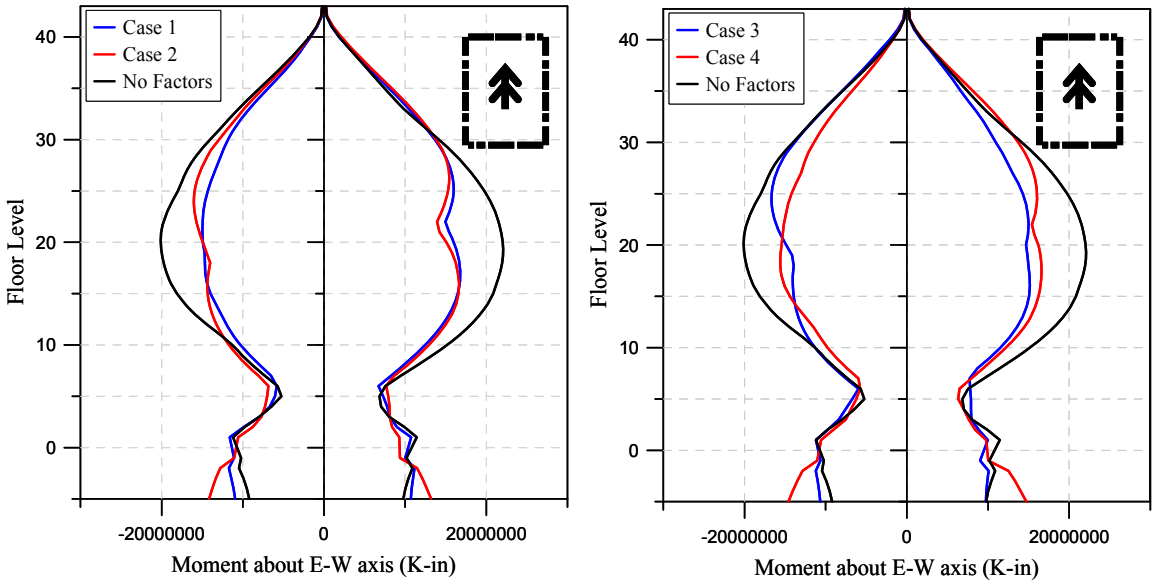

Figure 4-40 Variation in moment over height in the east-west direction, for each case of relative stiffness.

To study this result, an alternative model was created with nonlinear fiber elements provided over the full height of the wall. This model was used to assess the impact of yielding in the upper levels of the core wall, and to determine the magnitude and distribution of wall strains at various locations over the height. A comparison between shear and moment distributions over height for the base model (fiber hinge) and this alternative model (fiber all) is provided in Figure 4-41 and Figure 4-42.

Differences in the shear force distributions in Figure 4-41 indicate that yielding in the upper stories has a significant impact on the magnitude and distribution of shear forces, which are substantially reduced, especially within the hinge region. Figure 4-42 shows that moment magnitude in the

upper levels is also substantially reduced as a result of yielding (as would be expected).

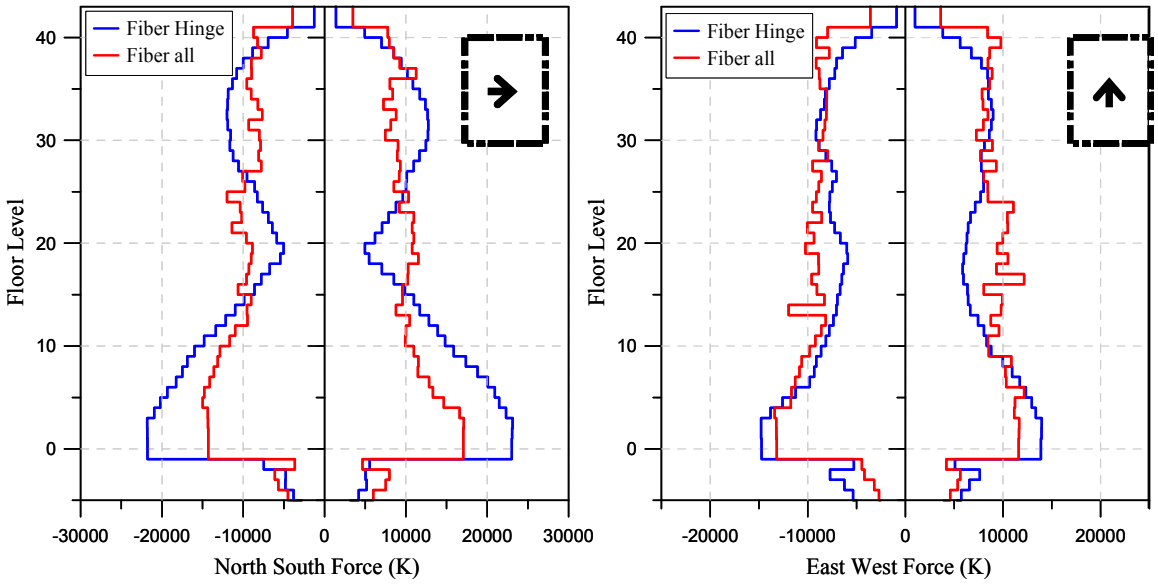

Figure 4-41 Comparison of shear force distribution over height for fiber-hinge and fiber-all models.

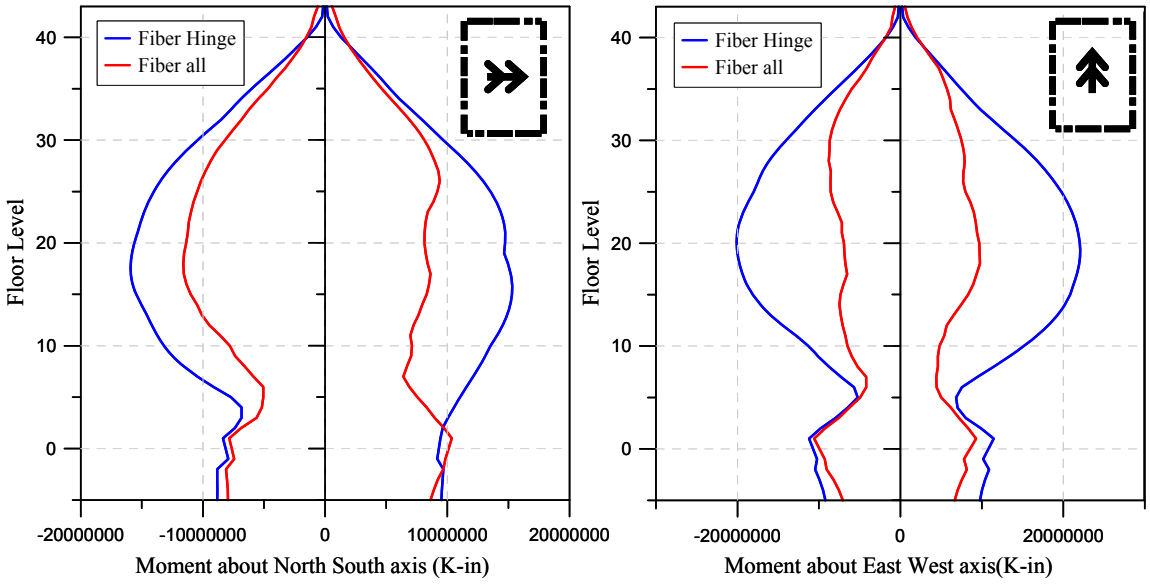

Figure 4-42 Comparison of moment distribution over height for fiber-hinge and fiber-all models.

Comparisons between shear and moment distributions over height for the base model (fiber hinge) and the alternative model (fiber all), considering the relative stiffness cases identified in Table 4-2, are provided in Figure 4-43 and Figure 4-44. Results again indicate that shear force above the hinge zone is relatively insensitive to variations in shear stiffness; however, the

magnitude of the shear force transferred in the podium level diaphragms is quite sensitive to yielding in the upper levels of the core wall. Incorporation of nonlinear behavior in the upper levels of the core wall is necessary for the evaluation of diaphragm transfer forces, and variations in shear stiffness have a large effect.

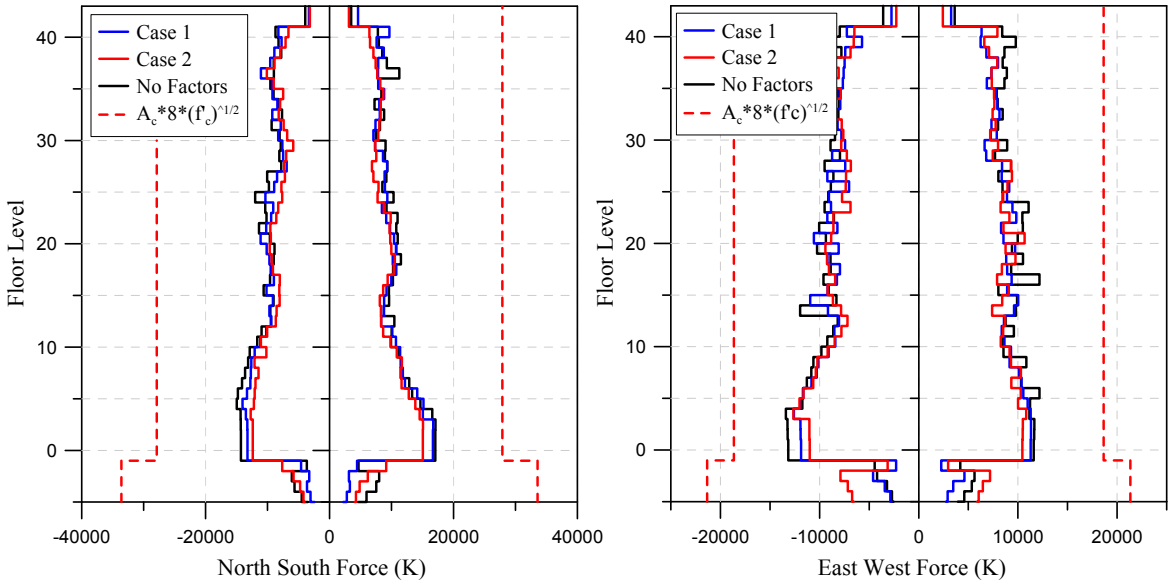

Figure 4-43 Comparison of shear force distribution over height for fiber-hinge and fiber-all models, for each case of relative stiffness.

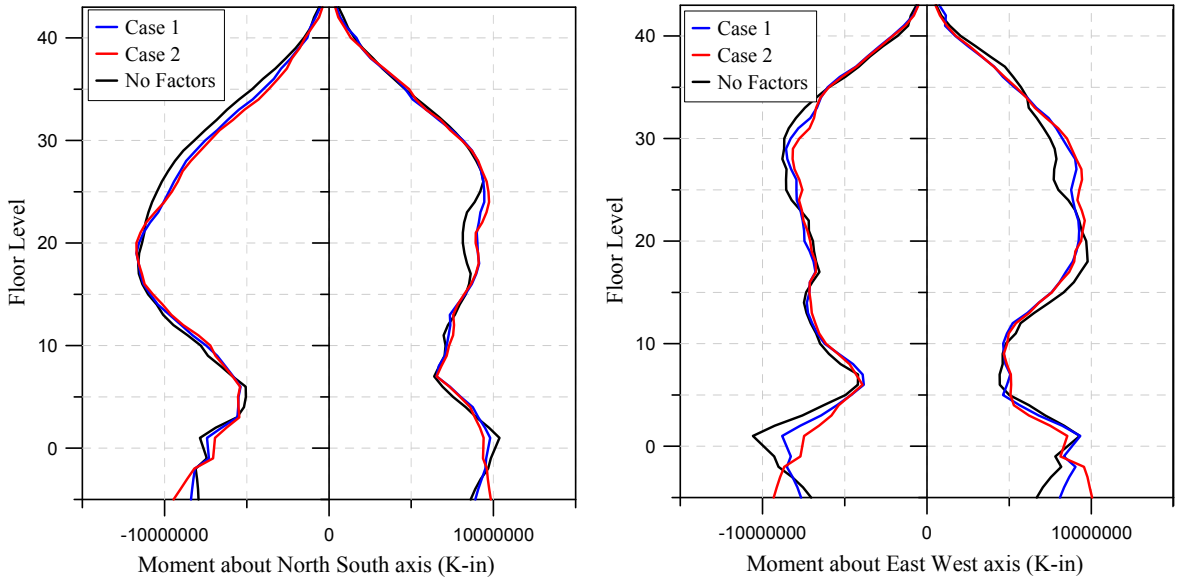

Figure 4-44 Comparison of moment distribution over height for fiber-hinge and fiber-all models, for each case of relative stiffness.

Results for moment distribution over height shown in Figure 4-44 confirm prior results that yielding in the upper levels substantially reduces moment

magnitudes, and that variation in shear stiffness has little effect on moment distribution.

The maximum strain values for core wall concrete in compression and core wall reinforcement in tension over height are plotted below. Distributions of maximum compression and tension strains for elements along the north wall of the core are shown in Figure 4-45.

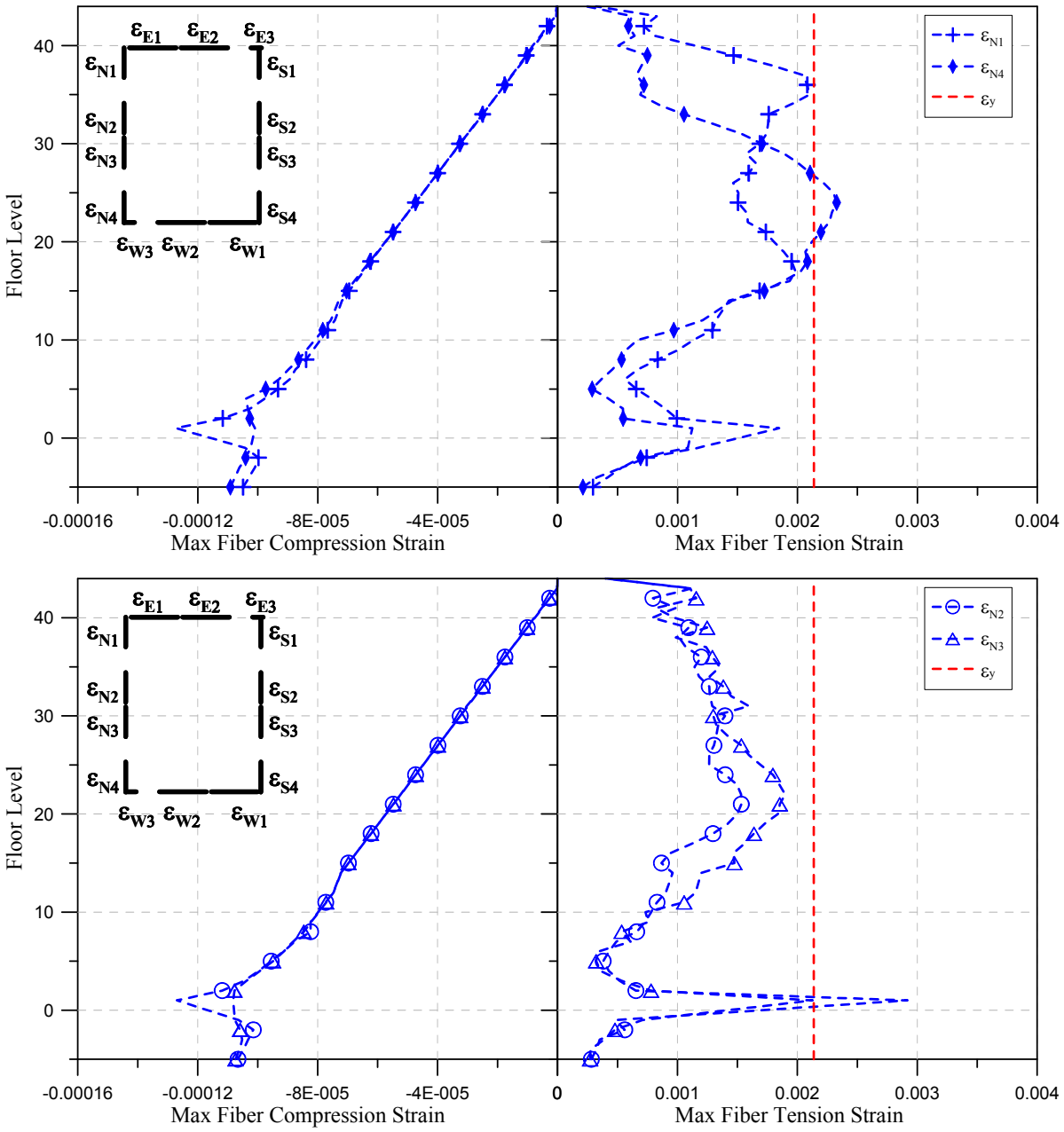

Figure 4-45 Distribution of maximum compression and tension strains over height for elements along the north wall of the core.

Variation in peak compressive strain over height is nearly linear, except at the base, and peak compressive strains are relatively low. Tensile strains in the north wall slightly exceed the yield strain, indicating modest yielding in tension in the upper levels and at the podium level. Similar results were observed for the south wall.

Distributions of maximum compression and tension strains for elements along the east wall of the core are shown in Figure 4-46. Peak compressive strain is nearly linear over height, and peak tensile strains indicate yielding in tension in the upper levels. Although the concrete compressive strains and reinforcement tensile strains increase modestly at the podium level, the peak compressive strain is low (0.0012), and the peak tensile strain is well below the yield value.

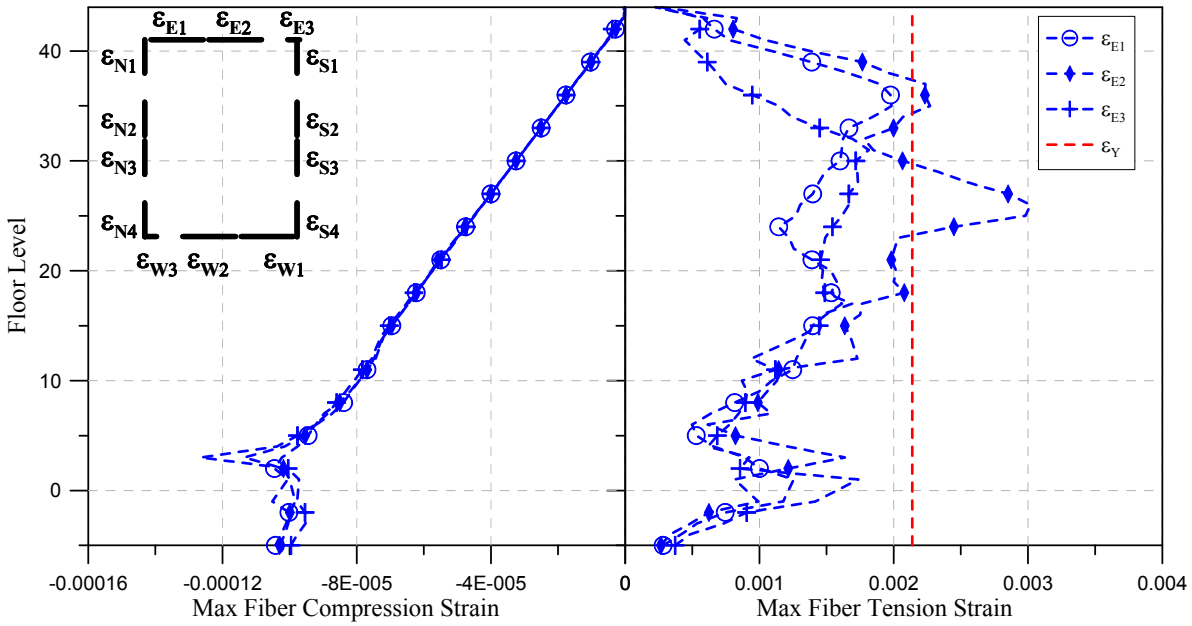

Figure 4-46 Distribution of maximum compression and tension strains over height for elements along the east wall of the core.

Longitudinal reinforcement over the height of the wall was varied to assess the effect of shear and flexural strength on response. Maximum longitudinal reinforcement was provided over the hinge region of the wall in levels 1 through 8. Below the hinge region, wall reinforcement was reduced 30% in levels B5 to B1. Above the hinge region, wall reinforcement was reduced 18% in levels 9 to 12, 35% in levels 14 to 21, 55% in levels 22 to 31, 67% in levels 32 to 37, and 82% in levels 38 to 43.

A comparison between shear and moment distributions over height for the base model (100% Steel) and the alternative model (Reduced Steel) is provided in Figure 4-47. Changes in the shear and flexural strength of the

wall over height had only a minor impact on core wall peak shear and moment values for the cases considered.

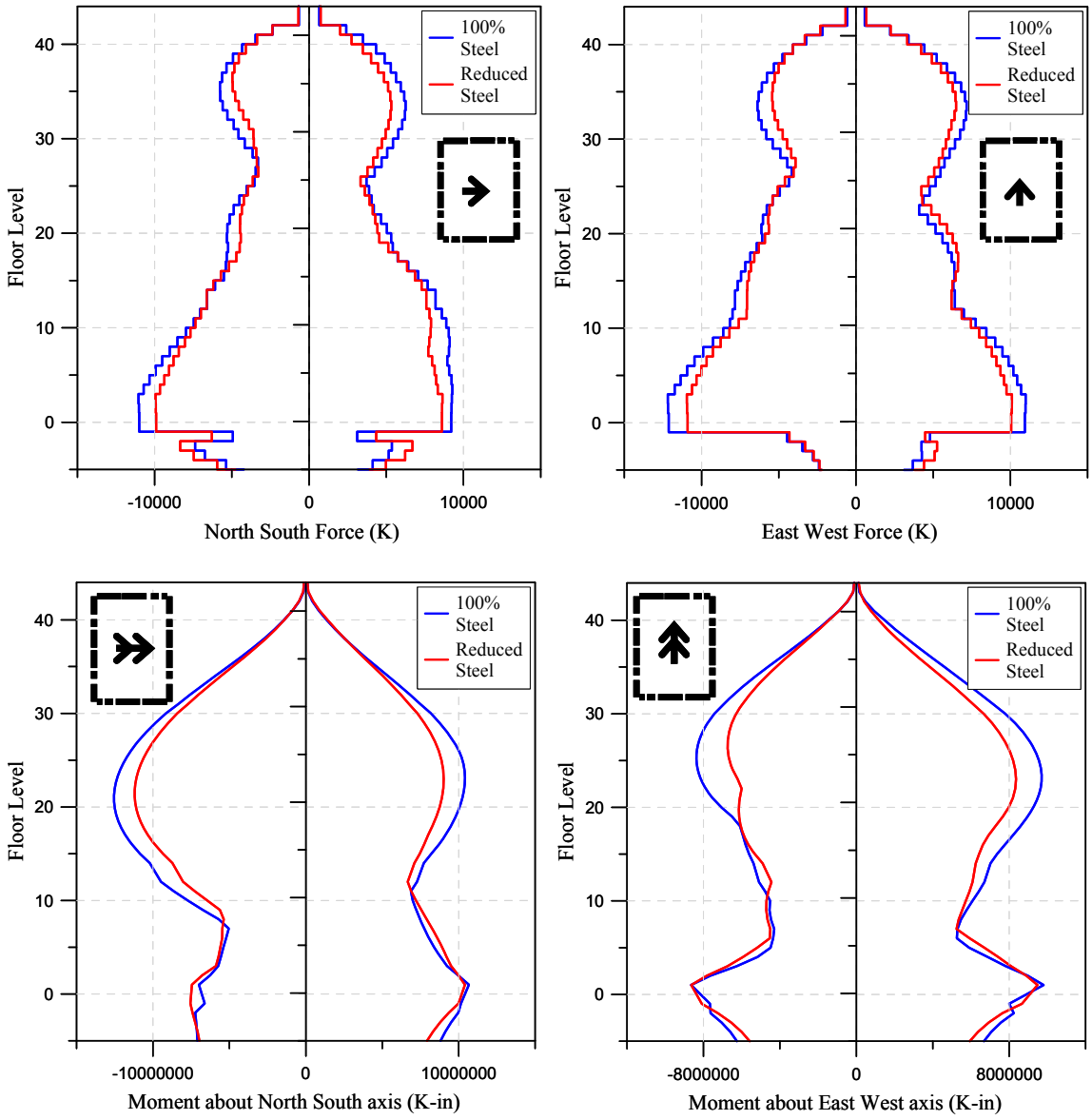

Figure 4-47 Comparison of shear and moment distributions over height for the 100% Steel and Reduced Steel models.

4.4.2 Summary Findings for Core Wall Response and Behavior

Summary findings related to core wall response and behavior include:

- Variation in wall shear stiffness values had a minor impact on the magnitude of shear and moment forces in the core wall above the podium level; however, the magnitude of force transfer between the core wall and exterior basement walls via the podium level diaphragms was

significantly impacted. Collector (or distributor) forces are sensitive to the selection of shear stiffness, and bounding cases (e.g., stiff core, soft diaphragm; soft core, stiff diaphragm) should be considered to determine the potential range of diaphragm deformations and collector forces.

- Elastic modeling above the anticipated hinge region of the wall is sometimes used to simplify modeling and reduce computer run time. Yielding is likely to occur in the upper levels, and nonlinear elements should be used over the full height of the wall to capture this behavior. Even minor yielding in the upper levels was observed to substantially reduce shear and moment magnitudes in the lower levels of the wall.

- Yielding in the upper levels of the wall should be limited to relatively low tensile strains (e.g., twice the yield strain) or plastic rotations (e.g., $\theta_{pl} = 1.2\theta_y$) to avoid concentrating nonlinear deformations in the upper levels.

- Reducing the quantity of wall longitudinal reinforcement over the height had only a minor effect on reducing the magnitude of peak shear and moment values over the height of the wall.

4.5 Modeling of Slab-Column Frame Components and Connections

Modeling of slab-column frames, commonly used as gravity systems in tall core wall buildings, involves assigning appropriate values for stiffness and strength, and includes consideration of punching failures. Current information on modeling of slab-column frames can be found in ASCE/SEI 41-06 *Supplement No. 1*, and in Elwood et al. (2007).

4.5.1 Quantification of Properties for Slab-Column Frames

The effective flexural stiffness of the slab is modeled using slab effective beam-width models from sources such as Allen and Darvall (1977). In this model, the centerline panel-to-panel transverse width measured perpendicular to the direction of loading under consideration, is reduced by the normalized effective stiffness, $\alpha\beta$, as given in Equation 4-10.

$$E_c I_{effective} = E_c \beta \left[\frac{\alpha l_2 h^3}{12} \right] \tag{4-10}$$

where h is the total slab thickness, and the other parameters are described below.

The elastic effective width is represented by αl_2, which depends on c_1, the column dimension parallel to the slab, and l_1, the center-to-center span length in the direction under consideration. Hwang and Moehle (2000) recommend the following equations to determine the elastic slab effective width:

$$\alpha l_2 = 2c_1 + l_1/3 \tag{4-11a}$$

for interior frames, including the exterior connections thereof, and

$$\alpha l_2 = c_1 + l_1/6 \tag{4-11b}$$

for exterior frames loaded parallel to the edge. The effective width given by Equation 4-10 is applicable for slab-column frame models in which the slab-beam is modeled as rigid over the width of the column (i.e., the joint region). Typical values of α for interior frames vary from 1/2 to 3/4 for reinforced concrete construction, and 1/2 to 2/3 for post-tensioned construction. Values for exterior frames transferring load parallel to the edge are about half of those for interior connections.

A further stiffness reduction due to concrete cracking is represented by β. Stiffness reduction due to cracking depends on a number of factors including construction, service loads, and earthquake loads, as well as the degree of post-tensioning. Typical values for β vary from 1/3 to 1/2 for reinforced concrete construction, and 1/3 to 1 for post-tensioned construction (Allen and Darvall, 1977; Vanderbilt and Corley, 1983; Grossman, 1997; FEMA, 1997; Hwang and Moehle, 2000; Kang and Wallace, 2005). For non-prestressed construction, the commentary of ASCE/SEI 41-06 *Supplement No. 1* recommends the following equation from Hwang and Moehle (2000):

$$\beta = 4c_1/l_1 \geq 1/3 \tag{4-12}$$

For prestressed slabs, a larger value of β is appropriate because of the reduced potential for cracking due to prestressing. Following the work of Kang and Wallace (2005), the commentary of ASCE/SEI 41-06 *Supplement No. 1* recommends a value of β=1/2.

Figure 4-48 shows the normalized effective stiffness, $\alpha\beta$, for interior connections calculated using Equations 4-10 through 4-12 over a range of span ratios, l_2/l_1. Also shown are typical ranges recommended in the literature for post-tensioned and reinforced concrete connections. Effective stiffness values for exterior connections can be estimated as half of the values shown in the figure.

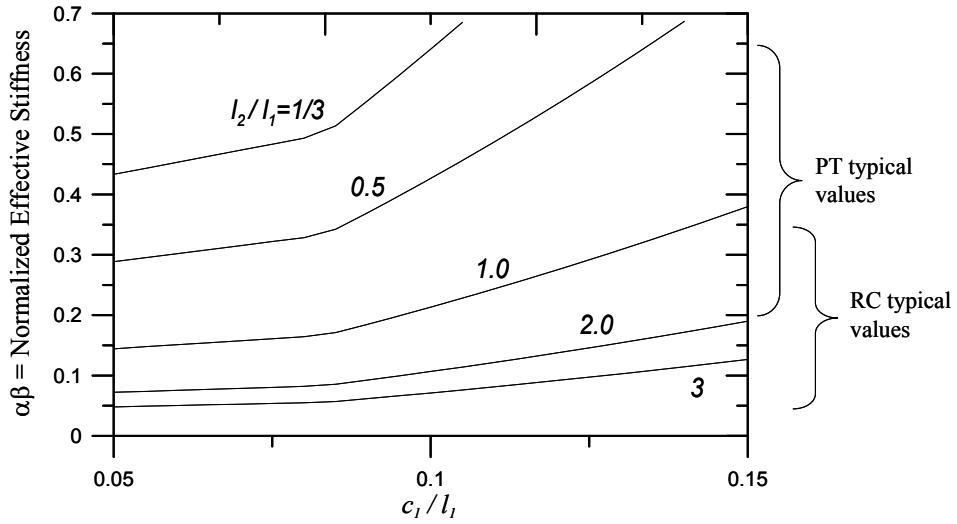

Figure 4-48 Normalized effective stiffness factors for interior slab-column frames based on Equations 4-10 through 4-12.

Connections in which continuity reinforcement is provided are classified as deformation-controlled, and nonlinear behavior, both before and after punching, should be incorporated in the structural model. In a slab-column frame the connection occurs "around" the column, and this can lead to complications in modeling nonlinear behavior. One way to model this connection is through the inclusion of a zero-length torsional member that connects the column to adjacent slab-beams, as shown in Figure 4-49.

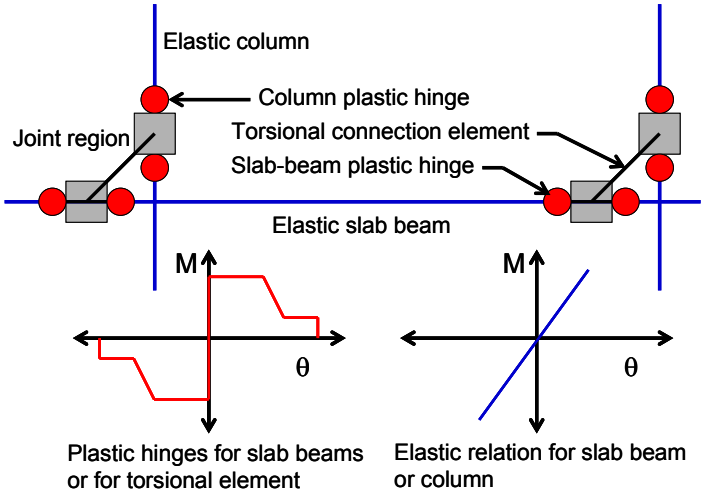

Figure 4-49 Model of slab-column connection.

In this model, the column and slab-beam are modeled with concentrated hinges at each end representing the flexural strengths of the members. The torsion member is rigid until the connection strength is reached, after which nonlinear rotation is represented. An advantage of this model is that it

enables the "unbalanced" moment, M_{con}, transferred from the slab to the column, as illustrated in Figure 4-50, to be tracked directly during the analysis.

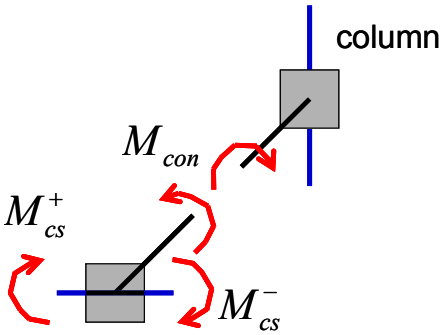

Figure 4-50 Unbalanced moment transferred between the slab and column in a torsional connection element.

The strength of the torsional connection element is given by:

$$M_{n,con} = \min\{M_f / \gamma_f ; M_v / \gamma_v\} \tag{4-13}$$

where M_f / γ_f is the moment transferred in flexure, divided by the fraction of unbalanced moment transferred in flexure, and M_v / γ_v is the moment transferred by eccentric shear, divided by the fraction of unbalanced moment transferred in eccentric shear, in accordance with Chapter 21 in ACI 318-05.

To accurately model the response of slab-column frames, the total drift, including all sources of yielding, should be monitored until the drift exceeds the limits shown in Figure 4-51. Although such a model has been proposed (Kang et al., 2006), most commercially available analysis programs do not currently have this capability; hence an alternate model is proposed.

If the punching capacity of the slab-column connection in Equation 4-13 is insufficient to develop the nominal capacity of the developed slab flexural reinforcement provided within the column strip, then all yielding is assumed to occur in the torsional element using the modeling parameters provided in ASCE/SEI 41-06 *Supplement No. 1*. For cases where yielding of slab reinforcement within the column strip is expected (i.e., strong connection), plastic rotations should be modeled only within the slab-beam elements (i.e., plastic hinges with positive and negative nominal capacities) using the plastic rotation modeling parameters from ASCE/SEI 41-06 *Supplement No. 1*. Figure 4-51 compares these modeling parameters with test data. Modeling parameters for connections with and without continuity reinforcement are approximately mean values and mean minus one sigma values, respectively (Elwood et al., 2007).

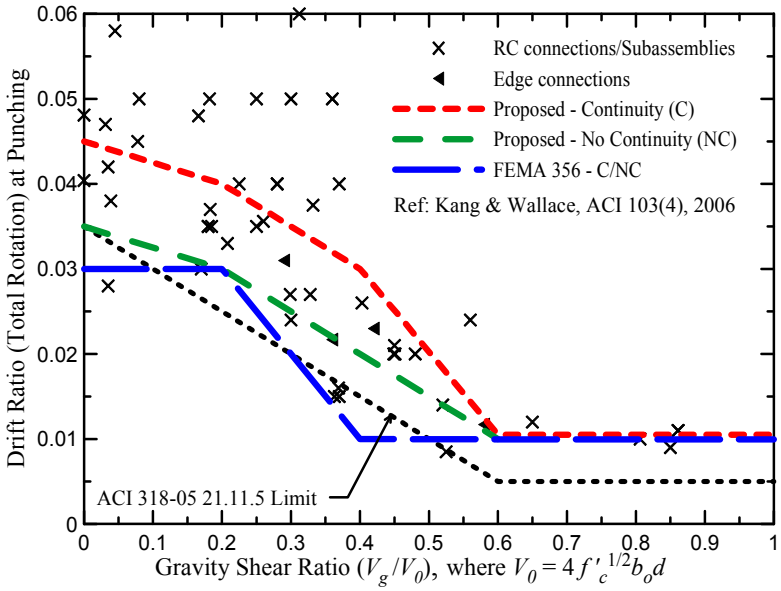

(a) Reinforced concrete slab-column connection

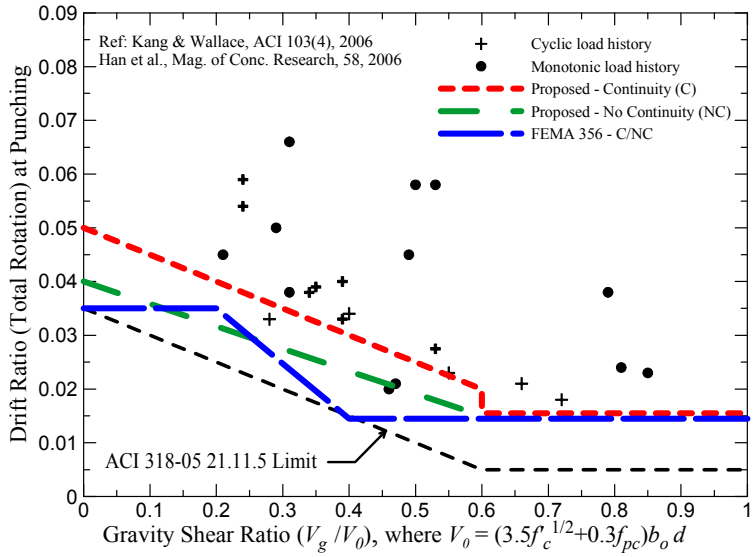

(b) Post-tensioned slab-column connection

Figure 4-51 ASCE/SEI 41-06 *Supplement No. 1* modeling parameter *a* for reinforced concrete and post-tensioned slab-column connections (Kang and Wallace, 2006).

4.5.2 Application to Core Wall Systems

A slab-column system was incorporated into the core-wall system investigated in Section 4.4, to assess the potential impact of the gravity framing on response quantities of interest, including story drift, column axial load, and the potential for slab-column punching failures.

The floor plan and simplified model of the combined slab-column frame and core wall system are shown in Figure 4-52. A simplified model was used to reduce computer run time. Four equivalent columns were used to represent the behavior of the gravity columns. Coupling between the core wall and the gravity columns is modeled using an equivalent slab-beam, with properties determined using the effective beam width model.

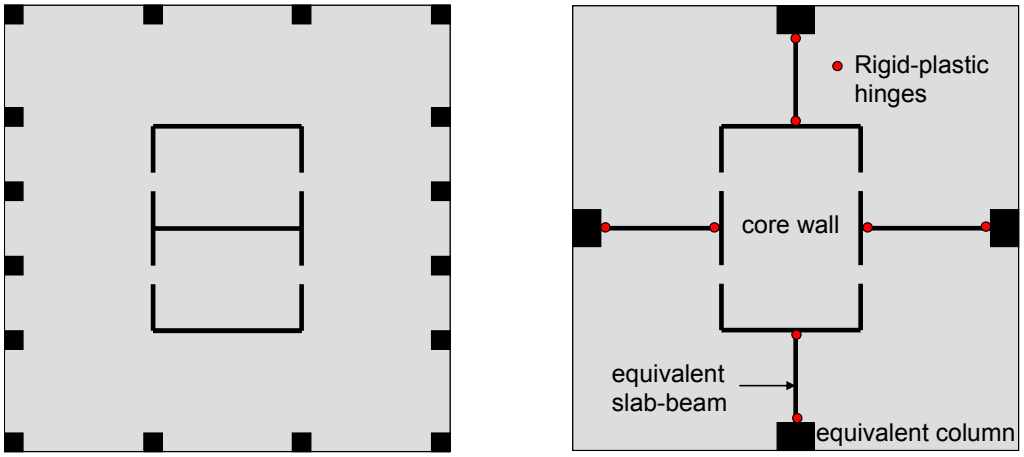

(a) Floor plan (b) Simplified model

Figure 4-52 Floor plan and simplified model of the combined slab-column frame and core wall system.

The stiffness of the equivalent slab-beams were determined as shown in Figure 4-53. Two slab effective widths were used to model spans with different elastic effective beam widths at each end.

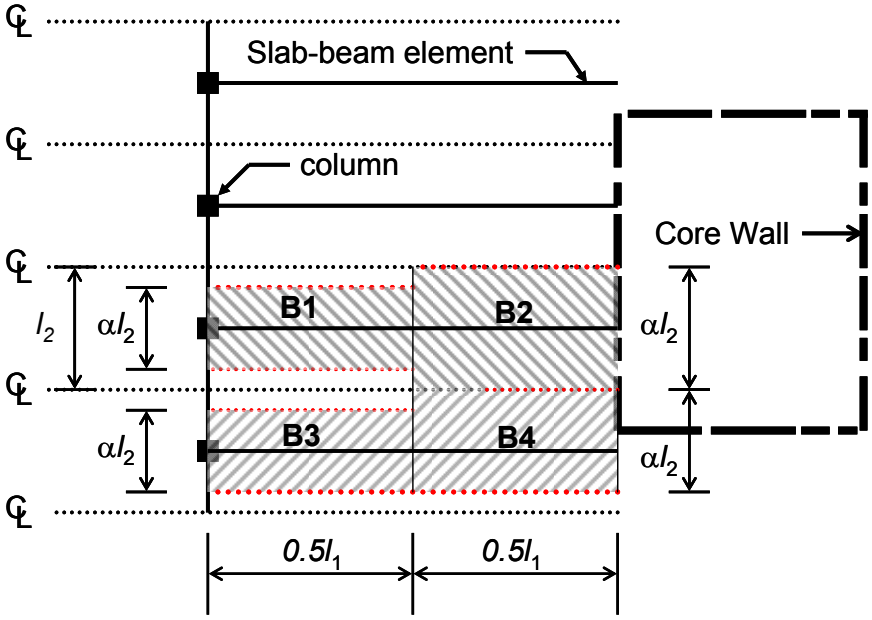

Figure 4-53 Application of effective width model to core wall.

The effective width for beam B1 was determined by the ratios of c_1 / l_1 and c_2 / l_2, and the effective width of B2 was set equal to l_2, given that the core wall spans the entire width of the beam. The two beams (B1 and B2) meet at a nodal point located at the center of the span, based on the approach recommended by Hwang and Moehle (2000). Effective *EI* values determined for the slab were multiplied by the β-factor to account for cracking. Yield moments in positive and negative bending for the slab-beams were determined based on fully anchored slab flexural reinforcement within the effective beam widths. A schematic of the slab model is provided in Figure 4-54.

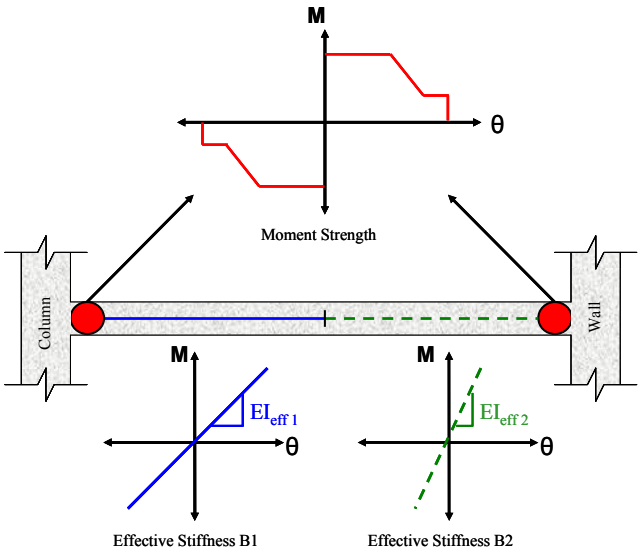

Figure 4-54 Schematic of the slab model.

To further reduce computer run time, an additional simplification was made. Plastic hinges were not included at the ends of the equivalent slab-beams. Yielding in the slab would be expected to reduce the interaction between the slab-column frame and the core wall elements. As such, results represent an upper-bound measure of the effects of the gravity frame on response quantities of interest.

A comparison between story drifts for the core wall model and coupled core wall-slab column model is shown in Figure 4-55. In this case, coupling between the core walls and the slab-column frame did not significantly impact story drift in the north-south or east-west directions.

A comparison between column axial stresses for the core wall model and coupled core wall-slab column model is shown in Figure 4-56. Results are plotted for two different load cases: (a) 1.2*D* + 1.6*L*, and (b) 1.0*D* + *E* (for a single ground motion record).

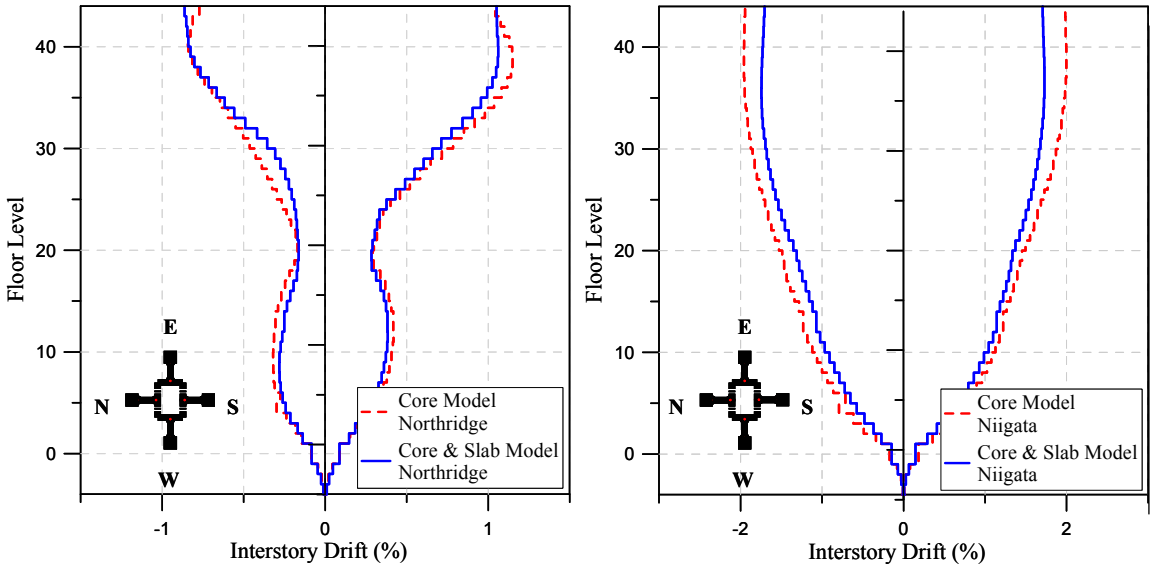

Figure 4-55 Comparison of story drifts in the north-south and east-west directions for the core wall model and coupled core-slab model.

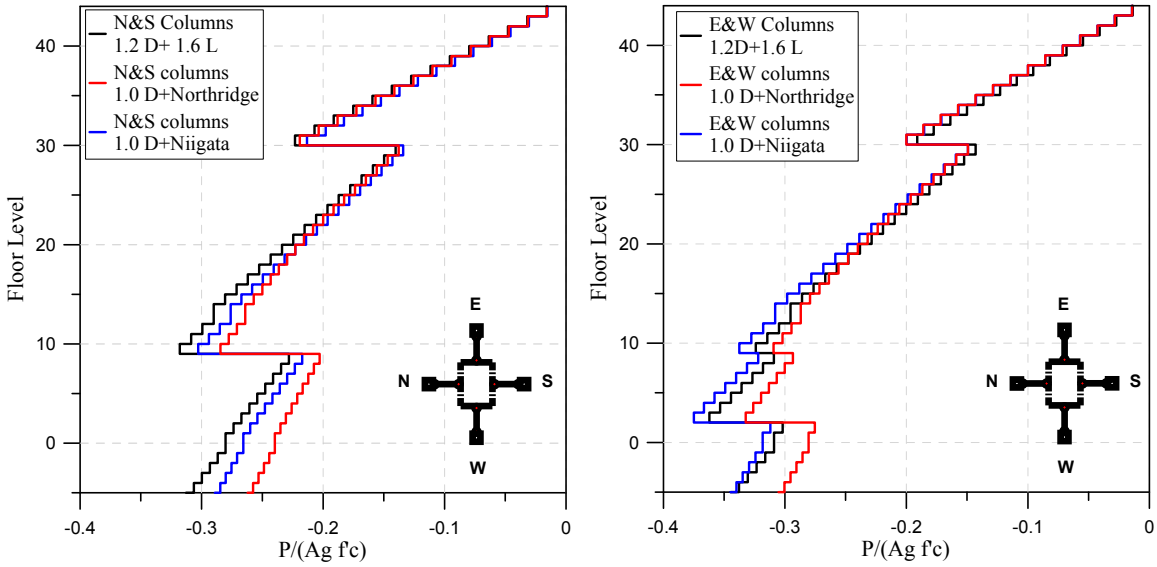

Figure 4-56 Comparison of column axial stress in the north-south and east-west directions for the core wall model and coupled core-slab model.

Sudden changes in axial stress at levels 9 and 30 are due to changes in the column cross-section at these levels. Results for this case study building and the given ground motion suggest that the variation in column axial load due to coupling between the core wall and the slab-column frame is not significant relative to the pure gravity load case. This is not necessarily a general result. For slabs with more longitudinal reinforcement and shorter spans, a greater variation in column axial load would be expected.

4.5.3 *Summary Recommendations for Modeling of Slab-Column Frames*

Summary recommendations for modeling of slab-column frames are as follows:

1. A significant body of work is available for reinforced concrete slab-column connections. Relatively few tests have been conducted on post-tensioned slab-column connections, and test information for post-tensioned connections with shear reinforcement is very limited. Information on modeling of slab-column frames can be found in ASCE/SEI 41-06 *Supplement No. 1*, and in Elwood et al. (2007).
2. Modeling parameters and acceptance criteria published in ASCE/SEI 41-06 *Supplement No. 1* are based on mean values of test results for conforming connections. These criteria allow substantially higher interstory drift (or total rotation) at slab-column connections prior to predicted punching failure. While use of mean values might be appropriate for seismic rehabilitation, lower values should be used for new construction. For service-level analyses, use of mean minus one standard deviation values is recommended. For MCE level analyses, use of mean values is recommended.
3. Use of the effective slab width model is recommended to model coupling between the core wall and the slab-column frame. Although this coupling is generally not considered, the potential adverse impacts of additional axial load induced on the gravity system columns should be considered.

4.6 Performance of Post-Tensioned Slab-Wall Connections

Post-tensioned slab-column frames are commonly used as gravity systems in tall core wall construction. Given that core wall strain gradients can be quite large, the core wall can impose large rotations on the slab, particularly at the slab-wall interface where the core wall is in tension. When subjected to these large rotation demands, the slab-wall connection must be capable of maintaining the ability to transfer gravity loads to the core wall.

Test data on slab-wall connections, however, are limited. Pantazopoulou and Imran (1992) present test results for reinforced concrete slabs, and recommend a limiting shear stress that depends on the quantity of slab reinforcement provided.

To speed up construction in tall buildings, slip-forming is sometimes used, i.e., the core wall is cast prior to the floor slab, creating a potential weak

connection at the slab-wall interface. One approach that has been used to accomplish this connection is shown in Figure 4-57, where the post-tensioning strands that stop short of the wall interface connect to the wall via mechanical couplers. In addition, shear keys are typically provided.

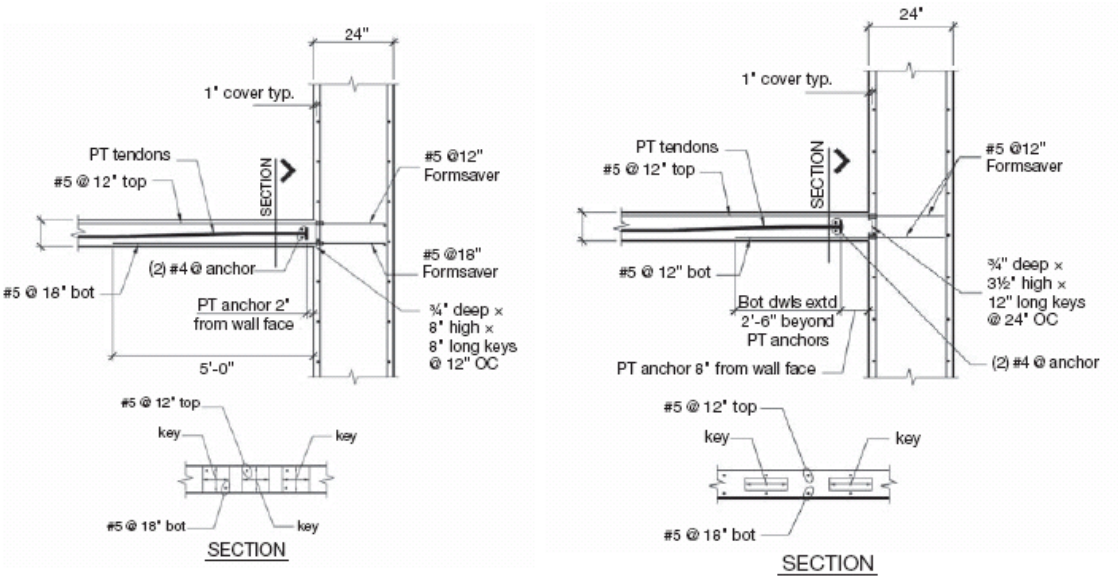

Figure 4-57 Slab-to-wall connection details for Specimen 1 (left) and Specimen 2 (right) (Klemencic et al., 2006).

Two full-scale tests were undertaken by Klemencic et al. (2006) to investigate the behavior of slab-wall connections, and to demonstrate that the connection can achieve Collapse Prevention performance for story drift ratios up to 2%. The two specimens were configured with common architectural dimensions, as shown in Figure 4-58.

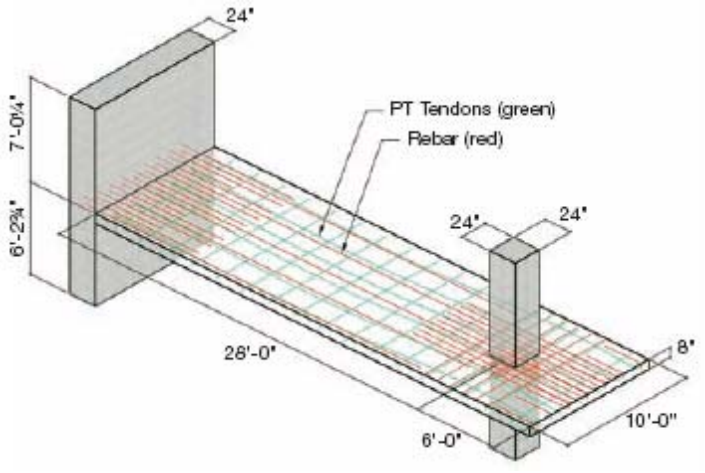

Figure 4-58 Overall test specimen geometry (Klemencic et al., 2006).

Other goals for these tests included assessing the impact of lateral drift on the degree of cracking in the connection region, the influence of varying the location of the anchor on the unbonded post tensioning cables, and the behavior of the mechanical couplers at slab-wall interface. Specimens were subjected to constant gravity load and then increasing lateral deformation. The displacement history included the application of negative peak drift values equal to twice the positive peak drift values to account for the impact of wall "growth" (due to core wall tension) on rotation demand.

Test results are shown in Figure 4-59. Elastic behavior was observed up to a peak drift ratio of 0.85%, with significant yielding at a drift ratio of approximately 1.0%.

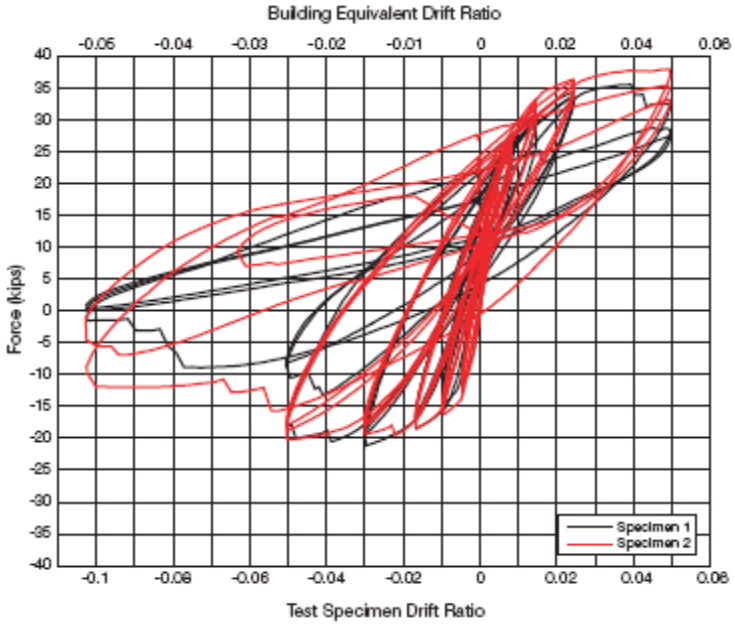

Figure 4-59 Force-displacement relations for slab-wall connection Specimens 1 and 2.

In Specimen 1, lateral strength degradation caused by pullout of top dowels was initiated in the first cycle at 2.5% drift, but the specimen was subjected to multiple cycles at 2.5% drift without loss of gravity load-carrying ability. Flexural strength loss occurred in the first cycle at 2.5% drift, caused by the pullout failures of the top dowels.

In Specimen 2, lateral strength degradation caused by bar buckling was initiated in the first cycle at 5.0% drift, but the specimen was subjected to multiple cycles at 5.0% drift without loss of gravity load-carrying ability.

The biggest difference in performance between the two specimens was the degree of cracking at the slab-wall interface, shown in Figure 4-60. In

Specimen 1, where the anchor for the post-tensioning tendons was placed 2 inches from the face of the wall, large cracks were observed between the anchor and the wall. In Specimen 2, where the anchor was placed 8 inches from the face of the wall, cracks were more distributed and narrower. Moderate improvement in performance was observed for Specimen 2, which had an equal amount of bonded reinforcement at the top and bottom of the slab.

Figure 4-60 Observed cracking at 2.5% drift in Specimen 1 (left) and Specimen 2 (right).

Appendix A

Modeling of Podium Diaphragms, Collectors, and Backstay Effects

The base of a tall building is often referred to as a *podium*. Any lower part of a tall building structure that is larger in floor plate, and contains substantially increased seismic-force resistance in comparison to the tower above, can be considered a podium.

Floor and roof slabs are key components in a podium. They act as *diaphragms* in shear and flexure, distributing forces to the vertical elements of the seismic-force-resisting system. Within the diaphragms, *collectors*, acting in axial tension and compression, accumulate forces in the diaphragm and assist in the transfer of forces to walls and frames.

Backstay effects are the transfer of lateral forces from the seismic-force-resisting elements in the tower into additional elements that exist within the podium, typically through one or more floor diaphragms. The lateral force resistance in the podium levels, and force transfer through floor diaphragms at these levels, helps a tall building resist seismic overturning forces. This component of overturning resistance is referred to as the backstay effect, based on its similarity to the back-span of a cantilever beam. It is also sometimes called "shear reversal" because the shear in the seismic-force-resisting elements can change direction within the podium levels.

This appendix discusses podium and backstay effects, provides guidance on the modeling and seismic design of floor diaphragms and collectors, and recommends element stiffness properties for use in modeling.

A.1 Podium and Backstay Effects

An example of a tall building structural system consisting of a concrete core wall superstructure and a below-grade podium, is shown in Figure A-1. Interaction between the tower and the below grade diaphragms and perimeter walls causes a backstay effect. Most tall buildings have configurations that cause backstay effects.

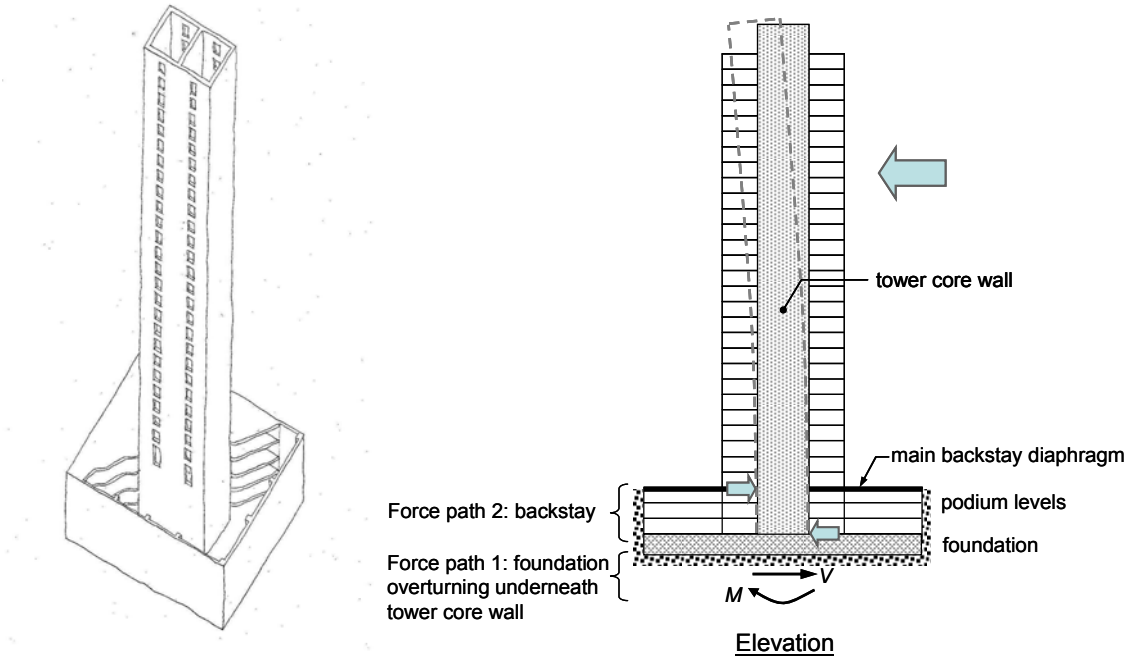

Figure A-1 Example of a tall building structural system with a concrete core wall superstructure and below-grade perimeter retaining walls forming a podium.

Buildings with below-grade levels require reinforced concrete retaining walls (i.e., perimeter basement walls) to retain the soil. If the building superstructure is connected to below-grade perimeter walls, and if the seismic-force-resisting elements in the tower are not aligned with the perimeter walls below, then a transfer of lateral forces will need to occur. This transfer occurs through one or more floor diaphragms in the podium, and the relative stiffness of all the elements in this load path determines how the force is transferred. In the case of podium elements responding nonlinearly, their strength rather than stiffness will govern the distribution of forces. Significant nonlinearity in the structural elements of the podium, however, is undesirable.

While larger below-grade stories almost always constitute a podium condition, levels above grade can also act as a podium if they contain additional seismic-force-resisting elements that do not extend the full height of the building. Many tall buildings have a configuration in which the first few stories above grade have a larger footprint than the tower or towers above. This condition is common in multi-use tall buildings where the lowest stories above grade often contain public, retail, and lobby spaces, hotel ballrooms and meeting rooms, or parking.

Podium and backstay effects are influenced by the type of structural system in the building. Designing for backstay effects requires careful consideration

of element stiffness, and use of bounding assumptions to bracket anticipated behavior. For tall buildings in high seismic regions, a capacity design approach and nonlinear response history analysis are recommended. Isolated models of particular diaphragm elements or structural subassemblies may be needed to ensure that the resulting design satisfies equilibrium and compatibility concerns.

A.1.1 Structural Elements of the Podium

Key elements of the podium include the reinforced concrete perimeter walls at the below-grade levels, floor diaphragms at the below-grade levels, and the foundations and supporting soils. The most critical diaphragm is the main backstay diaphragm, which is located at the top of the perimeter walls.

In structures with concrete gravity framing, podium floor diaphragms can be cast-in-place reinforced concrete slabs. In structures with steel gravity framing, podium floor diaphragms can be constructed with concrete fill on steel deck. Figure A-2 shows the construction of below-grade levels of a tall core wall building with steel gravity framing.

Figure A-2 Construction of a concrete core and below-grade levels of a high-rise building (courtesy of Magnusson Klemencic Associates).

A.1.2 Seismic-Force-Resisting Elements of the Tower

Seismic-force-resisting systems that extend above the podium are often reinforced concrete core walls with coupling beams. Tower systems can also include steel or concrete moment frames, and dual systems consisting of moment frames in combination with concrete walls, steel braced frames, or steel plate shear walls. Steel braced frames can be buckling-restrained braced frames, eccentrically braced frames, or concentrically braced frames.

Prescriptive requirements in ASCE/SEI 7-10, *Minimum Design Loads for Buildings and Other Structures* (ASCE, 2010), require buildings taller than 240 feet (160 feet in some cases) located in high seismic zones to have a seismic-force-resisting system consisting of special moment frames, or a dual system that includes special moment frames. Tall buildings not meeting these requirements achieve code compliance using non-prescriptive procedures, typically with a design process that utilizes capacity design and nonlinear response history analysis along with seismic peer review (SEAONC, 2007; Maffei and Yuen, 2007).

Not all concrete walls in tall buildings are arranged in a core configuration. The core arrangement works well for buildings where service functions such as elevators, stairs, mechanical rooms, and restrooms are located near the center of the floor plan. Buildings in which these elements are offset, or buildings with L-shaped or other irregular plan configurations, may need a series of individual walls or multiple cores, as shown in Figure A-3. Architectural constraints that affect the location and configuration of concrete walls apply similarly to the location and configuration of steel braced frames.

Figure A-3 Construction of concrete walls for a high-rise apartment building. The structural system has two individual walls, at left, and a concrete core, at right (courtesy of KPFF).

A.1.3 Consideration of Backstay Effects

Evaluation of backstay effects requires consideration of two seismic load paths, both of which contribute to the overturning resistance of the building. These paths are illustrated in Figure A-1, where one path is the overturning resistance provided by the foundation directly beneath the seismic-force-resisting elements of the tower, and the second path is the backstay resistance provided by in-plane forces in the lower floor diaphragms and perimeter walls. Seismic design for backstay effects requires: (1) an assessment of what portion of the overall building overturning is resisted by each load path; and (2) a design to provide adequate strength in the structural elements of each load path.

For the direct load path through the foundation, it is important to consider the vertical stiffness of the piles or the supporting soil below the foundation. For the backstay load path, it is important to consider the relative stiffness of the diaphragms and the perimeter walls, including consideration of horizontal pressures on the walls, and vertical in-plane rocking resistance below the walls, provided by the surrounding soil.

The elements in both load paths must have sufficient stiffness and strength to validate local modeling assumptions. Use of well-designed elements in redundant load paths is beneficial to the seismic performance of the building, and can result in an economical design.

A.1.4 Impact of Structural System Type and Configuration on Backstay Effects

The type and configuration of the structural system affects the location and magnitude of forces that are transferred through the podium. In seismic-force-resisting systems composed of central cores (e.g., shear walls or braced frames), the foundation directly below the core is often less stiff than the backstay load path. Pile foundations, however, tend to be stiffer than mat slabs, resulting in comparatively less reliance on the backstay load path. Seismic-force-resisting systems that are more distributed over the building floor plan tend to have more inherent overturning resistance, and rely less on the backstay load path.

Generally, the main backstay diaphragm located at the top of the podium perimeter walls will transfer more force than any other diaphragm. During preliminary design, it is prudent to assume that this diaphragm will need to be a structural slab that is significantly thicker than the other floors in the building, and to plan openings at locations that will not interrupt critical load paths.

A.2 Effects of Other Structural Configurations

Podium and backstay effects are not limited to tall buildings. Low- and mid-rise buildings can be subject to the same effects. Similar effects can occur at any location over the height of a building where lateral elements are discontinued or reduced in stiffness, such as at building setbacks or step-backs.

A.2.1 Buildings Without Backstay Effects

While most tall buildings have configurations that result in podium and backstay effects, there are exceptions. Examples of building configurations that will not result in backstay effects include:

- Buildings without below-grade levels, or buildings without significantly increased seismic-force-resistance at the base.
- Buildings that extend below grade, but have structural separations between the superstructure and the podium structure that accommodate seismic deformations without the transfer of seismic forces.
- Buildings with perimeter basement walls, but the walls are located directly below the seismic-force-resisting elements of the superstructure above. While there could be a marked change in lateral strength and stiffness, lateral forces will not be transferred through the floor diaphragms.

A.2.2 Setback or Step-Back Effects

Effects similar to backstay effects can occur anywhere in a building where there is a significant change in lateral strength or stiffness in one story relative to adjacent stories. In tall buildings, this can occur at setbacks or step-backs, which are locations where the seismic-force-resisting system significantly changes in dimension above the base, as shown in Figure A-4.

Because of deformation compatibility and relative stiffness effects, the shorter element in such a configuration will attract larger seismic forces through the floor diaphragms and collectors at the top of the setback. This is true for cantilever walls, coupled walls, braced frames, and moment frame systems.

Setbacks or step-backs can also create a strength discontinuity that can result in concentrated nonlinear behavior in the system at the location of the setback. In the case of concrete walls, the most desirable nonlinear behavior is a flexural plastic hinge mechanism at the base of the wall. Setbacks can

result in plastic hinging at elevations above the base of the walls, and structural elements should be designed to ensure essentially elastic behavior above the setback.

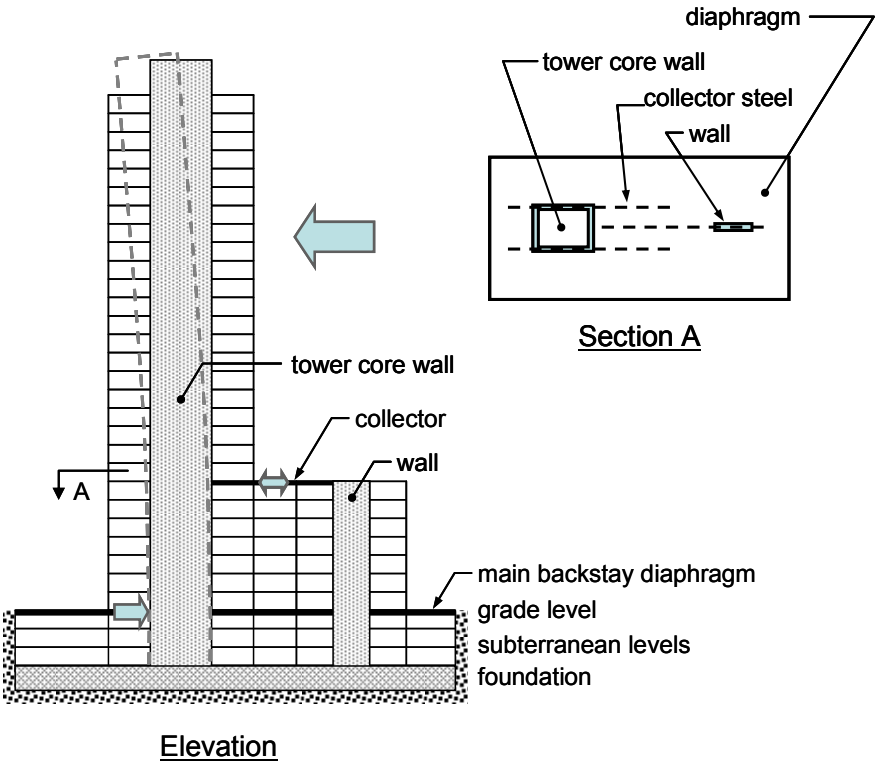

Figure A-4 Example of a setback in a concrete core wall building in which an additional concrete wall extends above the lower podium, but not the full height of the building.

A.2.3 Multiple Towers on a Common Base

Tall building developments can include two or more towers on the same site, as shown in Figure A-5. Multiple towers are often founded on a common base structure, and are likely to differ from each other in mass, stiffness, and other physical properties.

When subjected to earthquake shaking, individual towers will, at different times, be moving towards each other, away from each other, in-phase, or out-of-phase. Floor diaphragms and collectors that connect two or more tower structures are likely to be subjected to large forces associated with the relative movement. Connecting diaphragms and collectors should be designed to resist the envelope of forces that can be generated by this interaction.

In the case of a symmetric structure with two identical towers, an analytical model with coherent ground motion input will show synchronized movement

of the towers and negligible transfer of forces. In a real earthquake, however, incoherency of the ground motion (i.e., earthquake waves arriving at different parts of the structure at different times), as well as small differences in dynamic properties, will produce unsynchronized movement of the towers and more significant transfer of forces.

Figure A-5 Example of two towers on a common base (courtesy of Jones Kwong Kishi Architects and ABKJ Structural Engineers).

Nonlinear response history analysis is the best way to evaluate the effects of multiple towers on a common base, and the transfer forces that can occur in the connecting floor diaphragms and collectors. In the case of towers with similar dynamic properties, the potential for unsynchronized movement should be considered. Although there are no standard criteria for doing so, one approach would be the application of incoherent ground motions in a nonlinear response history analysis of the combined structure. Another approach would include varying the mass, stiffness, and other properties of the towers, in an attempt to bound the magnitude of potential transfer forces caused by unsynchronized movement.

Depending on the architectural configuration, the topmost diaphragm connecting multiple towers may, or may not, coincide with the main backstay diaphragm at the podium level. Where multiple towers are architecturally connected above the podium, it might be beneficial to keep the tower structures seismically separated at these levels. Limiting structural connections to the podium levels and below has the advantage of concentrating design for force transfers in areas where they are already being

considered, and where they can be transferred directly from the towers to the perimeter walls.

A.2.4 Buildings on Sloping Sites

In buildings on sloping sites, it is possible for retaining walls on the high side of the site to extend one or more levels above the walls on the low side of the site. If connected to the structure at all levels, unsymmetric retaining wall configurations cause unbalanced lateral resistance and undesirable torsional response. Sloping sites can also cause unequal horizontal soil pressures applied to the building, which should be considered in the design of below-grade floor diaphragms and walls.

A design objective for such buildings would be to minimize torsional eccentricities at the base of the structure. A possible solution includes seismic separations between the structure and one or more levels of the unequal-height retaining walls.

A.3 Nonlinear Seismic Response and Capacity Design

Most buildings are designed to experience nonlinear behavior under strong earthquake shaking. Typically, the vertical elements of the seismic-force-resisting system (e.g., concrete walls, steel or concrete moment frames, and steel braced frames) are intended to respond nonlinearly. These elements are expected to undergo inelastic deformation without significant strength degradation.

For the overall structure to respond as intended, other parts of the seismic load path (e.g., floor and roof diaphragms, collectors, and connections to the vertical seismic-force-resisting elements) should experience little or no inelastic deformation. This philosophy is incorporated into building codes through the use of the Ω_0 factor, which amplifies design forces to a level that is intended to approach the capacity of the adjacent vertical seismic-force-resisting elements in the system. A more direct, and more accurate way to protect non-yielding elements is to use a capacity design approach as part of a two-stage design process outlined below.

A.3.1 Capacity Design

Recommendations for addressing backstay effects are based on a capacity design philosophy and use of nonlinear response history analyses. Basic capacity design principles include the following:

- Selection of a desirable mechanism for nonlinear lateral deformation identifying which structural elements and actions are intended to undergo

nonlinear response. The mechanism should not lead to concentrated inelastic deformations.

- Adequate detailing of the designated nonlinear elements to provide ductility, i.e., capacity to deform beyond the yield point without significant strength degradation.
- Design of all other elements and actions for elastic, or near-elastic, response.

In a concrete core wall building, a desired nonlinear mechanism consists of flexural plastic hinging near the base, and ductile flexural yielding in coupling beams over the height, as shown in Figure A-6. Cantilever walls without coupling beams are designed to develop a single plastic hinge at the base. In each plan direction, flanges formed by the intersecting walls of the core contribute to global moment capacity.

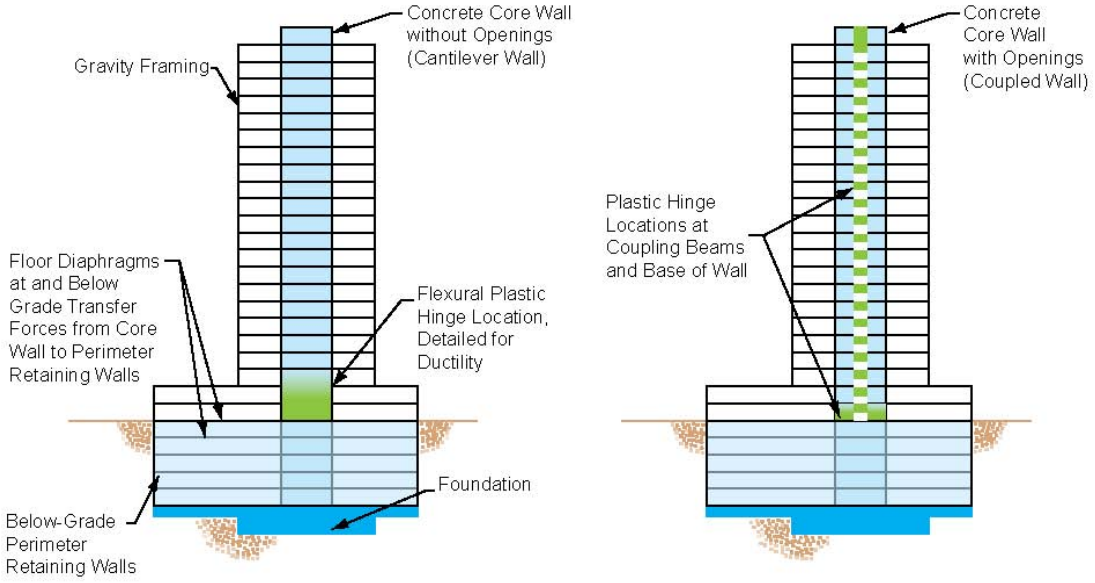

(a) Cantilever wall (b) Coupled wall

Figure A-6 Desirable nonlinear mechanisms for: (a) cantilever wall; and (b) coupled wall.

Designated nonlinear elements are detailed for ductile response. Other elements are designed with sufficient strength so that their behavior will be essentially elastic, with the required strength determined from Maximum Considered Earthquake (MCE) level nonlinear response history analysis. Capacity-protected elements in a typical building include the following:

- Walls in shear and sliding shear
- Walls in flexure outside the designated hinge zone(s)

- Floor and roof diaphragms and collectors
- Floor and roof slabs in punching shear
- Columns
- Foundation perimeter walls
- Foundations

Capacity design concepts for concrete members were introduced by Blume, Newmark, and Corning (1961), at a time when analytical capabilities in engineering practice were limited. Nonlinear response history analyses were only feasible on large university computers using two-dimensional models of simplified structures. Researchers used such analyses to derive requirements for capacity design that could be applied in simpler linear static analyses and structural design practices (Paulay and Priestley, 1992).

These requirements, such as dynamic shear amplification factors, are still useful, particularly for regular structures less than 20 stories in height, and for preliminary design of taller structures. Today, with recent advances in structural analysis software, a capacity design approach can be combined with building-specific analyses to design tall buildings for acceptable seismic performance.

A.3.2 Two-Stage Design Process

Tall buildings can be designed in a two-stage process that follows an approach that has been used for non-prescriptive seismic design of tall buildings (SEAONC, 2007). This process consists of: (1) preliminary code-level design of the system; and (2) performance verification using MCE level nonlinear response history analysis

The first stage of the process determines the strength of yielding elements. Typically, this is accomplished by designing the building to comply with all applicable code provisions (except for identified exceptions such as the height limit). This means that the designated yielding elements are designed for code-level demands including the R factor. For tall buildings with long periods, code-level demands are typically governed by minimum base shear requirements. Alternatively, a code-level analysis could be replaced with an elastic analysis that is scaled to the service level earthquake.

The second stage of the process is to analyze the structure with a nonlinear response history analysis using Maximum Considered Earthquake (MCE) level ground motions. This analysis is intended to:

- Verify that the expected seismic behavior of the structure is governed by the intended mechanism, with nonlinear behavior occurring only in the designated yielding elements.
- Verify that all other potential mechanisms and actions remain essentially elastic.

Record-to-record variability is often the largest source of dispersion in analytical results. However, other assumptions that can potentially have a large effect on the resulting design should also be considered. These can include effective gravity load and strength and stiffness properties of the structural elements. In the case of backstay effects, assumptions regarding stiffness properties are typically the most important variable to bracket.

Nonlinear response history analysis at the MCE level using expected material properties replaces the application of the code-prescribed overstrength factor, Ω_0, on actions designed to remain elastic. When evaluating actions that are to remain elastic, the design should consider the dispersion in the nonlinear response history analysis results, rather than just the average response.

A.4 Modeling of Structural Elements

All structural elements contributing to the backstay effect should be explicitly included in the analytical model, with suitable stiffness assumptions, so that appropriate design forces can be determined. The following elements should be modeled: floor diaphragms and collectors, structural walls and frames, foundation mat slabs, pile caps, footings, and soil or pile springs.

To get appropriate diaphragm and wall forces, the analytical model should include mass at all levels. In code procedures for calculating equivalent static lateral story forces, it is often appropriate to neglect mass below grade; however, this mass should be included in the dynamic analytical model for backstay effects.

A.4.1 Bracketing of Stiffness Properties

In general, there is uncertainty in the properties of structural components. In the case of reinforced concrete components, a number of variables can affect concrete stiffness properties, including cracking, strain penetration, bond slip, panel zone deformation, and tension shift associated with shear cracking.

The properties of supporting soils below a foundation are typically even more uncertain. Design practice for soil stiffness modeling often includes

analyzing a structural system with 0.5 times the expected soil properties, and again with 2 times expected properties, and then enveloping design forces for the two cases.

This type of design practice is known as "bracketing" assumptions. Typically, it is important to bracket assumptions if two conditions are present: (1) the assumptions are uncertain or variable; and (2) the assumptions are influential on the resulting design.

When applied to podium and backstay effects, stiffness properties of the following structural elements should be bracketed:

- Perimeter walls and their foundation support
- Shear and flexural action of backstay floor diaphragms
- Foundation support under the tower seismic-force-resisting system

A.5 Collectors and Diaphragm Segments

In general, floor diaphragms should be designed for: (1) inertial forces due to seismic acceleration of the mass tributary to the floor; and (2) seismic forces that are redistributed between different elements of the seismic-force-resisting system.

Seismic forces in diaphragms originate where the mass of the building is located, or where a vertical discontinuity or stiffness variation causes a redistribution of forces between the vertical elements of the seismic-force-resisting system.

A.5.1 Role of Collectors

Collectors are often called "collector elements," and sometimes referred to as "drag struts," "drag elements," or "tie elements." While diaphragms resist lateral forces through in-plane shear and bending, collectors act in axial tension or compression to accumulate (or distribute) forces along the length of a diaphragm, as illustrated in Figure A-7.

A.5.2 Design for System Overstrength

In order to limit inelastic behavior, ASCE/SEI 7-10, requires collectors to be designed for seismic forces amplified by an overstrength factor Ω_0, which is equal to 2.5 or 3 for most common systems. When walls or frames of a building respond inelastically, seismic forces in the building are estimated to be approximately Ω_0 times the code design forces.

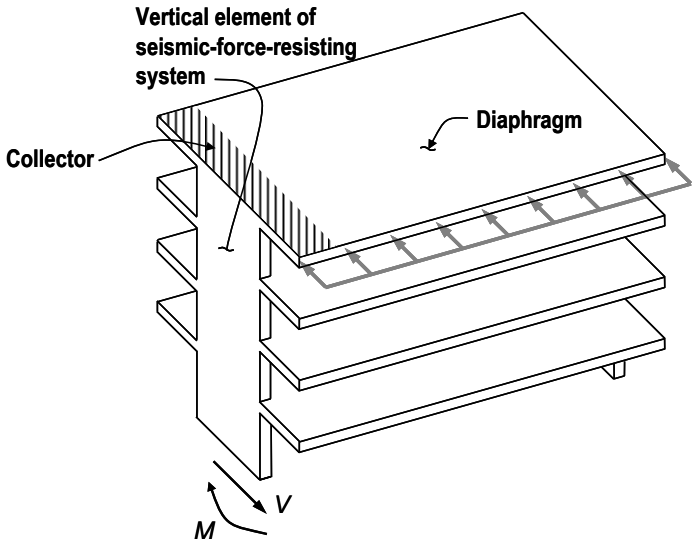

Figure A-7 Example location of a collector (shown hatched).

ASCE/SEI 7-10 specifies that the overstrength requirement is applied to collector elements, splices, and connections to vertical elements of the seismic-force-resisting system, but not the diaphragm as a whole. It might be more appropriate, however, to design the entire diaphragm for forces amplified by Ω_0, because the design intent for most structures is for all actions in diaphragms to remain elastic or near-elastic. Unreduced forces from nonlinear response history analysis can be used in lieu of the application of Ω_0.

A.5.3 Collector Eccentricity and Diaphragm Segments

In the case of very large collector forces, it is often not possible for the collector element to be concentric with the connecting wall or frame in the vertical seismic-force-resisting system. Figure A-8 illustrates a collector in which a portion of the seismic force is transferred directly into the end of the wall, and the balance is transferred through reinforcing bars placed outside the wall and shear-friction along the joint between the slab and the wall.

This load path creates an eccentricity between the collector forces and the reaction within the wall, and creates concentrated levels of diaphragm shear along the wall. This eccentricity induces additional stresses in the diaphragm segment adjacent to the wall.

The portion of the diaphragm adjacent to the wall, referred to as a *diaphragm segment*, functions to resist the concentration of diaphragm shears eccentricity of collector forces. Designing for these effects requires a process of checking forces at successive critical sections, ensuring a complete and adequate load path. It is recommended that diaphragm

segments be designed for the same amplified forces as collectors. That is, forces amplified by the system overstrength factor, Ω_0, are used to design diaphragm segments for: (1) collector eccentricity; and (2) concentrated shear resulting from the collector load path.

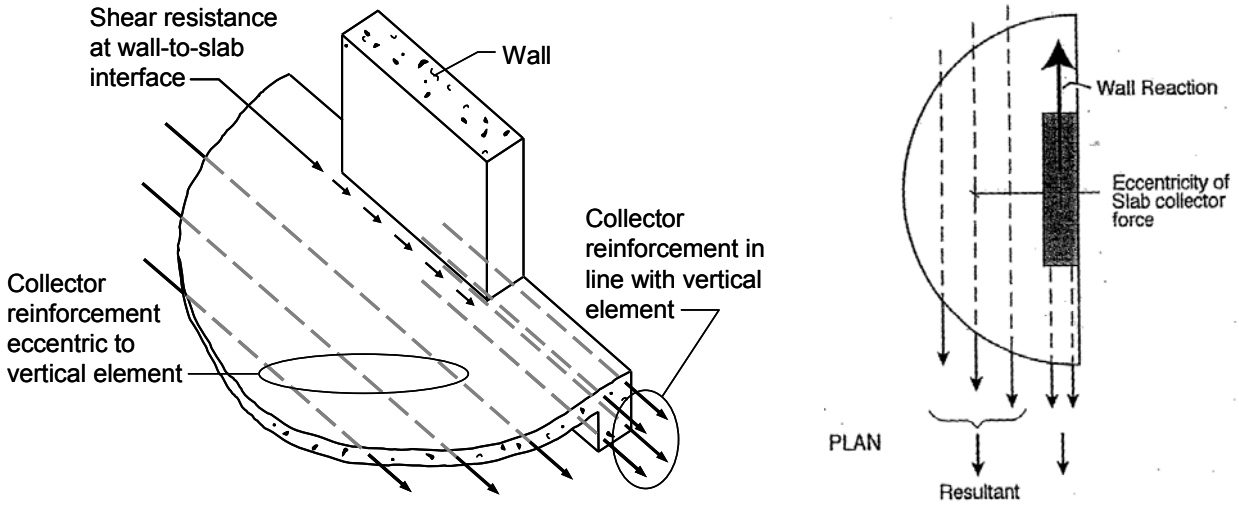

Figure A-8 Eccentric collector and reinforcement into, and alongside, a shear wall.

A.6 Diaphragm Flexibility

Diaphragms can be modeled as rigid, semi-rigid, or flexible. Applicability of each modeling approach is summarized in Table A-1. Relative stiffness assumptions associated with each are illustrated in Figure A-9.

Table A-1 Diaphragm Flexibility and Applicability of Modeling Assumptions

Modeling Assumption	*Description*	*Applicability*
Rigid	Diaphragm is assumed to be infinitely rigid compared to the vertical elements of the seismic-force-resisting system. Distribution of lateral forces is based on the relative stiffness of the vertical elements. Differences between center of mass and center of rigidity cause plan torsion that is distributed to vertical elements.	This is the most common approach for modeling concrete and concrete-on-steel-deck diaphragms. Widely used in commercially available structural analysis programs for buildings.
Semi-rigid	Finite diaphragm stiffness is included in the analytical model. Stiffness is computed based on diaphragm thickness, dimensions, and material properties.	The most realistic model, but more time-consuming and difficult to apply. Available in some three-dimensional structural analysis programs. Should be used to model diaphragms for backstay effects.
Flexible	Diaphragm is assumed to be infinitely flexible compared to the vertical elements of the seismic-force-resisting system. Spans of a diaphragm are considered simple shear spans, and distribution of lateral forces to vertical elements is based on tributary mass.	Typically not applicable for concrete or concrete-on-steel-deck diaphragms. Used most commonly for timber and un-topped steel deck diaphragms. Typically used with hand or spreadsheet calculations rather than in structural analysis programs.

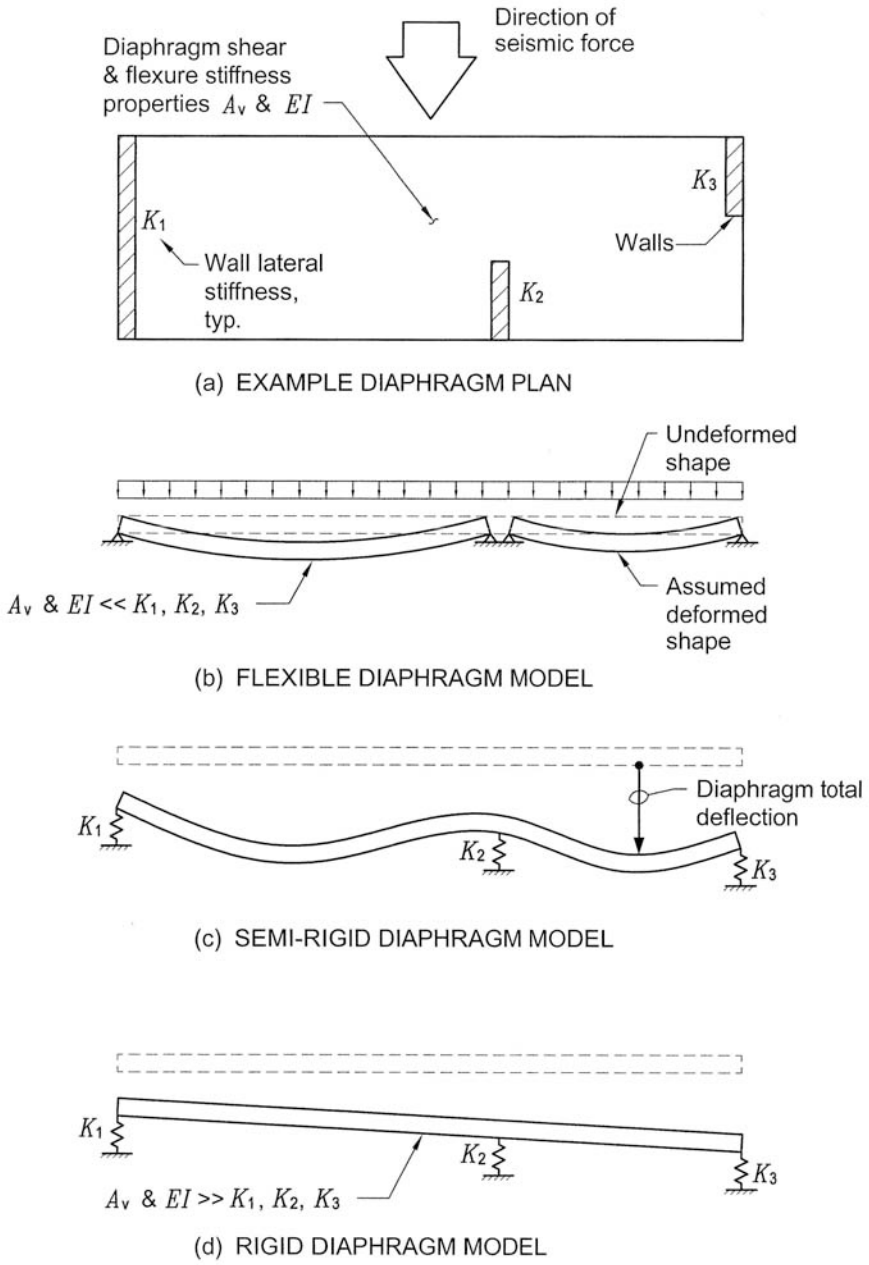

Figure A-9 Relative stiffness assumptions associated with diaphragm flexibility models.

In reality, all floor and roof diaphragms are semi-rigid because they have a finite value of in-plane stiffness. However, for practical design purposes, an idealized rigid or flexible diaphragm is often used to simplify the analysis. In some cases ASCE/SEI 7-10 requires semi-rigid modeling.

A semi-rigid diaphragm model is considered more accurate, particularly for irregular configurations or diaphragms with large openings, because it explicitly considers the diaphragm stiffness properties. It also provides

design forces for diaphragm shear and moment more directly. The chief disadvantage of a semi-rigid diaphragm model is that it can add significantly to the analytical work, including computer input and analysis run time.

Concrete, or concrete-on-steel-deck, diaphragms common in tall buildings are typically modeled as rigid or semi-rigid. A rigid diaphragm model is usually appropriate for regular structures. Diaphragms that make large force transfers, such as backstay diaphragms, should be modeled as semi-rigid. Other floors in tall buildings, i.e., those that do not carry significant force transfers, can often be modeled as rigid without significant loss in accuracy.

A.6.1 Relative Stiffness of Diaphragms and Vertical Elements

A rigid diaphragm assumption is most appropriate for stiff diaphragms with less stiff vertical seismic-resisting elements. Large openings or thin or narrow sections make a diaphragm less stiff. In the case of podium floor levels, a rigid diaphragm assumption can overestimate the transfer of forces as part of the backstay effect. A semi-rigid diaphragm model can lead to more economical designs for the floor diaphragm, and possibly the walls.

A comparison of stiffness between diaphragms and walls or frames should consider the anticipated nonlinear behavior. Under linear-elastic behavior, relative stiffness may be comparable. However, if the diaphragms remain elastic while the vertical elements yield, then the relative stiffness would change, and a rigid diaphragm assumption might become more appropriate.

A.6.2 Building Code Requirements

Prior to 2005, building codes did not regulate the choice between diaphragm modeling assumptions. Beginning with ASCE/SEI 7-05 (ASCE, 2006), use of a rigid diaphragm assumption for concrete diaphragms required that no horizontal irregularities be present in the building. Diaphragms in buildings not meeting this requirement must be modeled as semi-rigid.

This requirement can be unnecessarily burdensome because not all of the horizontal irregularities specified in ASCE/SEI 7-05 affect the appropriateness of diaphragm modeling assumptions. When choosing an appropriate diaphragm model, it is recommended that the following factors be considered. The specified horizontal irregularities that trigger semi-rigid diaphragm modeling are:

- Plan-torsional deformation
- Non-parallel systems
- Re-entrant corners

- Diaphragm discontinuities
- Out-of-plane offsets

Of these, plan-torsional deformation and non-parallel systems relate to the vertical elements of the seismic-force-resisting system, and can occur in systems where rigid diaphragm modeling is completely appropriate.

Re-entrant corners in a floor plan can make a semi-rigid diaphragm model appropriate, but generally this would only be the case only for very large re-entrant corners (e.g., L-shaped buildings). The irregularity provision is triggered when a re-entrant corner dimension exceeds 15% of the overall plan dimension. However, buildings can have re-entrant corners of this size, or larger, and still have essentially rigid diaphragms.

A diaphragm discontinuity is triggered by openings larger than 50% of the diaphragm area. In diaphragms with large openings, local deformations and long collectors result in diaphragm flexibility and force distributions that may not be adequately captured in a rigid diaphragm analysis. This is a good application for a semi-rigid diaphragm model.

Out-of-plane offsets can be the cause of large force transfers in diaphragms, which, as discussed above, are best analyzed with a semi-rigid diaphragm assumption that can lead to a more economical design.

A.7 Semi-Rigid Diaphragm Modeling

Semi-rigid diaphragm modeling is normally performed with a finite-element mesh that represents the in-plane stiffness of the diaphragm. Including finite elements for the diaphragms in the model can greatly increase the number of degrees of freedom in the analysis and the analysis run time. It will also increase the volume of output.

Successful implementation of such a model requires appropriate input assumptions and a thorough understanding of the output. Selection of an appropriate mesh size is important. If the mesh is too fine, the analysis can be overwhelmed by excessive run time. If the mesh is too coarse, results may not be realistic. If there are walls that are also modeled with finite elements, the nodes of diaphragm elements should be aligned with the nodes of the wall elements.

In semi-rigid diaphragm modeling, the mass at each level needs to be distributed to match the actual distribution of mass over the plan area. This is in contrast to rigid-diaphragm modeling, in which lumped mass properties at the center of rigidity of each level can be used.

Output from finite element models includes the forces and displacements at the element nodes. Some structural analysis programs allows the user to define sections across a diaphragm so that total design forces are reported over a series of nodes.

A.7.1 Linear Versus Nonlinear Analysis

Typically, semi-rigid diaphragms are linear elements. In some structural analysis programs, it is also possible to model diaphragms as nonlinear. This is not necessary if the diaphragms are intended to remain essentially elastic.

A linear-elastic semi-rigid diaphragm can be included in an overall analysis that is either linear or nonlinear. In a linear analysis, the resulting diaphragm force output will need to be amplified by the overstrength factor, Ω_0. In a nonlinear response history analysis, the resulting diaphragm force output can be used directly for design.

A.8 Design of Diaphragms and Collectors

A.8.1 Diaphragm In-Plane Shear

For reinforced concrete diaphragms, in-plane shear strength is based on the nominal shear strength specified in ACI 318-08, *Building Code Requirements for Structural Concrete* (ACI, 2008):

$$V_n = A_{cv}(2\sqrt{f_c'} + \rho_n f_y) \qquad \text{(A-1)}$$

where A_{cv} is the net area of concrete section bounded by the slab thickness and length in the direction of shear force considered. The quantity, $2\sqrt{f_c'}$, represents the nominal shear strength of the concrete section, and the reinforcement ratio, ρ_n, refers to the reinforcing steel placed parallel to the direction of shear force considered. For concrete-on-steel deck diaphragms, the same approach is often used, considering the net thickness of the concrete topping above the flutes of the deck.

A.8.2 Strut-and-Tie Models

Strut-and-tie models can be used to design diaphragms for shear and flexure. The design of collectors and diaphragm segments could also be considered in the strut-and-tie model, if the forces for the whole model are amplified by Ω_0. Code provisions for strut-and-tie models are given in ACI 318-08, Appendix A.

Strut-and-tie methods are more directly applicable to reinforced concrete slabs, but could possibly be applied to concrete-on-steel-deck diaphragms with modifications to account for the strength contribution of the steel deck.

Potentially, strut and tie methods could be a logical way of considering the contribution of steel floor beams to in-plane diaphragm strength. Such models are useful for analyzing complicated floor diaphragms with multiple floor openings and collector requirements where standard beam analogy techniques may not be appropriate.

Example applications, such as Reineck (2002), show that strut-and-tie models for seismic forces can become complex. This is due, in part, because of numerous possible load paths. Because of differences in the specified force reduction factors (ϕ), designs based on Appendix A of ACI 318-08 can result in more reinforcement than conventional design approaches used for reinforced concrete design. While strut-and-tie models can provide good design insight, especially in the case of diaphragms with significant openings (Paulay and Priestley, 1992), more development and calibration is needed before such models can be used as part of the basic design process.

A.8.3 Diaphragm In-Plane Flexure

For reinforced concrete diaphragms, a beam analogy is used to consider in-plane flexure. The nominal flexural strength can be calculated using the same procedure specified in ACI 318-08 for beams and walls, considering a force couple between concrete in compression and reinforcing steel in tension. For concrete-on-steel deck diaphragms, a similar approach can be used, with the possible consideration of additional strength provided by steel floor beams and by the steel deck in the direction parallel to the flutes.

A.8.4 Distribution of Collector Forces

Collectors are designed for tension and compression based on a calculated or assumed distribution of axial force along the length of the collector. Past design practices, such as assuming uniform shear along a collector, can overestimate demands because the assumed load path differs from the actual path. Such practices were more common under previous procedures when unamplified collector forces where used, but are impractical when applied to collector forces amplified by Ω_0 or taken from nonlinear response history analyses.

The recommended design approach is to choose a reasonable distribution of forces that satisfies equilibrium and does not exceed the capacities of the collector elements and shear transfer mechanisms provided. Forces assumed should be consistent with those taken from the semi-rigid diaphragm model. Such an approach is possible because a well-configured cast-in-place concrete slab or concrete-on-steel deck diaphragm would typically be expected to have the ability to redistribute high in-plane diaphragm or

collector stresses through cracking and limited bond slip and yielding of reinforcement. Mild steel reinforcement in each direction helps provide this inherent ductility. Use of deformed bars rather than welded wire reinforcement is recommended because tests have shown that welded wire reinforcement has limited ductility capacity. Gross reinforcement ratios greater than 0.7% or 0.8% are generally effective in causing distributed, rather than concentrated, cracking in slabs.

A.8.4.1 Procedure for Determining Forces on Collectors and Diaphragm Segments

A general procedure for designing collectors and diaphragm segments for collector eccentricity and localized diaphragm shear involves the following steps:

- Identify potential critical sections across which diaphragm strength and collector forces will be evaluated.
- Delineate free-body portions of the slab that correspond to each potential critical section and enable determination of forces at the critical section.
- Provide reinforcing steel necessary to resist calculated forces.

Identification of critical sections, and the necessary free-body diagrams, requires consideration of the geometry of the diaphragm and anticipation of potential sections where failures could occur. The process of checking forces at successive critical sections is how the adequacy and continuity of the seismic load path is verified. The choice of how collector eccentricity is resisted can depend on the geometry of the diaphragm, including the location of openings relative to walls, moment frames, or braced frames.

A.8.5 Slab Reinforcement for Gravity and Seismic Forces

Typically a floor or roof slab is designed first for gravity loads, then subsequently checked for in-plane diaphragm forces. The slab reinforcement utilized for resisting gravity loads should not be considered for resisting in-plane diaphragm forces. Reinforcement in excess of what is needed to resist the typical gravity load combinations can be used to resist collector or diaphragm forces. A portion of all such reinforcement in the top and bottom of the slab should be continuous, and all lap splices should be Class B.

A.8.5.1 Excess Capacity

Code provisions specify the gravity load combinations to be used for design of the slab reinforcement, including the effect of patterned live loads. When a slab is designed for gravity loads, it usually has some excess strength due to

the use of repetitive bar size and spacing increments. This is one source of excess strength that can be used to help resist in-plane diaphragm forces.

Different load factors are specified for gravity loads in combination with earthquake forces than specified for gravity loads alone. Typically, gravity loads assumed in combination with earthquake forces are smaller, which is a second source of excess capacity that can be used to help resist in-plane diaphragm forces.

A.8.5.2 Symmetry of Slab Reinforcement

Slab reinforcement used to resist diaphragm and collector forces should be positioned so that the resultant of the tensile forces is near the mid-depth of the slab to minimize eccentricity, which can induce additional slab bending moments. When slab gravity reinforcement is used to resist diaphragm and collector forces, the area of top and bottom reinforcement that is available for seismic force resistance is usually not equal. It is recommended, however, to assume that only the minimum of the available top or bottom reinforcement at a given section is effective. This ensures that the resultant of assumed tensile forces is symmetric in the section. If the sum of the top and bottom reinforcement calculated in this manner is not adequate to resist the prescribed diaphragm or collector forces, then additional reinforcement should be provided, and placed symmetrically in the top and bottom of the slab.

A.8.5.3 Reinforcement for Collector Eccentricity and Localized Diaphragm Shear

When a collector is not placed directly in line with the vertical elements of the seismic-force-resisting system (see Figure A-8), the eccentricity of the collector force is countered by in-plane slab moments. Diaphragm segments around walls (or frames) must be designed for these in-plane moments and localized increases in diaphragm shear.

Diaphragm segments need to be checked to ensure that they provide the necessary in-plane moment resistance. Depending on the configuration of the diaphragm and location of openings, moment resistance could be provided by reinforcement perpendicular to the collector, additional reinforcement parallel to the collector, or a combination of both. Localized increases in diaphragm shear are resisted by additional reinforcement parallel to the wall (in-plane shear strength) and additional reinforcement perpendicular to the wall (shear friction across the slab-wall joint).

A.9 Recommended Stiffness Properties for Modeling of Backstay Effects

Evaluation of backstay effects requires consideration of the overturning resistance provided by the foundation directly beneath the seismic-force-resisting elements of the tower, and the backstay resistance provided by the floor diaphragms and perimeter walls of the podium. Seismic design for backstay effects requires an assessment of what portion of the overall building overturning is resisted by each load path. Since the stiffness properties of the elements in each load path are both influential on the seismic design and uncertain, the use of bracketing assumptions is recommended.

Upper-bound and lower-bound stiffness properties should be considered for each critical element. To determine governing design forces for the elements in each load path, assumptions can be grouped into two overall cases:

- *Case 1 – Upper bound backstay effect*. A set of assumptions that provides an upper-bound estimate of forces in the backstay load path and a lower bound estimate of forces in the foundation below the tower. This case will govern the design forces for the podium floor diaphragms and perimeter walls, and the associated connections.
- *Case 2 – Lower bound backstay effect*. A set of assumptions that provides a lower-bound estimate of forces in the backstay load path and an upper-bound estimate of forces in the foundation below the tower. This case will govern the design forces for the tower foundation elements.

Recommended stiffness properties, and bracketing upper-bound and lower-bound assumptions (if applicable), are shown for the podium elements and supporting foundation in Table A-2 and the tower elements and supporting foundation in Table A-3.

Table A-2 Recommended Stiffness Assumptions for Structural Elements of a Podium and Foundation

Structural element or property	*Assumptions for Case 1*	*Assumptions for Case 2*	*Notes*
Concrete diaphragms/perimeter concrete walls – effective flexural stiffness (E_cI_{eff})	0.5 times gross section properties	0.2 times gross section properties, or fully cracked, transformed section properties.	Flexural stiffness should be reduced for strain penetration effects. Including sources of additional deformation, such as strain penetration, can reduce effective stiffness to a small fraction of gross properties.
Concrete diaphragms/perimeter concrete walls – effective shear stiffness (G_cA)	0.5 times gross section properties	0.05 to 0.2 times gross section properties	Shear stiffness should be reduced upon initiation of diagonal cracking (when average shear stress exceeds $3\sqrt{f_c'}$)
Supporting soil/piles – vertical spring stiffness below perimeter concrete walls	Upper-bound soil properties	Lower-bound soil properties	A fixed base assumption can be used in lieu of upper-bound properties.
Supporting soil – horizontal spring stiffness on face of perimeter concrete walls	Lower-bound soil properties (alternatively soil springs can be omitted)	Upper-bound soil properties (will increase overall backstay effect, but will also take force out of diaphragms)	Passive resistance occurs in compression but not tension. The stiffness of passive resistance can be small compared to the stiffness of the perimeter walls, and thus can often be neglected.

Table A-3 Recommended Stiffness Assumptions for Structural Elements of a Tower and Foundation

Structural element or property	*Assumptions for Case 1*	*Assumptions for Case 2*	*Notes*
Concrete core wall – effective flexural (E_cI_{eff}) and shear (G_cA) stiffness	Values recommended in Chapter 4		In typical cases, these stiffness assumptions are less influential to backstay effects and are not bracketed.
Concrete moment frames – effective flexural (E_cI_{eff})and shear (G_cA) stiffness	Values recommended in Chapter 3		In typical cases, these stiffness assumptions are less influential to backstay effects and are not bracketed.
Steel moment frames – effective flexural (E_cI_{eff}) and shear (G_cA) stiffness	Values recommended in Chapter 3		In typical cases, these stiffness assumptions are less influential to backstay effects and are not bracketed.
Foundation mat/pile cap – effective flexural stiffness (E_cI_{eff})	0.3 times gross section properties, or fully cracked, transformed section properties.		In typical cases, this stiffness is not influential or uncertain, and need not be bracketed.
Foundation mat/pile cap – effective shear stiffness (G_cA)	0.3 times gross section properties, or smaller if shear cracking is expected, based on shear stress exceeding $3\sqrt{f_c'}$.		In typical cases, this stiffness is not influential, and need not be bracketed.
Supporting soil/piles – vertical spring stiffness	Lower-bound soil properties	Upper-bound soil properties	A fixed base assumption can be used in lieu of upper-bound properties.

A.9.1 Lateral Stiffness for Passive Soil Resistance

Passive soil resistance occurs under compression, but not tension. Lateral soil springs used to represent passive resistance in the model must consider this behavior. Springs can be compression-only elements, or can be approximated as tension and compression springs on each side of the below-grade structure, but modeled with half of the compression stiffness.

The lateral stiffness of passive soil resistance may or may not be important to model. Often, the stiffness of this load path is small compared to the in-plane stiffness of the below grade perimeter walls, allowing lateral soil springs to be omitted.

Upper-bound stiffness properties for lateral soil springs would produce larger forces in a backstay mechanism overall, but higher passive stiffness will tend to reduce forces in the below-grade diaphragms and walls, which may not be conservative. This is particularly true for floor diaphragms in large below grade structures, where the diaphragm spans are long.

Upper-bound properties for the lateral springs will give larger passive soil pressures on the perimeter walls, which can govern out-of-plane design of the walls. Additionally, upper-bound properties for passive soil springs could govern the shear reversal in a core wall below the main backstay diaphragm. Appropriate use of upper-bound passive stiffness properties will depend on the element that is being designed.

Glossary

Definitions

Backbone Curve: A reference force-deformation relationship that defines the bounds within which the hysteretic response of a component is confined.

Backstay Effects: The transfer of lateral and overturning forces from seismic-force-resisting elements within the tower, into seismic-force-resisting elements within the podium, typically through one or more floor diaphragms.

Capping Deformation: The deformation associated with the capping point.

Capping Point: The point along a reference force-deformation curve at which the maximum strength is attained.

Capping Strength: The strength associated with the capping point.

Continuum (Finite Element) Model: Nonlinear element that explicitly models the underlying physics of the material response, and does not enforce any predefined component behavioral modes.

Cyclic Backbone Curve: A backbone curve that is continuously updated to account for cyclic deterioration. The branches of a cyclic backbone curve translate towards the origin or rotate relative to the initial backbone curve.

Cyclic Deterioration: Hysteretic reduction in strength, stiffness, or both, as a function of the damage and energy dissipated in a yielding component.

Cyclic Envelope (Skeleton) Curve: A force-deformation curve formed by connecting the peak points in the first loading cycle under increasing deformations in a given loading protocol. A cyclic envelope varies with the loading protocol.

Diaphragm Segment: A portion of a diaphragm, adjacent to a vertical element of a seismic-force-resisting system, which serves to resist a concentration of diaphragm shear and eccentricity of collector forces.

Distributed Inelasticity (Fiber) Model: Nonlinear element that explicitly models uniaxial material response in combination with implicit

enforcement of some component behavior assumptions (e.g., plane sections remain plane).

Expected Properties: Stiffness, strength, or deformation characteristics based on median values from a population of materials or components.

Initial Backbone Curve: A backbone curve that is close to the monotonic loading curve because cyclic deterioration has not occurred.

Lumped Plasticity (Concentrated Hinge) Model: Nonlinear element that represents nonlinear behavior in a phenomenological way, with inelastic deformation rules that are associated with the force-deformation behavior and hysteretic response of components observed in tests.

Member P-delta effects: The local effects of loads acting on the deflected shape of a member between joints in a model.

Onset of Structural Damage: Forces and deformations beyond the yield point, with some permanent deformation associated with yielding of steel and cracking of concrete.

Onset of Structural Degradation: Forces and deformations beyond the capping point, associated with significant strength loss and negative post-capping tangent stiffness.

Podium: The lower portion of a tall building structure that is larger in floor plate, and contains substantially increased seismic-force resistance, in comparison to the superstructure above.

Residual strength: The strength level associated with stabilized hysteresis loops at large inelastic cycles, which is maintained until final failure occurs.

Structure P-Delta Effects: The global effects of gravity loads acting on the displaced location of joints in a model.

References

ACI, 2005, *Building Code Requirements for Structural Concrete* (ACI 318-05) *and Commentary*, (ACI 318R-05), American Concrete Institute, Farmington Hills, Michigan.

ACI, 2008, *Building Code Requirements for Structural Concrete* (ACI 318-08) *and Commentary* (ACI 318R-08), American Concrete Institute, Farmington Hills, Michigan.

Adam, C., Ibarra, L.F., and Krawinkler, H., 2004, "Evaluation of P-delta effects in non-deteriorating MDOF structures from equivalent SDOF systems," *Proceedings of the 13th World Conference on Earthquake Engineering*, Paper 3407, Vancouver, Canada.

Adebar, P., Ibrahim, A.M.M., and Bryson, M., 2007, "Test of high-rise core wall: Effective stiffness for seismic analysis," *Structural Journal*, ACI, Vol. 104, No. 5, pp. 549-559.

AISC, 2005a, *Prequalified Connections for Special and Intermediate Steel Moment Frames for Seismic Applications*, ANSI/AISC 358-05, American Institute for Steel Construction, Chicago, Illinois.

AISC, 2005b, *Seismic Provisions for Structural Steel Buildings*, ANSI/AISC 341-05, American Institute for Steel Construction, Chicago, Illinois.

Aktan, A.E., Bertero, V., and Sakino, K., 1985, "Lateral stiffness characteristics of reinforced concrete frame-wall structures", *Structural Journal*, ACI, Vol. 86, No. 10, pp. 231-262.

Aktan, A.E., Bertero, V.V., Chowdhury, A.A., Nagashima, T., 1983, *Experimental and Analytical Predictions of the Mechanical Characteristics of a 1/5-Scale Model of a 7-Story R/C Frame-Wall Building Structure*, UCB/EERC Report 83/13, University of California, Berkeley, California.

Allen, F.H., and Darvall, P., 1977, "Lateral load equivalent frame," *ACI Journal Proceedings,* Vol. 74, No. 7, pp. 294-299.

Alsiwat, J., and Saatcioglu, M., 1992, "Reinforcement anchorage slip under monotonic loading," *Journal of Structural Engineering*, American Society of Civil Engineers, Vol. 118, No. 9, pp. 2421-2438.

ASCE, 2006, *Minimum Design Loads for Buildings and Other Structures,* ASCE Standard ASCE/SEI 7-05, including Supplement No. 1, American Society of Civil Engineers, Reston, Virginia.

ASCE, 2007a, *Seismic Rehabilitation of Existing Buildings*, ASCE Standard ASCE/SEI 41-06, American Society of Civil Engineers, Reston, Virginia.

ASCE, 2007b, *Supplement No. 1 to ASCE 41,* available at http://content.seinstitute.org/publications/ASCE41supplement.html. (Not included in the current printing of ASCE/SEI 41-06).

ASCE, 2010, *Minimum Design Loads for Buildings and Other Structures,* ASCE Standard ASCE/SEI 7-10, American Society of Civil Engineers/Structural Engineering Institute, Reston, Virginia.

ASCE-ACI, 1973, "The shear strength of reinforced concrete members," prepared by the joint ASCE-ACI Task Committee 426 on Shear and Diagonal Tension, *Journal of the Structural Division,* American Society of Civil Engineers, Vol. 99, No. 6, pp. 1091-1187.

ATC, 1992, *Guidelines for Seismic Testing of Components of Steel Structures*, ATC-24 Report*,* Applied Technology Council, Redwood City, California.

Baber, T.T., and Wen, Y., 1981, "Random vibration hysteretic of degrading systems," *Journal of the Engineering Mechanics Division,* Vol. 107, No. 6, pp. 1069-1087.

Barda, F., Hanson, J.M., and Corley, W.G., 1977, "Shear strength of low-rise walls with boundary elements," *Reinforced Concrete Structures in Seismic Zones*, Publication SP-53, American Concrete Institute, Farmington Hills, Michigan, pp. 149-202.

Barney, G.B., Shiu, K.N., Rabbit, B.G., Fiorato, A.E., Russell, H.G., and Corley, W.G., 1980, *Behavior of Coupling Beams Under Load Reversals*, Research and Development Bulletin RD068.01B, Portland Cement Association, Skokie, Illinois.

Bernal, D., 1994, "Viscous damping in inelastic structural response," *Journal of Structural Engineering,* American Society of Civil Engineers, Vol. 120, No. 4, pp. 1240-1254.

Bernal, D., 1998, "Instability of buildings during seismic response," *Engineering Structures,* Vol. 20, No. 4-6, pp. 496-502.

Berry, M., Parrish, M., and Eberhard, M., 2004, *PEER Structural Performance Database User's Manual*, Pacific Earthquake

Engineering Research Center, University of California, Berkeley, California. (Available at *http://nisee.berkeley.edu/spd/* and *http://maximus.ce.washington.edu/~peera1/*.)

Bertero, V.V., Aktan, A.E., Charney, F.A., and Sause, R., 1984, *US-Japan Cooperative Earthquake Research Program: Earthquake Simulation Tests and Associated Studies of a 1/5th-scale Model of a 7-Story Reinforced Concrete Test Structure*, UCB/EERC Report 84/05, University of California, Berkeley, California.

Blume, J.A., Newmark, N.M., and Corning, L.H., 1961, *Design of Multistorey Reinforced Concrete Buildings for Earthquake Motions,* Portland Cement Association, Chicago, Illinois.

Bouc, R., 1967, "Forced vibration of mechanical systems with hysteresis." *Proceedings, 4th Conference on Nonlinear Oscillations,* Prague, Czechoslovakia.

Bradford, S.C., Clinton, J.F., Favela, J., and Heaton, T.H., 2004, *Results of Millikan Library Forced Vibration Testing*, Report No. EERL 2004-03, California Institute of Technology, Pasadena, California.

Brown, P.C., and Lowes, L.N., 2007, "Fragility functions for modern reinforced-concrete beam-column joints," *Earthquake Spectra*, Vol. 23, No. 2, pp. 263-289.

Cardenas, A.E., Hanson, J.M., Corley, W.G., and Hognestad, E., 1973, "Design provisions for shearwalls," *Journal Proceedings*, ACI, Vol. 70, No. 3, pp. 221-230.

Cardenas, A.E., Russell, H.G., and Corley, W.G., 1980, "Strength of low rise structural walls," *Reinforced Concrete Structures Subjected to Wind and Earthquake Forces*, SP-63, American Concrete Institute, Farmington Hills, Michigan, pp. 221-241.

Carr, A.J., 2003, *Ruaumoko User Manual*, University of Canterbury, New Zealand.

Celebi, M., 2006, "Recorded earthquake responses from the integrated seismic monitoring network of the Atwood building, Anchorage, Alaska," *Earthquake Spectra,* Vol. 22, No. 4, pp. 847-864.

Celebi, M., 1998, "Performance of building structures – a summary," *The Loma Prieta, California, Earthquake of October 17, 1989 – Building Structures, Performance of the Built Environment*, USGS Professional Paper 1552-C, United States Geological Survey.

Challa, V.R.M., and Hall, J.F., 1994, "Earthquake collapse analysis of steel frames," *Earthquake Engineering and Structural Dynamics*, Vol. 23, No. 11, pp. 1199-1218.

Chang, G.A., and Mander, J.B., 1994, *Seismic Energy Based Fatigue Damage Analysis of Bridge Columns: Part I – Evaluation of Seismic Capacity*, NCEER Technical Report No. NCEER-94-0006; State University of New York, Buffalo, New York.

Charney, F.A., 2006, "Unintended consequence of modeling damping in structures: Rayleigh damping," *Procedures of 17th Analysis and Computation Specialty Conference*, American Society of Civil Engineers.

Cho, J.Y., and Pincheira, J.A., 2006, "Inelastic analysis of reinforced concrete columns with short lap splices subjected to reversed cyclic loads," *Structural Journal*, ACI, Vol. 103, No. 2, pp. 280-290.

Chopra, A., 2007, *Dynamics of Structures: Theory and Application to Earthquake Engineering,* Prentice Hall, New Jersey.

Corley, W.G., Fiorato, A.E., and Oesterle, R.G., 1981,"Structural walls," *Structural Journal*, ACI, Vol. 72, No. 4, pp. 77-131.

CTBUH, 2008, *Recommendations for the Seismic Design of High-Rise Buildings*, Report of the Working Group on the Seismic Design of Tall Buildings, prepared by Willford, M., Whittaker, A.S., and Klemencic, R., edited by Wood, A., for the Council on Tall Buildings and Urban Habitat, Chicago, Illinois.

Diebold, J., and Moehle, J.P., 1984, *Experimental Study of the Seismic Response of a Two-Story Flat-Plate Structure*, UCB/EERC Report 84/08, University of California, Berkeley, California.

Elwood, K.J., and Moehle, J.P., 2003, *Shake-Table Tests and Analytical Studies on the Gravity Load Collapse of Reinforced Concrete Frames*, PEER Report 2003/01, Pacific Earthquake Engineering Research Center, University of California, Berkeley, California.

Elwood, K.J., and Eberhard, M.O., 2006, *Effective Stiffness of Reinforced Concrete Columns*, PEER Research Digest No. 2006-1, Pacific Earthquake Engineering Research Center, University of California, Berkeley, California.

Elwood, K.J., Matamoros, A.B., Wallace, J.W., Lehman, D.E., Heintz, J.A., Mitchell, A.D., Moore, M.A., Valley, M.T., Lowes, L.N., Comartin,

C.D., and Moehle, J.P., 2007, "Update to ASCE/SEI 41 concrete provisions," Earthquake Spectra, Vol. 23, No. 3, pp. 493-523.

Fang, J.Q., Li, Q.S., Jeary, A.P., and Liu, D.K., 1999, "Damping of tall buildings: Its evaluation and probabilistic characteristics," *Structural Design of Tall Buildings*, Wiley Interscience, Vol. 8, pp. 145-153.

Farvashany, F.E., Foster, S.J., and Rangan, B.V., 2008, "Strength and deformation of high-strength concrete shearwalls," *Structural Journal*, ACI, Vol. 105, No. 1, pp. 21-29.

FEMA, 1997, *NEHRP Commentary on the Guidelines for Seismic Rehabilitation of Buildings*, FEMA 274 Report, prepared by the Building Seismic Safety Council and the Applied Technology Council for the Federal Emergency Management Agency, Washington, D.C.

FEMA, 2000a, *Recommended Seismic Design Criteria for New Steel Moment Frame Buildings*, FEMA 350 Report, prepared by the SAC Joint Venture Partnership for the Federal Emergency Management Agency, Washington, D.C.

FEMA, 2000b, *State of the Art Report on System Performance of Steel Moment Frames Subject to Earthquake Ground Shaking*, FEMA 355C Report, prepared by the SAC Joint Venture Partnership for the Federal Emergency Management Agency, Washington, D.C.

FEMA, 2000c, *State of the Art Report on Connection Performance*," FEMA 355D Report, prepared by the SAC Joint Venture Partnership for the Federal Emergency Management Agency, Washington, D.C.

FEMA, 2000d*, Prestandard and Commentary for the Seismic Rehabilitation of Buildings,* FEMA 356 Report, prepared by the American Society of Civil Engineers for the Federal Emergency Management Agency, Washington, D.C.

FEMA, 2009a, *Effects of Strength and Stiffness Degradation on Seismic Response,* FEMA P-440A Report, prepared by the Applied Technology Council for the Federal Emergency Management Agency, Washington, D.C.

FEMA, 2009b, *Quantification of Building Seismic Performance Factors*, FEMA P-695 Report, prepared by the Applied Technology Council for the Federal Emergency Management Agency, Washington, D.C.

FIB, 2004, *Seismic Design of Precast Concrete Building Structures*, Bulletin 27, State of the Art Report prepared by Task Group 7.3, International Federation for Structural Concrete (FIB), Lausanne, Switzerland.

Filippou, F.C., Popov, E.G., and Bertero, V.V., 1983, *Effects of Bond Deterioration on Hysteretic Behavior of Reinforced Concrete Joints*, UCB/EERC Report 83/19, University of California, Berkeley, California.

Foliente, G.C., 1995, "Hysteresis modeling of wood joints and structural systems," *Journal of Structural Engineering,* American Society of Civil Engineers, Vol. 121, No. 6, pp. 1013-1021.

Galano, L., and Vignoli, A., 2000, "Seismic behavior of short coupling beams with different reinforcement layouts," *Structural Journal*, ACI, Vol. 97, No. 6, pp. 876-885.

Gatto, K.S., and Uang, C.M., 2002, "Effects of loading protocol and rate of loading on woodframe shearwall response," *Seventh U.S. National Conference on Earthquake Engineering,* Earthquake Engineering Research Institute, Oakland, California.

Gioncu, V., and Mazzolani, F.M., 2002, *Ductility of Seismic Resistant Steel Structures*, Spon Press, New York.

Goel, R.K., and Chopra, A.K., 1997, *Vibration Properties of Buildings Determined from Recorded Earthquake Motions*, UCB/EERC Report 97/14, University of California, Berkeley, California..

Grossman, J., 1997, "Verification of proposed design methodologies for effective width of slabs in slab column frames," *Structural Journal*, ACI*,* Vol. 94, No. 2, pp. 181-196.

Gulkan, P., and Sozen, M.A., 1974, "Inelastic responses of reinforced concrete structures to earthquake motions," *Journal Proceedings,* ACI, Vol. 71, No. 12, pp. 604-610.

Gupta, A., and Krawinkler, H., 2000, "Dynamic P-delta effects for flexible inelastic steel structures," *Journal of Structural Engineering*, American Society of Civil Engineers, Vol. 126, No. 1, pp. 145-154.

Hall, J.F., 2005, "Problems encountered from the use (or misuse) of Raleigh damping," *Earthquake Engineering and Structural Dynamics*, Vol. 35, No. 5, pp. 525-545.

Harder, R., 1989, "Los Angeles City dynamic analysis," Professional Paper 89-2, Los Angeles Tall Buildings Structural Design Council.

Haselton, C.B., and Deierlein G.G., 2007, *Assessing Seismic Collapse Safety of Modern Reinforced Concrete Moment Frame Buildings*, PEER Report 2007/08, Pacific Earthquake Engineering Research Center, University of California, Berkeley, California.

Haselton, C.B., Liel, A.B., Taylor Lange, S., and Deierlein, G.G., 2008, *Beam-Column Element Model Calibrated for Predicting Flexural Response Leading to Global Collapse of RC Frame Buildings*, PEER Report 2007/03, Pacific Earthquake Engineering Research Center, University of California, Berkeley, California.

Haselton, C.B., Liel, A.B., Taylor Lange, S., and Deierlein, G.G., 2010, *Beam-Column Element Model Calibrated for Predicting Flexural Response Leading to Global Collapse of RC Frame Buildings* (updated report), in preparation.

Hidalgo, P.A., Ledezma, C.A., and Jordan, R.M., 2002, "Seismic behavior of squat reinforced concrete shear walls," *Earthquake Spectra*, Vol. 18, No. 2, pp. 287-308.

Hirosawa, M., 1975, "Past experimental results on reinforced concrete shear walls and analysis on them," Building Research Institute, Ministry of Construction, No. 6, (in Japanese).

Hudson, D.E., and Housner, G.W., 1954, "Vibration tests of a steel-frame building," *Technical Report*, California Institute of Technology, Pasadena, California.

Hwang, S., and Moehle, J.P., 2000, "Models for laterally loaded slab-column frames," *Structural Journal*, ACI, Vol. 97, No. 2, pp. 345-353.

Ibarra, L.F., Medina, R., and Krawinkler, H., 2002, "Collapse assessment of deteriorating SDOF systems," *Proceedings of the 12th European Conference on Earthquake Engineering*, Paper No. 665, Elsevier Science, London.

Ibarra, L.F., and Krawinkler, H., 2005, *Global Collapse of Frame Structures Under Seismic Excitations*, John A. Blume Earthquake Engineering Center Report No. TR 152, Department of Civil Engineering, Stanford University, Stanford, California and PEER Report 2005/06 Pacific Earthquake Engineering Research Center, University of California, Berkeley, California.

Ibarra L.F., Medina R.A., and Krawinkler, H., 2005, "Hysteretic models that incorporate strength and stiffness deterioration," *Earthquake Engineering and Structural Dynamics*, Vol. 34, No. 12, pp. 1489-1511.

ICBO, 1997, *Uniform Building Code*, 1997 Edition, Volume 2, International Conference of Building Officials, Whittier, California.

ICC, 2003, *International Building Code,* International Code Council, Washington, D.C.

ISO, 1997, *Wind Actions on Structures*, ISO 4354:1997, International Organization for Standardization, Geneva, Switzerland.

Janoyan, K., Stewart, J.P., and Wallace, J.W., 2006, "Full scale cyclic lateral load test of a reinforced concrete shaft-column," *Structural Journal*, ACI*,* Vol. 103, No. 2, pp. 178-187.

Jeary, A.P., 1986, "Damping in tall buildings – A mechanism and a predictor," *Earthquake Engineering and Structural Dynamics*, Vol. 14, No. 5, pp. 733-750.

Jin, J., and El-Tawil, S., 2005, "Seismic performance of steel panel zones," *Journal of Structural Engineering,* American Society of Civil Engineers, Vol. 131, No. 2, pp. 250-258.

Kang, T.H-K,. and Wallace, J.W., 2005, "Dynamic responses of flat plate systems with shear reinforcement," *Structural Journal*, ACI, Vol. 102, No. 5, pp. 763-773.

Kang, T.H-K., and Wallace, J.W., 2006, "Punching of reinforced and post-tensioned concrete slab-column connections," *Structural Journal*, ACI, Vol. 103, No. 4, pp. 531-540.

Kang, T.H-K., Wallace, J.W., and Elwood, K.J., 2009, "Nonlinear modeling of flat plate systems," *Journal of Structural Engineering*, American Society of Civil Engineers, Vol. 135, No. 2, pp. 147-158.

Kabeyasawa, T., and Hiraishi, H., 1998, "Tests and analyses of high-strength reinforced concrete shear walls in Japan," *Special Publication*, ACI, Vol. 176, pp. 281-310.

Kawashima, K., 2007, *Cyclic Loading Test Data of Reinforced Concrete Bridge Piers*, Kawashima Laboratory, at http://seismic.cv.titech.ac.jp/ja/titdata/titdata.html.

Kilic, S.A., 1996, *Stability Issues in Frames under Lateral Loads*, Ph.D. Dissertation, Department of Civil Engineering, Stanford University, California.

Kijewski-Correa, T., and Pirnia, J.D., 2007, "Dynamic behavior of tall buildings under wind: Insights from full-scale monitoring," *Structural Design of Tall and Special Buildings*, Vol. 16, pp. 471-486.

Kim, K., and Engelhardt, M.D., 1995, "Development of analytical models for earthquake analysis of steel moment frames," *Report No. PMFSEL 95-2,* Department of Civil Engineering, University of Texas at Austin, Texas.

Klemencic, R., Fry, J.A., Hurtado ,G., and Moehle, J.P., 2006, "Performance of post-tensioned slab-core wall connections", *PTI Journal*, Vol. 4, No. 2.

Krawinkler, H., 1978, "Shear design of steel frame joints," *Engineering Journal*, AISC, Vol. 15, No. 3.

Krawinkler, H., Zohrei, M., Lashkari-Irvani, B., Cofie, N.G., and Hadidi-Tamjed, H., 1983, *Recommendations for Experimental Studies on the Seismic Behavior of Steel Components and Materials*, Report No. 61, John A. Blume Earthquake Engineering Center, Department of Civil and Environmental Engineering, Stanford University, Stanford, California.

Krawinkler, H., and Ibarra, L., 2004, "Sidesway collapse of frames with deteriorating properties," *Proceedings of the 2004 SEAOC Convention*, Structural Engineers Association of California, Sacramento, pp. 239-250.

Kunnath, S.K., 2000, *IDASS - A Program for Inelastic Damage Analysis of Structural Systems*, Technical Report, Department of Civil Engineering, University of Central Florida, Orlando, Florida.

Kwan, A.K.H., and Zhao, Z.Z., 2002, "Cyclic behavior of deep reinforced concrete coupling beams," *Structures & Buildings*, Vol. 152, No. 3, pp. 283-293.

Li, Q.S., Yang, K., Zhang, N., Wong, C.K., and Jeary, A.P., 2002, "Field measurements of amplitude dependent damping in a 79-storey tall building and its effects on the structural dynamic response," *Structural Design of Tall Buildings*, Vol. 11, pp. 129-153.

Li, Q.S., Fang, J.Q., Jeary, A.P., Wong, C.K., and Liu, D.K., 2000, "Evaluation of wind effects on a supertall building based on full-scale measurement," *Earthquake Engineering and Structural Dynamics,* Vol. 29, pp. 1845-1862.

Li, Q.S., Wu, J.R., Liang, S.G., Xiao, Y.Q., and Wong, C.K., 2004, "Full-scale measurements and numerical evaluation of wind-induced vibration of a 63-story reinforced concrete tall building," *Engineering Structures,* Vol. 26, pp. 1779-1794.

Li, Q.S., Xiao, Y.Q., Wong, C.K., and Jeary, A.P., 2003, "Field measurements of wind effects on the tallest building in Hong Kong," *Structural Design of Tall Buildings*, Vol. 12, pp. 67-82.

Li, Y., and Mau, S.T., 1997, "Learning from recorded earthquake motion of buildings," *Journal of Structural Engineering,* Vol. 123, No. 1, pp. 62-69.

Liel, A.B., Haselton, C.B., Deierlein, G.G., and Baker, J.W., 2009, "Incorporating modeling uncertainties in the assessment of seismic collapse risk of buildings," *Structural Safety*, Vol. 31, No. 2*,* pp. 197-211.

Liew, J.Y.R., White, D.W., and Chen, W.F., 1993, "Second-order refined plastic-hinge analysis for frame design. Part I," *Journal of Structural Engineering,* American Society of Civil Engineers, Vol. 119, No. 11, pp. 3196-3216.

Lignos, D.G., and Krawinkler, H., 2007, "A database in support of modeling of component deterioration for collapse prediction of steel frame structures," *ASCE Structures Congress 2007*, Long Beach, California.

Lignos D.G., and Krawinkler H., 2009, *Sidesway Collapse of Deteriorating Structural Systems under Seismic Excitations*, Report No. TR 172, John A. Blume Earthquake Engineering Center, Department of Civil Engineering, Stanford University, Stanford, California.

Lignos, D.G., 2008, *Sidesway Collapse of Deteriorating Structural Systems under Seismic Excitations*, Ph.D Thesis, Department of Civil and Environmental Engineering, Stanford University, Stanford, California.

Liu, J., and Astaneh-Asl, A., 2000, "Cyclic testing of simple connections including effects of slab," *Journal of Structural Engineering,* Vol. 126, No.1, pp. 32–39.

Liu, J., and Astaneh-Asl, A., 2004, "Moment-rotation parameters for composite shear tab connections," *Journal of Structural Engineering,* Vol. 130, No. 9, pp. 1371-1380.

Maffei, J.R., and Yuen, N., 2007, "Seismic performance and design requirements for high-rise buildings," *Structure Magazine*, April 2007, pp. 28-32.

Mander, J.B., Priestley, M.J.N., and Park, R., 1988, "Theoretical stress-strain model for confined concrete," *Journal of Structural Engineering*, Vol. 114, No. 8, pp. 1804-1825.

Maragakis, E., Saiidi, M, and Abdel-Ghaffar, S., 1993, "Response of R/C buildings during the 1987 Whittier Narrows Earthquake," *Earthquake Spectra,* Vol. 9, No. 1, pp. 67-95.

Martin, J.A., and Harder, R.N., 1989, "Seismic design requirements for tall buildings in Los Angeles," *Proceedings*, 1989 Annual Meeting of Los Angeles Tall Buildings Structural Design Council.

Massone, L.M., 2006, *RC Wall Shear – Flexure Interaction: Analytical and Experimental Responses*, Ph.D. Dissertation, University of California, Department of Civil & Environmental Engineering, Los Angeles, California, 398 pages.

Medina, R., and Krawinkler, H., 2003, *Seismic Demands for Nondeteriorating Frame Structures and Their Dependence on Ground Motions*, Report No. TR 144, John A. Blume Earthquake Engineering Center, Department of Civil Engineering, Stanford University, Stanford, California, and PEER Report 2003/15, Pacific Earthquake Engineering Research Center, University of California, Berkeley, California.

Menegotto, M., and Pinto, P., 1973, "Method of analysis for cyclically loaded RC plane frames including changes in geometry and non-elastic behavior of elements under combined normal force and bending." *Proceedings of Symposium on Resistance and Ultimate Deformability of Structures Acted on by Well-Defined Repeated Loads*, IABSE Reports, Vol. 13, pp. 2557-2573.

Mitra, N., and Lowes, L.M., 2007, "Evaluation, Calibration, and Verification of a Reinforced Concrete Beam-Column Joint Model," *Journal of Structural Engineering*, Vol. 133, No. 1, pp. 105-120.

Moehle, J.P., Ghannoum, W., and Bozorgnia, Y., 2006, "Collapse of lightly confined reinforced concrete frames during earthquakes," *Procedure of 8th U.S. National Conference on Earthquake Engineering*, San Francisco, California.

Naish, D., Fry J.A., Klemencic, R., and Wallace, J.W., 2009, *Experimental Evaluation and Analytical Modeling of ACI 318-05/08 Reinforced Concrete Coupling Beams Subjected to Reversed Cyclic Loading*, Report No. SGEL 2009/06, Department of Civil & Environmental Engineering, University of California, Los Angeles, California.

NZS, 1995, *NZS 3101:1995, Concrete Structures Standard*, New Zealand Standards Association, Wellington, New Zealand.

Newell, J., and Uang, C.M., 2006, *Cyclic Behavior of Steel Columns with Combined High Axial Load and Drift Demand*, Report No. SSRP-06/22, Structural Systems Research Project, Department of Structural Engineering, University of California, San Diego, California.

Newell, J., and Uang, C.M., 2008, "Cyclic Behavior of Steel Wide-Flange Columns Subjected to Large Drift," *Journal of Structural Engineering*, Vol. 134, No. 8, pp. 1334-1342.

Oesterle, R.G., Aristizabal-Ochoa, J.D., Shiu, K.N., and Corley, W.G., 1984, "Web crushing of reinforced concrete structural walls," *Journal Proceedings,* ACI, Vol. 81, No. 3, pp. 231-241.

Oliva, M.G., 1980, *Shaking Table Testing of a Reinforced Concrete Frame with Biaxial Response*, UCB/EERC Report 80/28, University of California, Berkeley, California.

Orakcal, K., and Wallace, J.W., 2004, "Modeling of slender reinforced concrete walls," *Proceedings of the 13th World Conference on Earthquake Engineering,* Vancouver, Canada.

Orakcal, K., and Wallace, J.W., 2006, "Flexural modeling of reinforced concrete walls-Experimental verification," *Structural Journal*, ACI, Vol. 103, No. 2, pp. 196-206.

Orakcal, K., Wallace, J.W., and Conte, J.P., 2004, "Nonlinear modeling and analysis of slender reinforced concrete walls," *Structural Journal*, ACI, Vol. 101, No. 5, pp. 688-699.

Orakcal, K., Massone, L.M., and Wallace, J.W., 2009, "Shear strength of lightly reinforced wall piers and spandrels," *Structural Journal*, ACI, Vol. 106, No 4, pp. 455-465.

OpenSees, 2007, *Open System for Earthquake Engineering Simulation*, Pacific Earthquake Engineering Research Center, University of California, Berkeley, California, online at *http://opensees.berkeley.edu/*.

Panagiotakos, T.B., and Fardis, M.N., 2001, "Deformations of reinforced concrete members at yielding and ultimate," *Structural Journal*, ACI, Vol. 98, No. 2, pp. 135-148.

Panagiotou, M., and Restrepo, J.I., 2007, "Lessons learnt from the UCSD full-scale shake table testing on a 7-story residential building slice,"

Proceedings of the 2007 Structural Engineers Association of California Convention, pp. 57-74, Squaw Creek, California.

Pantazopoulou, S., and Imran, I., 1992, "Slab-wall connections under lateral forces," *Structural Journal*, ACI, Vol. 89, No. 5, pp. 515-527.

Park, R., and Paulay, T., 1975, *Reinforced Concrete Structures,* John Wiley & Sons, New York, New York.

Paulay, T., 1971, "Coupling beams of reinforced concrete shear walls," *Journal of the Structural Division,* American Society of Civil Engineers, Vol. 97, No. 3, pp. 843-862.

Paulay, T., 1980, "Earthquake-resisting shearwalls - New Zealand design trends," *Journal Proceedings*, ACI, Vol. 77, No. 3**,** pp. 144-152.

Paulay, T., and Binney J.R., 1974, "Diagonally reinforced coupling beams of shear walls," *Special Publication SP-42*, American Concrete Institute, Farmington Hills, Michigan, pp. 579-598.

Paulay, T., and Priestley, M.J.N., 1992, *Seismic Design of Reinforced Concrete and Masonry Buildings*, John Wiley and Sons, New York, New York.

Paulay, T., Priestley, M.J.N., and Synge, A.J., 1982, "Ductility in earthquake resisting squat shearwalls," *ACI Journal Proceedings*, Vol. 79, No. 4, pp. 257-269.

PEER, 2007, *PEER Column Database*, Pacific Earthquake Engineering Research Center, University of California, Berkeley, California, *http://nisee.berkeley.edu/spd/*.

PEER, 2008, *Seismic Performance Objectives for Tall Buildings*, PEER Report 2008/101*,* Pacific Earthquake Engineering Research Center, University of California, Berkeley, California.

PEER, 2010, *Seismic Design Guidelines for Tall Buildings*, PEER Report 2010/05, Pacific Earthquake Engineering Research Center, University of California, Berkeley, California.

Petrangeli, M., Pinto, P.E., and Ciampi, V., 1999, "Fiber element for cyclic bending and shear of RC structures. I: Theory," *Journal of Engineering Mechanics*, American Society of Civil Engineers, Vol. 125, No. 9, pp. 994-1001.

Petrini, L., Maggi, C., Priestley, N., and Calvi, M., 2008, "Experimental verification of viscous damping modeling for inelastic time history analyses," *Journal of Earthquake Engineering*, Vol. 12, No. 1, pp. 125-145.

Priestley, M.J.N., and Grant, D.N., 2005, "Viscous damping in seismic design and analysis," *Journal of Earthquake Engineering*, Vol. 9, No. 2, pp. 229-255.

Porter, K., Kennedy, R., and Bachman, R., 2007, "Creating Fragility Functions for Performance-Based Earthquake Engineering," *Earthquake Spectra,* Vol. 23, No. 2, pp. 471-489.

Powell, G., 2008, *Damping Models for Nonlinear Dynamic Analysis: Survey Results, Analyses and Conclusions – Including Addendums 1-4*, unpublished papers, April to November, 2008.

Razvi S., and Saatcioglu, M., 1999, "Confinement model for high-strength concrete," *Journal of Structural Engineering*, Vol. 125, No. 3, pp. 281-289.

Reineck, K.H., 2002, *Examples for the Design of Structural Concrete with Strut-and-Tie Models*, editor, Special Publication 208, American Concrete Institute, Farmington Hills, Michigan.

Ricles, J.M., Zhang, X., Lu, L.W., Fisher, J., 2004, *Development of Seismic Guidelines for Deep-Column Steel Moment Connections*, ATLSS Report No. 04-13, Center for Advanced Technology for Large Structural Systems, Lehigh University, Bethlehem, Pennsylvania.

Rodgers, J.E., and Celebi, M., 2006, "Seismic response and damage detection analyses of an instrumented steel moment-framed building," *Journal of Structural Engineering*, Vol. 132, No. 10, pp. 1543-1552.

Roeder, C.W., 2002a, "General issues influencing connection performance," *Journal of Structural Engineering*, American Society of Civil Engineers, Vol. 128, No. 4, pp. 420-428.

Roeder, C.W., 2002b, "Connection performance for seismic design of steel moment frames," *Journal of Structural Engineering*, American Society of Civil Engineers, Vol. 128, No. 4, pp. 517-525.

Saatcioglu M., Alsiwat, J.M., and Ozcebe, G., 1992, "Hysteretic behavior of anchorage slip in R/C members," *Journal of Structural Engineering*, American Society of Civil Engineers, Vol. 118, No. 9, pp. 2439-2458.

Saatcioglu, M., and Razvi, S.R., 1992, "Strength and ductility of confined concrete," *Journal of Structural Engineering*, American Society of Civil Engineers, Vol. 118, No. 6, pp. 1590-1607.

SAC, 1996, *Analytical and Field Investigations of Buildings Affected by the Northridge Earthquake*, Report No. SAC-95-04, prepared by SAC Joint Venture, a partnership of Structural Engineers Association of California, Applied Technology Council, and California Universities for Research in Earthquake Engineering.

SAC, 1999a, *Prediction of Seismic Demands for SMRFs with Ductile Connections and Elements,* Report No. SAC/BD-99/06 prepared by Gupta, A., and Krawinkler, H., for SAC Joint Venture, a partnership of Structural Engineers Association of California, Applied Technology Council, and California Universities for Research in Earthquake Engineering.

SAC, 1999b, *Effect of Hysteretic Deterioration Characteristics on Seismic Response of Moment Resisting Steel Structures,* Report No. SAC/BD-99/18, prepared by Naeim, F., Skliros, S., and Sivaselvan, M.V., for SAC Joint Venture, a partnership of Structural Engineers Association of California, Applied Technology Council, and California Universities for Research in Earthquake Engineering.

Salas, M.C., 2008, *Modeling of Tall Reinforced Concrete Wall Buildings*, MSCE Thesis, Department of Civil and Environmental Engineering, University of California, Los Angeles, California.

Satake, N., Suda, K, Arakawa, T., Sasaki, A., and Tamura, Y., 2003, "Damping evaluation using full-scale data of buildings in Japan," *Journal of Structural Engineering,* American Society of Civil Engineers, Vol. 129, No. 4, pp. 470-477.

Schotanus, M.IJ, and Maffei, J.R., 2008, "Computer modeling and effective stiffness of concrete wall buildings," *Proceedings of the International FIB Symposium on Tailor Made Concrete Structures – New Solutions for Our Society,* Amsterdam, Netherlands.

Scott, B.D., Park, R., and Priestley, M.J.N., 1982, "Stress-strain behavior of concrete confined by overlapping hoops at high and low strain rates." *ACI Journal Proceedings*, Vol. 79, No. 1, pp. 13-27.

Scott, M.H., Franchin, P., Fenves, G.L., and Filippou, F.C., 2004, "Response sensitivity for nonlinear beam-column elements," *Journal of Structural Engineering,* American Society of Civil Engineers, Vol. 130, No. 9 , pp. 1281-1288.

SEAONC, 2007, *Recommended Administrative Bulletin on the Seismic Design and Review of Tall Buildings Using Non-Prescriptive*

Procedures, Structural Engineers Association of Northern California, San Francisco, California.

Sezen, H., and Moehle, J.P., 2004, "Shear strength model for lightly reinforced concrete columns," *Journal of Structural Engineering,* American Society of Civil Engineers, Vol. 130, No. 11, pp. 1692-1703.

SFDBI, 2007, "Requirements and Guidelines for the Seismic Design and Review of New Tall Buildings using Non-Prescriptive Seismic-Design Procedures," *Administrative Bulletin 83,* San Francisco Department of Building Inspection, San Francisco, California.

Shahrooz, B.M., and Moehle, J.P., 1987, *Experimental Study of Seismic Response of R.C. Setback Buildings,* UCB/EERC Report 87/16, University of California, Berkeley, California.

Shin, Y., and Moehle, J.P., 2007, *Quarter-Scale Reinforced Concrete Specimen Test, Internal Technical Report*, University of California, Berkeley, California.

Sivaselvan, M., and Reinhorn, A.M., 2000, "Hysteretic models for deteriorating inelastic structures", *Journal of Engineering Mechanics*, American Society of Civil Engineers, Vol. 126, No. 6, pp. 633-640.

Skolnik, D., Lei, Y., Yu, E., and Wallace, J.W., 2006, "Identification, model updating, and response prediction of an instrumented 15-story steel-frame building," *Earthquake Spectra,* Vol. 22, No. 3, pp. 781-802.

Song, J.K., and Pincheira, J.A., 2000, "Spectral displacement demands of stiffness- and strength-degrading systems," *Earthquake Spectra*, Vol. 16, No. 4, pp. 817-851.

Sozen, M.A., and Moehle, J.P., 1993, *Stiffness of Reinforced Concrete Walls Resisting In-Plane Shear*, Electric Power Research Institute, Palo Alto, California.

Spacone, E., Filippou, F.C., and Taucer, F., 1996, "Fiber beam-column model for nonlinear analysis of R/C frames: I. Formulation," *International Journal of Earthquake Engineering and Structural Dynamics*, Vol. 25, No. 7, pp. 711-725.

Stephen, R.M., Wilson, E.L., and Stander, N., 1985, *Dynamic Properties of a Thirty-Story Condominium Tower Building*, UCB/EERC Report 85/03, University of California, Berkeley, California.

Takeda T., Sozen, M.A., and Nielsen, N.N., 1970, "Reinforced concrete response to simulated earthquakes," *Journal of the Structural Division,* American Society of Civil Engineers ,Vol. 96, No. 12, pp. 2557-2573.

Tassios, T.P., Moretti, M., and Bezas, A., 1996, "On the behavior and ductility of reinforced concrete coupling beams of shear walls," *Structural Journal*, American Concrete Institute, Vol. 93, No. 6, pp. 711-720.

Taylor, C.P., Cote, P.A., and Wallace, J.W., 1998, "Design of slender RC walls with openings," *Structural Journal*, American Concrete Institute, Vol. 95, No. 4, pp. 420-433.

Taylor, R.L., Filippou, F.C., Saritas, A., and Auricchio, F., 2003, "A mixed finite element method for beam and frame problems," *Computational Mechanics,* Vol. 31, No. 1-2, pp. 192-20.

Thomsen IV, J.H., and Wallace, J.W., 2004, "Experimental verification of displacement-based design procedures for slender reinforced concrete structural walls," *Journal of Structural Engineering*, American Society of Civil Engineers, Vol. 130, No. 4, pp. 618-630.

Tremblay, R., Tchebotarev, N., and Filiatrault, A., 1997, "Seismic performance of RBS connections for steel moment-resisting frames: influence of loading rate and floor slab", *Behavior of Steel Structures in Seismic Areas, Proceedings of the Second International Conference*, STESSA, Kyoto, Japan, pp. 664-671.

Trifunac, M.D., 1970, "Ambient Vibration Test of a Thirty-Nine Story Steel Frame Building," *EERL 70-02,* California Institute of Technology, Pasadena, California.

Tsai, K.C., and Popov, E.P., 1988, *Steel Beam-Column Joints in Seismic Moment Resisting Frames*, Report No. UCB/EERC-88/19, University of California, Berkeley, California.

Uang, C.M., Yu, Q.S., and Gilton, C.S., 2000, "Effects of loading history on cyclic performance of steel RBS moment connections," *Proceedings of the 12th World Conference on Earthquake Engineering*, Upper Hutt, New Zealand.

Valenas, J.M., Bertero, V.V., and Popov, E.P., 1979, *Hysteretic Behavior of Re-inforced Concrete Structural Walls*, Report No. UCB/EERC-79/20, University of California, Berkeley, California.

Vanderbilt, M.D., and Corley, W.G., 1983, "Frame analysis of concrete building," *Concrete International*, Vol. 5, No. 12, pp. 33-43.

Wallace, J.W., 1994, "A new methodology for seismic design of reinforced concrete shear walls," *Journal of Structural Engineering*, American Society of Civil Engineers, Vol. 120, No. 3, pp. 863-884.

Wallace, J.W., 2007, "Modeling issues for tall reinforced concrete core wall buildings," *The Structural Design of Tall and Special Buildings*, Vol. 16, No. 5, pp. 615-632.

Wallace, J.W., Moehle, J.P., and Martinez-Cruzado, J., 1990, "Implications for the design of shear wall buildings using data from recent earthquakes," *Proceedings from the Fourth U.S. National Conference on Earthquake Engineering*, pp. 359-368.

Wallace, J.W., 1998, "Behavior and design of high-strength RC walls," *Special Publication*, American Concrete Institute, Farmington Hills, Michigan, Vol. 176, pp. 259-279.

Wallace, J.W., and Moehle, J.P., 1992, "Ductility and detailing requirements of bearing wall buildings," *Journal of Structural Engineering,* American Society of Civil Engineers, Vol. 118, No. 6, pp. 1625-1644.

Wang, T.Y., Bertero, V.V., and Popov, E.P., 1975, *Hysteretic Behavior of Reinforced Concrete Framed Walls,* UCB/EERC Report 75/23, University of California, Berkeley, California.

Whittaker, A.S., Uang, C-M., and Bertero, V.V., 1987, *Earthquake Simulation Tests and Associated Studies of a 0.3-Scale Model of a Six-Story Eccentrically Braced Steel Frame Structure,* UCB/EERC Report 87/02, University of California, Berkeley, California.

Whittaker, A.S., Uang, C-M., and Bertero, V.V., 1988, *An Experimental Study of the Behavior of Dual Steel Systems*, UCB/EERC Report 88/14, University of California, Berkeley, California.

Wood, S.L., 1990, "Shear strength of low-rise reinforced concrete walls," *Structural Journal*, American Concrete Institute, Vol. 87, No. 1, pp. 99-107.

Xiao, Y., Esmaeily-Ghasemabadi, A., and Wu, H., 1999, "High-strength concrete short beams subjected to cyclic shear," *Structural Journal*, American Concrete Institute, Vol. 96, No. 3, pp. 392-399.

Yan, W., and Wallace, J.W., 1993, *Analytical Studies of Four Shear Wall Buildings Using Data From Recent California Earthquakes,* Report

No. CU/CEE-93/15, Department of Civil and Environmental Engineering, Clarkson University, Potsdam, New York.

Yassin, M.H.M., 1994, *Nonlinear analysis of prestressed concrete structures under monotonic and cyclic loads*, Ph.D. Dissertation, University of California, Berkeley, California.

Zareian, F., 2006, *Simplified Performance-Based Earthquake Engineering*, Ph.D. Dissertation, Department of Civil and Environmental Engineering, Stanford University, Stanford, California.

Zareian, F., and Krawinkler, H., 2007, "Assessment of probability of collapse and design for collapse safety," *Earthquake Engineering and Structural Dynamics*, Vol. 36, No. 13, pp.1901-1914.

Zhu, L., Elwood, K.J., and Haukaas, T., 2007, "Classification and seismic safety evaluation of existing reinforced concrete columns," *Journal of Structural Engineering,* American Society of Civil Engineers, Vol. 133, No. 9, pp. 1316-1330.

Ziemian, R.D., McGuire, W., and Deierlein, G.G., 1992a, "Inelastic limit states design. Part I: Planar frame studies," *Journal of Structural Engineering,* American Society of Civil Engineers, Vol. 118, No. 9, pp. 2532-2549.

Ziemian, R.D., McGuire, W., and Deierlein, G.G., 1992b, "Inelastic limit states design. Part II: Three-dimensional frame study," *Journal of Structural Engineering,* American Society of Civil Engineers, Vol. 118, No. 9, pp. 2550-2568.

Project Participants

PEER Task 7 Project Core Group Participants

James O. Malley (Project Technical Director)
Degenkolb Engineers
235 Montgomery Street, Suite 500
San Francisco, California 94104

Gregory Deierlein
Stanford University
Dept. of Civil and Environmental Engineering
Blume Earthquake Engineering Center, M3037
Stanford, California 94305

Jon A. Heintz
Applied Technology Council
201 Redwood Shores Parkway, Suite 240
Redwood City, California 94065

Helmut Krawinkler
Stanford University
Dept. of Civil and Environmental Engineering
473 Via Ortega
Stanford, California 94305

Joseph R. Maffei
Rutherford & Chekene
55 Second Street, Suite 600
San Francisco, California 94105

Mehran Pourzanjani
Saiful/Bouquet Inc.
385 E. Colorado Boulevard, Suite 200
Pasadena, California 91101

John Wallace
University of California, Los Angeles
Dept. of Civil Engineering
5731 Boelter Hall
Los Angeles, California 90095

PEER Tall Buildings Project Advisory Committee

Jack Moehle (Principal Investigator)
Pacific Earthquake Engineering Research Center
University of California, Berkeley
325 Davis Hall, MC1792
Berkeley, California 94720

Yousef Bozorgnia
Pacific Earthquake Engineering Research Center
University of California, Berkeley
325 Davis Hall, MC1792
Berkeley, California 94720

Norm Abrahamson
Pacific Gas & Electric Company
Geosciences Department
245 Market Street, Room 403
San Francisco, California 94177

Ronald O. Hamburger
Simpson Gumpertz & Heger
The Landmark @ One Market, Suite 600
San Francisco, California 94105

Helmut Krawinkler
Stanford University
Dept. of Civil and Environmental Engineering
473 Via Ortega
Stanford, California 94305

Marshall Lew
MACTEC Engineering & Consulting, Inc.
200 Citadel Drive
Los Angeles, California 90040

Ray Lui
Department of Building Inspection
1660 Mission Street, 2nd Floor
San Francisco, California 94103

Mark Moore
ZFA Consulting
555 Howard Street, Suite 202
San Francisco, California 94105

Farzad Naeim
John A. Martin & Associates, Inc.
1212 S. Flower Street, 4th Floor
Los Angeles, California 90015

Paul Somerville
URS Corp
566 El Dorado Street, 2nd Floor
Pasadena, California 91101

Expert Review Panel

Lawrence G. Griffis
Walter P. Moore
221 W. 6th Street, Suite 800
Austin, Texas 78701

Robert D. Hanson
2926 Saklan Indian Drive
Walnut Creek, California 94595

Leonard M. Joseph
Thornton Tomasetti
2415 Campus Drive, Suite 110
Irvine, California 92612

Ron Klemencic
Magnusson Klemencic Associates
1301 Fifth Avenue, Suite 3200
Seattle, Washington 98101

Graham Powell
Graham H. Powell, Inc.
14710 Wolfgang Road
Truckee, California 96161

Mike Mehrain
URS Corporation
915 Wilshire Blvd., Suite 700
Los Angeles, California 90017

Jose Restrepo
University of California San Diego
Dept. of Structural Engineering
9500 Gilman Drive, MC 0085
La Jolla, California 92093

Charles Roeder
University of Washington
Department of Civil Engineering
233B More Hall
Seattle, Washington 98195

Michael Willford
ARUP
560 Mission Street, 7th Floor
San Francisco, California 94105

Nabih Youssef
Nabih Youssef and Associates
800 Wilshire Blvd., Suite 200
Los Angeles, California 90017